UNIVERSITA' DEGLI STUDI DI PADOVA

DIPARTIMENTO DI INGEGNERIA CIVILE, EDILE E AMBIENTALE

CORSO DI LAUREA MAGISTRALE IN INGEGNERIA CIVILE

Tesi di Laurea Magistrale in Ingegneria Civile - Indirizzo Strutture

SISTEMA ANTISISMICO INNOVATIVO CON FUSIBILI DISSIPATIVI PER STRUTTURE IN ACCIAIO FORMATO A FREDDO – PROGETTAZIONE E MODELLAZIONE NUMERICA

Relatore:	Prof. Roberto Scotta	*Università degli Studi di Padova*
Correlatore:	Prof. Benjamin W. Schafer	*Johns Hopkins University*
Correlatore:	Prof. Grunde Jomaas	*Technical University of Denmark*

Laureando: ROBERTO COMINI

ANNO ACCADEMICO 2013 - 2014

M.Sc. Thesis for the Master-level double-degree program TIME
(Top Industrial Managers for Europe)

INSTITUTIONS:
Università degli Studi di Padova
Technical University of Denmark

Original title:

INNOVATIVE SEISMIC SYSTEM WITH REPLACEABLE ENERGY-DISSIPATING FUSES FOR COLD-FORMED STEEL STRUCTURES – MODELING AND DESIGN

Thesis written at: Johns Hopkins University, Department of Civil Engineering

Roberto Comini

Supervisor
Roberto Scotta
Professor
Department of Civil, Environmental and Architectural Engineering
University of Padova

Supervisor
Benjamin W. Schafer
Professor and Chair
Department of Civil Engineering
Johns Hopkins University

Supervisor
Grunde Jomaas
Associate Professor
Department of Civil Engineering
Technical University of Denmark

October 2013

Riassunto

Il sistema antisismico più diffuso per edifici in acciaio formato a freddo è la parete di taglio. Essa è normalmente costituita da pannelli in legno truciolato (Oriented Strand Board) fissati al telaio in acciaio mediante appositi connettori autofilettanti. In caso di terremoti significativi questi pannelli vengono danneggiati estesamente ma non dissipano sufficiente energia, e di conseguenza la capacità antisismica dell'intero sistema è limitata. A questo scopo, un innovativo sistema dissipativo per strutture in acciaio formato a freddo viene proposto mediante simulazioni numeriche agli elementi finiti. Il sistema consiste in pareti di taglio con elementi di acciaio a forma di farfalla inseriti tra i montanti e progettati per snervarsi durante i terremoti: tali elementi sono perciò fusibili dissipativi che possono essere facilmente sostituiti una volta danneggiati. Per effetto del sisma, il telaio subisce una deformazione tagliante che induce sollecitazioni di taglio e flessione nei fusibili che, grazie alla forma a farfalla, si snervano in maniera uniforme su tutta la loro lunghezza, massimizzando così la dissipazione energetica. Tali fusibili sono però elementi particolarmente snelli, potenzialmente soggetti a instabilità che ridurrebbe la capacità dissipativa del sistema. Per consentire il dimensionamento preliminare della parete antisismica proposta sono state derivate formule analitiche per valutare capacità massima e resistenza a instabilità dei fusibili, nonché la capacità complessiva della parete di taglio. Sono presentati i risultati di simulazioni numeriche, eseguite sia per i singoli elementi fusibili che per l'intero sistema parete, mediante un software commerciale agli elementi finiti. E' stato effettuato uno studio parametrico sui singoli fusibili, con lo scopo di validare le formule analitiche e generalizzare il loro utilizzo, nonché per osservare l'effettivo comportamento di tali elementi. In base a questo studio, vengono fornite tabelle per il dimensionamento della parete: tali tabelle, insieme alle formule proposte, consentono di scegliere numero e dimensione dei fusibili necessari ad ottenere la prestazione desiderata per il sistema, in termini di resistenza e capacità di spostamento laterale (drift). I risultati numerici ottenuti modellando l'intera parete evidenziano un comportamento isteretico migliore rispetto ai telai tradizionali in acciaio formato a freddo, rivestiti da pannelli strutturali lignei; questo a condizione di prevenire una prematura instabilità dei fusibili. E' così dimostrata la potenziale applicabilità del sistema proposto nel settore edilizio. Si forniscono inoltre indicazioni per un'eventuale prosecuzione dell'attività di ricerca che dovrebbe includere, in particolare, analisi dinamiche di modelli dell'intero edificio che utilizzano il sistema antisismico proposto, nonché prove di laboratorio per validare ulteriormente i risultati qui presentati.

Preface

This work is the Master thesis for the M.Sc. program in Civil Engineering at the Technical University of Denmark (DTU) and University of Padova, within the Master-level double-degree program TIME (Top Industrial Managers for Europe). The thesis, worth 32.5 ECTS points, has been written in the period April-October 2013.

The project has been conducted at Johns Hopkins University, under the supervision of Dr. Benjamin W. Schafer, Professor and Chair of the Department of Civil Engineering.

The internal supervisors of the project have been Dr. Grunde Jomaas, Associate Professor and Head of Studies for the Civil Engineering program at the Technical University of Denmark, and Dr. Roberto Scotta, Professor at the University of Padova.

Acknowledgements

First, I would like to thank Prof. Benjamin W. Schafer for welcoming me in his Thin-Walled Structures research group at Johns Hopkins University, where this project has been carried out. Prof. Schafer's expertise guided me through the development of the Thesis, and his deep passion for research has been undoubtedly inspiring to overcome the difficulties faced along the way.

A special thanks must be given to all the students of the Thin-Walled Structures research group, for making me feel immediately part of the group and creating an inspiring research environment. My visit there has been very educative from an academic perspective, and the overall experience has proved to be unique for my cultural and personal growth.

Appreciation is dedicated to all the fellow students who helped me with my work, in particular to Baofeng Zheng for his patient answers to my numerous Abaqus related questions. It is also thanks to him I could overcome several difficulties and proceed with the development of the project.

I am immeasurably grateful to Prof. Grunde Jomaas (DTU), who dedicated an enormous amount of time for making this exchange visit possible and helping me to find the financial support. Besides that, he has been and continues to be a unique source of inspiration: during my years of study, I have never met anyone so passionately dedicated to his work and his students. His mentoring goes far beyond this project, and it will be certainly determinant for future choice of occupation.

I would like to thank Prof. Roberto Scotta (University of Padova) for his precious comments and suggestions, very helpful to the final draft of the Thesis and encouraging for an eventual prosecution of this research work.

I thank the University of Padova, the Technical University of Denmark and the Otto Mønsted Foundation for the received financial support.

Last but not least, I am very grateful to my parents who have always supported me morally and financially, and who have given me full freedom in my educational choices even when these led me away from home.

Content

Nomenclature

a	Height of the middle section of the fuse link.
a_i	Amplitude of the ith step in the FEMA loading protocol.
b	Height of the end sections of the fuse link.
$\overline{b}$	Height of the quarter-point section of the fuse link.
E	Young modulus.
$\mathbf{f_0}$	Imperfection field.
F	Lateral force on the shear wall.
F_{frame}	Contribution of the CFS frame to the total capacity of the wall system.
$\overline{F}_{wall}$	Maximum lateral capacity of the shear wall with integrated fuses.
h	Height of the shear wall.
$\overline{I}$	Moment of inertia of the simplified straight fuse link.
k, k'	Measures of stiffness in the fuse links.
k_{31}	Stiffness coefficient relative to the moment at the end section of a beam.
L	length of the fuse link.
L_{plate}	Length of the fuse side plates.
M	Bending moment in the fuse link.
M_0	bending moment at the end of the fuse link.
$M_{0,y}$	Bending moment at the end sections of the fuse link, causing first yielding in the link.
$M_{0,p}$	Bending moment at the end sections of the fuse link, causing plastic hinge in the link.
$M_{y,x=\frac{L}{4}}$	Bending moment at the quarter-point section of the fuse link, causing yielding in the same section.
n_{fuse}	Number of fuse links installed in the shear wall.
N	Axial force at the bottom of the studs (or number of steps for the FEMA loading protocol, according to the context).
P	Axial load of a column.
P_{cr}	Critical axial load of a column.
q	Behavior factor.
R	response modification coefficient.
R^2	Coefficient of determination.

t	thickness of the fuse links (or time, according to the context).
u	Relative vertical displacement of the fuse end sections.
u_{top}	Horizontal displacement of the track.
u_y	Relative vertical displacement of the fuse end sections, causing first yielding in the fuse.
v	Lateral displacement of a column.
v_0	Initial geometric imperfection of a column.
$v_{0,fuse}$	Initial geometric imperfection of the fuse link.
V	Shear force in the fuse link.
V_{cr}	Critical shear force of the fuse link.
V_{peak}	Post-buckling peak capacity of the fuse link.
V_y	Shear force causing yielding in the fuse link.
$\overline{V}_{fuse}$	Shear capacity of the fuse link.
w	Width of the shear wall.
α	Inclination angle of the studs in a pin-connected frame.
$\overline{\alpha}$	Inclination angle of the studs in fixed frame
Δ	Drift of the shear wall.
Δ_0	Targeted smallest drift for the FEMA loading protocol.
Δ_{cr}	Wall drift causing buckling in the fuse link.
$\Delta_{cr,fuse}$	Fuse drift causing buckling in the fuse link.
Δ_{fuse}	Drift of the fuse link.
Δ_m	Targeted maximum drift for the FEMA loading protocol.
Δ_y	Wall drift causing first yielding in the fuse link.
$\Delta_{y,fuse}$	Fuse drift causing first yielding in the fuse link.
$\overline{\Delta}$	Normalized critical drift of the fuse.
λ	Fuse slenderness.
σ_y	Yielding stress .
$\mathbf{\Phi_1}$	Lowest eigenmode of the fuse link.
φ	Actual rotation of the fuses (equal for link and side plates).

List of Figures

List of Tables

Chapter 1

Introduction

1.1 General

Earthquake engineering deals with the design of structures capable of withstanding dynamic loadings induced by seismic ground acceleration. Such loadings depend both on the earthquake's magnitude (peak ground acceleration) and the mass of the building, according to Newton's law. Designing structures to remain elastic during seismic excitation is not convenient, because requires over-dimensioning of the components, which in turn increases the mass and therefore the seismic load.

For this reason, earthquake building codes, both in Europe and North-America, allow the structural systems to resist seismic actions in the non-linear range [1], thus developing post-elastic energy dissipation [2]. The structural systems are therefore designed to resist seismic forces smaller than those corresponding to a linear elastic response [1]; this reduction is accomplished by introducing the behavior factor q [1] or the response modification coefficient R [2]. Both factors are a measure of the ratio between the elastic and design loads.

To allow such reduction of seismic loading, structures are expected to undergo plastic deformation, but at the same time they have to maintain a sufficient resistance and prevent collapse in the post-elastic regime. The inelastic deformation capacity can be guaranteed by providing sufficient ductility to the structural systems. For moment-resisting frames, plastic deformation normally occurs in the beam-column joints; concentrically braced frames rely mainly on buckling of the braces; for eccentrically braced frames, inelastic deformation is localized in the link beam.

Structures designed according to this approach are expected, after a major earthquake, to undergo inelastic damage distributed throughout the seismic force resisting system. In fact, the building codes are intended to prevent large failures and loss of life, but not to significantly limit the structural damage. However, this approach is inadequate to satisfy the rising demand for continued occupancy of the building after large earthquake events. The extensive damage, allowed to dissipate seismic energy, is often irreparable, thus forcing building downtime and even the structure to be torn down: the social and financial costs of reconstruction, as many past earthquakes have recorded, are enormous.

For these reasons, a recent trend in earthquake engineering is the development of energy dissipation systems which reduce structural damage and maintain building functionality even after major seismic events. Many techniques have been developed in the past years, and a review of these can be found in [3]. Control systems to improve seismic (and wind) performance of building and bridges can be classified into two main categories:

- passive systems;
- active systems.

Passive seismic solutions do not require any additional energy source to operate and are activated simply by seismic motion. They can be subdivided into [4]:

- energy dissipation devices;
- base isolation techniques;
- dynamic oscillators.

Energy dissipation devices are designed to absorb most of the seismic input energy through deformation or yielding, thus preventing the main structural members to undergo plastic deformation. Examples are metallic yielding dampers, friction dampers, visco-elastic dampers and fluid-viscous dampers [4]. The basic principle of these systems is the conversion of the mechanical energy induced by seismic motion into thermal energy, thus enhancing structural damping.

On the other hand, base isolation increases the fundamental period of a structure by means of a flexible interface between the structure itself and its foundation. The interface is very stiff along the vertical direction but flexible in the lateral direction so that the amount of lateral force transferred to the superstructure is limited.

The main category of dynamic oscillators are tuned-mass dampers. These are additional masses attached to the main structural system, designed to have their frequency tuned to the exciting frequency and moving out-of-phase compared to the main structure.

Contrary to passive systems, active control devices require an energy source and computer-controlled actuators to apply forces counterbalancing the action induced by earthquakes. They are intrinsically more complex than passive systems, because they make combined use of computer-control, motion sensors, etc., requiring an interdisciplinary approach. The sensors positioned throughout the building measure the seismic excitation and accordingly determine the direction and weight of the necessary counter-balancing forces to be applied. This technology is complex and expensive, still rather new for civil constructions and probably feasible only for very specific buildings and infrastructures of vital importance.

A control system combining the features of both passive and active systems is defined hybrid.

1.2 Cold-formed steel structures

The thesis aims to propose an innovative seismic system, among those presented above, for structures made of cold-formed steel (CFS), which have almost exclusively relied on conventional lateral force resisting systems characterized by extensive damage and large repair costs.

Cold-formed steel structures are currently diffused in many countries, particularly in North-America, for residential and industrial buildings, bridges, storage racks and several other applications other than those related to the construction industry [5]. Cold-formed steel products are shaped at ambient temperature from steel sheet, strip plates or flat bars by rolling, press or bending brake operations [6]. The rising success of this structural material is due to its many advantages compared to more traditional

materials like hot-rolled steel, concrete or timber. In the following, some of these advantages are briefly summarized, but a full overview of cold-formed steel is left to more specific publications.

Members made of cold-formed steel are often referred to as thin-walled or thin-gauge members. In fact, they are characterized by a large width-to-thickness ratio that, combined with high strength and stiffness, allows building structural components with a significantly reduced amount of material. Thus, CFS structures are light, with a small structural dead load: when compared to concrete structures, the reduction in weight is remarkable, but CFS components are also approximately 35% to 50% lighter than their timber counterparts [6]. The reduced weight facilitates handling, transportation and erection. Other positive features are durability (resistance to termites and rotting, and long-term resistance to corrosion, if galvanized), non-combustibility, recyclability. In brief, cold-formed steel is often chosen for its cost-effectiveness (savings in the amount of steel required) and rapidity and easiness of construction.

On the other hand, the large width-to-thickness ratios combined with high strength makes CFS members prone to many instability problems. Apart from the global buckling modes (flexural, torsional and lateral-torsional buckling), there are also other buckling modes, referred to as distortional and local buckling.

Although the first applications of cold-formed steel as a construction material date back to the 1850s in both United States and Great Britain [5], CFS was not widely used until the 1940s. The reason for this was mainly lack of standardized design methodologies and non-inclusion to Building Codes [6]. The publication of the first AISI *Specification for the Design of Cold Formed Steel Structural Members* (1946) and the *Design Manual* (1949), following the research at Cornell University under the direction of George Winter, accelerated its diffusion. After the second edition of the *Specification* (1956), cold-formed steel was also adopted by the Building Code.

Many are the applications of cold-formed steel, but the present Thesis focuses only on its structural use for building constructions. Cold-formed steel is currently used for load-bearing applications in three primary areas: framing, metal buildings and racks [7]. Despite being often associated with low-rise buildings, CFS mid-rise framing have recently become more common in the United States, even in seismic areas [7]: for example, Fig. 1.1(a) is an example of building entirely made of CFS members, while Fig. 1.1(b) shows a six-story building with CFS framing in the United States. In this work, framing applications for cold-formed steel are mainly addressed, in particular the lateral force resisting system, which is of main interest in earthquake engineering.

(a) (b)

Fig. 1.1 (a) CFS building; (b) exterior CFS framing (from [7], with permission)

1.3 Structural fuses as energy-dissipation devices

The success and diffusion of cold-formed steel buildings is strongly dependent on the low cost and reduced construction time, compared to other traditional structural materials. Furthermore, cold-formed steel is mainly used for low and mid-rise industrial and residential buildings, which do not require the same seismic control systems used for tall skyscrapers or building of strategic significance.

Thus, any seismic control system (other than the traditional lateral resisting system) proposed for cold-formed steel structures has to be cheap, easy to install and without specific maintenance requirements; otherwise, the more traditional timber, hot-rolled steel and concrete may be preferable solutions for structural applications. This immediately excludes the use of sophisticated active systems or particular dampers, also because (even neglecting the financial aspect) they would be probably disproportional compared to the relatively small energy dissipation requirements for conventional cold-formed steel buildings.

Based also on past research and proposals for innovative seismic control devices, the typology more likely to be feasible for cold-formed steel structures is based on metal yielding. Such devices are often referred to as *fuses*, because they are designed to perform the same function as electric fuses for appliances. It is well known that traditional fuses are sacrificial devices providing overcurrent protection: the metal wire in the fuse melts when excessive current flows, thus preventing further damage to appliances and risk for people. Once the fuse melts, it can be easily replaced with a cost remarkably smaller than substituting the full electrical appliance to which was connected. The analogy is evident: a structural fuse in earthquake engineering is designed to dissipate most of the input seismic energy by plastic deformation, thus preventing or minimizing the damage in the main structure. After the earthquake, the fuses can be easily replaced with a small cost and avoiding building downtime.

The Thesis will discuss the design and application of dissipative fuses, to be installed within conventional CFS frames. Although the idea of using metal devices designed to yield to dissipate energy is not new in earthquake engineering, it is almost unexplored in cold-formed steel building, and the proposed system is completely original.

1.4 Thesis overview

The Thesis is structured as follows:

- After discussing the lateral force resisting systems conventionally used for CFS structures, an overview of the main energy-dissipation devices based on metal yielding is presented (Chapter 2).

- The innovative seismic protection system for CFS is introduced and the main design equations are derived (Chapter 3).

- A parametric study of the structural fuses employed by the proposed seismic system is performed, to investigate the relative influence of the relevant parameters (Chapter 4). The parametric study is conducted by means of finite element analyses. This also allows to verify the design formulas and provides additional information for the actual design.

- Numerical models of the entire wall system with integrated fuses are presented to discuss their seismic performance, in terms of hysteretic behavior and energy-dissipation capacity (Chapter 5). The innovative seismic system is compared to conventional lateral force resisting systems, to show the benefits and improvements that can be achieved.

- The simplifications introduced and the main limitations present in the models are addressed, and indication for future research is provided (Chapter 6).

Chapter 2

Seismic resisting systems for CFS structures and energy-dissipation devices

2.1 Traditional lateral force resisting systems for CFS framing

The primary lateral force resisting system for cold-formed steel framing is the shear-wall [7]. Different types of shear-wall solutions are available: the most common is the wood-sheathed wall, in which oriented strand board (OSB) panels are attached to the cold-formed steel studs by means of fasteners, usually steel tapping screws [8, 9]; in alternative, strap-braced walls are also used [10].

In the most recent version of the American Iron and Steel Institution *Lateral Design Standard* (AISI S213-07-S1-09), shear strength is provided for different wall configurations [11]. However, the *Lateral Design Standard* does not provide specific insight on the hysteretic performance of shear walls, which is a fundamental piece of information needed to understand their behavior under seismic action. On the other hand, experimental investigations have been performed to characterize hysteretic response and failure mode of such lateral force resisting systems [8, 9, 12].

Hysteresis describes the dependence of a system on its past environment, and this is particularly relevant for structures under cyclic seismic loading. Hysteretic curves provide direct insight on the system capacity to maintain sufficient resistance in the inelastic range, expected to occur during earthquakes. Any failure or material degradation in structural members reduces the overall capacity available in the next loading cycles, thus affecting the seismic performance of the system. Hysteresis also indicates the amount of energy that can be dissipated through inelastic deformation of the structure, which is a fundamental parameter in earthquake engineering.

The behavior of wood-sheathed shear walls has been studied quite extensively. Recent experiments show that failure occurs at sheathing-to-stud fastener locations [8]. Some failure modes are shown in Fig. 2.1. Experiments focusing on the hysteretic behavior of the fasteners loaded in shear show pinched hysteretic curves with essentially no force in the second and fourth quadrant of the force-deformation diagram [9]. This behavior is reflected in the hysteretic curve of the entire shear wall, as found in [8]. Fig. 2.2 represents the hysteresis for the fasteners and the entire wall, which is qualitatively similar in the two cases. These curves are characterized by pinching, essentially no force in the second-fourth quadrant and therefore not optimal energy dissipation capacity.

Strap-braced walls make use of diagonal flat steel strap cross bracing to resist seismic actions [10] (Fig. 2.3). The lateral forces induced by earthquakes are transferred from the roof and floor levels to the foundation by means of this bracing system. Ideally, the strap bracing are designed to be the elements dissipating energy through yielding; the wall would behave in a ductile way, without failure of the other components such as connections, studs, track and hold-downs. However, experimental campaign

carried out in Australia [10] showed that the wall actual behavior is often very far from the desired one, so that ductility and energy dissipation capacity are relatively small. This is because yielding of the straps is accompanied by other non-ductile failure modes, which result in a pinched hysteretic curve (Fig. 2.3c) and essentially no force in the second and fourth quadrant of the force-displacement diagram.

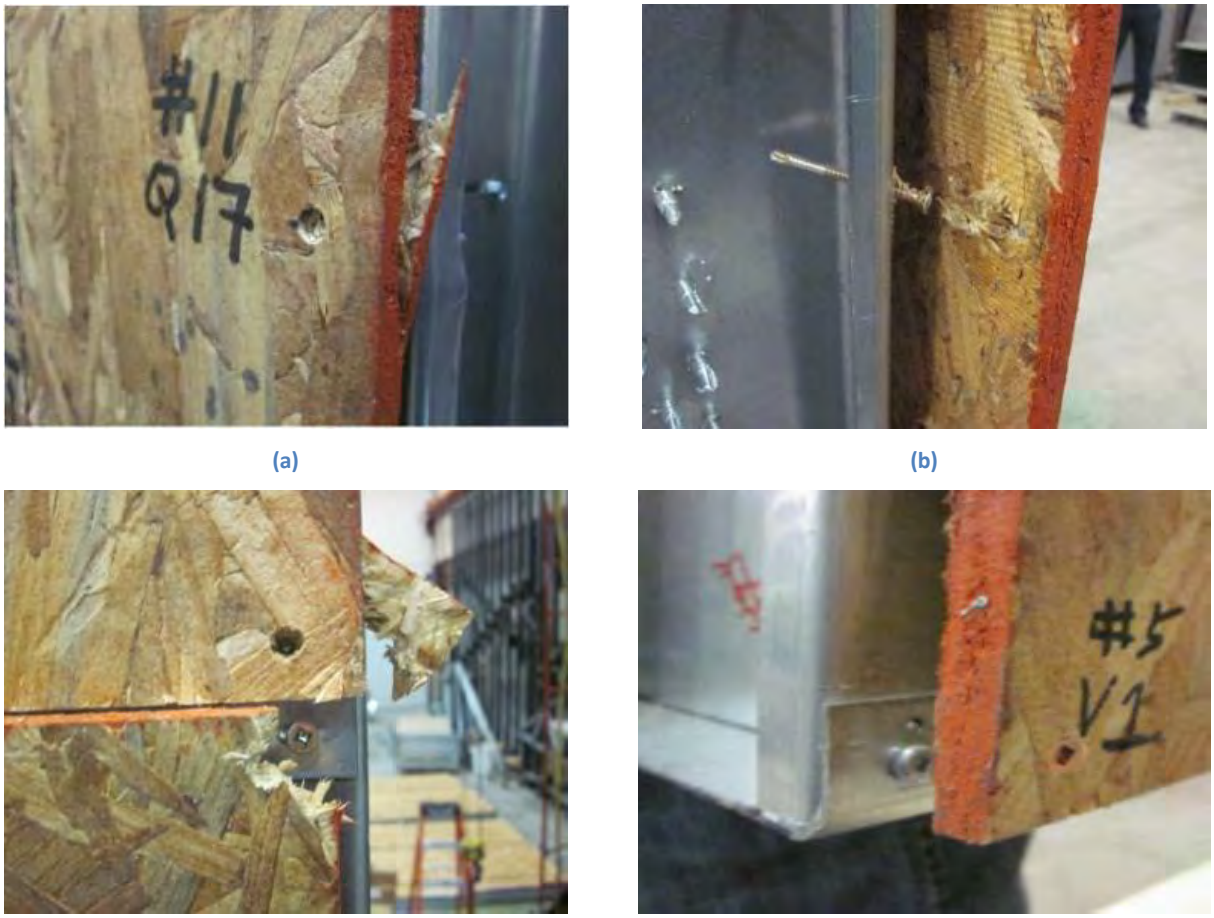

(a) (b)

(c) (d)

Fig. 2.1 **Failure modes at the stud-OSB connections (from [8]). (a) wood bearing failure; (b) pull-through; (c) cut off head (screw shear); d) tear out of sheathing.**

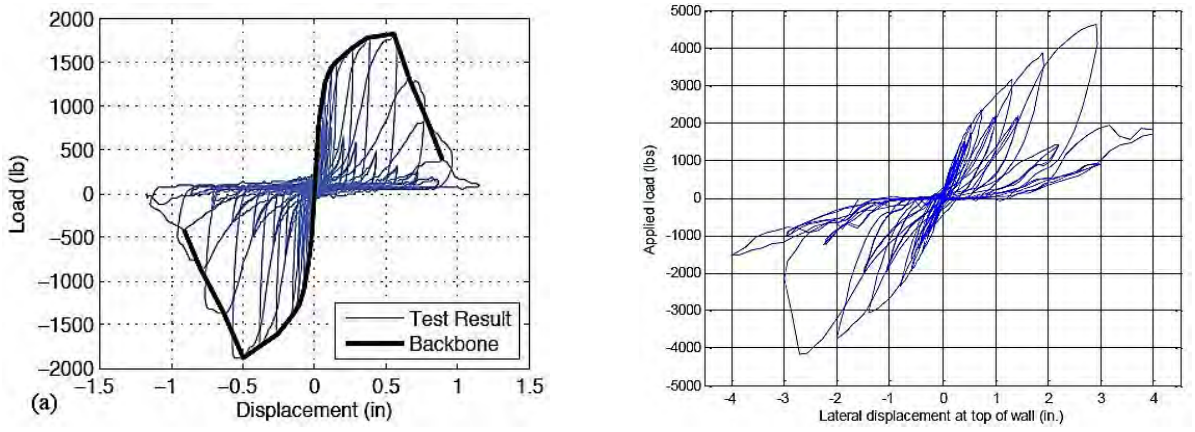

(a) (b)

Fig. 2.2 **Hysteretic behavior in the OSB shear wall (from [8, 9]). (a) Fasteners loaded in shear; (b) Entire shear wall**

(a)

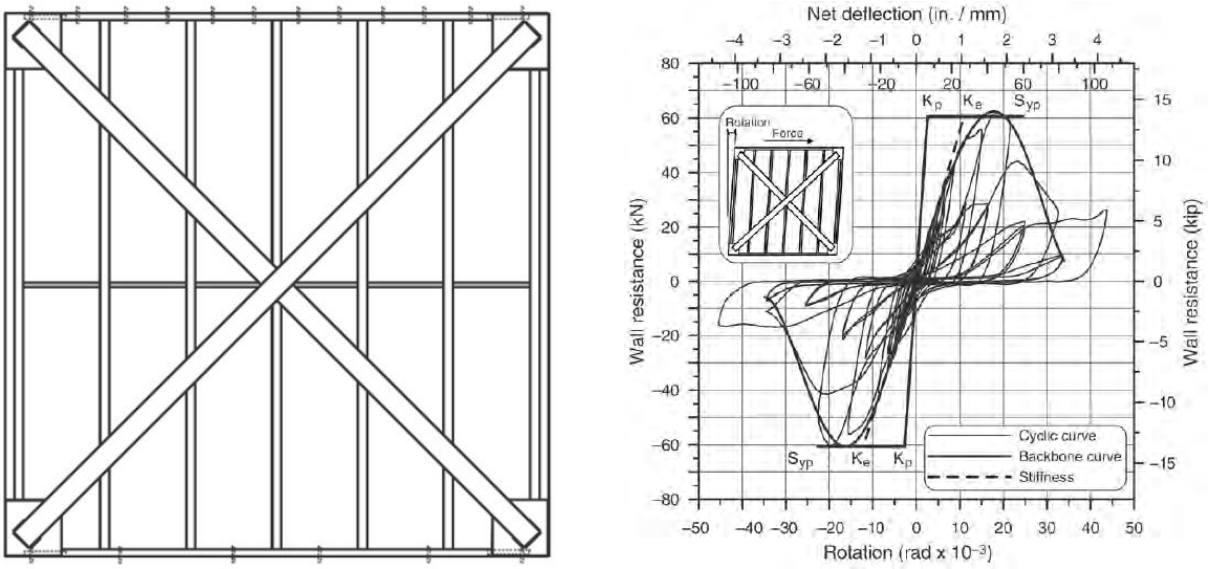

(b) (c)

Fig. 2.3 Strap-braced wall (from [10]). a) during construction; b) schematic view; c) hysteretic behavior

2.2 Energy dissipation devices based on metal yielding

A building without any supplemental seismic control device dissipates energy by means of inelastic deformation throughout its structural components: for instance, in the systems presented in Chapter 1, the actual failure mode involves members and connections. This Thesis presents an innovative seismic system that may eliminate the inconveniences and drawbacks of the traditional wood-sheathed CFS frame, but at the same time feasible for practical usage in the construction industry.

It has been observed in Chapter 1.3 that a convenient solution to dissipate seismic energy is through yielding of metal elements. However, to avoid extensive plastic deformation and allow easy replacement, such elements should present the characteristics of structural fuses. In the following, some of the recent proposals for energy dissipation systems based on the concept of fuse are

presented. This allows to understand which are the solutions used in current design, and to define the background from which the idea for the proposed system has been taken.

The following overview is quite general and may refer to structures made of different materials, other than cold-formed steel. It is also said from the outset that not all of the following solutions are feasible for cold-formed steel buildings, but are nevertheless presented to introduce general design principles that may be applied, with minor modifications, to other building types. The applications described below are:

- Steel plate shear walls (flat or stiffened, with or without openings);
- Steel braced-frames with integrated fuses;
- Self-centering steel frames with post-tensioning strands and fuses;
- CFS shear walls with fuses in the hold-downs.

2.2.1 Steel plate shear walls

First, the use of steel plates as shear walls is addressed. Extensive research and experiments have been conducted in the past years [13-16], and steel plate shear walls have been used for building design especially in North America and Japan. A wall made of steel is inherently more ductile than a wooden counterpart, provided its failure mode involves extensive metal yielding instead of buckling or connection failure. In order to prevent global buckling of the steel sheet, which would result in pinching of the hysteretic curve and reduction of dissipation capacity, different stiffeners configurations have been proposed [14, 15]. The buckling behavior of the shear panel can be transformed from global to local by adding stiffeners; stiffened plates have also higher stiffness and strength, but in general the construction cost is quite large due to the presence of stiffeners. For this reason, trapezoidally corrugated plates have been proposed [14], to avoid the cost of the stiffener installation, while keeping the same beneficial effects of preventing global buckling. Fig. 2.4 shows three different configurations of steel plate shear walls, where the surrounding frame is made of traditional hot-rolled steel. The unstiffened plate is characterized by global shear buckling behavior, resulting in evident pinching of the hysteretic curve, although the development of tension fields keeps the capacity approximately constant even after instability. Also the corrugated plates undergo buckling which, unlike the unstiffened specimen, is local. For this reason, only in the unstiffened specimen pinching is evident in the hysteretic loop, which results in a lower energy dissipation compared to the specimens 2 and 3.

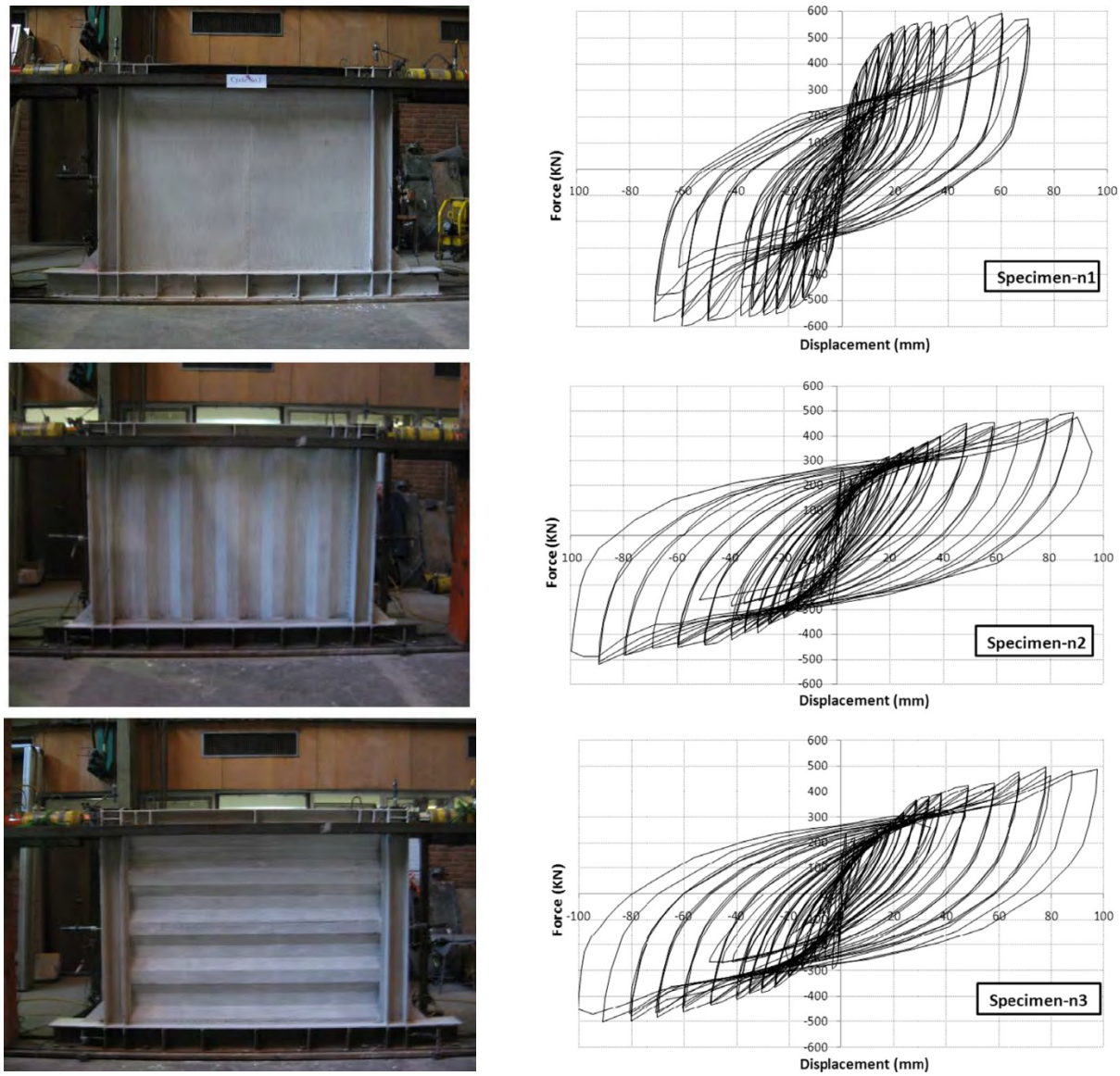

Fig. 2.4 **Steel shear walls and their hysteretic behavior (from [14]). From top to bottom: unstiffened shear wall; trapezoidally vertical corrugated shear wall; trapezoidally horizontal corrugated shear wall**

As a design criterion for steel plate shear walls, the plate has to yield prior to the boundary beams and columns, which should remain elastic as long as possible [14]. However, such shear walls hold very large stiffness which attracts significant seismic forces. This is beneficial in terms of energy dissipation, because most damage can be concentrated on such steel plate walls, but on the other hand large forces require boundary beams and columns to be very resistant. Thin-walled structural elements, like those made of cold-formed steel, are clearly unsuitable for such wall configuration.

To reduce wall stiffness and therefore attracting smaller horizontal forces, steel plates with openings (slits) have been proposed [13]. The steel plate segments between the slits behave as flexural links, providing a ductile response without the need of stiffening the wall. Use of *slit wall* is beneficial also because the strength and stiffness can be adjusted independently by changing the slit configuration. Fig. 2.5 shows an example of steel plate with vertical slits.

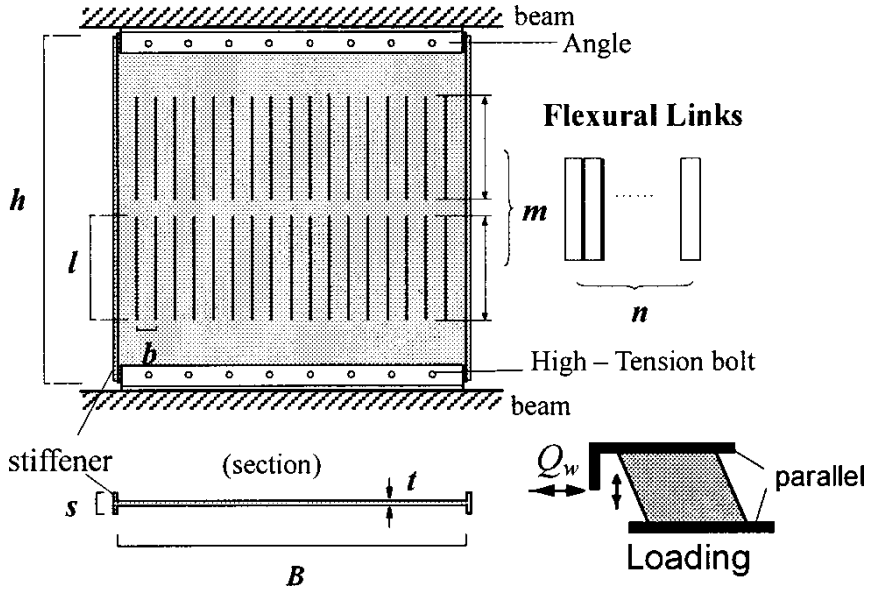

Fig. 2.5 Schematic of steel shear wall with slits (from [13])

2.2.2 Development of structural fuses and application to steel braced frames

Theoretically, steel plate shear walls may be considered examples of structural fuses, because they are designed to yield and undergo inelastic deformation while keeping the boundary structural elements in the elastic range as long as possible. On the other hand, they may also be considered more part of the structural system than specific energy dissipation fuses, also because their post-earthquake replacement is not as easy as for a compact fuse device.

A steel plate with slits, similar to the one presented above but much smaller and conceptually different, was proposed by Chan and Albermani [17]. This device can be installed on top of an inverted V-brace of a frame structure, as shown in Fig. 2.6(a). The vertical steel links between the openings behave as a series of partially-fixed beams under shear and deforming in double curvature; thus, energy is dissipated through flexural yielding of the steel links, when the device is subjected to inelastic cyclic deformation. Yielding first occurs at the end sections of the links, where the moment is the maximum. The specimens fail by fracture due to strain concentration at the end sections (Fig. 2.6b). Experimental results show that plastic deformation occurs at small angular distortion, so that energy is dissipated early during earthquakes. Furthermore, hysteretic behavior is stable and energy dissipation is large, as seen in Fig. 2.6(c).

In order to improve the energy dissipation capacity of such devices, their shape has been optimized to have more uniform and simultaneous yielding. For this purpose, X-shaped or butterfly-shaped steel links (Fig. 2.7) have been proposed to distribute yielding along the length of the links, due to the resemblance of their geometry to the moment diagram of beams deforming in double curvature [18]. Further details on fuse shape optimization will be given in Chapter 3.2.

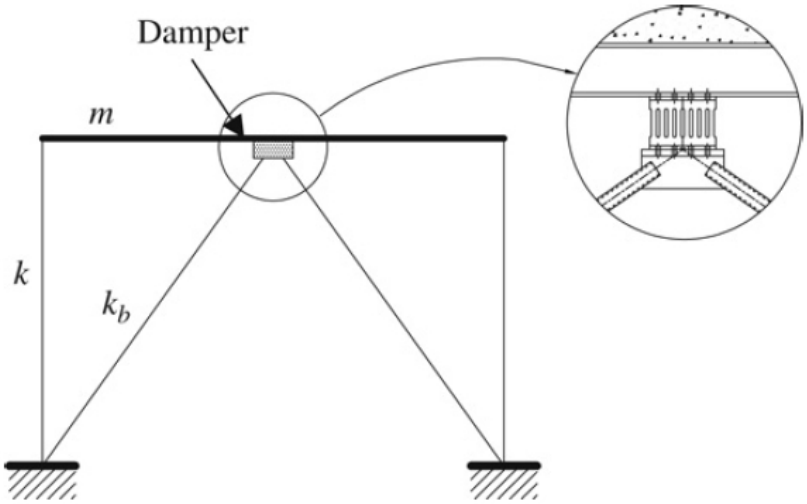

(a)

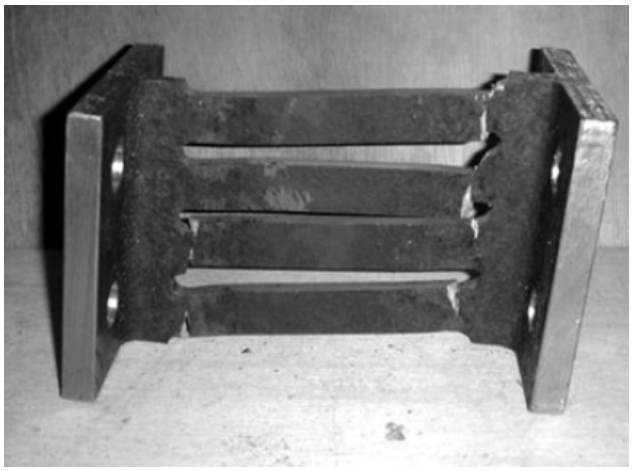

(b)

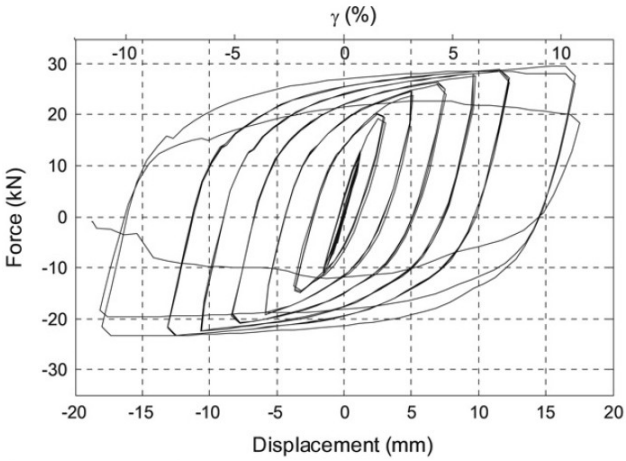

(c)

Fig. 2.6 From [17]: (a) Braced-frame with steel slit damper (fuse); (b) fracture of steel links; (c) hysteretic curve

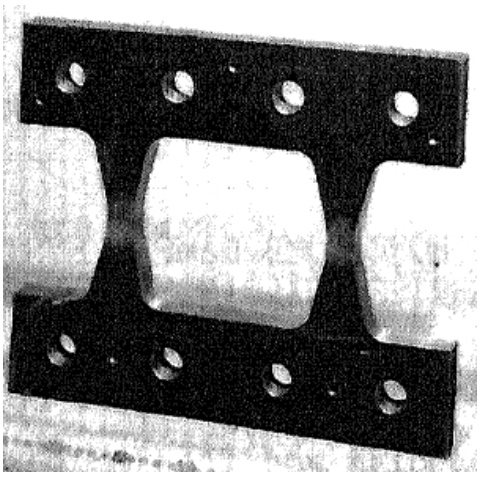

Fig. 2.7 Steel plate with butterfly-shaped links (From [18])

A very interesting application of such energy-dissipating device is within steel-braced frames with post-tensioning cables [19-22]. The proposed system is characterized by steel-braced frames, vertical post-

tensioning strands and replaceable fuses; two alternative configurations are shown in Fig. 2.8. The braced frames are allowed to uplift and rock upon the column base, the strands provide overturning resistance and self-centering capability, while the fuses dissipate energy. Frames and strands are designed to remain elastic, so that damage is only concentrated in the replaceable fuses. In the single frame configuration, the fuse shear deformation is activated by the cables attached to the fuses (Fig. 2.8a), whereas in the double frame is the relative shear deformation between frames to induce shear in the fuses. The advantage of the second solution is that fuse deformation is amplified thus providing greater mobilization of the fuses at low drift; furthermore, more fuses can be installed throughout the height of the frame, allowing for a larger dissipation capacity. For small drifts, the butterfly-shaped links resist shear force through in-plane flexural action with stable (fat) hysteresis loops. For larger drifts, buckling of the links occurs, accompanied by pinching of the hysteretic curve.

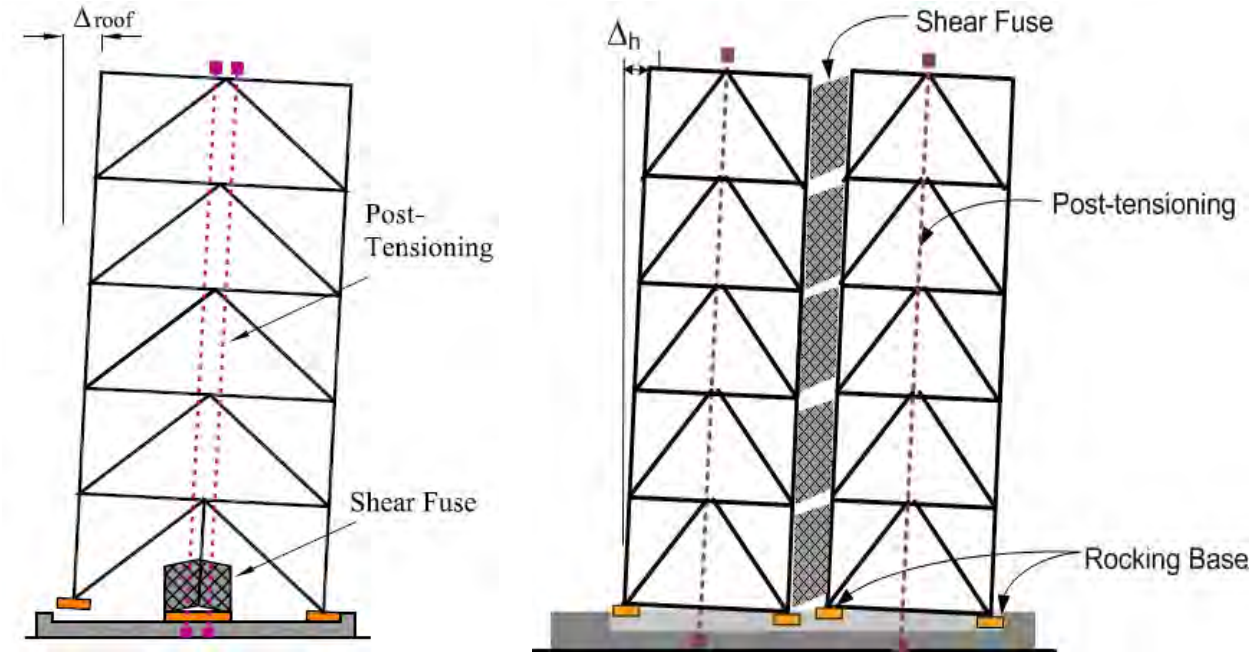

Fig. 2.8 Self-centering braced frames (from [19]): (a) single frame; (b) dual frame

2.2.3 Cold-formed steel frames with fuses in the hold-downs

The system of Fig. 2.8 is suitable for conventional (hot-rolled) steel structures, whose members are strong and stiff enough to allow the connection with post-tensioning cables; such application is probably unsuitable for buildings with thin-walled cold-formed steel members. However, energy dissipation fuse devices have been specifically designed also for thin-gauge structures. In particular, an innovative solution where fuses are placed in the hold-downs is proposed by Ozaky et al. [23, 24]. The fuse configuration is analogue to that proposed above (butterfly-shaped steel links), but the mechanics of the system is different. The fuse is placed between the rocking frame and the foundation, and is connected to a channel of the upper frame and an anchor bolt supported by the foundation (Fig. 2.9a). In conventional cold-formed steel structures hold-downs rigidly connect the frame to the foundation, so that seismic energy is mainly dissipated through plastic deformation of shear walls or structural

members; in this system, instead, members and walls sustain less damage because most energy is dissipated in the hold-downs. Fig. 2.9(b-c) shows that the hysteretic curves, for both the entire wall and the single fuse, are fat and stable up to a significant drift. The pinching, as already indicated, is due to buckling of the steel links.

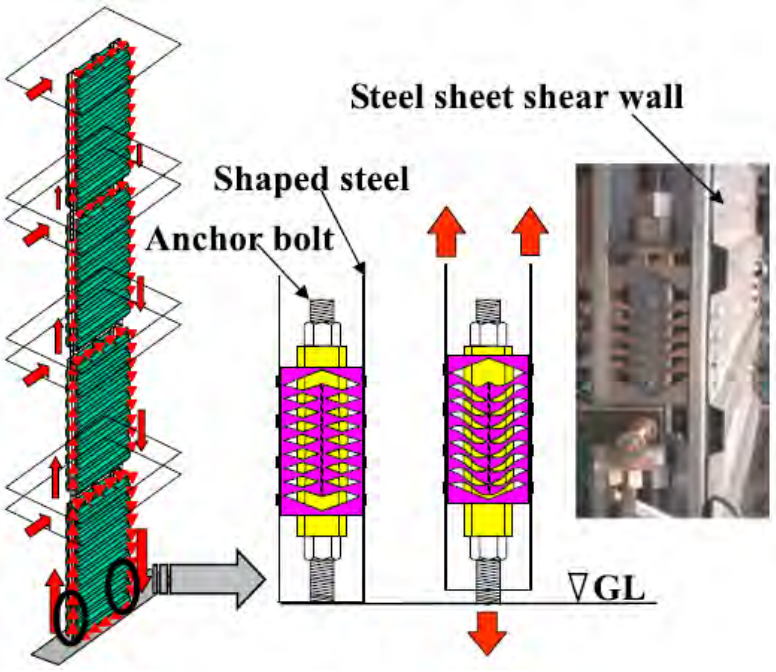

(a)

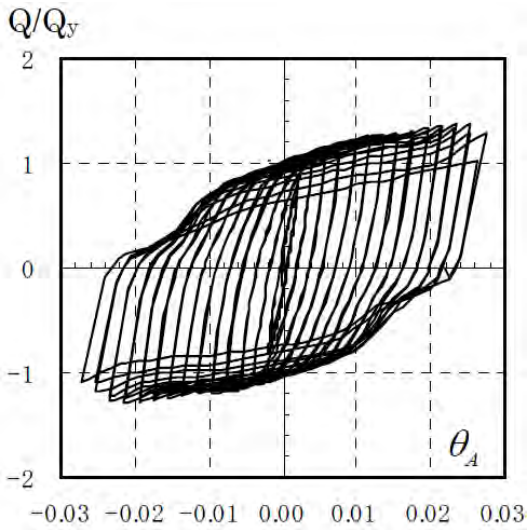

(b)

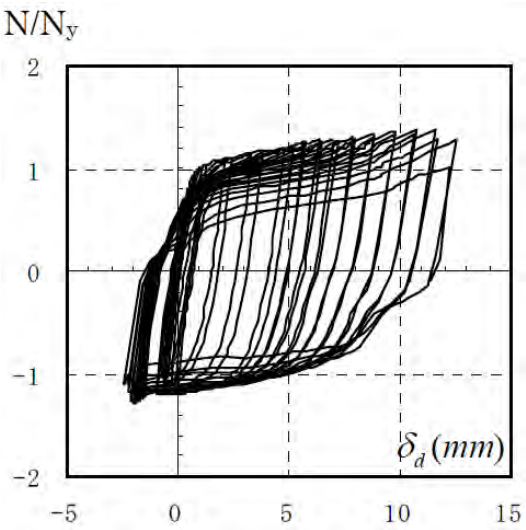

(c)

Fig. 2.9 **From [24]. (a) Multistory shear wall with hold-down fuses; (b) hysteretic curve of the wall; (c) hysteretic curve of the fuse**

2.2.4 Remarks

As a summary of the preceding overview of energy dissipation devices, a structural fuse has to:

- concentrate inelastic deformation to prevent or minimize damage in the main structural system;
- dissipate most of seismic input energy through stable (fat) hysteretic behavior;
- start yielding (and consequently dissipate energy) at relatively small drift;
- be inexpensive and easy to replace if damaged by earthquakes.

Other than adding structural damping, fuses may also increase significantly the stiffness and therefore the seismic-induced forces on the boundary members. In fact, they are also referred to as ADAS (added damping and stiffness) devices [25]. For instance, although not always considered as fuses, steel plate shear walls attract large forces and require the boundary structural elements to have sufficient strength and stiffness, which may not be guaranteed by thin-walled cold-formed steel members. The innovative CFS frame presented in the Thesis takes inspiration from the solutions described in the previous paragraph and combines some of the features typical of each system to fulfill the above-mentioned bullet points and be feasible for cold-formed steel framing. The effectiveness of such system will be mainly measured on the basis of comparison with the most common solution for lateral force resisting systems for cold-formed steel structures: the wood-sheathed CFS framed shear wall, described in Chapter 1. This type of shear wall is considered as a benchmark case also because it has been used in the CFS-NEES building, the first full-scale cold-formed steel building in the world to be tested by means of shake table [26, 27].

Chapter 3

Innovative shear wall with energy-dissipating fuses for CFS structures

3.1 Basics

It is well known that oriented strand board (OSB), sheathed to cold-formed steel frame in the conventional lateral force-resisting system, behaves approximately as a rigid body carrying most of the seismic lateral force. However, as rigid-body motion is not associated with energy dissipation, the force is entirely transferred to the boundary members by means of fasteners connecting OSB and studs. These connections have been proved to be the weak point of the wall, where the failure is localized (Chapter 1); thus, the overall hysteretic behavior of the wall is characterized by evident pinching and the energy dissipation capacity is small.

The basic idea for an innovative type of shear wall consists in substituting the traditional rigid OSB with several flexible steel plate elements spanning the width of the wall and connected to the vertical studs. Such elements should be capable not only of sustaining the lateral seismic force, but also of dissipating a relevant amount of energy through metal yielding while doing so. That is, they should act as energy-dissipating fuses. In this way, the surrounding structural members are less likely to be damaged, improving the system performance. Furthermore, by using multiple fuse elements it is possible to easily adjust the overall lateral capacity of the shear wall according to the specific necessity.

Fig. 3.1 shows a schematic sketch of the proposed wall system, where only one dissipating element is included for simplicity. The boundary frame is initially assumed to be pin-connected so that the only lateral resistance is given by the connector between the vertical studs. This flexible element is schematically represented in Fig. 3.1(a), but it may be thought of as a beam with relatively small bending stiffness. If the stiffness of the fuse is sufficiently small, compared to the other frame members, it can attract most of the deformation and yield, whereas the frame behaves like a rigid body.

Such behavior is clearly quite ideal, because actual frames are not pin-connected and the fuse link cannot be too flexible in order to sustain a sufficient lateral force. However, a properly designed system would have a good compromise between lateral capacity and fuse flexibility. For this purpose, instead of using a single connector as shown in Fig. 3.1, several fuses may be used so that the overall lateral capacity can be increased while maintaining the necessary flexibility of the single links.

Because the dissipation capacity of the wall relies upon yielding of the internal metal devices, it is important to understand how such plastic behavior can be induced. Shear walls under seismic action deform mainly in shear with inclination of the vertical studs; if a sufficiently flexible beam is connected to the studs, the two end sections of the beams will follow the stud rotation as shown in Fig. 3.1(b), so

that the beam undergoes bending deflection with double curvature. Bending moments are induced in both end sections, which have to be balanced by shear forces. The static equilibrium of the beam is represented in Fig. 3.2, where the distribution of shear and bending moment are indicated as well. It is evident that, in such a configuration, plasticity in the beam element is mainly governed by bending behavior.

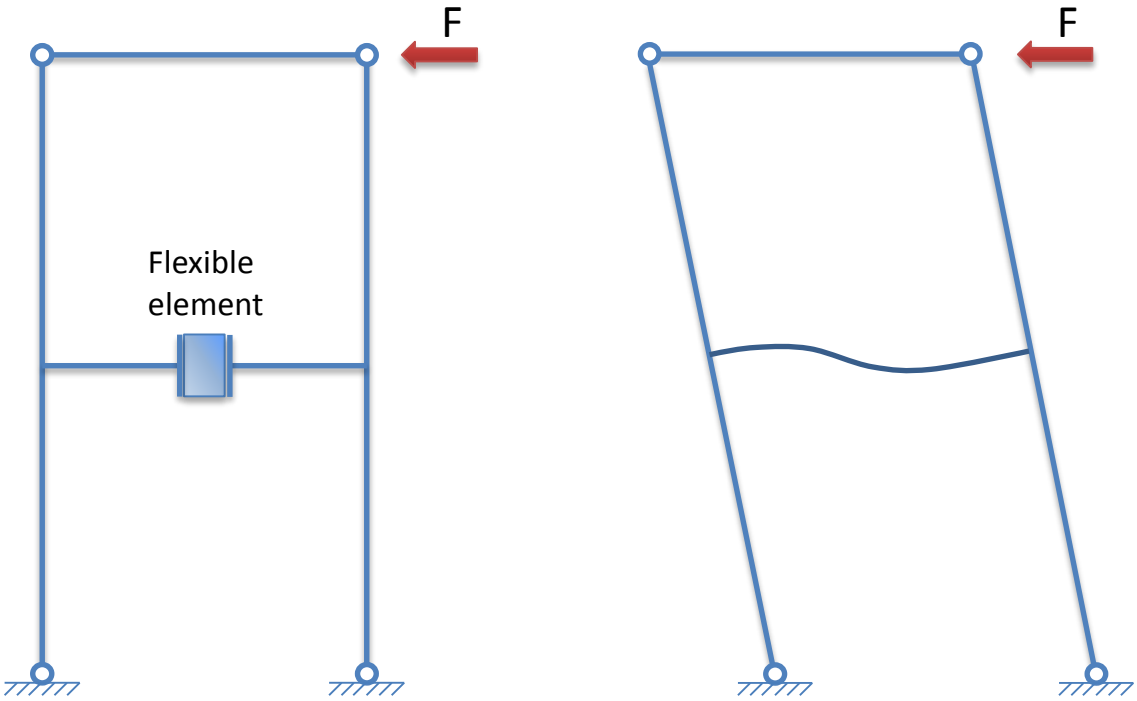

Fig. 3.1 Schematic representation of the shear wall with a single fuse (a) The lateral force is entirely sustained by means of a flexible element; (b) the deformation is localized in the fuse, while the frame behaves as a rigid body

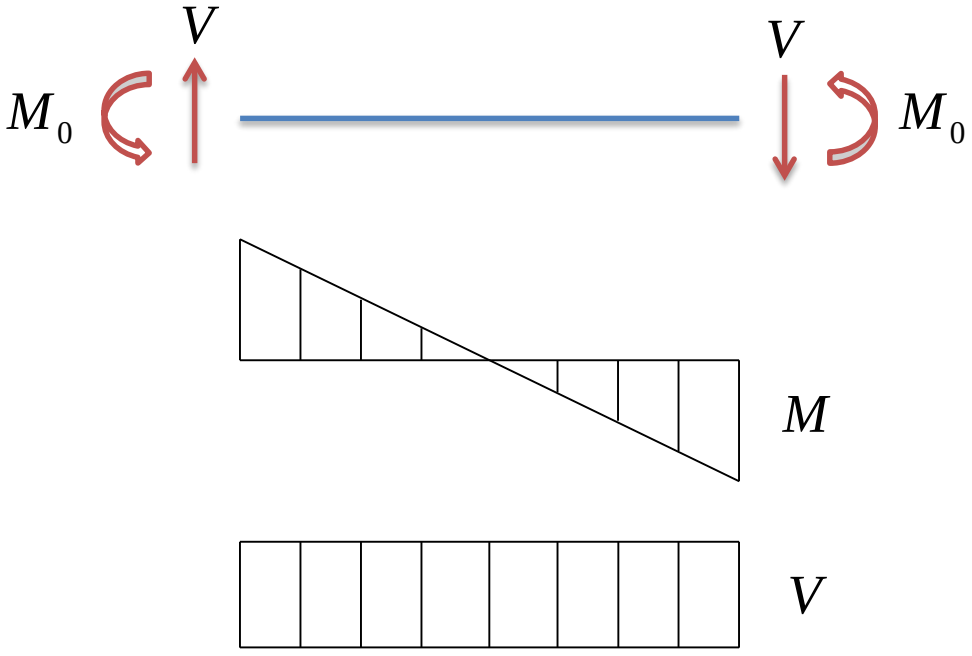

Fig. 3.2 Static equilibrium of the fuse link between the studs

3.2 Shape optimization and strength of fuse links

The shape of the fuse link is defined optimal when it maximizes its energy dissipation capacity. Energy dissipation relies on metal yielding, so the link should be proportioned to have simultaneous yielding in all points along its edges. However, as indicated in Ma et al. [22], this would result in an hourglass-shaped link with curved edges, which is not easy to design and manufacture. A good compromise between perfect simultaneous yielding and simplicity is a fuse with butterfly shape and straight edges [22] (Fig. 3.3). If compared to a straight link, a butterfly-shaped link better aligns its bending capacity with the distribution of the moment diagram shown in Fig. 3.2.

Once the overall geometry of the fuse is known, the ratio between the height of the middle section and the height of the end sections has to be determined. Such a ratio defines the location of the highest stress along the link, and is chosen based on considerations for fracture resistance. The sections of a link most vulnerable to fatigue and fracture are those with local change in geometry (stress concentrations) and with plastic hinges (strain localization). A butterfly fuse has local geometric changes (corners) both at the end and middle sections, so the plastic hinge should be located away from these sections. The optimal solution is therefore to design the link so that plastic hinges will be located at the quarter-point sections ($x = L/4$). Ma et al. derived a formula for the optimal ratio for this condition: $a/b = 1/3$ [22].

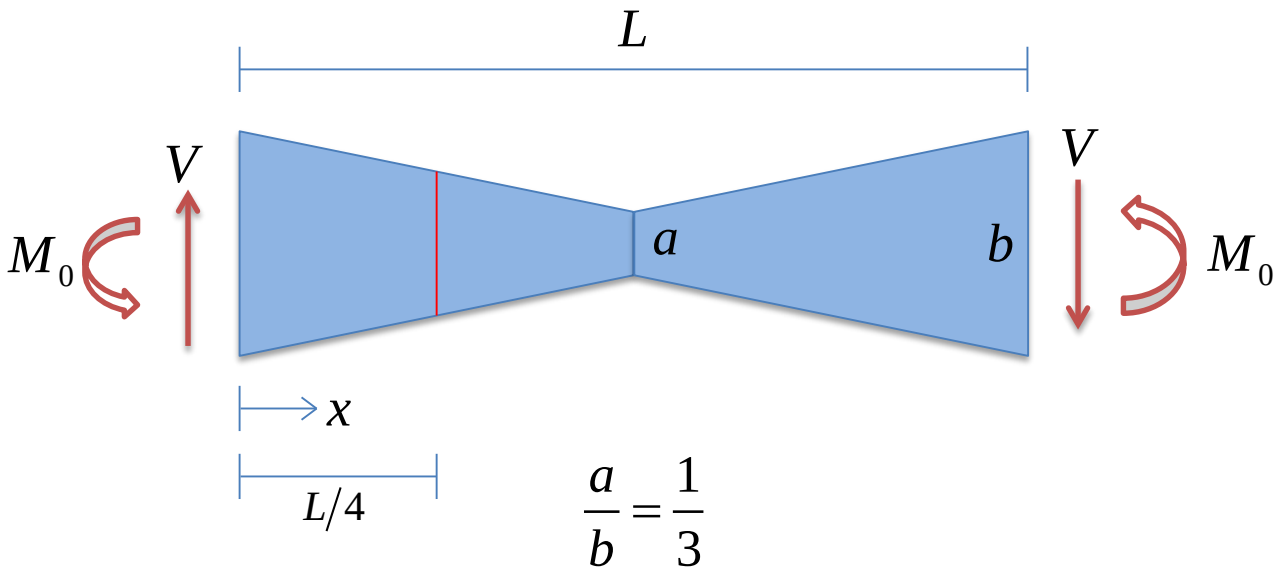

Fig. 3.3 Optimal butterfly-shaped fuse link, based on Ma et al. [22]

In the following, the shear and moment capacity of the fuse link are determined. First, a simple relation between shear and end moments in the fuse is given:

$$V = \frac{2M_0}{L} \tag{3.1}$$

where L is the length of the link.

Since the fuse is designed to have the critical section at $x = L/4$, first yielding is expected to occur at the external fiber of such section. The link height at the critical section is $\bar{b} = 2b/3$ and therefore the yielding moment at the same section is:

$$M_{y,x=\frac{L}{4}} = \frac{t\bar{b}^2}{6}\sigma_y = \frac{2}{27}tb^2\sigma_y \tag{3.2}$$

where t is the thickness and σ_y the yielding stress.

When first yielding occurs in the critical section, the corresponding maximum bending moment (at the end sections) is:

$$M_{0,y} = 2M_{y,x=\frac{L}{4}} = \frac{4}{27}tb^2\sigma_y \tag{3.3}$$

and the shear force (constant along the length of the fuse) is immediately found based on Eqn. (3.1):

$$V_y = \frac{8}{27}\frac{tb^2\sigma_y}{L} \tag{3.4}$$

It is known that the maximum moment (causing plastic hinge) for a rectangular cross section is 50% larger than the moment causing first yielding in the same section. Thus, the plastic moment at the critical section is simply obtained by multiplying Eqn. (3.2) by 1.5, and the corresponding end moment $M_{0,p}$ and shear $\bar{V}_{fuse}$ are:

$$M_{0,p} = \frac{2}{9}tb^2\sigma_y \tag{3.5}$$

$$\bar{V}_{fuse} = \frac{4}{9}\frac{tb^2\sigma_y}{L} \tag{3.6}$$

The latter is referred to as $\bar{V}_{fuse}$ to highlight its meaning of actual shear capacity of the fuse, an important parameter hereinafter. In Chapter 4, several numerical models of fuse links, under the same loading conditions as described here, will show an excellent correspondence to the analytical value provided by Eqn. (3.6).

3.3 Statics of the wall system – design equation

To design a shear wall with integrated fuse links, a fundamental parameter is the total lateral capacity. For traditional systems, where the shear wall is made of wood panels, steel sheets, gypsum board or fiberboard panels, the AISI Standard for lateral design of cold-formed steel framing [11] provides tabulated values for the shear strength under in-plane loading. It is therefore necessary, in order to make the innovative wall system available to actual implementation, to provide a relationship where the total lateral capacity can be estimated on the basis of number and size of fuses. In the following, a simple formula is derived based on equilibrium considerations. Validation of such formula will be given in Chapter 5 by presenting numerical result for the entire wall system.

A few simplifications on the safe side are first introduced. The actual cold-formed steel frame is fixed to the foundation by means of conventional hold-down fasteners, which resist elastically the overturning moments of the shear wall during earthquakes. The studs are therefore clamped to the foundation, although some rotational flexibility may exist. In the derivation of the formula for the wall capacity, it is instead assumed that the frame is pin-connected (also in the stud-to-track joints). This simplification is conservative as neglects the contribution of the hold-downs to the lateral resistance.

The simplified shear wall system with integrated fuses is sketched in Fig. 3.4. Further considerations on the single members of the frame and the connections between the studs and the fuses will be given in Chapter 3.5.

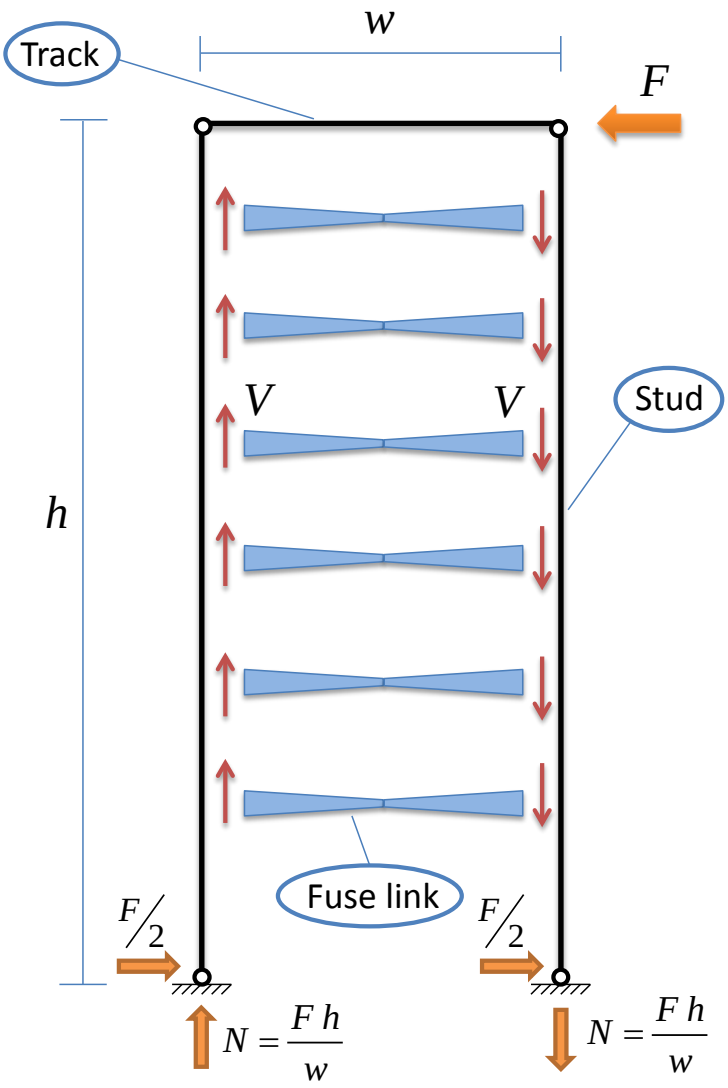

Fig. 3.4 Static equilibrium of the simplified shear wall

In a pin-jointed frame, the lateral force F induced by seismic action can only be sustained by the fuse links between the vertical studs; such links therefore become the actual lateral force resisting system of the wall. The shear force V developed in each link is transferred to the foundation through axial force N in the studs. The global equilibrium to rotation is expressed by:

$$F \cdot h = N \cdot w \tag{3.7}$$

which provides the axial force at the bottom of the studs:

$$N = \frac{F \cdot h}{w} \tag{3.8}$$

where h and w are, respectively, the height and the width of the frame.

N can be also thought as the sum of the contributions of each fuse. Assuming that all fuse links behave in the same way (same shear force V), their shear force can be easily related to the total lateral force F:

$$V = \frac{N}{n_{fuse}} = \frac{F \cdot h}{w} \cdot \frac{1}{n_{fuse}} \tag{3.9}$$

By rearranging Eqn. (3.9), one can obtain a simplified expression for the lateral force in the wall as a function of the shear force in the fuses:

$$F = n_{fuse} \cdot \frac{V \cdot w}{h} \tag{3.10}$$

For a certain lateral drift of the wall, the fuses start to yield: substitution of $V = V_y$ in Eqn. (3.10) gives the total force at which fuse yielding begins. Maximum capacity $\overline{F}_{wall}$ of the wall system occurs when nominal capacity $\overline{V}_{fuse}$ of the links is reached (this corresponds to formation of plastic hinges at the quarter-point sections of the fuses):

$$\overline{F}_{wall} = n_{fuse} \cdot \frac{\overline{V}_{fuse} \cdot w}{h} \tag{3.11}$$

However, this is a lower-bound estimation for the lateral capacity, because assumes that the frame, pin-connected, behaves like a rigid body without contributing to the wall strength. An actual cold-formed steel frame, however, does not have pin connections, since the hold-down fasteners can resist overturning moments. Thus, some additional lateral capacity is provided by the bare frame, which strongly depends on the members used. If the extra capacity, F_{frame}, is added to Eqn. (3.11), a more realistic expression for the design formula of the wall system is obtained:

$$\overline{F}_{wall} = F_{frame} + n_{fuse} \cdot \frac{\overline{V}_{fuse} \cdot w}{h} \tag{3.12}$$

Equation (3.12), together with the fuse capacity provided by Eqn. (3.6), is an excellent tool for the design of the shear wall with integrated fuses. For a certain geometry of the frame (w and h), it is possible to choose number and size of fuses to achieve the target capacity for the wall. Furthermore, whereas the strength of traditional shear walls is tabulated only for a limited range of dimensions and geometry [11], the previous formula allows the designer to choose any type of configuration, by changing either number or size of fuses according to the specific necessity.

However, such a simple and potentially powerful tool needs to be validated by numerical modeling. Chapter 5 will discuss finite element models of the entire wall where the maximum lateral force is compared to the values provided by Eqn. (3.12), showing a very satisfactory correspondence.

3.4 Kinematics of the wall system

The performance of the shear wall strongly depends on the characteristics and behavior of the fuse links: fuse capacity determines overall capacity, and buckling of the single links negatively affects the energy dissipation of the system. Thus, the fuse response can be analyzed separately to estimate the behavior of the entire wall. Chapter 4 will present an extensive parametric study for different fuse sizes; the fuses, cyclically loaded to replicate the effects of earthquakes, will be analyzed by means of finite element simulations. This avoids studying the behavior of the entire wall system, which would be computationally expensive.

In order to do so, the same loading as in the actual shear wall has to be applied to the single fuse links. This paragraph studies how cyclic loading of the shear wall is transferred to the fuses, and determines a relation between the global lateral drift of the frame and the local drift of the fuses.

It is assumed that the effects of seismic-induced loading on a frame can be replicated by means of cyclic lateral displacements at the top track [28]. The horizontal displacement of the track induces rotation in the vertical studs. It is the stud inclination to cause flexural behavior in the fuse links, which in fact are connected to the studs for this purpose. In a simple pin-connected frame as shown in Fig. 3.5(a), the lateral displacement u_{top} of the top track determines rigid body motion of the system. The inclination angle α of the studs, expressed in radians, is approximately:

$$\alpha\,[rad] \cong \frac{u_{top}}{h} \tag{3.13}$$

with h being the height of the frame. It can be seen that expression (3.13) also corresponds to the definition of the lateral drift of the wall Δ (ratio of the relative displacement by the total height).

However, an actual cold-formed steel frame is not pin-connected but clamped to the foundation by means of hold-downs; also the stud-to-track connection can be idealized as rigid (see Fig. 3.5b). In this case, the studs deform in bending and the rotation angle $\bar{\alpha}$ is variable along the length. Except for the lowest part where the fixed connection forces the rotation to be almost zero, the real inclination angle $\bar{\alpha}$ is well approximated by the idealized angle α of the pin-connected frame. Thus, the following relation is assumed valid except for the bottom of the studs:

$$\bar{\alpha} \cong \alpha \cong \Delta \tag{3.14}$$

The fuse links are now introduced in the CFS frame, to analyze how they deform in relation to the stud inclination. In the following, it is made the fundamental assumption that the fuses are significantly more flexible than the studs; in this way, in the force-transfer mechanism between fuse and studs, the former

can be considered as the weak element where most deformation is localized. Chapter 3.5 will provide additional considerations on the previous assumption.

For simplicity, in the next figures the fuse links are schematically represented by their centroidal axis, since this is sufficient to define their drift. If the fuses are connected directly to the studs so that they span the entire width of the frame (Fig. 3.6a), the end points A and B are horizontally aligned. In fact, the studs rotate parallel to each other and therefore the fuse ends undergo the same vertical displacement. It can be seen that the fuse deforms in bending and therefore drift occurs, which is computed in a rotated coordinated system (Fig. 3.6b). Each end of the link rotates by an angle α equal to the stud inclination, which has been proved by (3.14) to correspond to the drift Δ of the wall. But such angle α is also equal to the local drift of the fuse:

$$\Delta_{fuse} = \frac{u}{L} \tag{3.15}$$

where L, length of the fuse link, here corresponds to the width w of the frame.

One can hence conclude that, for a link length equal to the wall width, the local fuse drift and global wall drift coincide:

$$\Delta_{fuse} = \Delta \tag{3.16}$$

Thus, if the loading history of the entire shear wall is known in terms of total drift Δ, the corresponding loading history for a single-fuse model should be such that induces the same local drift to the fuse.

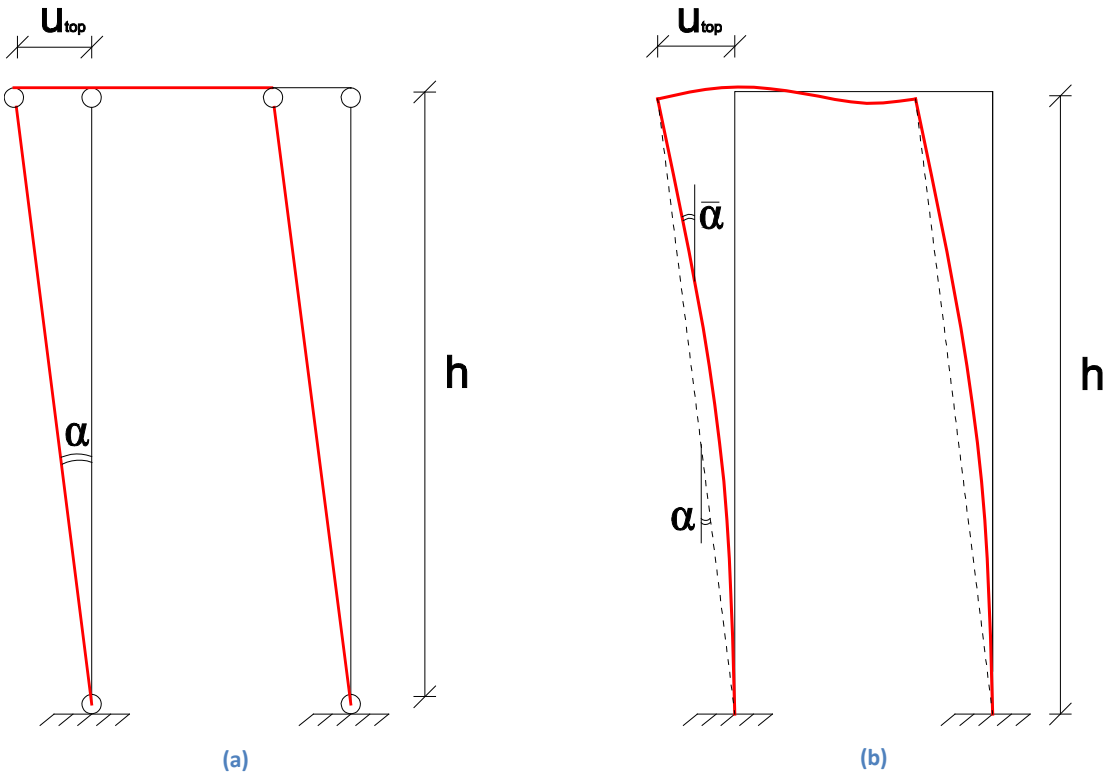

Fig. 3.5 Lateral deformation of a pin-connected (a) and fixed frame (b)

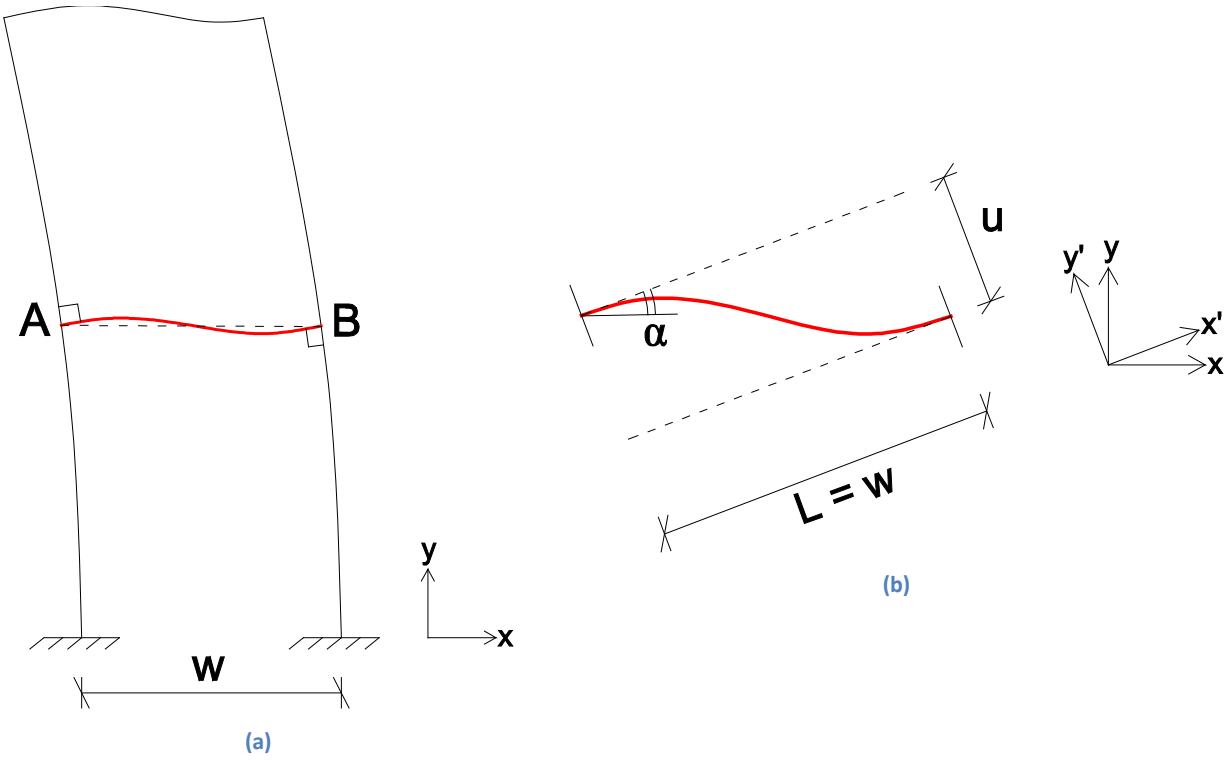

Fig. 3.6 (a) Lateral deformation of the shear wall with fuse; (b) local drift of the fuse

The length of the fuse is an important parameter in relation to shear capacity and buckling resistance: it may be therefore necessary to adjust such length to achieve a specific target behavior. On the other hand, the designer may need to keep the width of the wall constant. For this purpose, and also to practically connect the fuse links to the lateral studs, side plates are expected to be installed between the fuse and the stud. The actual design and shape of such plates is strongly dependent on the connection detailing, and is not discussed specifically in this work. The focus here is understanding how Eqn. (3.16) changes when fuse links shorter than the wall width are used.

Again, assumption is made that the fuse links are more flexible than the studs so that most deformation is localized in the latter, and the plates just behave as rigid bodies following the rotation of the studs. This important hypothesis can be fulfilled by properly designing the fuse dimensions and detailing the fuse-to-stud connection (in Chapter 5 additional explanations will be given).

It can be seen in Fig. 3.7 that, for $L < w$, the fuse ends C-D are not aligned along the horizontal direction, because the presence of side plates determines a relative vertical displacement:

$$v_{CD} = 2 \cdot L_{plate} \cdot \alpha = 2 \cdot L_{plate} \cdot \Delta \tag{3.17}$$

where Eqn. (3.14) has been introduced.

Other than a vertical displacement, the fuse ends are also characterized by the rotation angle α, which increases the fuse local drift because such drift has to be computed in a rotated coordinate system. It can be easily seen (Fig. 3.7b) that the total relative displacement of the fuse ends u is:

$$u = \left(L_{plate} + L + L_{plate}\right) \cdot \Delta = w \cdot \Delta \tag{3.18}$$

The local drift of the fuse is simply obtained by dividing the relative displacement by the fuse length:

$$\Delta_{fuse} = \frac{u}{L} \quad \rightarrow \quad \Delta_{fuse} = \frac{w}{L} \cdot \Delta \tag{3.19}$$

If $L = w$ (no side plates), Eqn. (3.16) is immediately recovered. Equation (3.19) shows that using short fuses, relatively to the width of the wall, amplifies their local drift and therefore should facilitate occurrence of yielding; on the other hand, also buckling may occur earlier, so that the use of short links is not necessarily beneficial.

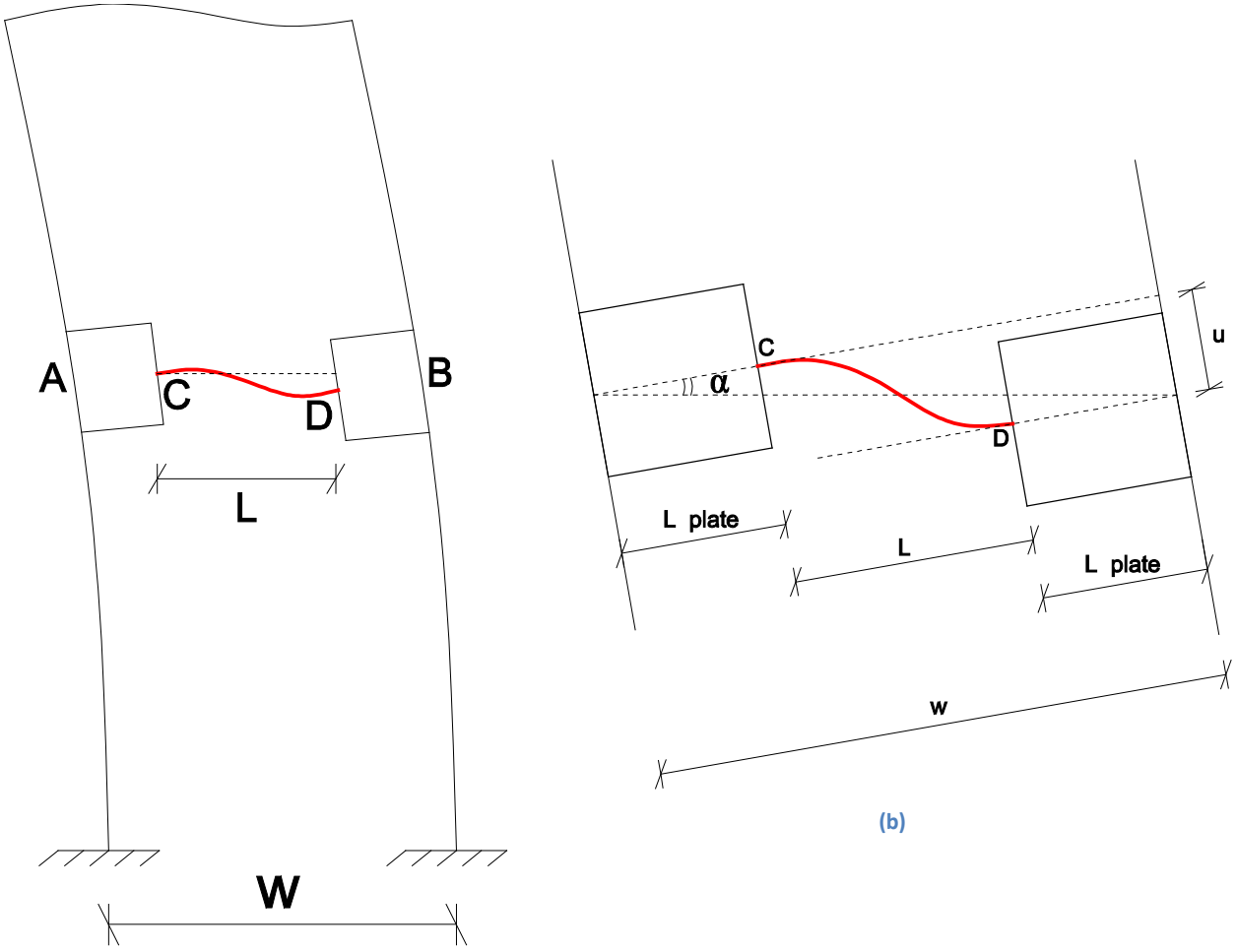

Fig. 3.7 (a) Lateral deformation of the shear wall with fuse and side plates; (b) local drift of the fuse

As already mentioned, the previous analysis of the kinematics of the fuses is preparatory for a parametric study. There are two possible alternatives to model the fuses, as described in Chapter 4 in more details:

- Model of the fuse link with side plates included;
- model only of the fuse link without side plates.

The loading conditions in the two models differ, because in the first case only rotations need to be applied at the fuse plates, whereas in the second case also a relative displacement of the link ends has to be introduced, as indicated by Eqn. (3.17).

3.5 Additional design considerations

The core of the innovative shear wall proposes is the fuse link, analyzed in details in the previous paragraphs where shape, capacity and deformation mechanism have been discussed. However, besides the fuses, the wall system consists of a cold-formed steel frame and the connections between studs and fuses.

The frame, made of vertical studs connected at the top by a horizontal track, is analogue to those employed for conventional cold-formed steel framing; however, the choice of stud dimensions turns out to be essential. First, it is noted that the static equilibrium of the wall system (Chapter 3.3) assumes that the capacity of each member is sufficient to resist the applied forces, which in an actual shear wall may not be the case. This is particularly true for the studs, which have to carry axial force according to the simplified Eqn. (3.8), where height and width of the wall play a relevant role. The height h is an architectural variable that cannot be easily modified, which means that particular care has to be taken in the choice of the width *w*. A large width is beneficial in reducing the axial force *N* but, on the other hand, the fuse links cannot be too long, since excessive slenderness may cause stability problems (and it would also be inconvenient to use very long side plates). The dissipation behavior of the wall system is thus effective for relatively small widths.

This leads to amplified axial forces in the studs, in particular when a large lateral capacity $\overline{F}_{wall}$ is required. Large capacity can be obtained by installing many fuse links, by choosing their size to allow for significant shear strength $\overline{V}_{fuse}$, or a combination of these. However, the potential lateral capacity cannot be achieved if premature failure occurs in the studs, which would prevent the system from behaving as expected. In such negative scenario, inelastic deformation would involve the main structure (studs) instead of the fuse links, leading to irreparable damage in the shear wall and decrease of energy dissipation capacity.

Thus, the choice of the studs is strongly dependent on the target capacity of the wall. For a desired $\overline{F}_{wall}$, the correspondent axial force in the studs can be immediately determined by Eqn. (3.8), and the stud dimensions will be chosen accordingly. It is also observed that the wall capacity $\overline{F}_{wall}$ partially depends on the stud capacity through the parameter F_{frame} in Eqn. (3.12): to account for this, a complete design procedure is defined in Fig. 3.8.

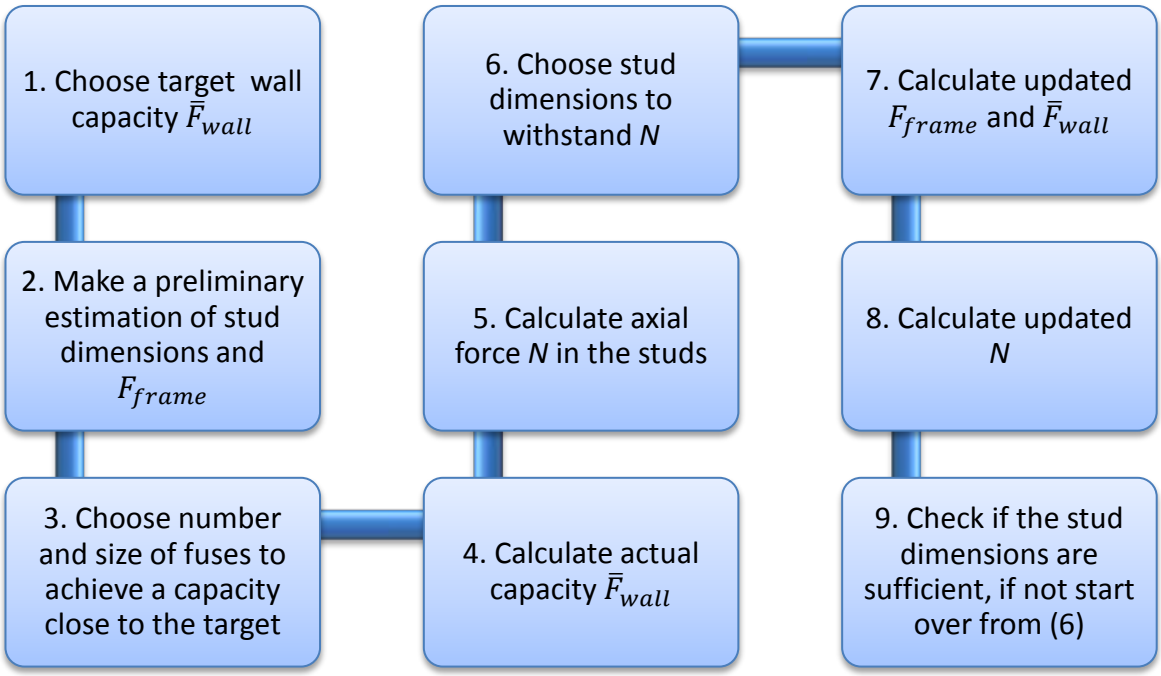

Fig. 3.8 Flow-chart for the design of the studs

One of the most crucial aspects of the entire wall system is the stud-to-fuse connection. So far, the fuse link has been assumed to be much more flexible than the studs, so that the entire deformation is localized in the fuse; however, in an actual frame, the in plane bending stiffness of the fuses in not negligible. In addition, cold-formed steel studs are not as strong as hot-rolled steel elements, and may therefore locally deform if the fuses offer excessive resistance to in plane-bending.

The worst-case scenario consists of very thin and flexible studs combined with thick and rigid fuse links, because all deformation is likely to be localized in the studs. As described in the previous paragraph, the top lateral displacement of the track induces rotation in the studs; however, such rotation would be locally restrained by the fuses if they are too rigid (Fig. 3.9). The proposed energy-dissipating shear wall is only effective for fuses deforming in bending and studs remaining mostly undamaged.

The previous considerations have to be accounted for in the design of the studs, and should therefore integrate the flow-chart of Fig. 3.8. Further information on typology and size of the studs will be given in Chapter 5.

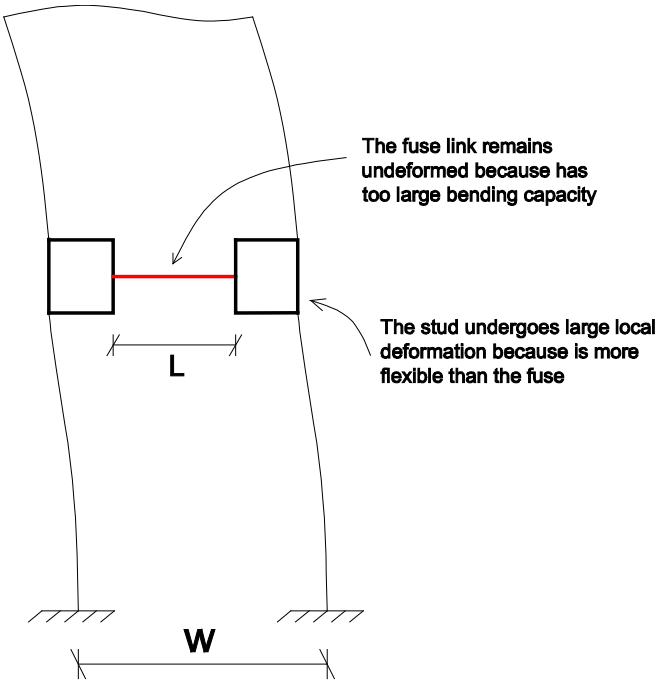

Fig. 3.9 Lateral deformation of the shear wall if the fuse is too rigid (no dissipation occurs)

So far, only the in-plane behavior of the fuse plates has been considered. However, as already mentioned in Chapter 2.2, out-of-plane displacements induced by instability are expected for relatively thin plates. In fact, since the fuses act as beams loaded in bending, lateral-torsional buckling is expected. Buckling is greatly detrimental for the energy-dissipation capacity of the shear wall because it is associated with a drop in the fuse capacity resulting in pinching of the hysteretic behavior.

Lateral-torsional buckling cannot be completely prevented because significant loading in the fuses (which have some initial imperfections) induces out-of-plane displacements, in particular for reversed loading typical of seismic actions. Nevertheless, knowledge of the drift which initiates buckling in the fuses would be very beneficial in the design of the wall system because, for a target allowable drift, fuses can be chosen to prevent instability up to that drift.

Since fuse buckling drift is strongly dependent on the applied loading history, there is no analytical formula for it; from the parametric study described in Chapter 4, estimation for the buckling drift for several fuses is provided, and a more generalized expression will be attempted.

3.6 Innovative shear wall vs. alternative configurations

After presenting the main characteristics of the proposed wall system, analogies and differences with respect to the alternative configurations introduced in Chapter 2.2 are now described. For this purpose, a more realistic representation of the innovative shear wall with fuse is given in Fig. 3.10.

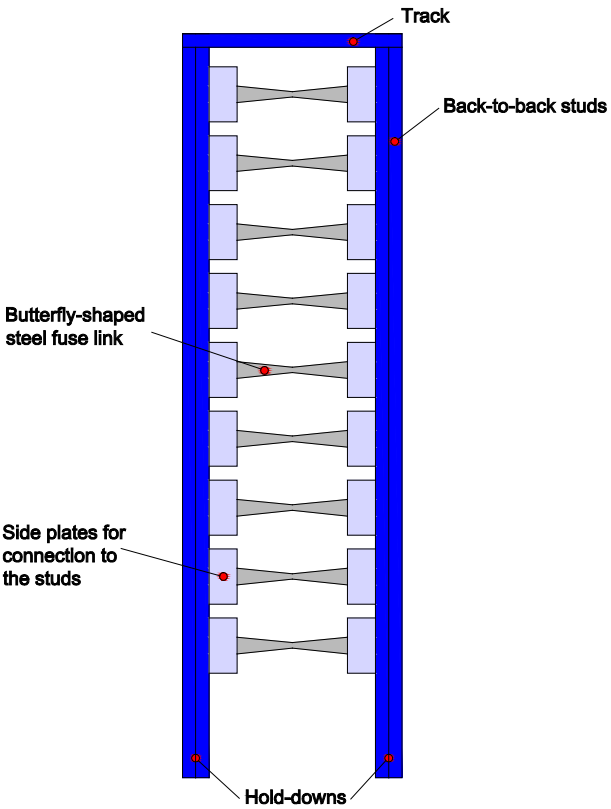

Fig. 3.10 CFS shear wall with integrated fuses

First, a comparison is made with the only system specifically designed for cold-formed steel structures, shown in Fig. 2.9 and described in [23, 24]. Fuse shape and principles of energy dissipation are the same, but different is the mechanics and overall behavior of the frame. In that system, the fuses (placed in the hold-downs) deform in shear and bending due to the rocking movement and uplift of the wall. Conversely, the shear wall described in the present Chapter is not allowed to rock, since makes use of the conventional hold-down fasteners, elastically resistant to overturning moments. It is the shear behavior of the entire wall, instead, to activate flexural deformation and yielding in the fuses. A clear advantage of installing fuses along the height of the frame is the lack of space constraint, which potentially allows the installation of any number of links. Thus, the lateral capacity of the wall together with the overall energy dissipation can be significantly adjusted. If the fuses are localized in the hold-downs, on the other hand, the limited space available may reduce the lateral capacity and energy dissipation of the system. This is also why hold-down fuses have to be associated with high-stiffness/high-strength steel sheet walls [24].

Similar considerations, in terms of space available for fuse installation, can be made when analyzing the system shown in Fig. 2.6, where the fuse plate is located on top of a braced-frame. Also the mechanic behavior of a braced-frame for conventional steel structures is significantly different from the behavior of the innovative cold-formed steel wall.

The idea of using shear walls made of steel plate segments behaving as flexural links can be traced back to the experimental work of Hitaka and Matsui [13], but in that case the plate segments were obtained by making several cuts in a large steel sheet (Fig. 2.5). A significant drawback of using the entire wall as

energy-dissipation device is the more difficult replacement, compared to separate fuse links. Furthermore, cutting steel plates to obtain internal butterfly-shaped links may be more time-consuming and expensive than fabricating single links. Finally, global shear buckling behavior of the entire plate may occur, which is detrimental for the wall performance.

Probably the system in which the mechanics of fuse deformation is the closest to the one proposed in this chapter is the self-centering double-frame with fuse plates installed in between, as shown in Fig. 2.8(b). In fact, shear deformation of the fuse links is mobilized by relative movement of the inner columns. However, the main difference of the innovative shear wall is that the relative movement of the columns (studs) is not due to rocking, prevented by base-fixed hold-downs, but to shear deformation of the frame itself. And this is made possible by the larger flexibility of a frame made of cold-formed steel than a hot-rolled steel counterpart.

It is also evident that rocking of the frame would amplify fuse deformation, thus increasing the energy dissipated by the fuse. On the other hand, rocking behavior with self-centering strands results in a flag-shape hysteretic response, because the system is designed to have approximately zero displacement as the force is removed [21, 29]. This means that almost no energy is dissipated in the second and fourth quadrant of the force-displacement diagram (Fig. 3.11), whereas the innovative shear wall can dissipate energy also in these quadrants, as described in Chapter 5.

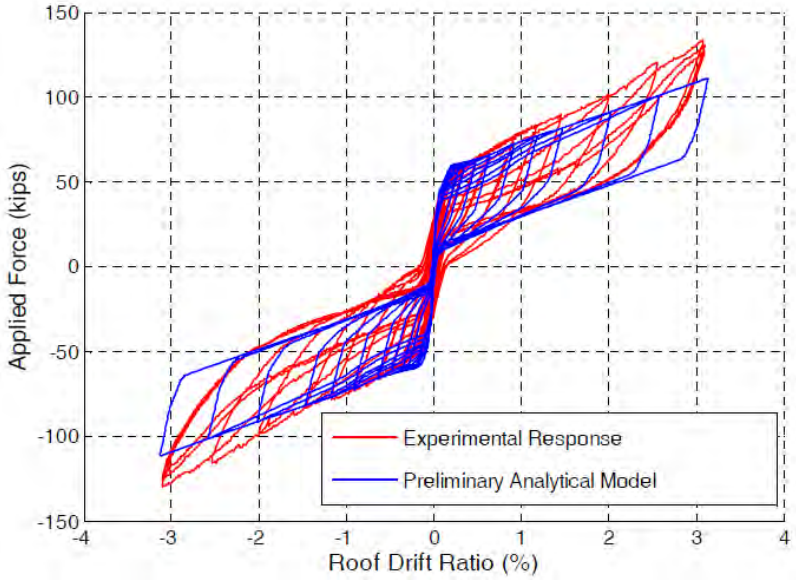

Fig. 3.11 Hysteretic behavior of the self-centering steel frame with fuses (from [21])

In summary, the main advantages of the proposed system are:

- Use of multiple independent fuse links allows significant adjustment of lateral capacity and energy dissipation of the wall system;
- Replacement of damaged links is easy and cost-effective;
- By installing the fuses along the height of the wall, it is possible to have a large number.
- Rocking behavior of the shear wall is not required, which allows using traditional hold-downs.

Chapter 4

Parametric study of single fuse models

4.1 Introduction

Chapter 3 described the behavior of the shear wall with integrated fuses, and provided practical information for its actual design: Eqn. (3.6) estimates analytically the shear capacity of the fuses $\bar{V}_{fuse}$ which, combined with Eqn. (3.12), gives the total lateral capacity of the wall F_{tot}; the studs should be designed for the axial force N expressed by Eqn. (3.8). It has also been shown that the response of the entire wall system can be estimated from the basic properties of the fuse links. Thus, estimation of the overall response does not require full wall models, but simpler analyses of single links (independently from the shear wall).

This Chapter presents a parametric study conducted on 60 fuses by means of numerical models. The purpose is to verify the accuracy of the analytical formulas derived in Chapter 3, and provide additional information on the out-of-plane behavior and instability of the fuse links. In fact, an analytical expression for the drift causing fuse buckling (buckling drift, in the following) is not available; but such drift is a fundamental parameter for a proper design of the system, because it marks the end of stable dissipation behavior. For this reason, several finite element models of fuses with different length, size and properties have been carried out to derive a generalized expression.

Later, in Chapter 5, a model of the entire wall with fuses will be presented to validate the results described here and provide overall information that cannot be attained by the partial models.

4.2 Modeling type

As already mentioned in Chapter 3.4, the fuse links can be modeled with or without side plates. This choice may lead to slightly different results, and pros and cons of both models are briefly summarized below.

4.2.1 Single fuse without side plates

Only the fuse link is modeled, thus eliminating the influence of the side plates (Fig. 4.1, on the right). It is the more general modeling choice, because the results are independent from the actual type of connection to the studs (shape and dimension of side plates). In order to reproduce on the fuse link the same loading conditions present in the actual shear wall, both rotation and displacement have to be applied to its end sections, as described in Chapter 3.4 and shown in Fig. 3.7(b). The vertical displacements are justified by rotation of the side plates, not included in the model; the rotation corresponds to the inclination of the studs.

If the loading history on the full wall is expressed by $\Delta = \Delta(t)$ (with Δ being the lateral drift), equivalent conditions on the single fuse models are given by the following loading history applied to their end sections:

$$\varphi(t) = \Delta(t)$$
$$u(t) = \Delta(t) \cdot L_{plate} = \Delta(t) \cdot \frac{w - L}{2} \tag{4.1}$$

where φ stand for rotation and u for displacement. It can be seen that the width of the wall w affects the magnitude of the load.

A drawback of this modeling choice is the application of the boundary conditions in the out-of-plane direction. In a real shear wall, as shown in Fig. 3.10, the end sections of the links are connected to side plates providing restraint against out-of-plane displacements. However, the flexibility of such restraint is affected by the characteristics (mainly thickness) of the plates, and this could be properly accounted for by means of springs. For simplicity, in the fuse models the end sections of the links have been instead fixed against out-of-plane displacement; this is not very conservative, particularly in relation to the buckling drift.

4.2.2 Single fuse with side plates

This modeling choice significantly depends on the actual connection between fuse links and studs. In the present Thesis, such connection is assumed to be realized by side plates having the same thickness of the links (Fig. 4.1, on the left). However, this is only one of many options and the practical connection detailing is left for future work: as a result, a change in the connection typology would partially invalidate the results obtained here. On the other hand, modeling fuses together with their side plates better reproduces the out-of-plane boundary conditions when installed within the wall system, as discussed in Chapter 4.2.1.

If $\Delta = \Delta(t)$ is the loading history on the entire wall, the equivalent loading corresponds to rotation of the two end sections of the plates (Fig. 3.7b):

$$\varphi(t) = \Delta(t) \tag{4.2}$$

It should be finally mentioned that including the side plates in the numerical models increases the computational cost compared to models of the simple links.

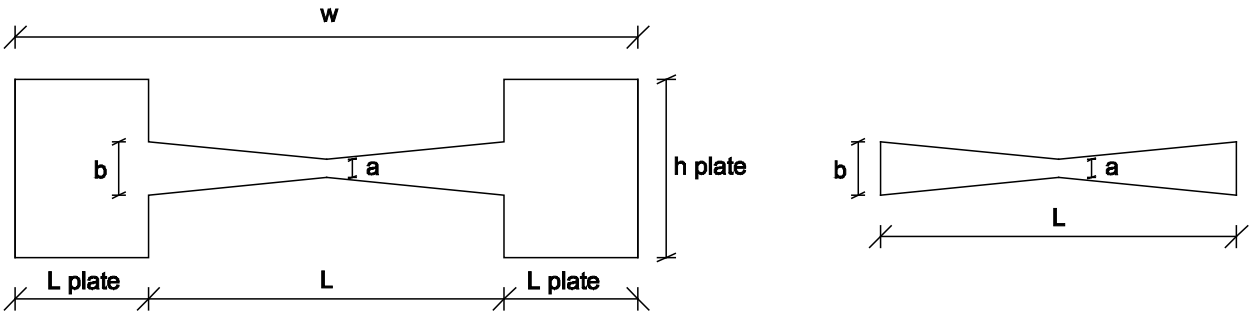

Fig. 4.1 Model of single fuses with and without side plates

4.3 Overview of the parametric study

Parametric studies execute a task many times with different sets of input parameters, to analyze how these parameters affect a specific response. In the parametric study here presented, the task consists in

a finite element analysis of single fuse models under cyclic loading; parameters are their dimensions and material properties; response is their shear capacity and buckling behavior.

The parameters mostly affecting fuse behavior are listed here and shown in Fig. 4.2 :

- length L;
- height of end sections b;
- thickness t;
- yielding stress σ_y.

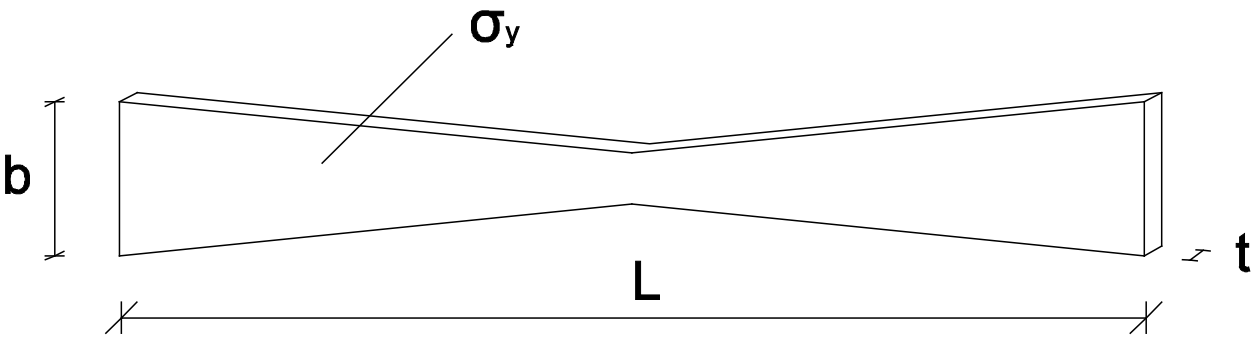

Fig. 4.2 Fuse parameters for the parametric study

Overall shape and ratio of the mid-section to the end-section height have been already determined in Chapter 3.2 and are therefore assumed constant. From the above-listed set of parameters, infinite combinations can be found, but a limited number is sufficient to obtain significant and generalized information on fuse behavior.

Fuse links are designed for installation within CFS frames, whose dimensions and properties strongly limit the feasible fuse parameters. For instance, length L has to be smaller than frame width w, which in turn has to comply with architectural constraints. The type of stud also affects the choice of the links: studs with a thickness of 2*mm* are not compatible with fuses 20*mm* thick, since the behavior shown in Fig. 3.9 would occur; similarly, an excessive height *b* would lead to a very large bending stiffness, resulting in the same undesired behavior. To conclude, there are fuses suitable for a wall system but not for another.

The Thesis provides basic tools for design and installation of steel links regardless geometry and characteristics of the boundary frame. On the other hand, a “benchmark wall” will be introduced in Chapter 5 ($w = 0.7m$, back-to-back studs 600S200-97 [30] with a thickness of 2.6*mm*) to present a numerical model of the entire system: the fuses for this parametric study have been chosen to be potentially suitable for that specific wall.

Different frames may require different fuses, but no specific guidelines are here provided to the designer; the examples shown in the following will hopefully help to form sound judgment, but are not intended to be exhaustive.

60 different fuse links are analyzed and, for each type, models both with and without side plates are carried out. The range for the parameters used is given by (4.3), and a complete list of the models in Table 4.1:

$$\begin{aligned} L &= 200, 250, 300, 350, 400\ mm \\ b &= 60, 75\ mm \\ t &= 5, 6, 7\ mm \\ \sigma_y &= 180, 250\ MPa \end{aligned} \tag{4.3}$$

Table 4.1 Matrix of fuse parameters used for the parametric study

Fuse No.	$L\,[mm]$	$b\,[mm]$	$t\,[mm]$	$\sigma_y\,[MPa]$
1	200	60	5	180
2	200	60	5	250
3	200	60	6	180
4	200	60	6	250
5	200	60	7	180
6	200	60	7	250
7	200	75	5	180
8	200	75	5	250
9	200	75	6	180
10	200	75	6	250
11	200	75	7	180
12	200	75	7	250
13	250	60	5	180
14	250	60	5	250
15	250	60	6	180
16	250	60	6	250
17	250	60	7	180
18	250	60	7	250
19	250	75	5	180
20	250	75	5	250
21	250	75	6	180
22	250	75	6	250
23	250	75	7	180
24	250	75	7	250
25	300	60	5	180
26	300	60	5	250
27	300	60	6	180
28	300	60	6	250
29	300	60	7	180
30	300	60	7	250
31	300	75	5	180
32	300	75	5	250
33	300	75	6	180
34	300	75	6	250
35	300	75	7	180
36	300	75	7	250
37	350	60	5	180
38	350	60	5	250
39	350	60	6	180
40	350	60	6	250
41	350	60	7	180
42	350	60	7	250
43	350	75	5	180
44	350	75	5	250
45	350	75	6	180
46	350	75	6	250
47	350	75	7	180
48	350	75	7	250
49	400	60	5	180
50	400	60	5	250
51	400	60	6	180
52	400	60	6	250
53	400	60	7	180
54	400	60	7	250
55	400	75	5	180
56	400	75	5	250
57	400	75	6	180
58	400	75	6	250
59	400	75	7	180
60	400	75	7	250

4.4 Loading protocol

The shear wall with energy-dissipating fuses is alternative to conventional lateral force resisting systems, and is designed to dissipate significant amount of energy through yielding of the steel links. The effectiveness of the system can be analyzed on the basis of its energy-dissipation performance and hysteretic behavior under earthquake loading.

The dynamic effects of earthquakes can be replicated experimentally by means of shake-table tests, or simulated numerically through dynamic finite element analyses. However, a preliminary evaluation of the system performance does not require advanced dynamic analyses or testing, because simple cyclic loading protocols can provide satisfactory information on the seismic response of the structure. This is particularly true if the main interest is on constituent force-deformation properties and hysteretic data [28], as for the shear wall with fuses. The loading protocols should be applied to models of the entire frame system (Chapter 5), but equivalent histories are first used in the parametric study for single fuse models.

Loading protocols are used in earthquake engineering because structural capacity depends on cumulative damage induced by consecutive cycles [31]; they should therefore replicate the same effects and damage produced by actual seismic actions, in a conservative way. Since loading protocols reproduce seismic events, there may be as many as the number of earthquakes: no optimal protocol exists, and several have been proposed in the past (an overview can be found in [31]).

In the numerical simulations performed here, the FEMA protocol defined by the U.S. Federal Emergency Management Agency has been used [28]. The loading history, generally used for performance assessment of building components and subsystems like shear walls and frames, is conveniently applied by displacement-control in a quasi-static way. A deformation control parameter is required, for instance the story drift that is very useful to evaluate the effects of earthquakes on building structures. The protocol consists of repeated cycles with increasing amplitude and, for each amplitude, two identical cycles are completed (Fig. 4.3).

Two drift values have to be defined:

- The targeted maximum drift, Δ_m, corresponding to initiation of the most severe damage
- The targeted smallest drift, Δ_0, which has to be lower than drift at which first damage begins.

The choice of Δ_m involves an estimation of the level of structural damage that may not be easy to perform. However, based on old prescriptive requirements for CFS framing ([2], Section 12.12-1), a reference drift:

$$\Delta_m = 2.5\% \tag{4.4}$$

is used, which is slightly smaller than the 3% suggested in the FEMA document [28].

The actual loading history is defined by the following equation:

$$a_{i+1} = 1.4\, a_i \tag{4.5}$$

where a_i and a_{i+1} are the amplitudes of the steps i and $i+1$.

The first amplitude a_1 corresponds to the targeted smallest drift, Δ_0, and has been defined using Eqn. (4.5) backwards by imposing $a_n = \Delta_m$. It turns out that:

$$\Delta_0 = 0.121\% \tag{4.6}$$

Ten steps are needed to reach Δ_m, which is the minimum value recommended by [28]. It may happen that, for some of the fuses analyzed, any evident damage state has not occurred at Δ_m, which requires to continue the loading history by adding increments of amplitude $0.3\Delta_m$.

Table 4.2 reports the peaks of lateral drift Δ for each step *N*, including two additional steps (in different colors) that may be added to reach damage. The loading history is represented in Fig. 4.3 , where the time unit in the horizontal axis is a fictitious time since the analysis is only numerical. To reduce the computational cost of the finite element models, the displacement rate increases for larger amplitudes, as shown in the last column of Table 4.2. It is finally noticed that the loading history $\Delta(t)$ refers to the entire shear wall but equivalent histories for the single fuse models can be determined using Eqns. (4.1)-(4.2).

Table 4.2 Drift amplitude of the FEMA loading protocol

N	$\Delta\,[\%]$	$Disp.\,rate\,[mm/s]$
1	0.12	1.0
2	0.17	1.0
3	0.24	1.5
4	0.33	1.5
5	0.47	2.0
6	0.65	2.5
7	0.91	3.0
8	1.28	3.5
9	1.79	4.0
10	2.50	5.0
11	3.25	6.0
12	4.00	7.0

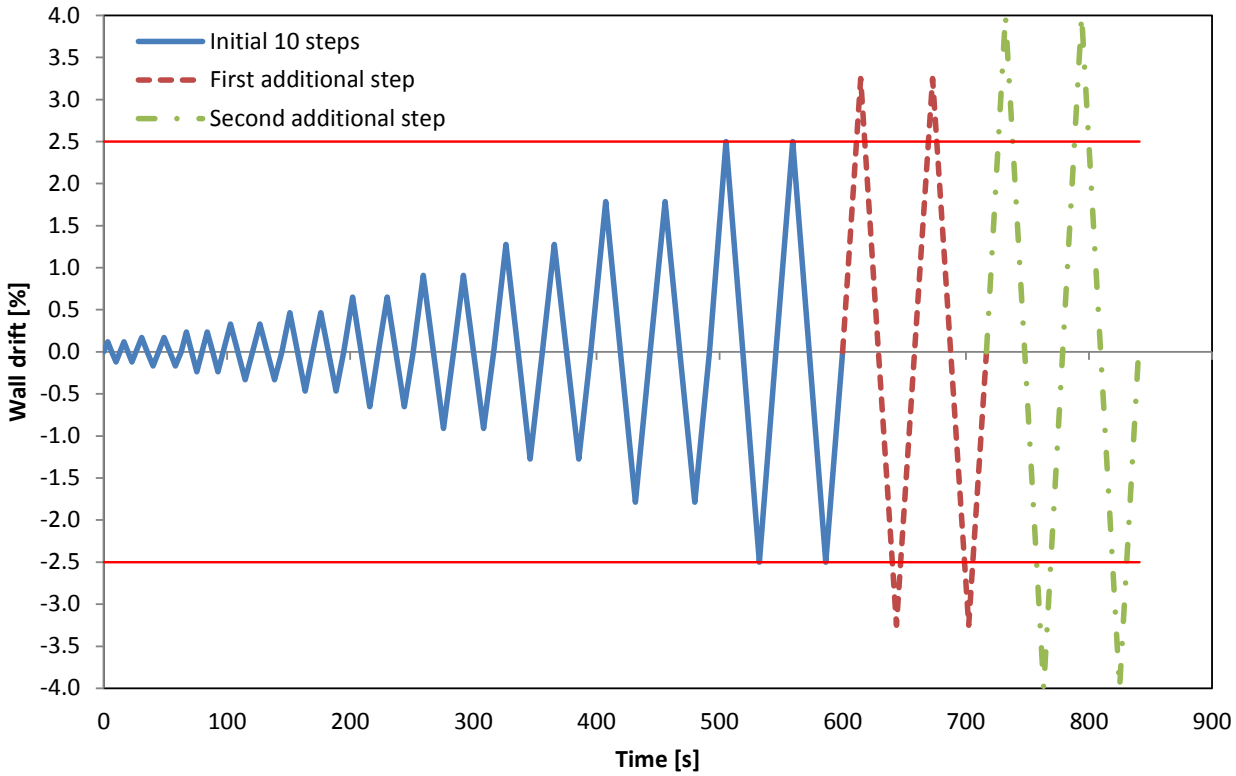

Fig. 4.3 FEMA loading protocol [28]. The horizontal red lines indicate the targeted drift equal to 2.5%.

4.5 Out-of-plane behavior of the fuses

While in-plane bending behavior of the fuse links is relatively simple to analyze, allowing the formulation of analytical expressions, more complicated and less predictable remains their out-of-plane behavior, associated with buckling. On the other hand, a good estimation of the buckling drift is important because affects the energy-dissipation performance of the wall system.

In the metallic energy-dissipating devices described in Chapter 2.2, initiation of buckling is detrimental to energy dissipation, because results in evident pinching of their hysteretic curves. Thus, an optimal system should prevent buckling as long as possible to guarantee stable and fat hysteresis even for large drifts, which is generally very difficult if not impossible to achieve. Nevertheless, the possibility of estimating buckling drift with good accuracy would allow the designer to choose the fuses necessary to obtain stable performance up to the desired drift.

This paragraph describes the buckling mechanism of the links, the influence of initial imperfections and the criteria to evaluate initiation of instability.

4.5.1 Buckling mechanism of the fuse links

The fuse links behave as beams under bending, and lateral-torsional buckling (LTB in the following) may occur for large loads. Formulas and tables for the elastic critical load V_{cr} exist for beams with constant section but not for butterfly-shaped links, and therefore the elastic buckling load has to be computed numerically. It turns out that, for the fuses listed in Table 4.1, $V_{cr} \gg \overline{V}_{fuse}$ so that plastic behavior is expected to anticipate and prevent LTB.

Nevertheless, when the loading protocol described in Chapter 4.4 is applied to the fuse models, instability occurs, due to a more complicated buckling mechanism triggered by:

- presence of initial geometric imperfections;
- load reversal associated with cyclic loading.

Small imperfections in the initial link geometry foster out-of-plane displacements in the following equilibrium states (when a geometric non-linear analysis is carried out) and the out-of-plane deformation is progressively accumulated. However, geometric imperfections alone could not lead to LTB, because the maximum force in the fuse remains much smaller than the critical load.

In fact, under monotonic loading, out-of-plane displacements remain small and LTB does not occur even for large drifts. Plastic hinges form at the quarter-point sections, which transform the link into three joined pieces, of which the central one behaves similarly to a column with pinned ends: stretching and elongation due to large drifts induce tension in the central column and prevent instability.

On the other hand, for cyclic loading, load reversal induces compression in the link, leading to a type of buckling analogue to flexural buckling of columns: instability determines out-of-plane displacements, drop in the strength and pinching of hysteretic curves (see example in Chapter 4.7.1). When the next peak in the opposite loading direction is then approached, the fuse exhibits again a tension field which temporarily stabilizes it, allowing to pick up significant strength, even larger than the in-plane capacity $\overline{V}_{fuse}$.

An analogue deformation mechanism is also described in [22], although in the experiments reported there tension mode is more relevant due to larger drifts.

4.5.2 Role of geometric imperfections

The buckling behavior of the fuses is affected by the presence of geometric imperfections; but why such imperfections should be introduced in the finite element models?

The main reason is that all structural members, as a result of manufacturing, shipping and installation, present small defects. The fuse links are thin steel plates designed to be straight, but some out-of-straightness is always present, normally not visible to the naked eye. Thus, applying a perturbation to the initial geometry aims to replicate the same flaws present in reality.

Another explanation is to avoid numerical problems in finite element analyses, since perfect geometries lead to bifurcation of the load-displacement curve (an abrupt change of equilibrium configuration at the critical load), as visualized in Fig. 4.4 for an axially-compressed column. The vertical axis represents the axial load P and the horizontal axis the lateral displacement v. A column without initial imperfections remains perfectly straight until the load reaches the critical value P_{cr}; for $P = P_{cr}$, instability occurs with a rapid increment of the lateral displacement. Since a finite element solver needs to find consequent equilibrium states to proceed with the analysis, at bifurcation (marked with a green circle in the figure) convergence may not be found, causing a premature interruption of the analysis. Instead, a continuous

response is accomplished by introducing an initial imperfection v_0 in the model: in this case (blue line in Fig. 4.4), no abrupt change of equilibrium states occurs, and the numerical analysis can continue without problems. On the other hand, less straightforward is evaluating the critical load because the curve is continuous, which may require a specific criterion to evaluate occurrence of buckling.

All the previous considerations for a column under compression can be applied to a fuse link under shear and bending.

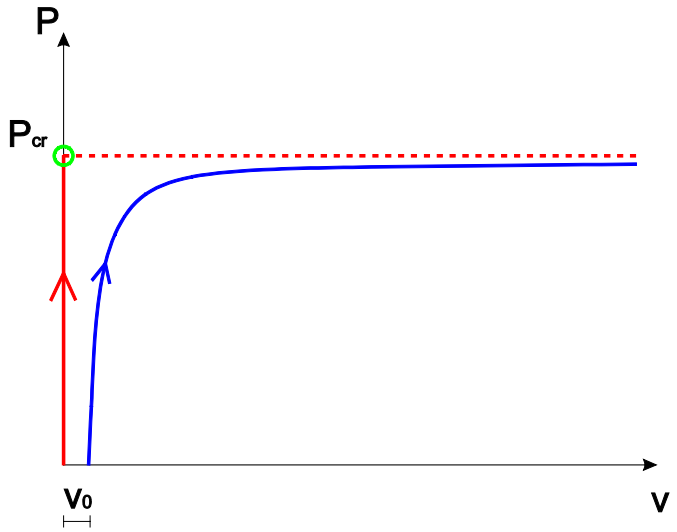

Fig. 4.4 Load-displacement curves for a perfect column (red) and a column with initial imperfection (blue)

4.5.3 Shape and magnitude of imperfections

There are several ways to implement imperfections into finite element models, and none of these is optimal in general, since the actual magnitude and shape of defects in a real structural element is unknown (or known in a statistical sense). Imperfections can be applied by means of a preliminary load which perturbs the perfect geometry; by specifying directly their values at each node; or as a linear superposition of buckling eigenmodes [32]. In the following, the last approach is used because relatively simple and widely accepted in the scientific community. The reason for using the buckling modes as imperfection shape is to perturb the geometry with a pattern resembling the buckling deformations that are first expected to occur.

Two analyses have to be conducted on the same model: first, an eigenvalue buckling analysis (linear buckling) on the perfect fuse, to determine its eigenmodes; then, the geometric imperfection is introduced by superposition of these modes and the loading protocol is applied to the perturbed geometry. In general, the lowest buckling modes are sufficient, and in all models for the parametric study only the first eigenmode has been used for simplicity.

The buckling modes provide the shape of imperfections, but their magnitude has to be decided differently. Several values have been proposed according to the type of element and expected buckling (local, distortional, global). A review of these, for cold-formed steel members, can be found in [33]. It is obvious that, the larger the imperfection, the smaller the buckling drift and vice versa. The fuse links are

steel plates for which no specific magnitude of the defects can be found in literature. However, since they act as beams undergoing lateral-torsional buckling (a form of global buckling), the classical value for global imperfection will be used [33], which corresponds to:

$$v_{0,\,fuse} = \frac{L}{1000} \tag{4.7}$$

where $v_{0,\,fuse}$ is the maximum value of imperfections and L the length of the link.

Thus, the imperfection field $\mathbf{f_0}$ can be defined as:

$$\mathbf{f_0} = v_{0,\,fuse}\,\mathbf{\Phi_1} \tag{4.8}$$

where $\mathbf{\Phi_1}$ is the lowest eigenmode. Bold symbols indicate vectors.

The magnitude defined in Eqn. (4.7) is conservative, because for short steel plates as the fuse links, the manufacturing process would probably allow for a smaller defect tolerance. For instance, according to the formula above, a fuse with $L = 300\,mm,$ is expected to have an out-of-straightness of 0.3*mm,* which is definitely larger than any manufacturing tolerance. However, since the buckling drifts obtained from the parametric study will provide a design formula for the estimation of fuse buckling, is good to be on the safe side.

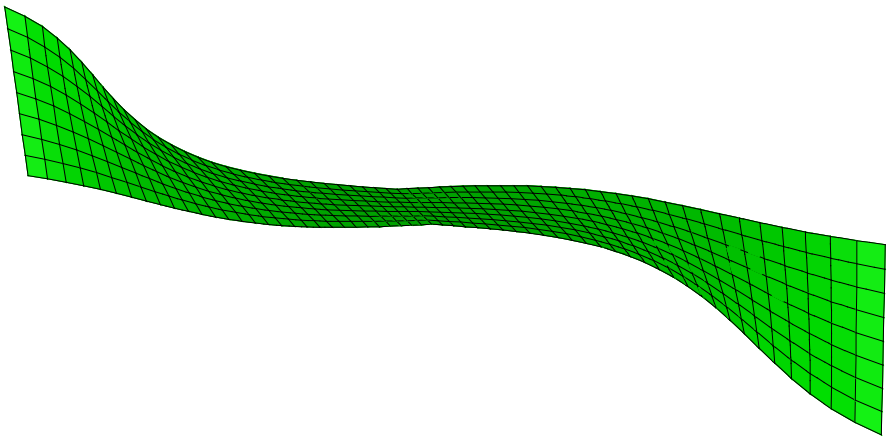

Fig. 4.5 Shape of imperfection field (first buckling mode) of the fuse link. A large deformation scale factor is used for clarity.

4.5.4 Criteria to evaluate buckling

The parametric study presented in this Chapter attempts to derive a formula for estimation of fuse buckling drift, which would be an important tool for the designer to choose the proper type of fuses. For each of the 60 “specimens”, the buckling drift has therefore to be determined.

Its evaluation is not straightforward as it would be for a perfect structure with bifurcation point in the load-displacement curve. In fact, since out-of-plane displacements progressively increase, the real curve is continuous as indicated in Fig. 4.4; what is more, the loading is not monotonic but cyclic, which means that a decrease in the force is not necessarily associated with a structural instability but may be simply due to reversal of loading.

It is therefore necessary to set a consistent criterion to evaluate occurrence of buckling. Since the most visible effect of unstable behavior is out-of-plane deformation, a possible criterion may rely upon the maximum transverse displacement. However, this choice has been discarded because not robust: some fuses may remain globally stable even after significant transverse displacement, while others suddenly buckle when they are still almost straight.

A more robust criterion is based on first occurrence of negative stiffness in the hysteretic curve. By definition, structural instability is a rapid change of the equilibrium configurations from the initial state (see Fig. 4.4), behavior often correlated with a reduction of force. Thus, it is assumed that buckling has occurred when the ratio between load increment and deformation increment is negative:

$$k = \frac{\Delta V}{\Delta u} < 0 \quad or \quad k' = \frac{\Delta M}{\Delta \varphi} < 0 \tag{4.9}$$

Buckling drift is therefore associated with the first occurrence of negative stiffness in the fuse. Negative stiffness means that a positive increment of the applied displacement (or rotation) determines a decrease of the shear force (or bending moment).

4.6 Finite element models of the fuses

Before presenting the results of the numerical simulations, the modeling with the commercial finite element software Abaqus [32] is discussed in this paragraph. For each type of fuse, two models have been analyzed, one with only the simple links and the other including the side plates also used for modeling the entire wall system (see Fig. 4.1). The results are expected to be the same in terms of maximum capacity, but the buckling drift may slightly change due to the difference in the boundary conditions (*BCs*) described in Chapter 4.2.

Models of single links are described in the following. The small thickness, relative to the other dimensions, suggests to apply plate theory for the finite element formulation; the modeling space is three-dimensional to catch out-of-plane deflection and buckling of the fuse links. General-purpose shell elements with reduced integration (4 nodes at the corners and only 1 integration point at the center) are used, with linear interpolation between nodes (Fig. 4.6). The mesh has to be sufficiently refined to simulate the twisting deformation associated with instability: six elements along the short edges have been used in [22]; here, eight elements are chosen instead. The number of elements along the long edges should keep the shape of each element approximately a square (since $a/b = 1/3$, the bias ratio along the long edges should be set equal to 3). The mesh is automatically created by Abaqus based on the seeds of nodes planted along the edges (Fig. 4.7)

The end sections can only undergo vertical displacement and in-plane rotation, whereas all the other degrees of freedom are fixed. To apply such BCs, at each side of the fuse a reference point is created (red circle in Fig. 4.7), to which the end sections are rigidly connected by multi-point constraints “beam” [32]. It is therefore possible to define BCs and loading history on these reference points.

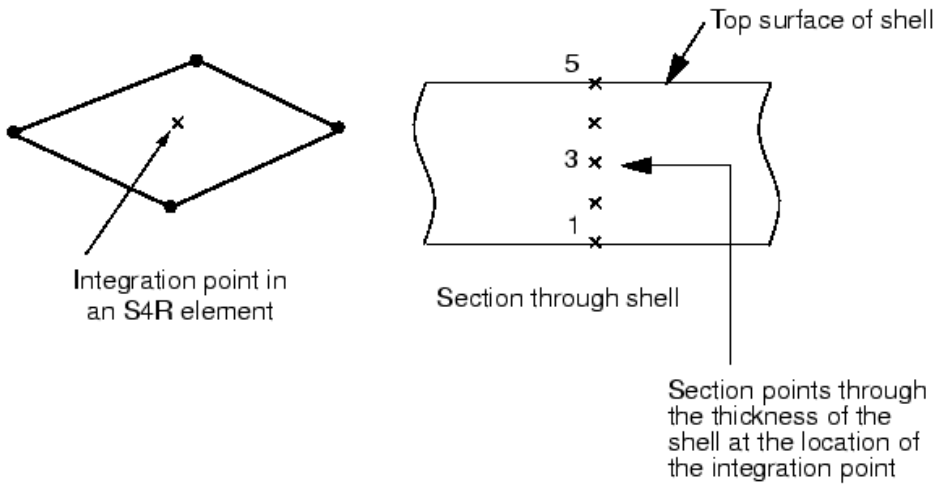

Fig. 4.6 S4R element, according to Abaqus convention, used to define the finite element mesh (from [32])

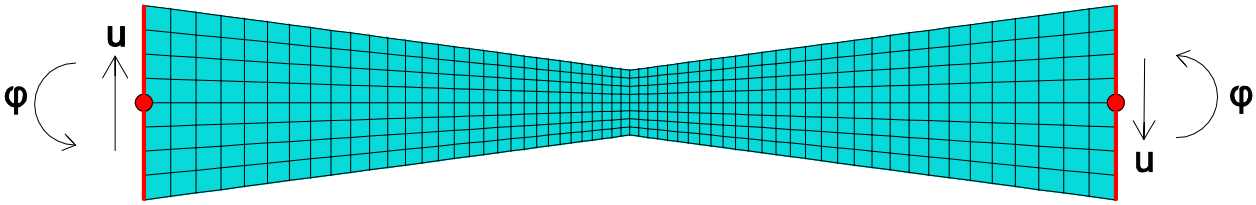

Fig. 4.7 Mesh and loading conditions of the fuse link

One of the main simplifications consists in the material modeling. Elastic-perfectly plastic behavior is assumed in each model, which neglects eventual hardening and failure associated with cracking (Fig. 4.8). This choice is justified by the fact that post-yielding plastic behavior is considered to be sufficient for analyzing the overall performance of the shear wall in terms of energy dissipation and hysteretic behavior. Use of more sophisticated material models is left for future investigations.

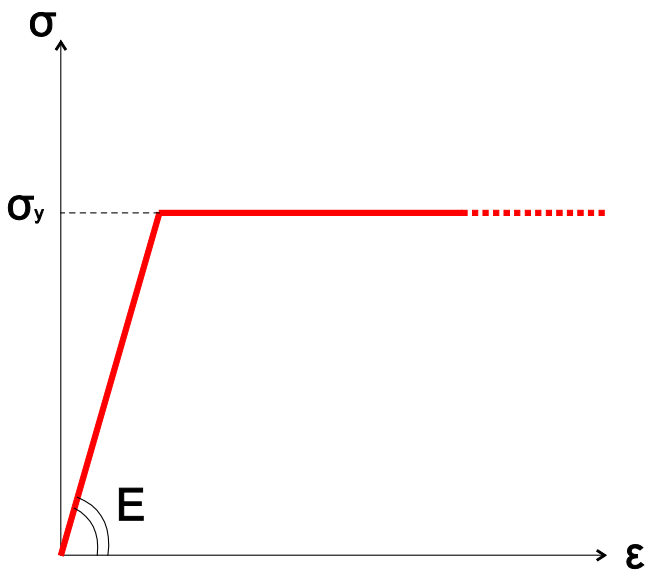

Fig. 4.8 Elastic-perfectly plastic material model

Initially, linear buckling analysis is performed with all degrees of freedom restrained, except for vertical displacements. This provides the elastic critical shear V_{cr} (that will be used to evaluate the fuse slenderness) and the buckling modes used to apply the geometric imperfections. Then, non-linear analysis is carried out (both geometric and material non-linearity are accounted for) on the fuse geometry perturbed by initial imperfections, according to Chapter 4.5.3. This type of analysis allows to investigate the post-buckling behavior of the links. Since the FEMA protocol (Chapter 4.4) is applied in displacement-control, the traditional Newton-Raphson non-linear solver can be used (force-control application of the loading history would have required a different approach based on the arch-length method).

Displacements and rotation are applied to the end sections according to Eqn. (4.1). The time scale for cyclic loading (see Fig. 4.3) is not a physical time as in experimental tests, but plays a role in the choice of the increment length for the numerical analysis. The maximum increment value used by the Abaqus automatic solver has been set small enough ($\Delta t = 1s$) to catch quite accurately the development also of the small initial cycles.

Since the targeted maximum drift of the FEMA protocol is associated to evident damage of the fuses (buckling), the duration and maximum drift of the protocol may vary to catch the unstable behavior (Fig. 4.3).

The model of the fuse with side plates is similar to the one just described. The only difference is obviously the geometry and boundary conditions. As Fig. 4.9 shows, rotations are applied to the end sections of the side plates, fixed for the other degrees of freedom. For all models, the height of the side plates has been set equal to 200*mm*; however, since the weak point of the fuse is the inner link and not the lateral plates, this choice should not be relevant for the results.

As described in Chapter 4.2.2, modeling the entire fuse with side plates should better reproduce the results of the full wall models. However, if different connection detailing will be used in the actual design, the results of the models without plates may be considered more general. Both modeling typology are presented in the Thesis to provide complete information that can be used according to the necessity.

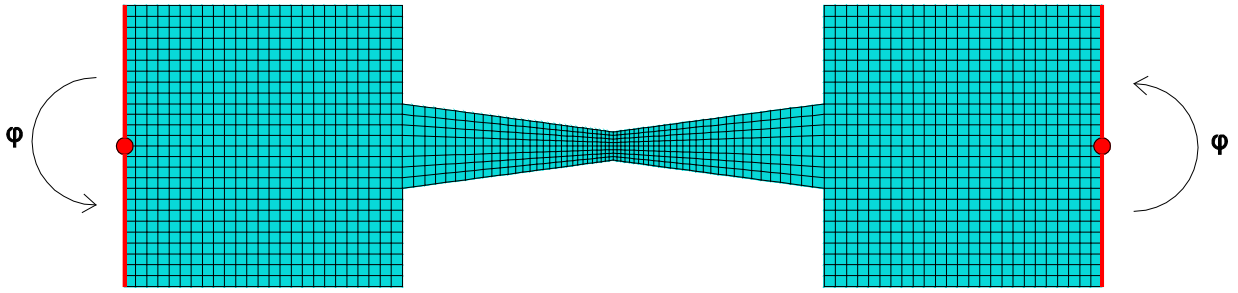

Fig. 4.9 Mesh and loading conditions of the fuse with side plates

4.7 Results of numerical simulations

Out of the numerical models, the following parameters are computed:

- elastic buckling force V_{cr} ;
- shear capacity $\overline{V}_{fuse}$ before buckling;
- eventual post-buckling peak capacity V_{peak} ;
- critical buckling drift of the fuse $\Delta_{cr,\,fuse}$ and corresponding critical drift of the wall Δ_{cr} .

V_{cr} , together with the yielding force V_y given in Eqn. (3.4), defines the slenderness of the fuses. The capacity $\overline{V}_{fuse}$ computed from the finite element analyses will validate Eqn. (3.6). The extra-capacity V_{peak} is reported only for additional information, to show that in some cases the fuses can pick up significant strength even after buckling. Finally, the buckling drifts of the 60 fuses will be used to obtain a generalized formula for estimating Δ_{cr} for any size of fuse.

4.7.1 Results for a sample fuse

First, the results for one of the 60 specimens are described here in detail. This provides a benchmark example to understand the response of all the fuses analyzed in the parametric study (the 59 remaining fuses have analogue behavior and their results are reported in the Appendix). The specimen presented here is the No. 27 (without plates) according to Table 4.1, but a different choice would have led to the same conclusions.

Due to their particular butterfly-shape defined in Chapter 3.2, fuse yielding is first expected at the external fibers of the quarter-point sections. Fig. 4.10 shows in red the areas where yielding stress has been reached; these areas spread from the quarter-point sections as anticipated. For larger drifts, plastic hinges form at the same sections (Fig. 4.11), and the corresponding shear force is given by Eqn. (3.6).

When $\overline{V}_{fuse}$ is reached, the behavior is still stable because the critical load is larger than the capacity. Fig. 4.12 is a top view of the link, at the time when plastic hinges form: it still lies in its own plane, with very small transverse displacements. With extension of plastic hinges, the link results almost divided in three pieces, of which the central one behaves like a column which buckle for the compression induced by load reversal. This behavior is observed in Fig. 4.13, where the extensive plastic region is now due to out-of-plane bending and the central part remain elastic. At this level, evident out-of-plane displacements are present, as shown in Fig. 4.14.

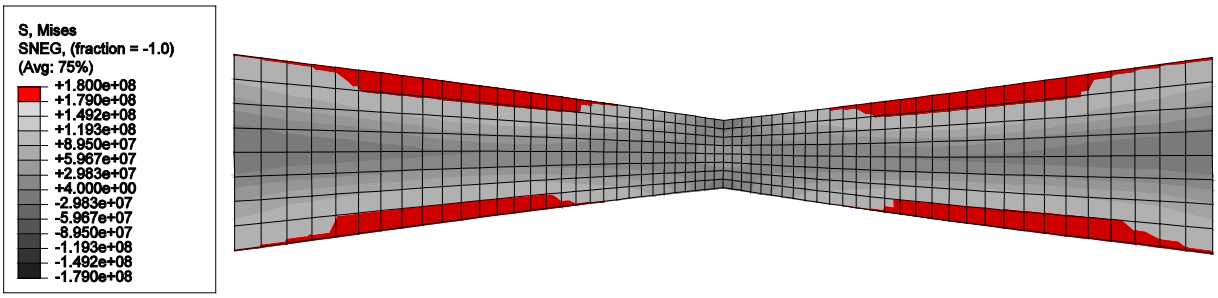

Fig. 4.10 First yielding starting at the external fibers of quarter-point sections (stresses in Pascal)

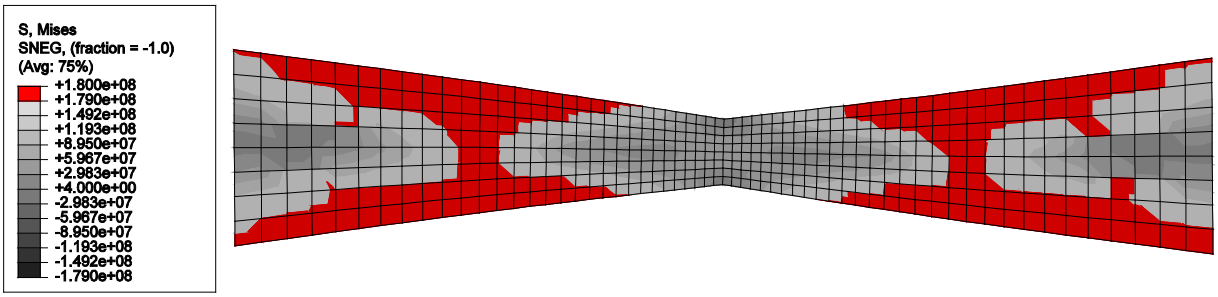

Fig. 4.11 Plastic hinges at the quarter-point sections (stresses in Pascal)

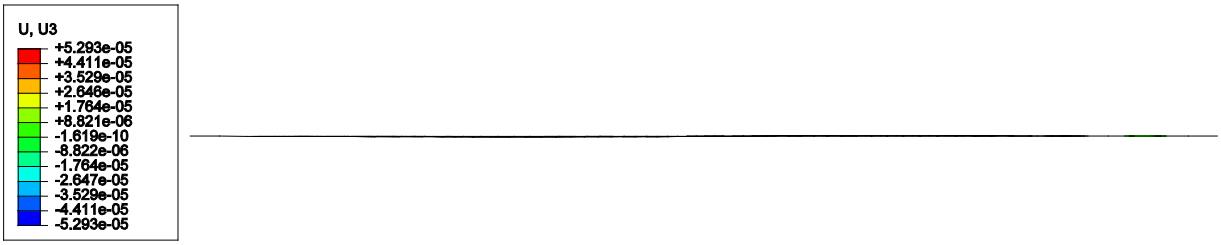

Fig. 4.12 Top view of the fuse before buckling (out-of-plane displacement in meter)

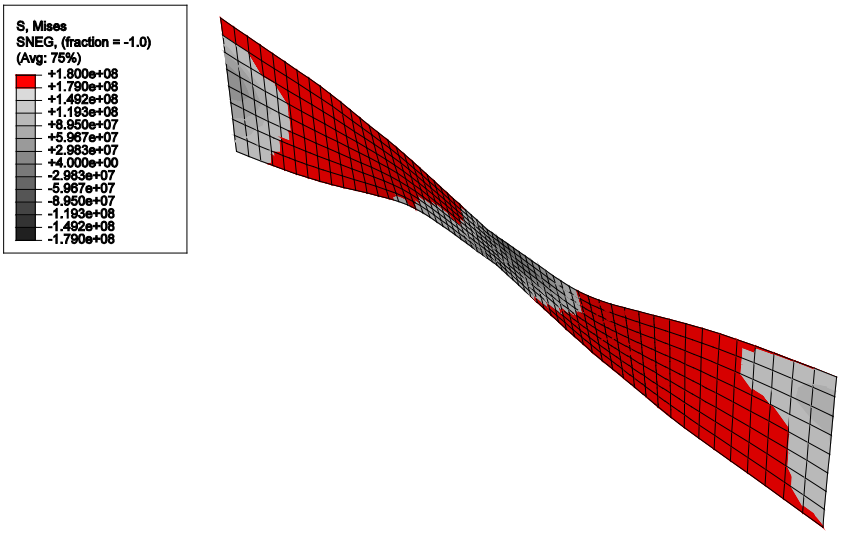

Fig. 4.13 Buckling of the fuse (stresses in Pascal)

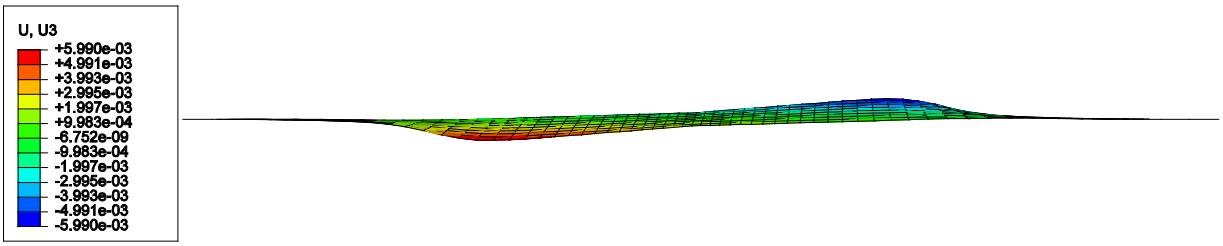

Fig. 4.14 Top view of the fuse after buckling (out-of-plane displacement in meter)

In general, the same deformation mechanism is expected also for the models with plates. However, due to the different boundary conditions, buckling may not involve only the link but extend also to the side plates. The plates are in fact restrained against out-of-plane displacements only at their end sections, so that they offer a weaker constraint in preventing instability of the links. This explains why the buckling drift measured for the models with plates is generally lower than for the models without.

Time-histories of fuse shear force are shown in Fig. 4.15 - Fig. 4.16. After the first cycles, the peaks of shear force converge to a value that remains constant for several cycles (is the capacity $\bar{V}_{fuse}$). The numerical capacity corresponds exactly to the analytical value, provided by Eqn. (3.6) and represented as red horizontal lines in Fig. 4.15.

Initiation of buckling, evaluated with the negative-stiffness criterion of Chapter 4.5.1, is highlighted by a green circle. It can be seen that instability does not start at the peak of the drift (when the fuse is stretched and in tension), but after loading reversal which induces compression. The critical drift is thus evaluated as the previous maximum peak.

Buckling drift is not associated with immediate large out-of-plane displacements and drop of shear capacity. In fact, the maximum transverse displacement at the initiation of buckling is 0.3*mm* for this example, and the post-buckling peaks can even exceed the estimated capacity. Only after a few cycles transverse displacements become evident and the capacity significantly drops.

The chart for the single link is compared to the results of the model with plates in Fig. 4.16. It can be seen that in the first cycles (corresponding to very small drift) the shear developed by the fuse is slightly smaller in the second model, probably due to the presence of the side plates. After that, the two curves are identical for several cycles, with peaks converging to the analytical solution. Then, buckling occurs approximately at the same time and is followed by a larger load degradation in the model with side plates, that is reflected by a more evident pinching in the hysteretic curves. However, also in this case the post-buckling peaks are not significantly smaller than the original capacity.

As a general conclusion, the analytical and the numerical capacity are exactly the same for the two models. Furthermore, buckling drift is not associated with immediate failure, but simply marks the beginning of a less stable behavior which will become more evident only after few more cycles. Δ_{cr} is therefore a conservative value for evaluating the lateral drift up to which optimal performance of the wall system, in terms of resistance and energy dissipation, is guaranteed.

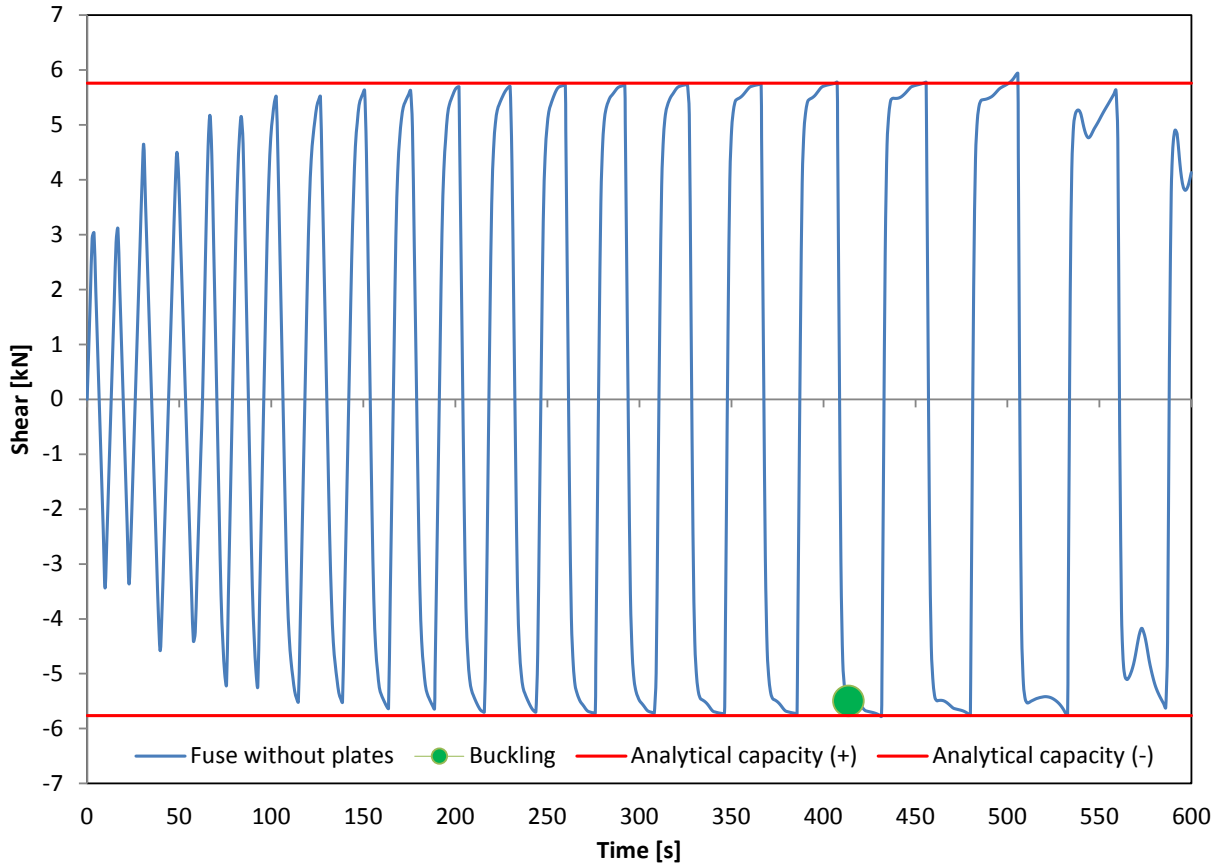

Fig. 4.15 Time history of the shear force (fuse No. 27, without plates)

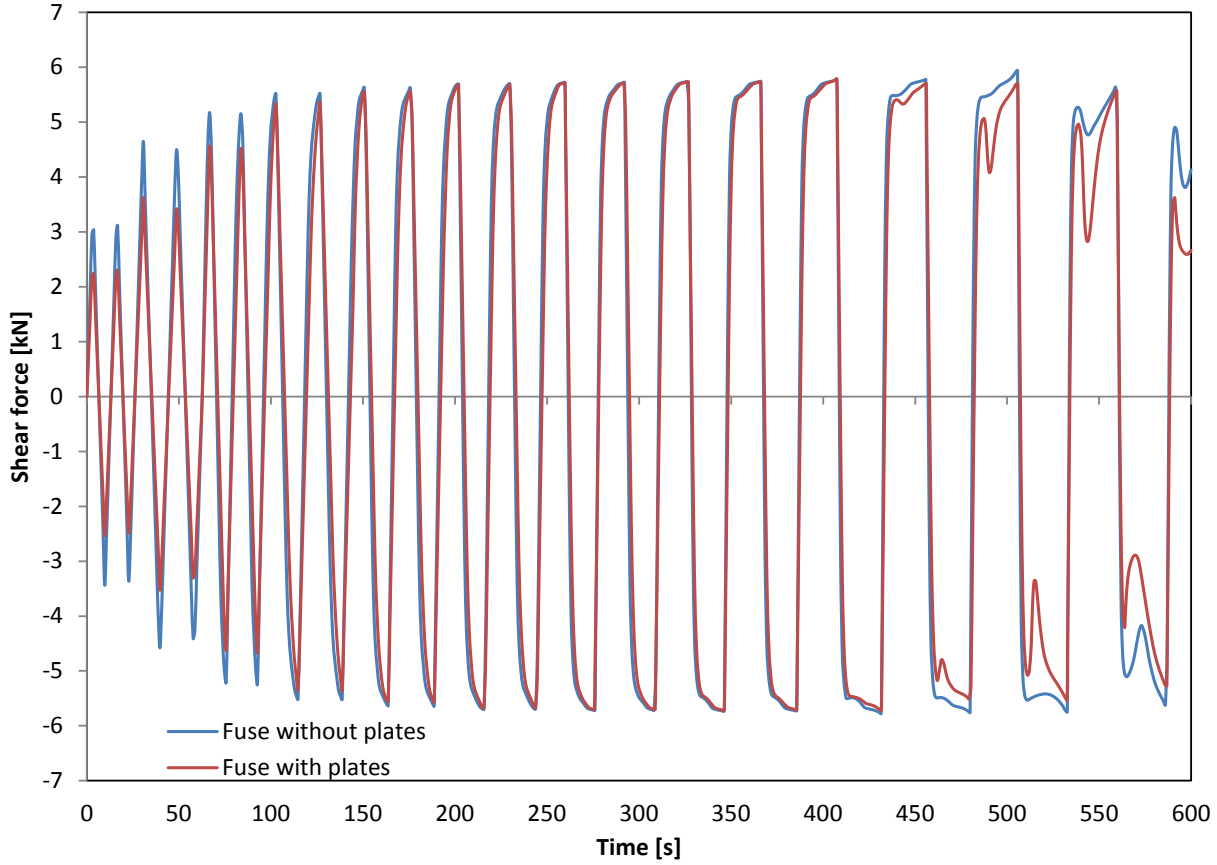

Fig. 4.16 Time history of the shear force (comparison of the fuse models with and without plates)

Finally, the hysteretic curves for both models are shown in Fig. 4.17. The two charts at the top refer to the fuse drift Δ_{fuse}, while those at the bottom refer to the lateral drift of the entire wall Δ: they are practically the same but scaled differently. Δ_{fuse} is more appropriate for evaluating the response of the fuse, whereas Δ provides information on the equivalent level of drift expected in the entire wall system. In general, the hysteretic behavior is very good, with fat and stable loops.

For the models without plates, buckling initiation is highlighted in red; pinching is present only in the last cycles, and more evident for the model with side plates (those on the right). Since the energy dissipated is equal to the area enclosed by the curve, pinching (corresponding to narrowing of loops due to a decrease of capacity) is detrimental for the fuses, and consequently for the wall. This is why estimation of buckling drift is so important for the design.

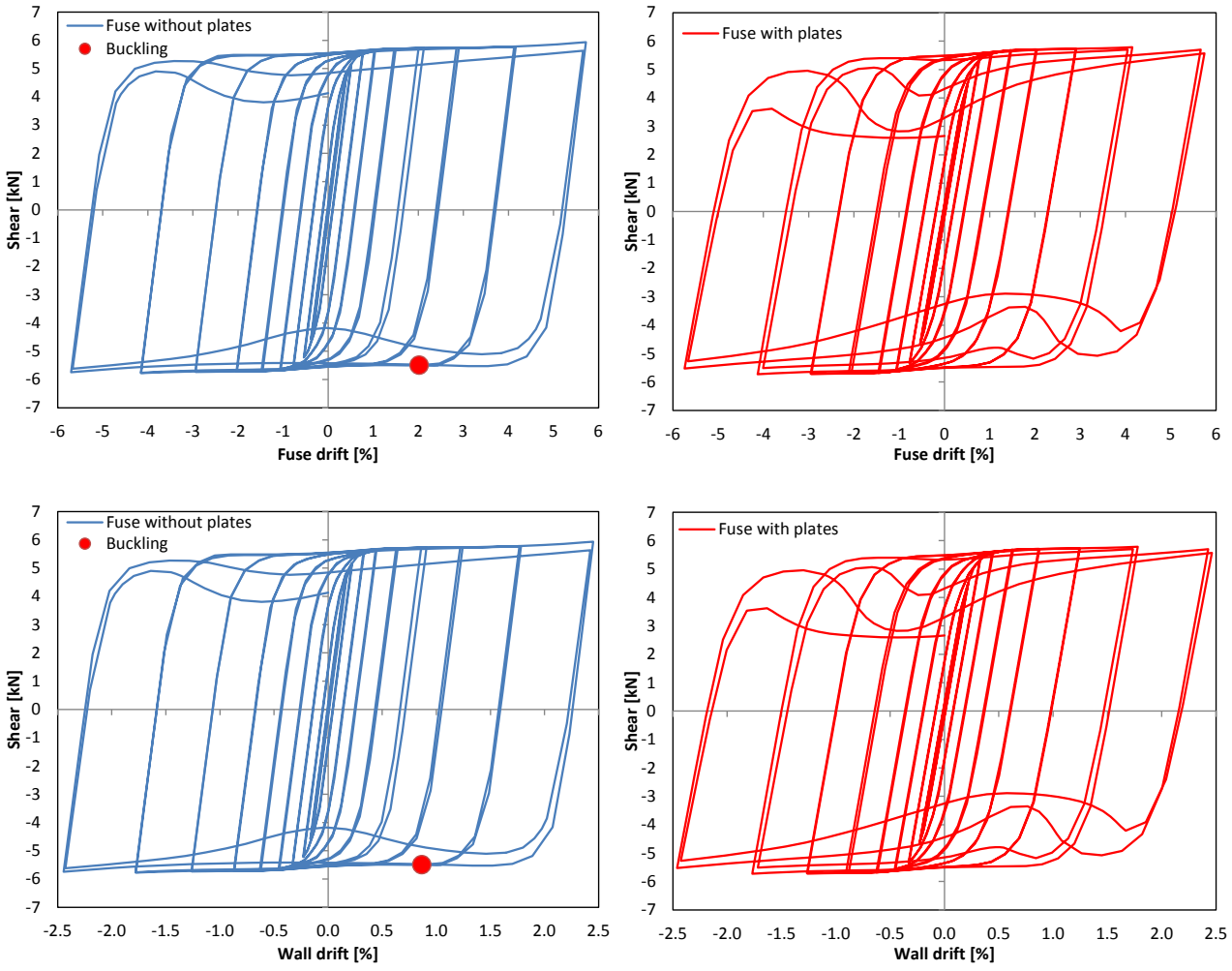

Fig. 4.17 Hysteretic curves of both fuse models

4.7.2 Final results for all fuses

The results of the parametric study are summarized in Table 4.3 and Table 4.4: Table 4.3 refers to the capacity of the fuses whereas Table 4.4 deals with their buckling resistance.

The nominal shear capacity of the fuse links has been derived in Chapter 3.2 and is expressed by Eqn. (3.6): the numerical models carried out for the parametric study allow to check the reliability of such formula. It should be noted that Eqn. (3.6) assumes in-plane behavior, whereas the presence of geometric imperfections associated with non-linear analysis leads to out-of-straightness which slightly reduces the actual capacity. On the other hand, plastic hinges may extend from the quarter-point sections, leading to a redistribution of section forces which increases the capacity. Combination of these two effects can explain discrepancies between analytical and numerical values. However, Table 4.3 shows that there is a great agreement between the results, for both the models without and with side plates.

Fig. 4.18 - Fig. 4.19 show in more details the relative difference between numerical and analytical capacity (positive difference means that the analytical capacity is larger than the numerical capacity). It can be seen that for most cases the measured capacity is slightly smaller than the value provided by Eqn. (3.6), which may be explained with the presence of out-of-plane displacements in the numerical models, neglected by the analytical formula. However, such formula is proved to be precise and reliable, since the relative difference is always smaller than 5% and, more often than not, also smaller than 2%.

The presence of an extra peak of strength for some of the models has been justified in Chapter 4.5.1. This extra capacity is generally quite small, and should not be accounted for in the design, since fuse buckling has already occurred. It is reported here to show that, although instability is associated with pinching of hysteretic curves, the fuses can still withstand a force similar or even larger to the pre-buckling capacity. The fuses with $V_{peak} \leq \overline{V}_{fuse}$ are indicated with a pound (#) in Table 4.3.

To conclude, the designer can use Eqn. (3.6) to determine the shear capacity for fuses of any size, even those not included in this parametric study. The formula can also be inverted to find the dimensions necessary to achieve the targeted capacity.

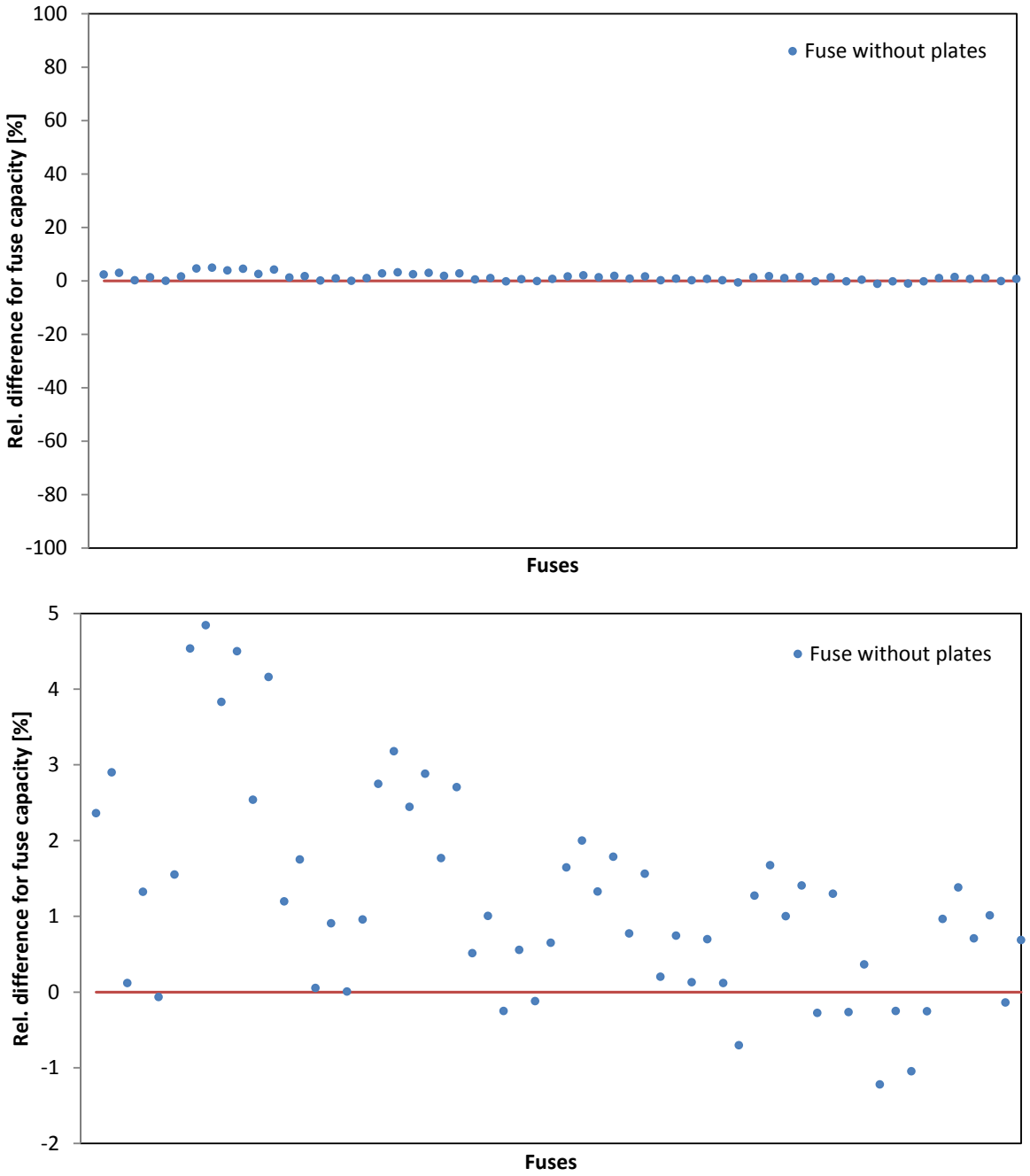

Fig. 4.18 Relative difference between numerical and analytical fuse capacity. Top: zoomed-out; Bottom: magnified.

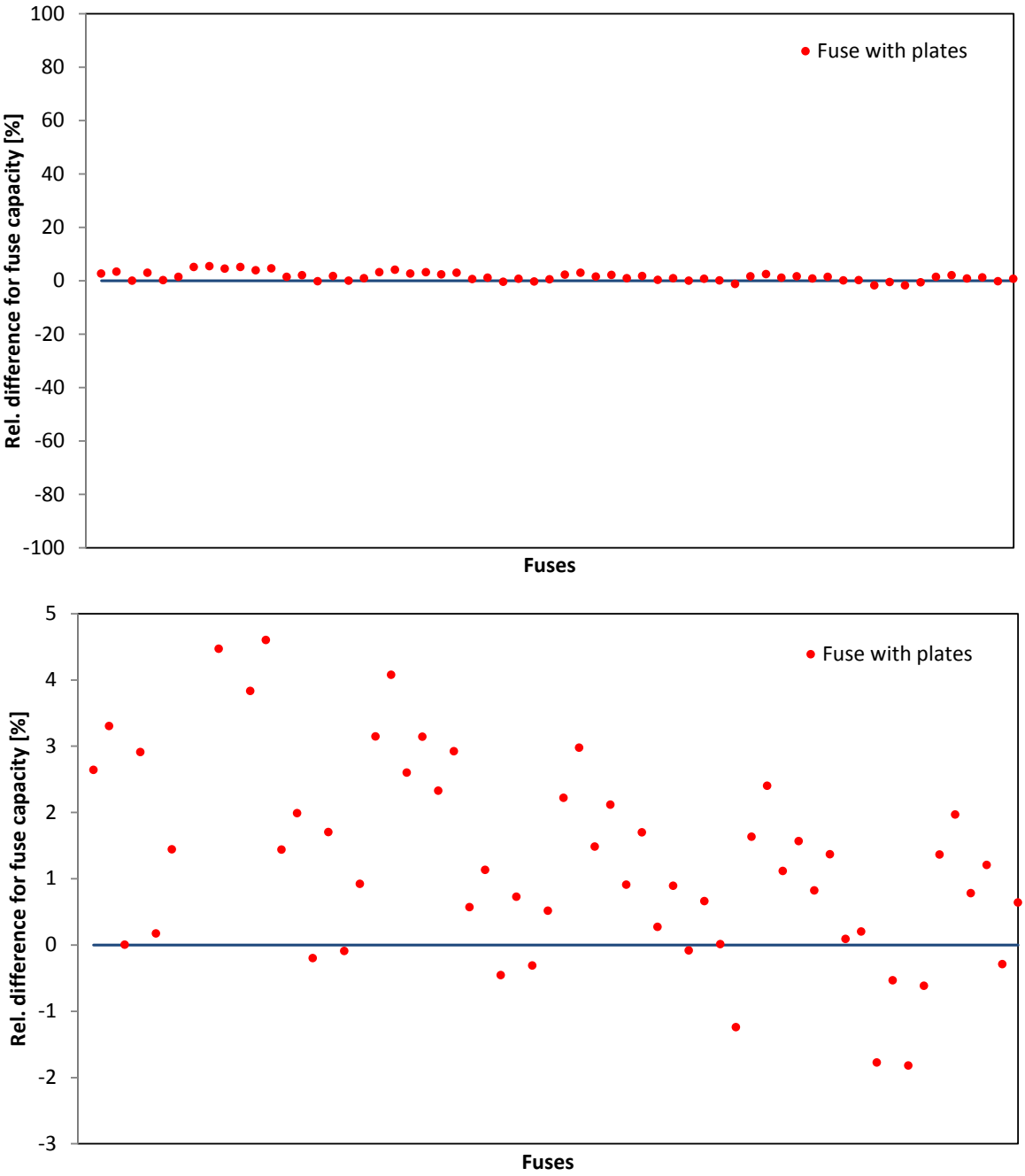

Fig. 4.19 Relative difference between numerical and analytical fuse capacity (fuses with plates). Top: zoomed-out; Bottom: magnified.

Table 4.3 Results of the parametric study (fuse capacity)

	Analytical	Numerical - Fuse without plates			Numerical - Fuse with plates		
N	$\bar{V}_{fuse}\,[kN]$	$\bar{V}_{fuse}\,[kN]$	Rel. diff. [%]	$V_{peak}\,[kN]$	$\bar{V}_{fuse}\,[kN]$	Rel. diff. [%]	$V_{peak}\,[kN]$
1	7.20	7.03	2.36	#	7.01	2.64	#
2	10.00	9.71	2.90	#	9.67	3.30	#
3	8.64	8.63	0.12	#	8.47	2.01	#
4	12.00	11.84	1.32	#	11.65	2.91	#
5	10.08	10.09	-0.07	10.57	10.06	0.17	#
6	14.00	13.78	1.55	14.48	13.80	1.44	14.00
7	11.25	10.74	4.53	#	10.67	5.12	#
8	15.63	14.87	4.84	#	14.78	5.41	#
9	13.50	12.98	3.83	#	12.90	4.47	#
10	18.75	17.91	4.50	#	17.80	5.06	#
11	15.75	15.35	2.54	#	15.15	3.83	#
12	21.88	20.97	4.16	#	20.87	4.60	#
13	5.76	5.69	1.20	#	5.68	1.44	#
14	8.00	7.86	1.75	#	7.84	1.99	#
15	6.91	6.91	0.05	6.98	6.93	-0.20	#
16	9.60	9.51	0.91	#	9.44	1.70	#
17	8.06	8.06	0.00	8.65	8.07	-0.09	8.45
18	11.20	11.09	0.96	11.59	11.10	0.92	11.55
19	9.00	8.75	2.75	#	8.72	3.15	#
20	12.50	12.10	3.18	#	11.99	4.08	#
21	10.80	10.54	2.44	#	10.52	2.60	#
22	15.00	14.57	2.88	#	14.53	3.14	#
23	12.60	12.38	1.77	#	12.31	2.32	#
24	17.50	17.03	2.70	#	16.99	2.92	#
25	4.80	4.78	0.51	#	4.77	0.57	#
26	6.67	6.60	1.00	#	6.59	1.13	#
27	5.76	5.77	-0.25	5.94	5.79	-0.46	#
28	8.00	7.96	0.55	8.12	7.94	0.72	8.00
29	6.72	6.73	-0.12	7.19	6.74	-0.31	#
30	9.33	9.27	0.65	9.65	9.29	0.52	9.65
31	7.50	7.38	1.64	#	7.33	2.22	#
32	10.42	10.21	2.00	#	10.11	2.98	#
33	9.00	8.88	1.32	#	8.87	1.48	#
34	12.50	12.28	1.79	#	12.24	2.11	#
35	10.50	10.42	0.77	#	10.40	0.91	#
36	14.58	14.36	1.56	#	14.34	1.70	#
37	4.11	4.11	0.20	#	4.10	0.27	#
38	5.71	5.67	0.74	#	5.66	0.89	#
39	4.94	4.93	0.13	5.04	4.94	-0.09	#
40	6.86	6.81	0.69	6.97	6.81	0.66	#
41	5.76	5.75	0.11	6.21	5.76	0.01	6.07
42	8.00	8.06	-0.70	8.53	8.10	-1.24	8.40
43	6.43	6.35	1.27	#	6.32	1.63	#
44	8.93	8.78	1.67	#	8.71	2.40	#
45	7.71	7.64	1.00	#	7.63	1.11	#
46	10.71	10.56	1.41	#	10.55	1.57	#
47	9.00	9.03	-0.28	#	8.93	0.82	#
48	12.50	12.34	1.29	12.40	12.33	1.37	#
49	3.60	3.61	-0.27	#	3.60	0.09	#
50	5.00	4.98	0.36	#	4.99	0.20	#
51	4.32	4.37	-1.22	4.42	4.40	-1.78	4.41
52	6.00	6.02	-0.25	6.08	6.03	-0.54	6.10
53	5.04	5.09	-1.05	5.39	5.13	-1.82	5.30
54	7.00	7.02	-0.26	7.35	7.04	-0.62	7.35
55	5.63	5.57	0.96	#	5.55	1.36	#
56	7.81	7.70	1.38	#	7.66	1.96	#
57	6.75	6.70	0.71	#	6.70	0.78	#
58	9.38	9.28	1.01	#	9.26	1.21	#
59	7.88	7.89	-0.14	#	7.90	-0.29	#
60	10.94	10.86	0.68	#	10.87	0.64	#

For each type of specimen, Table 4.4 provides the critical drift both in terms of lateral drift of the wall Δ_{cr} and internal drift of the fuse $\Delta_{cr,\,fuse}$. The former is more relevant for the actual wall design, since indicates the level of global drift up to which the seismic energy is dissipated in a stable way, with *fat* hysteretic curves and no pinching. The critical drift of the fuses is instead more significant to derive a generalized formula for their design. The relation between Δ and Δ_{fuse} is expressed by Eqn. (3.19).

From Table 4.4 one immediately notices that Δ_{cr} assumes only a few repetitive values (0.65%, 0.91%, 1.28%, 1.79% and 2.5%). This is explained by the nature of the FEMA loading protocol, which is not monotonically increasing but cyclic (Chapter 4.4). In fact, for a cyclic protocol the critical drift is defined as the maximum peak before initiation of buckling; but since the peak values are fixed by the protocol, Δ_{cr} necessarily corresponds to one of the values listed in Table 4.2.

Some fuses, if installed within the shear wall, would start to buckle for $\Delta < 1\%$, while others remain stable up to 2.5% wall drift, which was the prescriptive allowable drift for cold-formed steel frames. However, not only the critical drift is relevant for their design, but also the drift at which yielding starts, because this marks the beginning of energy-dissipation. For this reason, a simplified formula for $\Delta_{y,\,fuse}$ is derived in the following; the corresponding wall drift Δ_y is obtained from Eqn. (3.19).

To avoid complex integration over the fuse length, the butterfly-shape links are approximated by equivalent links with constant cross section. The height of the rectangular beam is the average between the end-section and mid-section heights ($\bar{b} = \frac{2}{3} b$), which leads to an equivalent moment of inertia $\bar{I} = \frac{t \bar{b}^3}{12}$ (see Fig. 4.20a). The bending behavior of a beam is described by four degrees of freedom, two at each end, and the stiffness coefficient k_{31} represents the moment at one end due to a unit vertical displacement at the same location. It is given by:

$$k_{31} = 6 \cdot \frac{E \bar{I}}{L^2} \tag{4.10}$$

For a general transverse displacement u, the bending moment is:

$$k_{31} = M(u) = 6 \cdot \frac{E \bar{I}}{L^2} u \tag{4.11}$$

The moment causing first yielding in the fuse links is defined by Eqn. (3.3) which, substituted into Eqn. (4.11), leads to the (approximate) value of "yielding displacement" u_y:

$$u_y = \frac{L^2 \sigma_y}{E b} \tag{4.12}$$

The corresponding yielding drift is simply obtained by dividing Eqn. (4.12) by the fuse length:

$$\Delta_{y,\,fuse} = \frac{u_y}{L} \qquad \rightarrow \qquad \Delta_{y,\,fuse} = \frac{L \sigma_y}{E b} \tag{4.13}$$

When installed into the CFS frame, the theoretical yielding drift of the wall, according to Eqn. (3.19), is:

$$\Delta_y = \frac{L}{w} \cdot \Delta_{y,\,fuse} \tag{4.14}$$

It should be noted, however, that (4.14) generally leads to very small values, which are only realistic if the fuses are much more flexible than the studs to which they are connected. For actual wall systems (Chapter 5), some flexibility and deformation in the studs will delay yielding in the fuses.

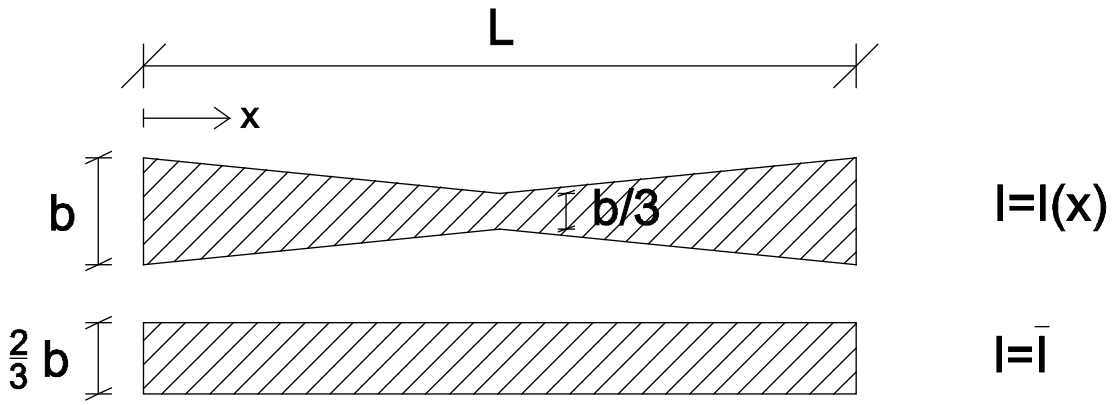

(a)

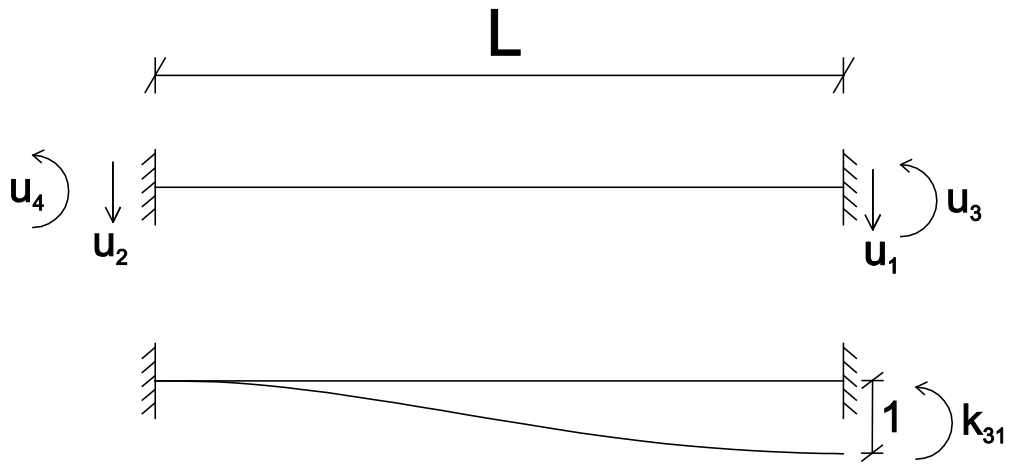

(b)

Fig. 4.20 **Simplified straight fuse to derive an approximate formula for the fuse yielding drift: (a) from butterfly-shape to approximately equivalent rectangular shape; (b) beam stiffness coefficient relative to bending moment**

Table 4.4 Results of the parametric study (buckling resistance of the fuses)

	Fuse slenderness properties				*Fuse without plates*		*Fuse with plates*	
N	$V_y\,[kN]$	$V_{cr}\,[kN]$	λ	$\Delta_{y,\,fuse}\,[\%]$	$\Delta_{cr}\,[\%]$	$\Delta_{cr,\,fuse}\,[\%]$	$\Delta_{cr}\,[\%]$	$\Delta_{cr,\,fuse}\,[\%]$
1	4.80	84.74	0.057	0.30	0.91	3.19	0.65	2.28
2	6.67	84.74	0.079	0.42	0.91	3.19	0.65	2.28
3	5.76	144.32	0.040	0.30	1.79	6.27	1.28	4.48
4	8.00	144.32	0.055	0.42	1.28	4.48	1.28	4.48
5	6.72	225.66	0.030	0.30	1.79	6.27	1.79	6.27
6	9.33	225.66	0.041	0.42	1.79	6.27	1.79	6.27
7	7.50	110.21	0.068	0.24	0.65	2.28	0.47	1.65
8	10.42	110.21	0.095	0.33	0.65	2.28	0.47	1.65
9	9.00	188.02	0.048	0.24	0.91	3.19	0.65	2.28
10	12.50	188.02	0.066	0.33	0.91	3.19	0.65	2.28
11	10.50	294.47	0.036	0.24	1.79	6.27	1.28	4.48
12	14.58	294.47	0.050	0.33	1.28	4.48	0.91	3.19
13	3.84	53.30	0.072	0.38	1.28	3.58	0.91	2.55
14	5.33	53.30	0.100	0.52	1.28	3.58	0.91	2.55
15	4.61	90.98	0.051	0.38	1.79	5.01	1.79	5.01
16	6.40	90.98	0.070	0.52	1.79	5.01	1.28	3.58
17	5.38	142.60	0.038	0.38	1.79	5.01	1.79	5.01
18	7.47	142.60	0.052	0.52	1.79	5.01	1.79	5.01
19	6.00	68.70	0.087	0.30	0.65	1.82	0.65	1.82
20	8.33	68.70	0.121	0.42	0.65	1.82	0.65	1.82
21	7.20	117.46	0.061	0.30	0.91	2.55	0.91	2.55
22	10.00	117.46	0.085	0.42	0.91	2.55	0.91	2.55
23	8.40	184.43	0.046	0.30	1.79	5.01	1.28	3.58
24	11.67	184.43	0.063	0.42	1.28	3.58	1.28	3.58
25	3.20	36.61	0.087	0.45	1.28	2.99	1.28	2.99
26	4.44	36.61	0.121	0.63	1.28	2.99	1.28	2.99
27	3.84	62.57	0.061	0.45	1.79	4.18	1.79	4.18
28	5.33	62.57	0.085	0.63	1.79	4.18	1.79	4.18
29	4.48	98.21	0.046	0.45	1.79	4.18	1.79	4.18
30	6.22	98.21	0.063	0.63	1.79	4.18	1.79	4.18
31	5.00	47.00	0.106	0.36	0.91	2.12	0.91	2.12
32	6.94	47.00	0.148	0.50	0.91	2.12	0.91	2.12
33	6.00	80.46	0.075	0.36	1.28	2.99	1.28	2.99
34	8.33	80.46	0.104	0.50	1.28	2.99	1.28	2.99
35	7.00	126.51	0.055	0.36	1.79	4.18	1.79	4.18
36	9.72	126.51	0.077	0.50	1.79	4.18	1.79	4.18
37	2.74	26.65	0.103	0.53	1.79	3.58	1.79	3.58
38	3.81	26.65	0.143	0.73	1.79	3.58	1.79	3.58
39	3.29	45.58	0.072	0.53	2.50	5.00	1.79	3.58
40	4.57	45.58	0.100	0.73	2.50	5.00	2.50	5.00
41	3.84	71.60	0.054	0.53	2.50	5.00	2.50	5.00
42	5.33	71.60	0.074	0.73	2.50	5.00	2.50	5.00
43	4.29	34.08	0.126	0.42	0.91	1.82	0.91	1.82
44	5.95	34.08	0.175	0.58	0.91	1.82	0.91	1.82
45	5.14	58.37	0.088	0.42	1.28	2.56	1.28	2.56
46	7.14	58.37	0.122	0.58	1.28	2.56	1.28	2.56
47	6.00	91.86	0.065	0.42	2.50	5.00	1.79	3.58
48	8.33	91.86	0.091	0.58	1.79	3.58	1.79	3.58
49	2.40	20.29	0.118	0.60	1.79	3.13	1.79	3.13
50	3.33	20.29	0.164	0.83	1.79	3.13	1.79	3.13
51	2.88	34.72	0.083	0.60	2.50	4.38	2.50	4.38
52	4.00	34.72	0.115	0.83	2.50	4.38	2.50	4.38
53	3.36	54.57	0.062	0.60	2.50	4.38	2.50	4.38
54	4.67	54.57	0.086	0.83	2.50	4.38	2.50	4.38
55	3.75	25.88	0.145	0.48	0.91	1.59	1.28	2.24
56	5.21	25.88	0.201	0.67	1.28	2.24	1.28	2.24
57	4.50	44.35	0.101	0.48	1.79	3.13	1.79	3.13
58	6.25	44.35	0.141	0.67	1.79	3.13	1.79	3.13
59	5.25	69.84	0.075	0.48	2.50	4.38	2.50	4.38
60	7.29	69.84	0.104	0.67	2.50	4.38	2.50	4.38

With the above data, it is now possible derive a formula for the critical drift, $\Delta_{cr,\,fuse}$, that can be extended to apply for any size of fuse. For this purpose, a chart is created where the measured buckling drifts are reported as a function of fuse slenderness:

$$\lambda = \frac{V_y}{V_{cr}} \tag{4.15}$$

Stocky links (small λ) are expected to have a large $\Delta_{cr,\,fuse}$, whereas slender links are more likely to buckle for small drifts. All slenderness values can be found in Table 4.4.

Since λ is dimension-less, it is convenient to normalize also the critical drift: the yielding drift $\Delta_{y,\,fuse}$ derived in Eqn. (4.13) and reported in Table 4.4 is used for such normalization. The parameter δ is therefore defined as:

$$\delta = \frac{\Delta_{cr,\,fuse}}{\Delta_{y,\,fuse}} \tag{4.16}$$

Fig. 4.21 shows the chart with all 60 models of links (without plates). The choice of using the simple fuse links eliminates the eventual influence of the plates on the results, and should therefore lead to a more general applicability.

Despite the approximations introduced ($\Delta_{cr,\,fuse}$ depends on the drift values of the FEMA loading protocol; $\Delta_{y,\,fuse}$ is computed approximately for an equivalent straight fuse), a clear trend can be seen, which is interpolated by a power trend-line, as shown in Fig. 4.21 along with the equation for the line. The exponent of the equation is very close to 1, which enables an approximation for the curve as a branch of a rectangular hyperbola:

$$\delta = \frac{0.57}{\lambda} \tag{4.17}$$

which can be rewritten, substituting Eqns. (4.15)-(4.16), in terms of critical drift:

$$\Delta_{cr,\,fuse} = 0.57 \cdot \frac{\Delta_{y,\,fuse}\, V_{cr}}{V_y} \tag{4.18}$$

The designer can therefore estimate the maximum drift that any butterfly-shaped fuse can sustain before buckling, and using Eqn. (3.19) also the corresponding lateral drift of the wall. In the formula above, $\Delta_{y,\,fuse}$ is given by Eqn.(4.13), V_y by Eqn. (3.4) and V_{cr} can be determined by an eigenvalue buckling analysis or an approximate estimation. Since generally the maximum drift for CFS shear walls does not go beyond 2-3%, there is no reason to install fuses which provide a larger buckling resistance.

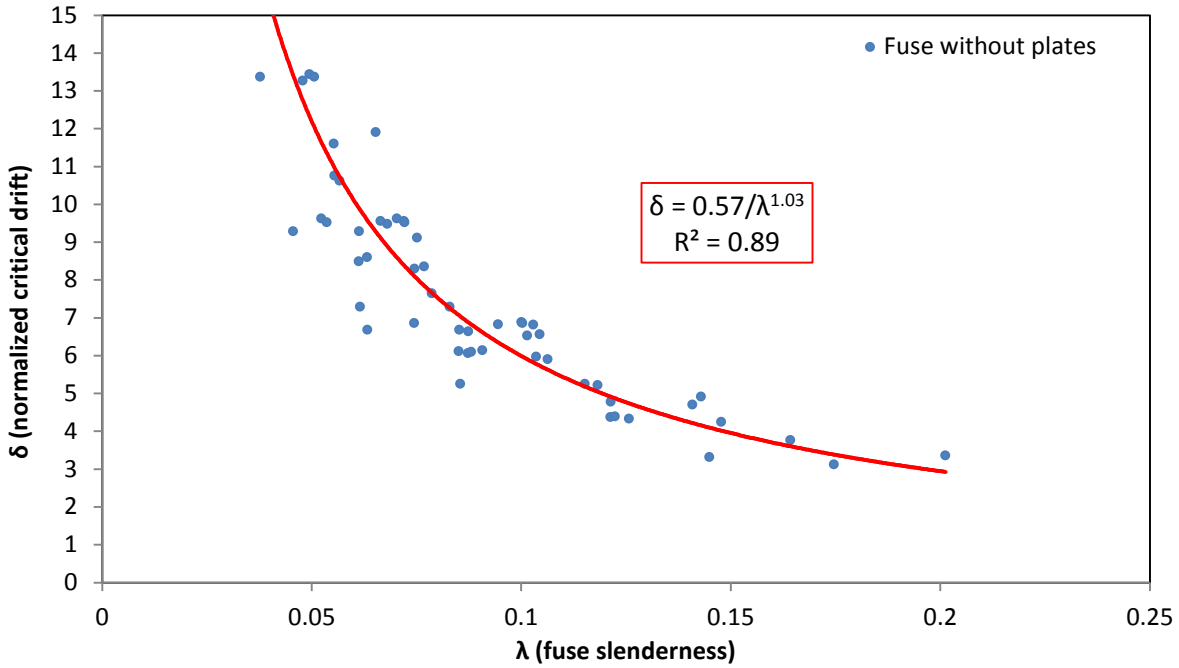

Fig. 4.21 Interpolation of numerical critical drifts of the fuses to derive an approximate generalized formula for the buckling drift

4.8 Remarks

The parametric study presented in this Chapter allows drawing the following conclusions:

- the yielding mechanism of the fuse links observed in the numerical simulations corresponds to the expected behavior described in Chapter 3.2;
- the analytical formula $\bar{V}_{fuse} = \frac{4}{9}\frac{t b^2 \sigma_y}{L}$ can be used to evaluate the capacity for any size of link, with very good precision;
- although their critical load V_{cr} is significantly larger than the capacity, the fuses buckle due to load reversal, and the critical drift Δ_{cr} is influenced by geometric imperfections;
- Δ_{cr} shows a clear dependency on the fuse slenderness, which allowed to derive a generalized formula for the buckling drift.

With the information provided in Chapter 3 and Chapter 4, the designer has the main tools and background for choosing the fuses necessary to achieve a targeted performance. However, it still remains to be proved that the results obtained for single models are also valid for the entire wall system. Furthermore, the hysteretic behavior and energy-dissipation performance of the full shear wall need to be evaluated to prove the actual efficiency of the proposed system. These topics will be addressed in the next Chapter.

Chapter 5

Model of the entire seismic wall system

5.1 Introduction

The parametric study, presented in Chapter 4, has analyzed 60 types of fuse separately from the frame they belong to. This Chapter describes instead the modeling of the entire wall, comprehensive of the boundary frame, to verify that the behavior assumed for the independent fuses actually corresponds to the behavior within the entire frame. Furthermore, full models provide several additional information, like interaction between structural components, lateral capacity, hysteretic behavior and energy-dissipation performance of the wall system.

On the other hand, a complete model of the dissipative wall introduces parameters that complicate the solution and its interpretation; the computational cost also becomes very large. For this reason, only few significant examples are presented here, sufficient anyway to provide relevant findings. The examples are preceded by a general overview of the shear wall features and the modeling techniques employed (Chapter 5.2).

As already mentioned, not every type of fuse is suitable for any shear wall. As a consequence, if 60 different links were installed within the same CFS frame, many would be completely inadequate to guarantee the expected behavior, only a few would be satisfactory and among these the final choice should be made. Chapter 5.3 will present a wall system with evident undesired behavior due to an improper choice of the fuses. Chapter 5.4, on the contrary, will present an example with the expected behavior, discuss the principal results and show the actual feasibility of the innovative seismic system.

5.2 Cold-formed steel frame and modeling

The conventional OSB-sheathed walls, whose experimental results are reported in [8], have been the benchmark for the choice of the frame for the innovative system. This will allow to compare the new with the conventional system, for which extensive information is available. The frames tested in [8] are 4*ft* x 9*ft* (approximately 1.2*m* x 2.7*m*), and utilize 600S162-54 (back-to-back studs) and 600T150-54 (top track) as structural elements (Fig. 5.1). The nomenclature is based on the AISI Standard [30].

The characteristics and dimensions of the frame actually employed are discussed and justified in the following, together with the techniques and simplifications for the finite element modeling.

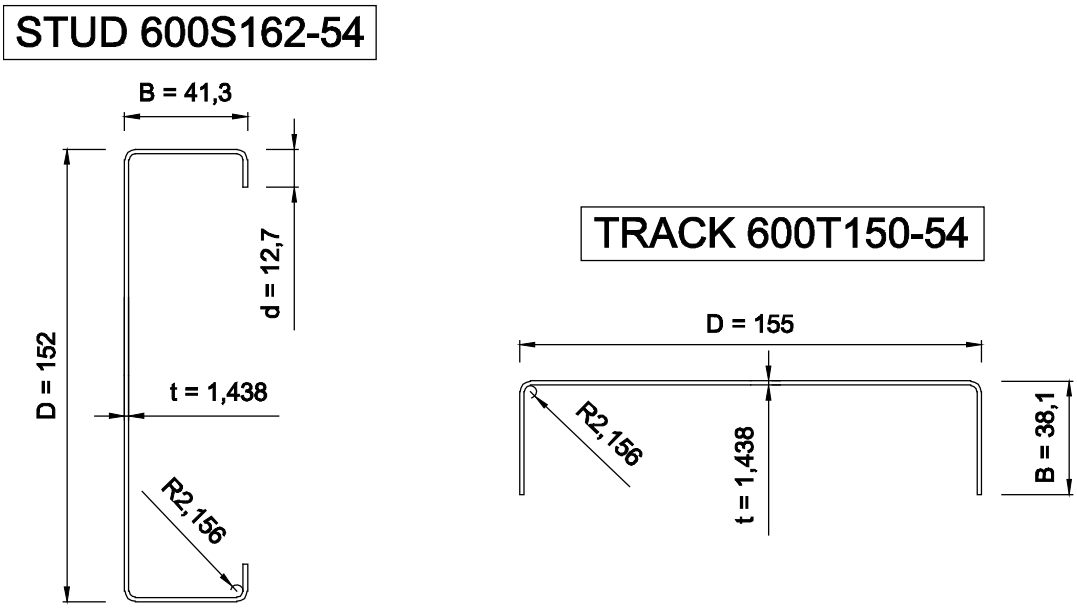

Fig. 5.1 CFS members of the shear walls tested in [8] (dimensions in *mm*)

5.2.1 Wall dimensions

Extremely slender fuses may cause premature instability and ensuing deterioration of the energy-dissipation capacity. As the height b and thickness t of the links is relatively small to limit their bending resistance, the fuse length L should be quite short as well, which forces to choose frames with reduced width w.

A shear wall with $w = 0.7m$ is used for the numerical models, while the height $h = 2.7m$ is maintained equal to the frames presented in [8]. A further reduction of the width is not recommended, to prevent significant amplification of the axial force *N* in the studs (according to Eqn. (3.8)), and to keep the aspect ratio of the wall $\frac{h}{w}$ smaller than 4, as recommended in [11]. It is noticed that the width is computed between the center-lines of the back-to-back studs.

5.2.2 Members of the cold-formed steel frame

The innovative wall system requires strong studs, to resist the significant axial forces induced by seismic action on a quite narrow frame (additional to gravity loads), and to avoid the undesired behavior of Fig. 3.9.

Back-to-back studs 600S200-97 (50*ksi*) are used, which are among the largest employed in the current building practice; the top track 600T200-97 (50*ksi*) is chosen accordingly. Compared to the members shown in Fig. 5.1, these have slightly longer flanges and larger thickness, as can be seen in Fig. 5.2 and Fig. 5.3. These figures provide the actual dimensions according to the AISI Design Manual [34], but the International System of units is used instead). For simplicity, in the numerical models the round corners of the cross sections have been straightened.

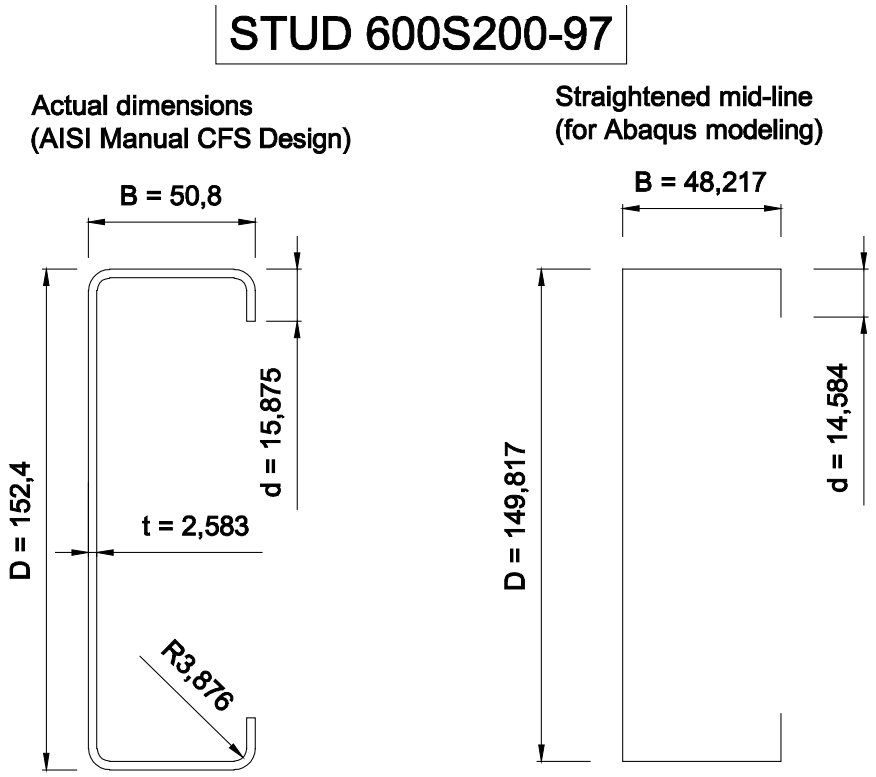

Fig. 5.2 Cross section of the studs used for the innovative shear wall. The actual section is shown on the left, whereas the simplified mid-line for the modeling in on the right (dimensions in mm)

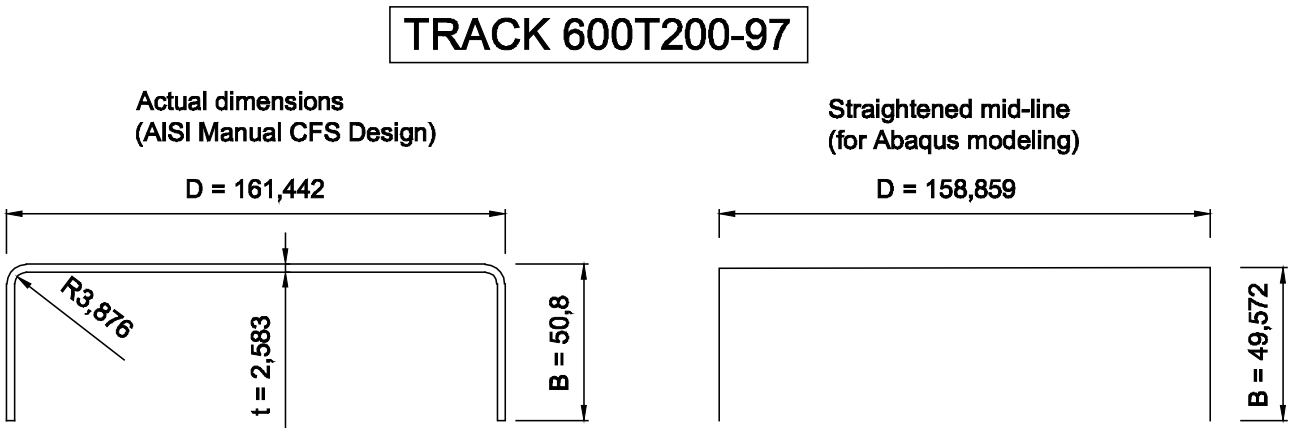

Fig. 5.3 Cross section of the track used for the innovative shear wall. The actual section is shown on the left, whereas the simplified mid-line for the modeling in on the right (dimensions in mm)

5.2.3 Connections and boundary conditions in the models

The chord studs are built-up members made of two 600S200-97 connected together back-to-back: in actual frames, the built-up members are realized by screw-connecting their webs together. However, to accurately reproduce such constraint in the models, flexible springs may be required and their stiffness needs to be calibrated, which would introduce additional uncertainty.

To avoid this, the entire webs have been tied together in Abaqus (using constraint type *tie*). Such choice is not conservative because introduces composite bending action of the webs (equivalent to a single web with double thickness) and prevents their eventual local buckling. However, it is justified as the

main focus of the models is not to investigate the local behavior of the studs but the fuse deformation and the overall performance of the wall.

As mentioned in Chapter 3.6, the frame is not allowed to rock because conventional hold-down fasteners (moment-resisting connectors) fix the studs to the foundation. The shear walls described in [8] make use of Simpson Strong-Tie® S/HDU6 hold-downs. To model such connectors, fixed boundary conditions have been applied, on the inward face at the bottom of the chord studs, to a surface approximately equal to the hold-down surface (Fig. 5.4).

As in actual buildings the floors or roof prevents out-of-plane displacements of the shear walls, the track has been restrained against transverse displacements, to force in-plane behavior of the system. The connection of the studs to the top track is assumed to be a moment-resisting joint, and is therefore modeled by means of a tie-constraint.

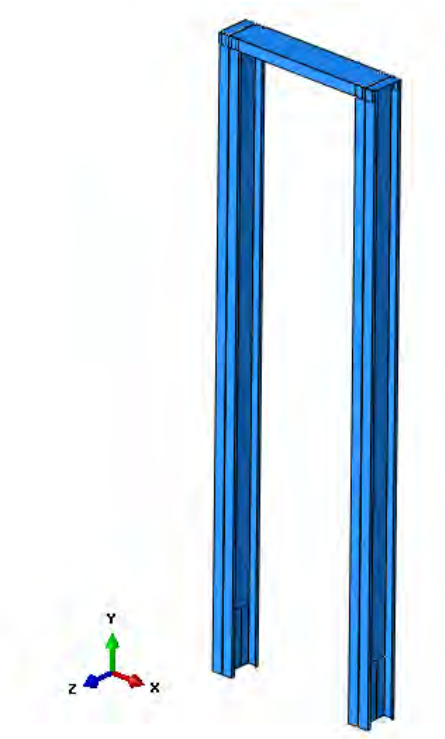

Fig. 5.4 Model of the cold-formed steel frame without fuses

5.2.4 Finite element mesh

Cold-formed steel members have very small thickness compared to other dimensions, and shell elements are therefore reasonable to create the finite element mesh. S4R Abaqus elements [32], with four nodes and reduced-integration scheme, are used (see Fig. 4.6). At least two elements are required along the lips of the studs, to catch their eventual local buckling; in order to maintain similar dimensions for all the other elements and keep the aspect ratio close to one, 4 elements are used along the flanges, 12 along the web and 225 along the height of the studs (Fig. 5.5a). Analogue element dimension has been used for the track (Fig. 5.5b). The material model is elastic-perfectly plastic (Fig. 4.8), with yielding stress $\sigma_y = 345MPa\ (\simeq 50ksi)$.

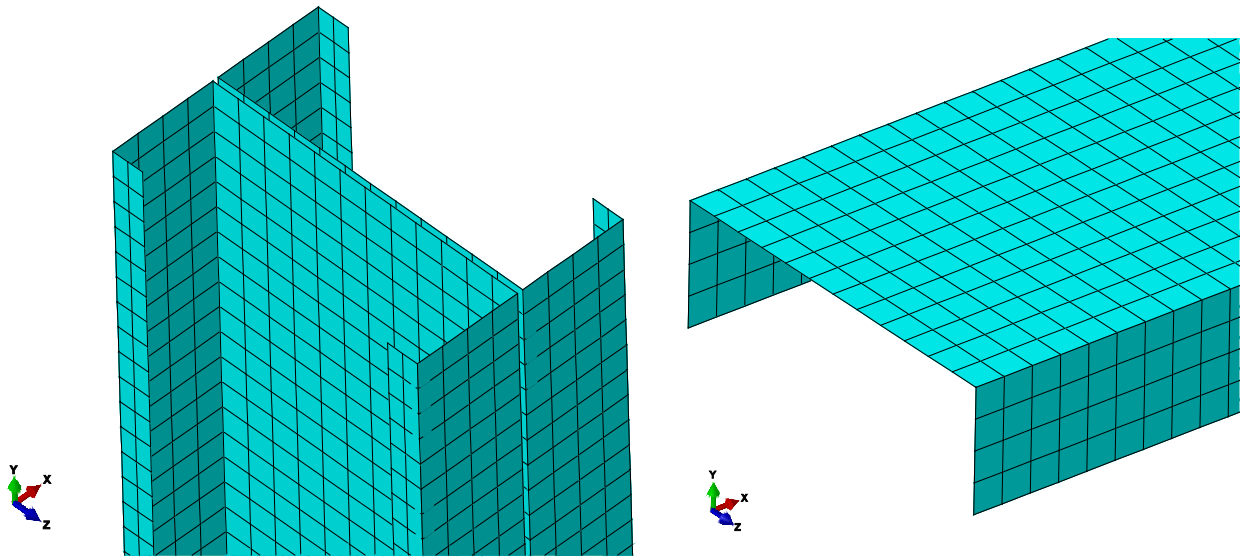

(a) (b)

Fig. 5.5 Finite element mesh of the back-to-back studs (a) and track (b)

5.2.5 Loading protocol and response of the frame

The FEMA loading protocol, already introduced in Chapter 4.4, is applied to the frame in displacement-control; this is done by imposing the proper displacement history along the x-axis to all nodes of the end cross-section of the track. Any loading eccentricity is therefore prevented.

As the bare frame provides the contribution F_{frame} to the overall shear-wall capacity $\overline{F}_{wall}$ (according to Eqn. (3.12)), the FEMA protocol has been first applied to the CFS frame without fuses, in order to estimate F_{frame}. This allows to separate the contribution of the frame from the contribution of the internal links in the calculation of $\overline{F}_{wall}$. The time history of F for the bare frame is shown in Fig. 5.6, where the last two blue peaks correspond to a lateral drift of 2.5%.

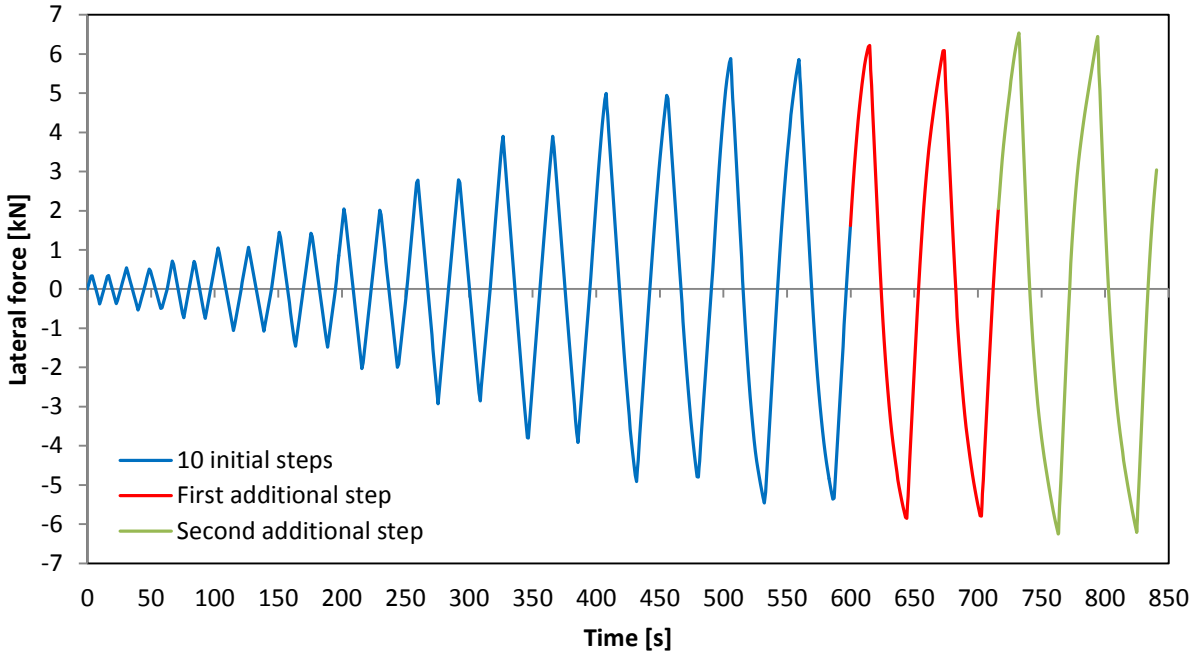

Fig. 5.6 Time history of the lateral force in the CFS frame

5.2.6 Fuse links and connections to the studs

To model the entire wall system, the fuse links need to be added to the frame and connected to the chord studs: details for modeling and mesh of the links can be found in Chapter 4. A central aspect remains their connection to the studs, because it affects the fuse bending behavior and ensuing yielding and energy dissipation. However, since the connection detailing is not the main object of the thesis, a very basic solution has been adopted in the numerical modeling; this type of connection will guarantee the desired behavior only for specific fuse dimensions.

The end section of the fuse side plates are connected to the web of the studs, by means of a tie-constraint which allows for moment-transfer (Fig. 5.7). This solution is simple to model and maintains the entire fuse within the central plane of the shear wall, but is certainly not optimal for practical constructability because the small out-of-plane bending resistance of the web may induce localized deformation in the studs.

A more extensive discussion on the connection choice can be found in the next paragraph and Chapter 6.

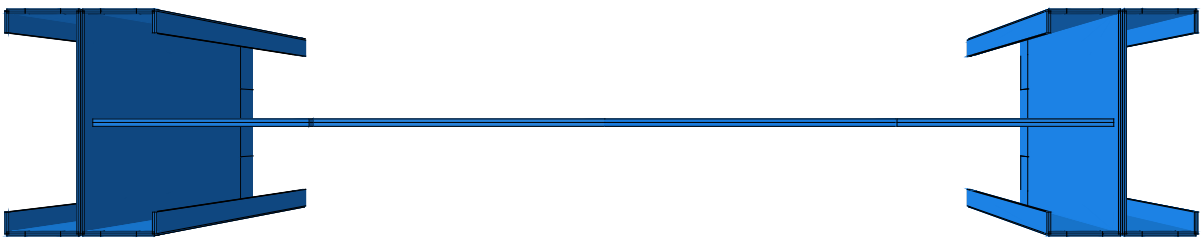

Fig. 5.7 Connection of the fuses to the web of the studs

5.3 Undesired behavior of the wall system

In the single fuse models described in Chapter 4.2.2, the side plates have been loaded with a rotation φ equal to the inclination of the studs (and to the wall drift Δ, according to Eqn. (4.2)). However, this is reasonable only if the links are much more flexible than the studs thus attracting all the deformation (Fig. 3.7).

In actual shear walls, the studs are thin structural members with limited resistance, and may locally deform due the not-negligible bending resistance offered by the fuses. The rotation of the side plates is therefore lower than the theoretical value:

$$\varphi(t) < \Delta(t) \tag{5.1}$$

In extreme cases where the links have very large bending resistance, they remain completely straight acting as rigid bodies between the studs (Fig. 3.9):

$$\varphi(t) = 0 \tag{5.2}$$

Such behavior is obviously undesired because not associated with energy dissipation and not beneficial to the seismic performance of the wall. The damage would affect the main structural members instead of the designated links.

This explains why not any type of fuse is suitable for any frame. To make a practical example, fuses with the following properties have been used in the entire wall model:

$L = 200\ mm$
$b = 75\ mm$
$t = 7\ mm$
$\sigma_y = 180\ MPa$

The dimensions above correspond to the fuse No. 11 in Table 4.1, which has bending resistance rather larger than most of the other specimens analyzed. Such bending capacity is also larger than the out-of-plane resistance of the stud webs, and the consequence is shown in Fig. 5.8. The rotation of the side plates is prevented by the resistance of the links, which cannot deform and yield; the studs, instead, are the weak component of the wall and suffer extensive deformation and damage.

In the model of the entire wall system, the rotation history $\varphi(t)$ almost corresponds to Eqn. (5.2), as Fig. 5.9 shows (the theoretical rotation history $\varphi(t) = \Delta(t)$ is also included for comparison). This example represents the worst-case scenario, but analogue results can be obtained with several other fuses listed in Table 4.1. More generally, an intermediate behavior defined by Eqn. (5.1) occurs, where the deformation is shared between fuse and stud according to their relative capacity.

It should be noticed, however, that the undesired deformation of Fig. 5.8 does not depend only on the bending resistance of the fuses, but also on their connection to the web of the studs. A better response could be achieved with a different connection detailing; for instance, attaching the fuses to the flanges

of the studs would exploit the in-plane bending capacity of the flanges, which is larger than the out-of-plane capacity of the web.

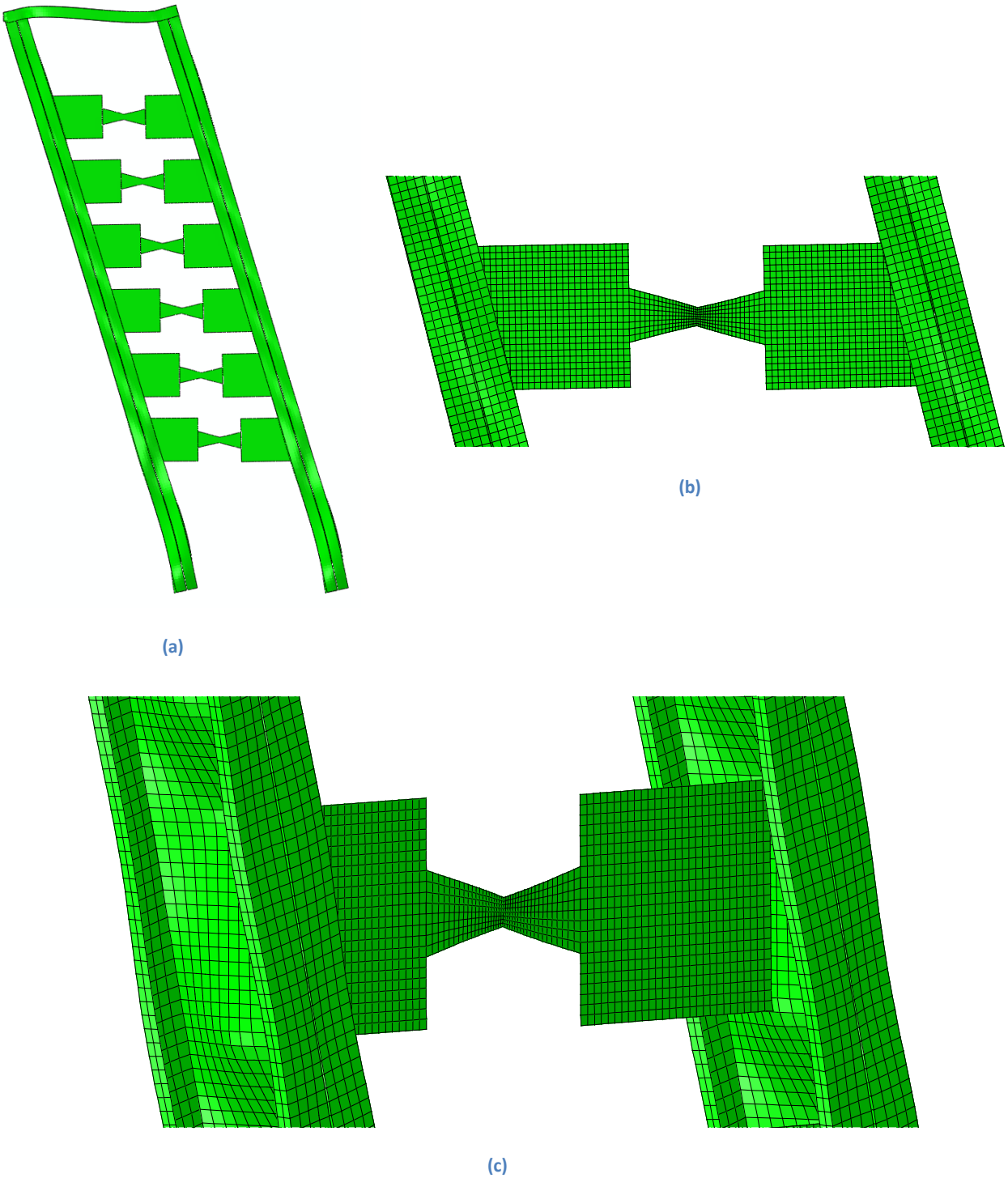

Fig. 5.8 Undesired behavior of the wall (deformation scale = 20). (a) overall deformation; (b) detail of an undeformed fuse; (c) detail of local deformation in the studs

If a different detailing allowed to attach the fuses to the flanges instead, a better response would be expected due to the larger in-plane bending capacity of the flanges, compared to the out-of-plane capacity of the web. To conclude, the undesired behavior described above is a combination of improper

choice of fuse dimensions and connection detail. Even maintaining the same type of fuse, the deformation behavior of the wall system would improve with a better connection.

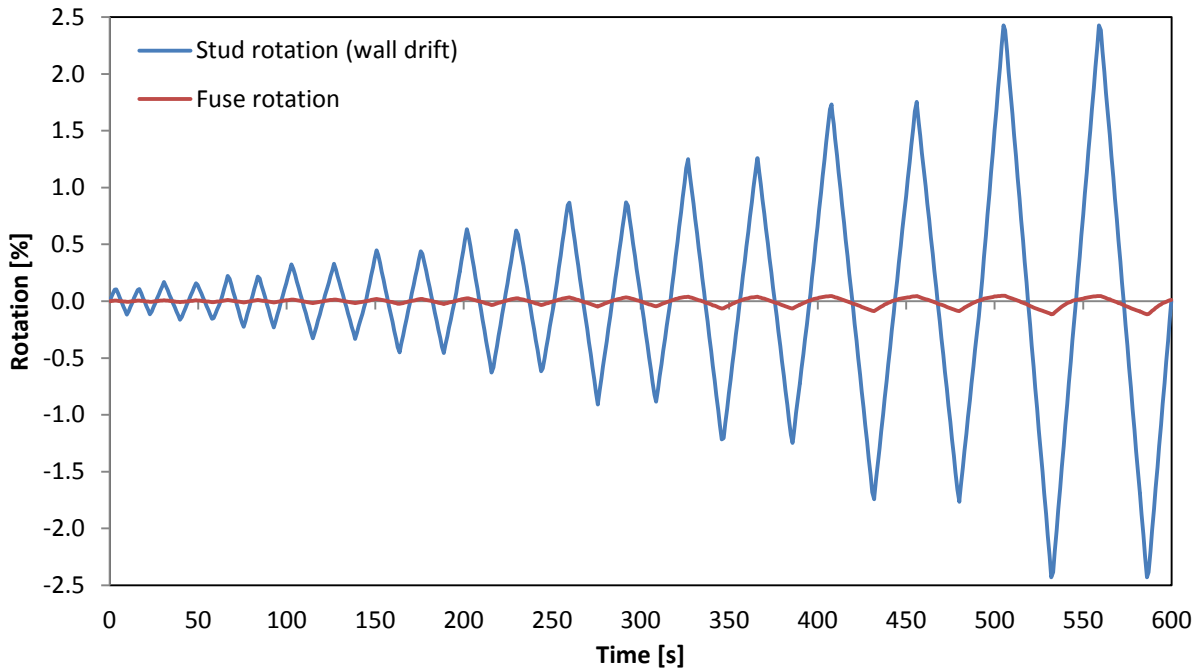

Fig. 5.9 Comparison between the theoretical and actual rotation history of the fuses

5.4 Expected behavior of the wall system and main results

The previous paragraph has illustrated the importance of the choice of fuse dimensions, in relation to the studs. This paragraph presents an example where, even maintaining the same connection to the web of the studs, the expected behavior of the wall is achieved by different fuses.

The fuse chosen is the No. 53 in Table 4.1, whose principal parameters are reported below:

$L = 400\ mm$
$b = 60\ mm$
$t = 7\ mm$
$\sigma_y = 180\ MPa$

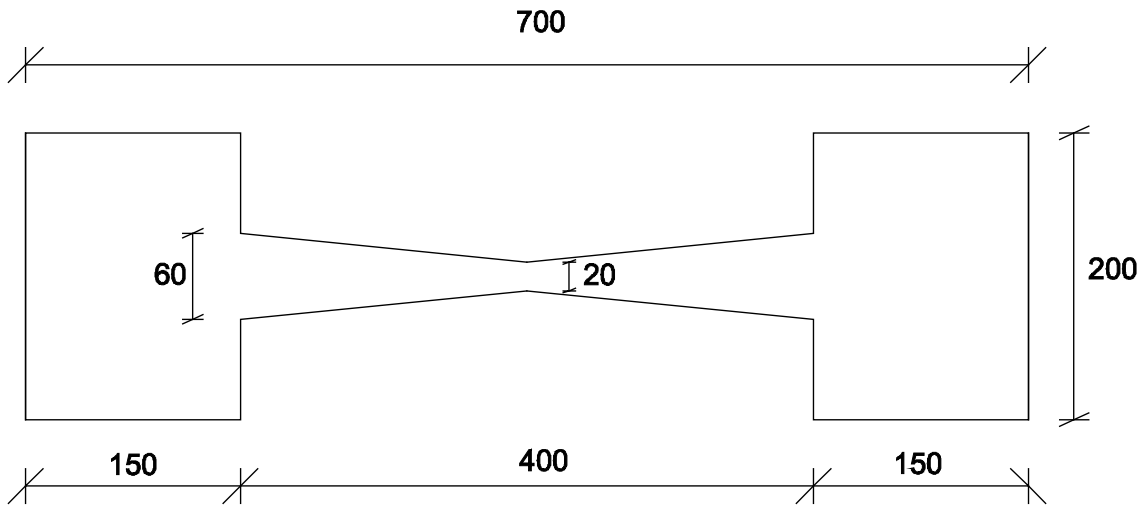

Fig. 5.10 Fuse used for the entire wall system (dimensions in *mm*)

The fuse link is flanked by two side plates which cover the distance necessary to reach the studs:

$$L_{plate} = \frac{w - L}{2} = 150mm \tag{5.3}$$

To provide sufficient lateral capacity to the shear wall (similar to the capacity of the walls tested in [8]), multiple links are installed throughout the height of the frame. The following example makes use of 9 fuses, attached for simplicity to the web of the studs (Fig. 5.11). Although this type of connection is generally not optimal, as previously discussed, here does not give any particular problem. No fuses are installed at the very bottom of the studs where their inclination is negligible due to the presence of the hold-downs.

It is noted from the outset that fuses with different dimensions could have been used to achieve the same or similar results. However, a single example is deemed to be sufficient to demonstrate that the innovative dissipative wall can actually perform well and be an effective alternative to conventional seismic systems.

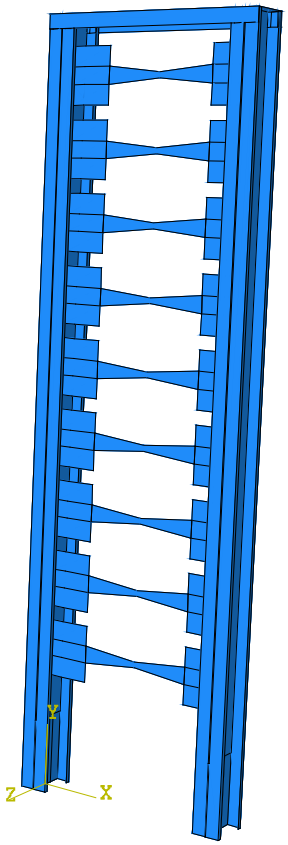

Fig. 5.11 Model of shear wall with 9 fuses

The most relevant parameters provided by the numerical analyses are:

- the lateral force F ;
- the shear force V in the fuse links;
- the rotation φ of the side plates;
- the drift Δ_{cr} at which buckling begins.

The lateral displacement u of the frame is given in input (see FEMA protocol in Fig. 4.3), and the wall drift Δ is immediately calculated:

$$\Delta[\%] = \frac{u}{h} \cdot 100\% \tag{5.4}$$

The lateral capacity of the shear wall is an important design parameter because provides information on the maximum seismic action the wall can sustain. In fact, it is normally one of the first parameter to decide, as the flow-chart in Fig. 3.8 indicates. Analyzing the statics of the wall system has led to the Eqn. (3.12) for estimation of the capacity $\bar{F}_{wall}$; such formula provides the following result:

$$\bar{F}_{wall}\left(analytical\right) = F_{frame} + n_{fuse} \cdot \frac{\bar{V}_{fuse} \cdot w}{h} = \left(6 + 9 \cdot \frac{5.04 \cdot 0.7}{2.7}\right) kN = 17.8 kN$$

where $F_{frame} = 6kN$ has been determined from Fig. 5.6, at the time instant of the peak of the total lateral force.

The capacity measured in the numerical model is:

$$\bar{F}_{wall}\left(numerical\right)=18.8kN$$

which is very close to the estimated value (the relative difference is approximately 5%). The same comparison has been made for a few other models (not reported here) where again $\bar{F}_{wall}\left(numerical\right)$ is about 5% larger than $\bar{F}_{wall}\left(analytical\right)$. This suggests that the approximate formula described by Eqn. (3.12) provides a satisfactory estimation of the lateral capacity (on the safe side), and may be used for a preliminary choice of number and size of fuse links.

Fig. 5.12 shows the time-history of the total force during the FEMA protocol: it can be seen that the maximum force is well approximated by the preliminary estimation (red horizontal lines).

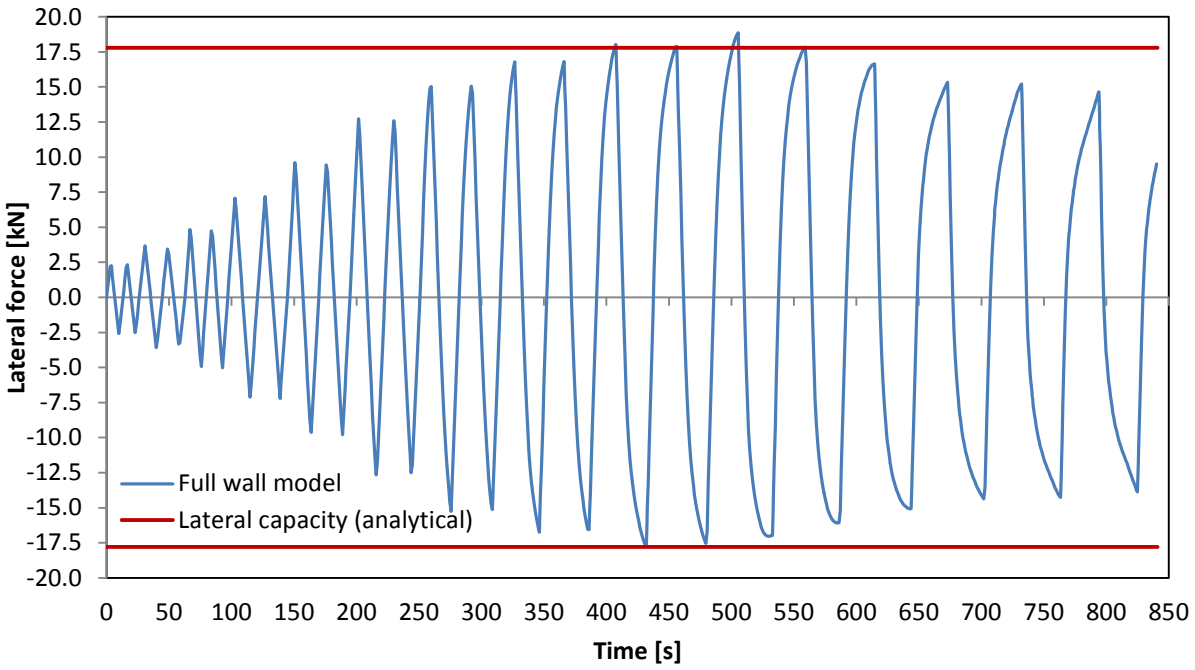

Fig. 5.12 Time-history of the lateral force of the wall

The parametric study of the single models has already verified the analytical formula for the shear capacity of the fuses. For the dimensions used in this example, the expected shear capacity is:

$$\bar{V}_{fuse}(analytical)=\frac{4}{9}\frac{t\,b^2\sigma_y}{L}=5.04kN$$

which corresponds exactly to the value measured in the numerical simulation:

$$\bar{V}_{fuse}(numerical)=5.04kN$$

This can be seen also in Fig. 5.13, showing the time-history of the shear force in one of the central links.

As already mentioned, connecting the fuses to the web of the studs is not optimal as may cause local deformation in the studs and smaller (or negligible) deformation in the links. In the present example,

this causes a delay in the development of the shear force and yielding of the fuses, consequence of a smaller rotation of the side plates compared to the theoretical expression given by Eqn. (4.2).

Fig. 5.14 shows that, in the first cycles with small drift, the rotation φ is smaller than the wall drift Δ (Eqn. (5.1) applies). This is reflected by the time-history of the shear force, which in the first cycles is smaller than the correspondent values obtained in the single model (Fig. 5.15).

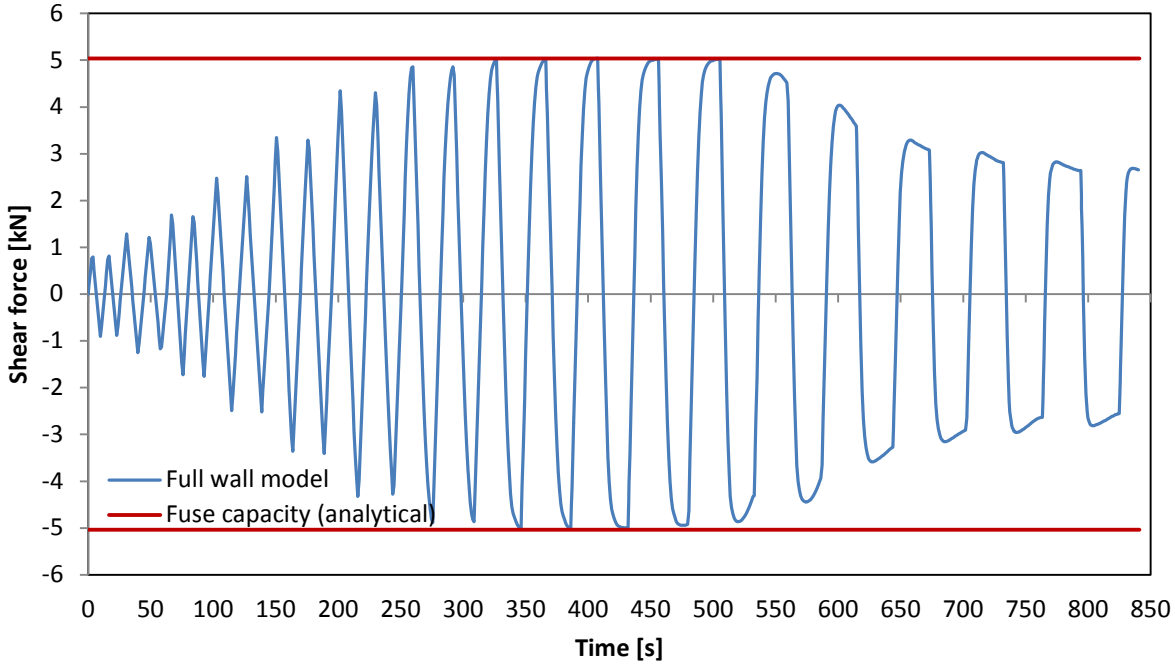

Fig. 5.13 Time history of the shear force in the fuses, computed in the full model

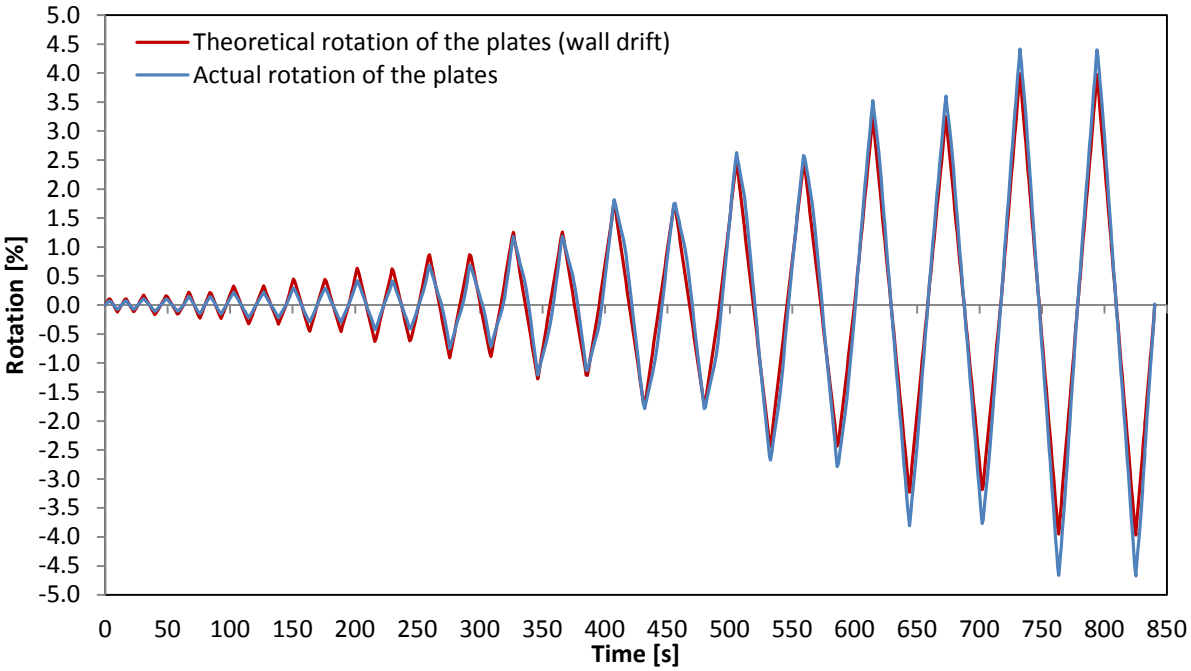

Fig. 5.14 Comparison between the theoretical rotation of the plates (if the fuses have negligible resistance) and the actual rotation computed in the numerical model

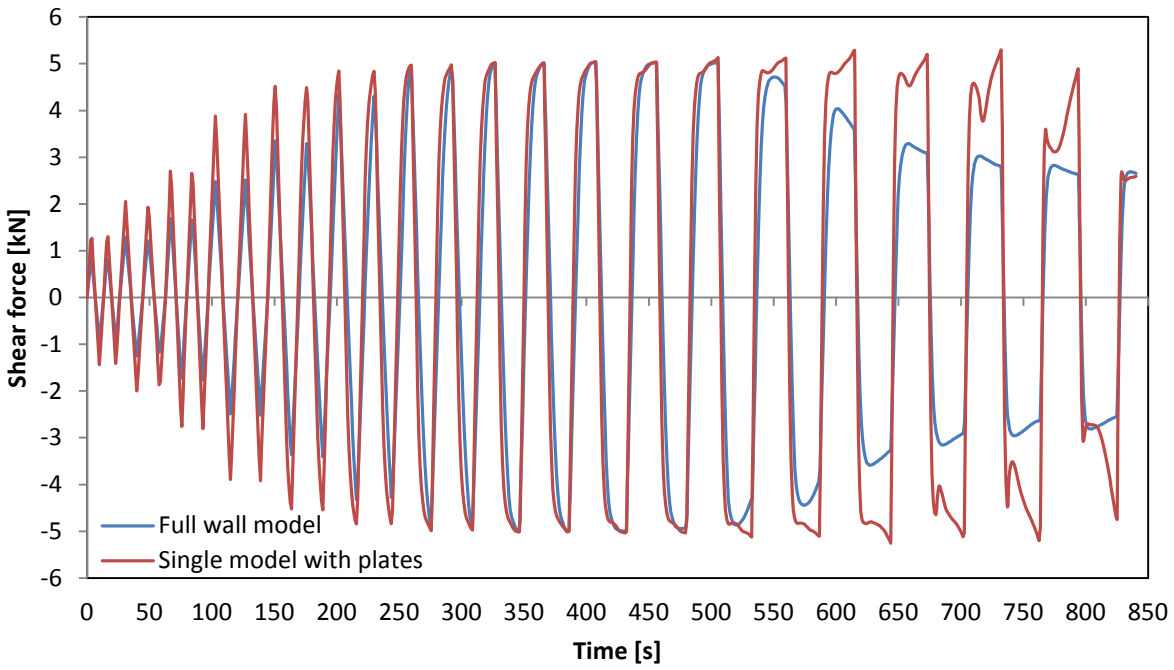

Fig. 5.15 Comparison between the fuse shear force computed in the full model and in the single model with side plates

The previous findings are relevant, but to evaluate the performance of the wall system and its dissipation capacity the overall hysteretic behavior has to be analyzed (Fig. 5.16). At first glance, one can immediately notice that the loops are fat and stable up to a drift of 2-2.5%; then, some pinching occurs due to fuse buckling, but the decrease of capacity is not dramatic. As the area enveloped by the hysteretic curves represents the energy dissipated by the system, the seismic performance seems to be very good.

With regard to the critical drift, the single models estimated $\Delta_{cr} = 2.5\%$ for this type of fuses; in the full model, the criterion of negative stiffness (Chapter 4.5.4) suggest that the unstable behavior already begins in the previous step $\left(\Delta_{cr} = 1.79\%\right)$, but until 2.5% no significant out-of-plane displacements are observed. Also from the hysteretic curve it can be seen that the maximum capacity is reached at 2.5% and only in the next cycles pinching becomes evident. Thus, the critical drift of the fuses, estimated by the parametric study, provides at least an approximate value for evaluating the beginning of instability in the entire wall.

However, a good performance of the wall system does not depend only on the buckling drift (that should be sufficiently large to maintain stable dissipation behavior for several loading cycles), but also on the drift at which the fuses start to yield. In fact, such drift marks the beginning of the energy dissipation. A very small yielding drift is not positive because the fuses may yield under very small seismic events which do not normally require any specific energy-dissipation device; furthermore, the fuses should be substituted quite often, which is not sustainable from a practical and economical perspective.

On the other hand, if the fuses start to yield too late, the energy dissipation is also delayed and this is detrimental to the structural integrity. In fact, as the links remain elastic during several loading cycles, it is the rest of the frame (studs, hold-downs, etc.) to undergo plastic deformation causing irreversible damage to the structure.

There is not an optimal value for the yielding drift of the wall: sound judgment may suggest a target Δ_y between 0.5% and 1%, but this does not apply to all possible design situations. An approximate estimation of the yielding drift of the fuses is given by Eqn.(4.13), while Eqn. (4.14) provides the corresponding drift of the wall. For the fuses considered in this example:

$$\Delta_y = 0.34\%$$

However, this is valid only for links with negligible flexural resistance. In practice, the actual rotation of the fuses is smaller than the theoretical Eqn. (4.2), and yielding is delayed. In the present example, first yielding occurs approximately at $\Delta = 0.5\%$, which is also shown by Fig. 5.16.

The actual deformation behavior of the shear wall during the simulation is shown in Fig. 5.17, where in the red areas the yielding stress has been reached (plasticity). It can be seen that, as expected, the plastic deformation is concentrated in the links and is associated to their bending behavior. The rest of the structure remains undamaged, except for small areas in the track, in proximity to the connection to the studs. However, this is due to the rigid joints and to the fact that the displacement is locally applied to the track; in actual frames this effect should be smaller and not affect the global performance.

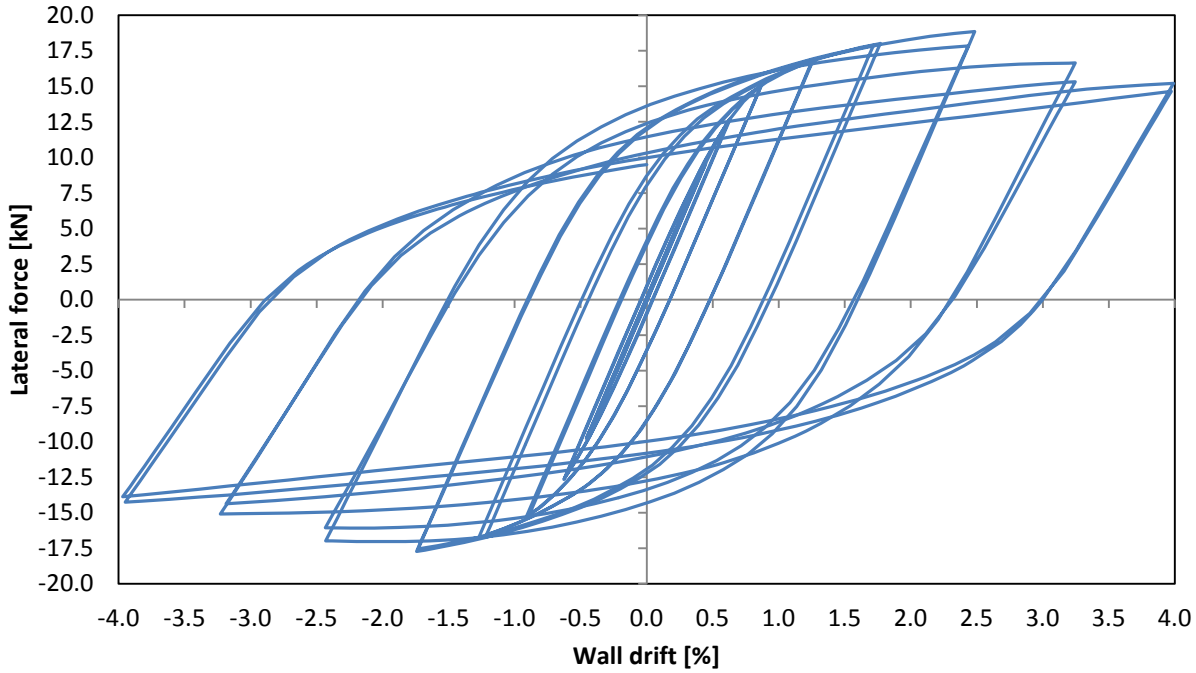

Fig. 5.16 Hysteretic behavior of the entire shear wall with fuses

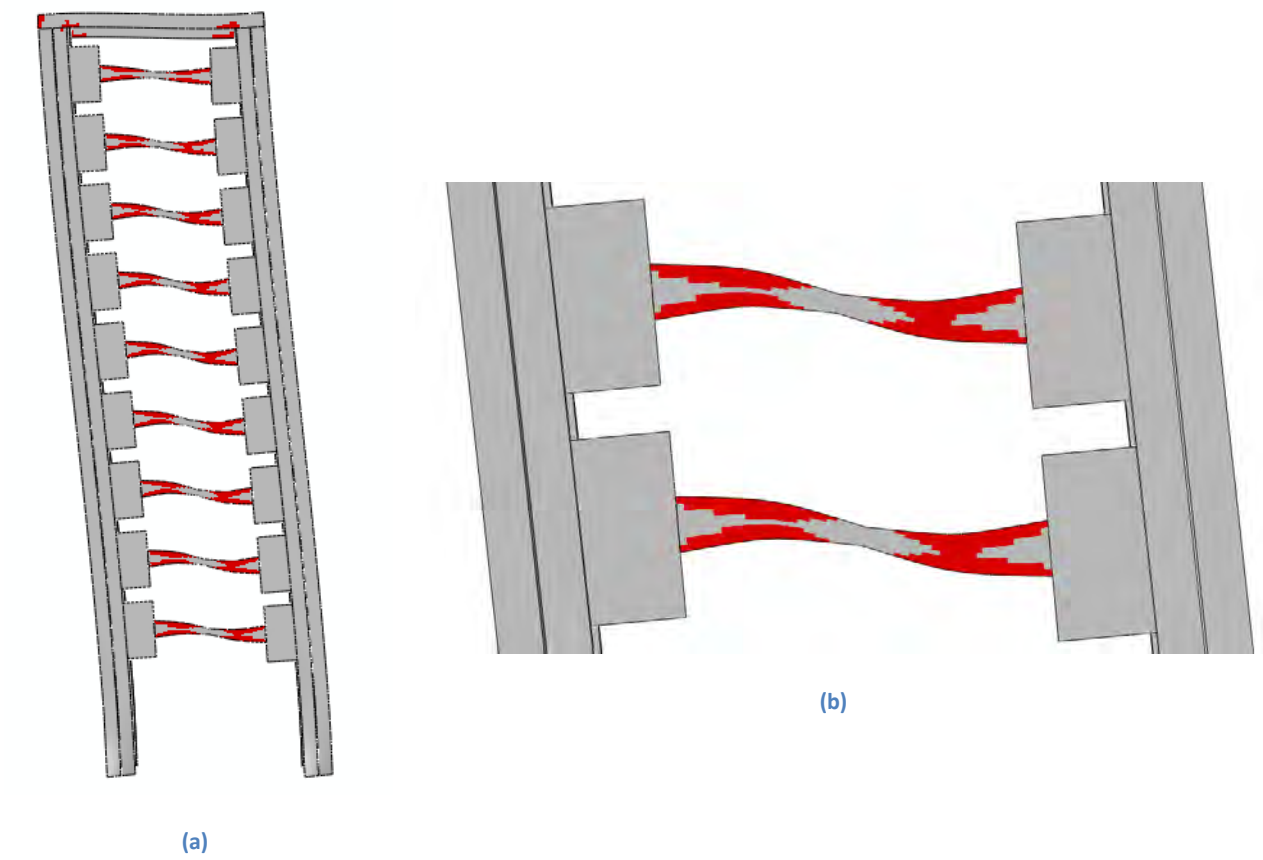

(a) (b)

Fig. 5.17 Deformation behavior of the shear wall: red areas indicates plasticity (deformation scale factor=5). (a) Entire wall; (b) detail of 2 fuse links

The main objective of the thesis is to demonstrate, at least in a preliminary stage, that the cold-formed steel frame with integrated fuses has a better seismic performance, in terms of energy-dissipation, than the conventional seismic systems for CFS structures (in particular the frames sheathed with wooden panels). For this purpose, the hysteretic behavior of the two systems have to be compared.

The frame used in the previous numerical model is similar to the one employed by the conventional shear walls whose experimental results are reported in [8]. The two frames are not identical, as indicated in Chapter 5.2, but the comparison is still significant to evaluate the different seismic performances. In fact, the OSB and the fuses provide, one for each system, the most of the total stiffness and lateral capacity.

The shear wall considered for the following comparison is the specimen No.2 according to [8], which only makes use of 7/16 inches OSB (approximately 11mm) at the front side of the wall (Fig. 5.18). The OSB is attached to the studs and track with flat-head fasteners.

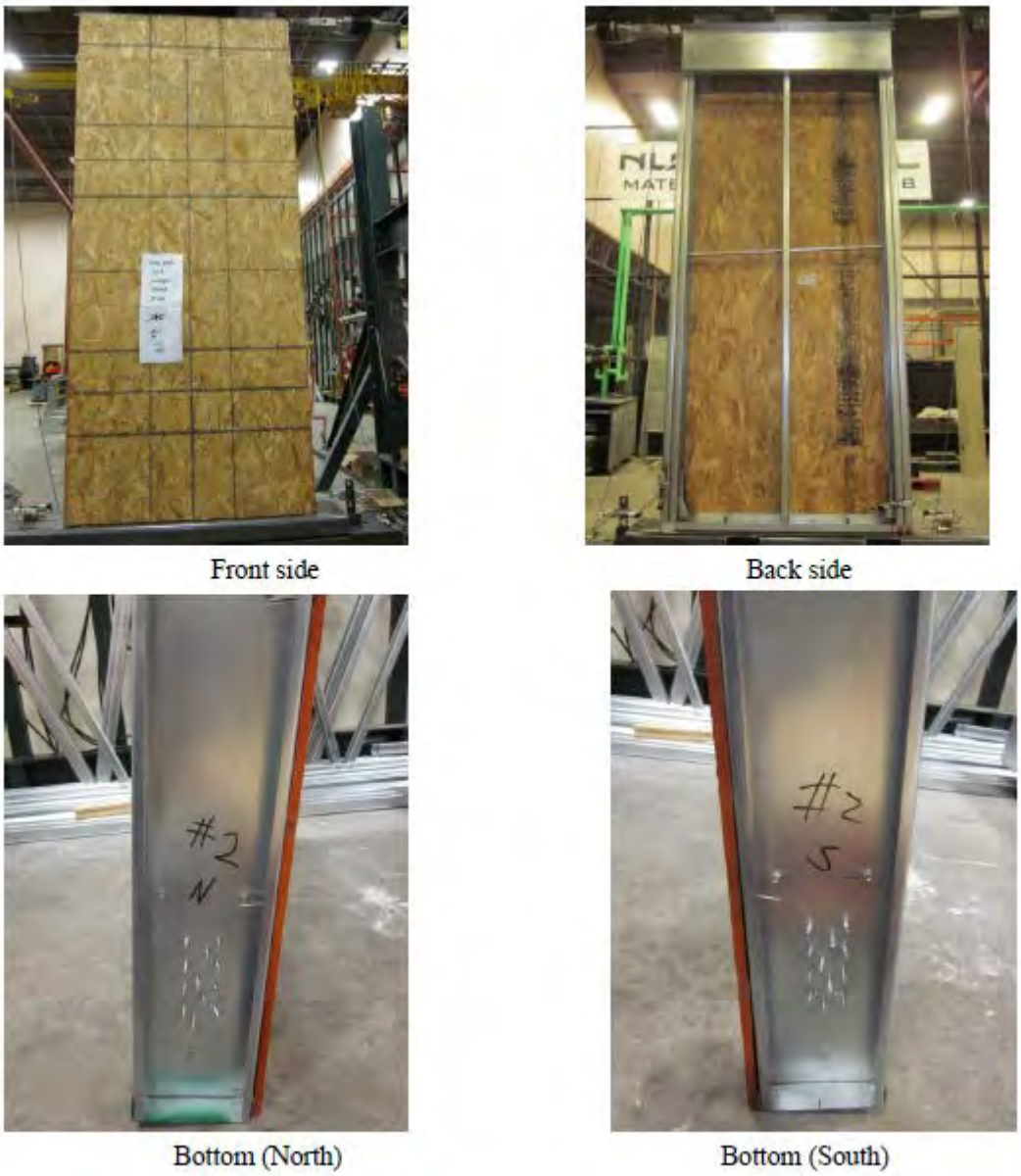

Fig. 5.18 Conventional shear wall with OSB sheathing (specimen No.2, from [8])

The comparison described in the following should be mainly interpreted from a qualitative perspective, because numerical results (with all their inherent limitations) are compared to experimental results, which include several variables not accounted for in the simulation. Secondly, the CFS frames used for the two wall systems are not the exactly the same and also the loading protocol is different, although similar maximum drift are applied.

The hysteretic curves of the two systems are shown in Fig. 5.19. It can be seen that the initial stiffness is similar in the two cases, although the wall with fuses can reach earlier a larger capacity. The main difference is associated to the deformation mechanism and development of damage. The wall with OSB sustains most of the seismic action through the rigid wooden panel that transfers the load to the CFS by means of fasteners. This allows to carry a significant force, but when the applied drift returns to zero almost no force is left in the system, as the ODB acts almost as a rigid body: as a consequence, the hysteretic loops are narrow and the energy dissipated is small. When, eventually, brittle failure occurs in

the connections (see Fig. 2.1), the reduction of capacity is quite dramatic, and the loops becomes even narrower.

On the contrary, the wall with fuses sustains most of the seismic action through shear and bending of the links, which are therefore the lateral-force resisting devices. Early plastic deformation of the fuses makes the system capable of carrying a residual force even when the drift is back to zero: the hysteretic cycles are therefore large and a lot of energy can be dissipated by yielding. When instability occurs in the links, the total capacity decreases, but the fuses can still absorb plastic energy although with a less stable mechanism. The overall dissipated energy, proportional to the area enclosed by the curves, is much larger in this system because there is significant force in the second and fourth quadrant of the load-drift diagram.

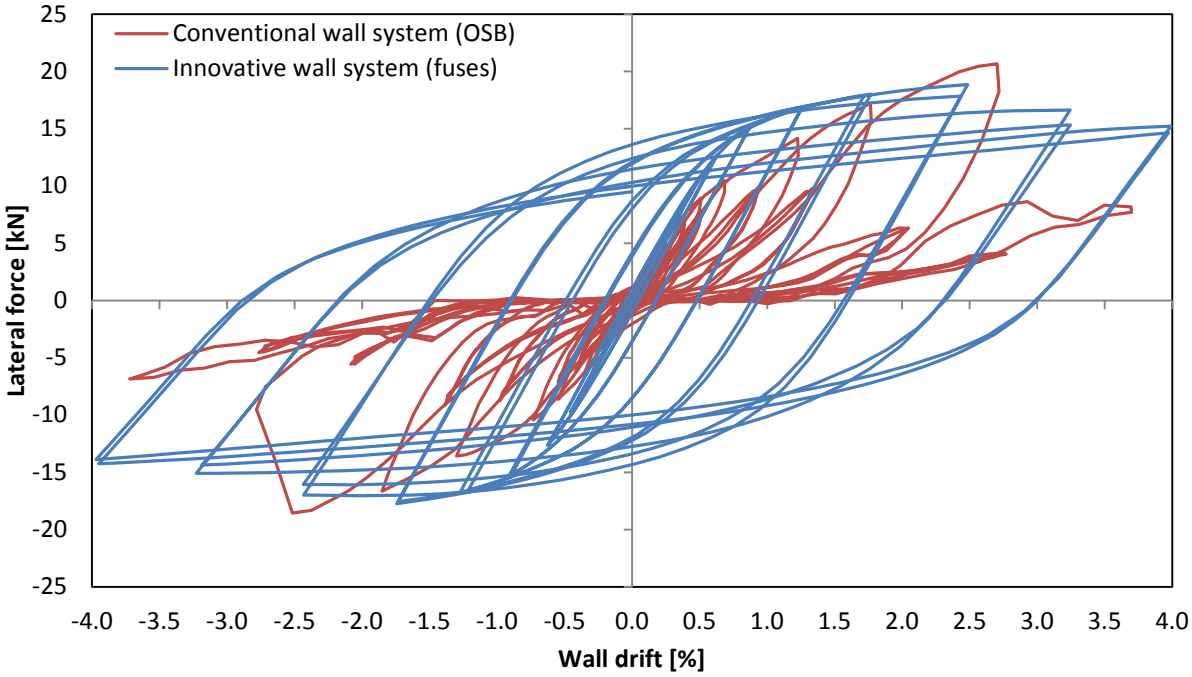

Fig. 5.19 **Hysteretic behavior of the wall system with fuses and comparison with the conventional OSB-sheathed frame (the hysteretic curve for the conventional wall system has been reproduced from [8], with permission)**

The shear wall with integrated steel fuses may therefore provide an effective alternative to conventional OSB-sheathed frames. Stiffness and capacity analogue or larger than the conventional walls can be achieved by a proper choice of number and dimensions of the links. The energy dissipation is much larger for the innovative system, which improves the overall performance of the building and prevents extensive damage in the main structural elements. Finally, the possibility of replacing the damaged devices should guarantee a more sustainable and cost-effective building solution.

Although promising, this is only preliminary research with many limitations, and needs to be further validated by additional investigations. The next Chapter, together with a summary of the work carried out, emphasizes once more the simplifications introduced, which may be gradually eliminated in updated models; furthermore, directions for future work are provided.

Chapter 6

Conclusions

6.1 Final remarks

The Thesis has presented an innovative shear wall for cold-formed steel buildings, employing structural fuses to dissipate the seismic energy by means of metal yielding. The fuses consist of butterfly-shaped thin beams (links) which are installed between the vertical studs of CFS framings. The lateral deformation of the frame induces inclination of the studs and flexural deformation in the attached fuse links. If properly designed, the links have smaller bending resistance than the studs, thus attracting almost all deformation. For this purpose, low-yield steel is a good material choice. The bending behavior of the fuses develops yielding and ensuing energy dissipation in the early phases of earthquakes. The shape of the links is optimized to guarantee uniform yielding along their length and maximize dissipation. Extensive yielding in the fuses should prevent or at least reduce inelastic deformation in the rest of the shear wall; in this way, after significant earthquakes, the main structure should remain undamaged while the fuses can be easily replaced. This should allow continued occupancy of the building and limited repair effort.

Other than improving the energy dissipation performance of the building, the fuses provide stiffness and lateral resistance to the structure. These important design parameters can be adjusted by choosing number and size of links. For this purpose, simple analytical formulas have been derived to determine the capacity of the single links and the lateral capacity of the entire wall. Finite element analyses of 60 fuses (separate from the CFS frame) with different parameters have then been performed to control the accuracy of such formulas and provide additional design information. In these analyses, it has been applied to the links the same cyclic loading they are expected to undergo when installed within the actual frame. The reliability of the formulas has been verified, and their application can be therefore extended beyond the fuses considered in the parametric study. The out-of-plane behavior of the links, associated to buckling, has also been investigated, because it significantly affects the energy-dissipation performance of the system. An approximate formula to estimate the drift at which fuses start to buckle has been proposed: the critical drift of the shear wall can therefore be evaluated and apposite links can be used to guarantee a stable behavior up to a targeted drift.

Finally, the overall behavior of the shear wall with fuses has been simulated by means of models of the entire system. Most of the results predicted by the analytical formulas and single models have been confirmed. The hysteretic behavior and seismic performance of the proposed system is significantly better than the conventional CFS frames sheathed with wooden panels: the total energy dissipation is larger, and concentrated in the fuse devices. These results suggest the possible applicability of the innovative seismic system in the construction industry.

6.2 Simplifications and limitations

Dimensions and properties of the cold-formed steel frame determine the range of fuses suitable for installation within the seismic system. The Thesis has considered only a single type of CFS frame, and the range of fuses analyzed has been chosen to fit this specific wall: this has been sufficient to prove the potential feasibility of the seismic system.

However, any frame configuration and CFS members could be employed, and for this purpose design criteria should be defined to guide the choice of fuses. In fact, using improper fuse dimensions may lead to undesired behavior for the entire system, where the studs become the weak component and deform instead of the links.

One of the key choices for the analysis and design of the seismic wall is the detailing of the connection between the fuses and the studs. To keep the models simple, the fuses have been attached to the web of the studs: this can be realized in practice by angular profiles (Fig. 6.1a). However, this choice turned out to be inconvenient due to excessive out-of-plane flexibility of the webs, which may be smaller than the links; in such case, inelastic deformation would be localized in the studs and the fuses would not work properly, because cannot yield and dissipate energy. Only a narrow range of link dimensions still allows the desired deformation behavior. A possible improvement is to detail the connection so as to attach the fuses to the flanges of the stud (Fig. 6.1b shows a very schematic connection configuration). The flanges have in fact in-plane bending resistance significantly larger than the out-of-plane resistance of the webs. This updated connection type is expected to generally avoid localized plasticity in the studs and keep inelastic deformation within the links. Another alternative, which avoids the use of specifically designed connection profiles, consists in changing the orientation of the CFS studs (Fig. 6.1c): in this way, the fuse links can be easily connected parallel to the web of the studs, exploiting their larger in-plane resistance. However, these are just a few schematic proposals that need to be further addressed, also taking into account the cost and ease of construction.

Other simplifications in the finite element analyses regard the modeling of the built-up members (chord studs), because the entire web surfaces have been tied together instead of modeling the discontinuous and punctual fasteners actually employed. Furthermore, the connection to the foundation by means of hold-downs has been assumed completely fixed; same for the stud-track joints. For both the CFS frame and the fuses, elastic-perfectly plastic material model has been used, which neglects hardening effects and eventual fracture, the latter particularly relevant for cyclic loading due to effect of fatigue.

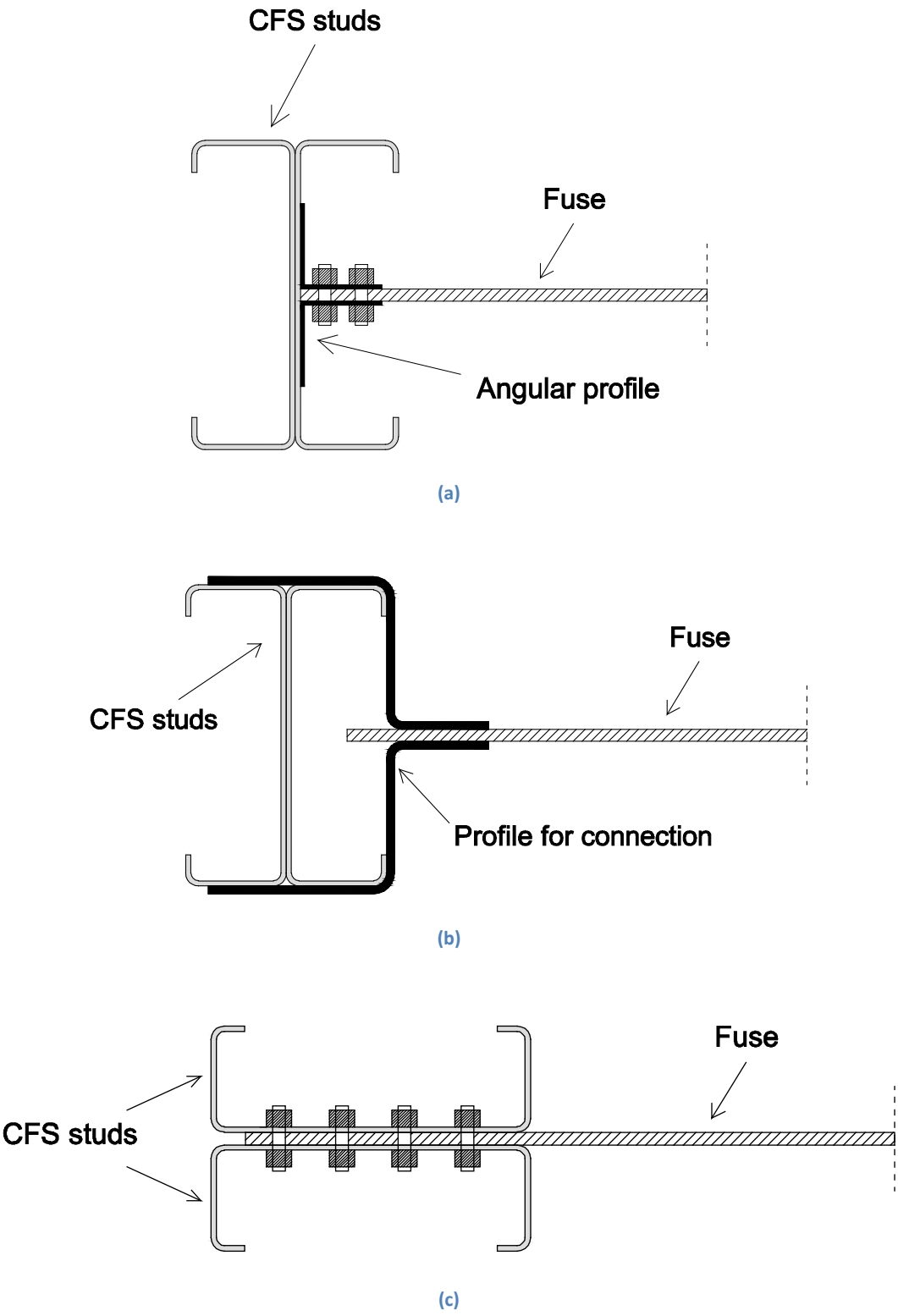

Fig. 6.1 Schematics for different fuse-to-stud connection proposals (top view): (a) fuse connected perpendicular to the web of the studs by means of angular profiles; (b) fuse connected to the flanges of the studs by a properly designed profile; (c) alternative orientation of the CFS studs in order to exploit the in-plane capacity of the web of the studs.

6.3 Future research

The Thesis represents an exploratory and preliminary work towards the development of the seismic system presented herein. Further research is necessary to validate and potentially improve these results and, for this purpose, suggestions for the next research steps are given here.

The non-linear static analyses (with cyclic loading protocol) carried out are only sufficient to evaluate the hysteretic performance and potential energy-dissipation capacity, but do not give insight on the dynamic response of the system. Thus, non-linear time-history analyses should be applied to the shear wall model, with application of proper seismic acceleration records. If the same ground acceleration is applied also to models of conventional OSB-sheathed frames, a valuable comparison may be established between the maximum amplification factors of the two configurations. Determining the maximum ground acceleration that can be sustained by the innovative and conventional wall systems also provides additional information on their response and capacity, which is complementary to that obtained by the hysteretic curves.

Vertical gravity loads reproducing the presence of the actual building structure should also be included to analyze the capacity of the CFS frame and the risk of buckling. In fact, although the models presented in the Thesis consider only seismic lateral loads, the CFS studs in real structures are also characterized by compressive loads, particularly large for mid-rise buildings. This may cause instability phenomena, for instance local buckling of the flanges and lips, if not properly restrained.

Eventually, experimental tests will be required to evaluate the actual response of the frame with integrated fuses in real structures. In particular, such experiments will provide insight on the fuse-to-stud connections and verify the actual behavior of the fuse links.

References

[1] **European Standard**. *Eurocode 8: Design of structures for earthquake resistance. Part 1: General rules, seismic actions and rules for buildings* (2004).

[2] **ASCE**. *Minimum Design Loads for Buildings and Other Structures (7-10)* (2010).

[3] **Soong T.T., Spencer Jr. B.F**. *Supplemental energy dissipation: state-of-the-art and state-of-the-practice.* Eng. Struct.; 24: 243-59 (2002).

[4] **Building Research Institute**. *http://www.buildingresearch.com.np/index.php* (Accessed 2013).

[5] **Yu W., LaBoube R.A.** *Cold-formed steel design*. John Wiley & Sons, Inc. (2010).

[6] **Steel Market Development Institution.** *Cold-formed steel in building construction* (2010).

[7] **Schafer B.W**. *Cold-formed steel structures around the world – A review of recent advances in applications, analysis and design.* Steel Construction; No. 3 (2011).

[8] **Liu P., Peterman K.D., Schafer B.W.** *Test report on cold-formed steel shear walls*. RR03 (2012).

[9] **Peterman K.D., Schafer B.W.** *Hysteretic shear response of fasteners connecting sheathing to cold-formed steel studs*. RR04 (2013).

[10] **Al-Kharat M., Rogers C.A.** *Inelastic performance of cold-formed steel strap braced walls*. Journal of Constructional Steel Research; 63: 460-74 (2007).

[11] **American Iron and Steel Institute.** *North American Standard for cold-formed steel framing - Lateral design*. S213-07-SI-09 (2009).

[12] **Iuorio O., Fiorino L., Macillo V., Landolfo R**. *Seismic design and experimental tests of an Italian cold formed steel structure* (2012).

[13] **Hitaka T., Matsui C.** *Experimental study on steel shear wall with slits.* Journal of Structural Engineering-Asce; 129: 586-95 (2003).

[14] **Emami F., Mofid M., Vafai A.** *Experimental study on cyclic behavior of trapezoidally corrugated steel shear walls.* Eng. Struct.; 48: 750-62 (2013).

[15] **Shimizu N., Kanno R., Ikarashi K., Sato K., Hanya K.** *Cyclic Behavior of Corrugated Steel Shear Diaphragms with End Failure.* Journal of Structural Engineering-Asce; 139: 796-806 (2013).

[16] **Astaneh-Asl A.** *Steel shear walls, behavior, modeling and design*. 2008 Seismic Engineering Conference Commemorating the 1908 Messina and Reggio Calabria Earthquake, Pts 1 and 2; 1020: 5-18 (2008).

[17] **Chan R.W.K., Albermani F**. *Experimental study of steel slit damper for passive energy dissipation.* Eng. Struct.; 30: 1058-66 (2008).

[18] **Kobori T., Miura Y., Fukuzawa E., Yamada T., Arita T., Takenaka Y. et al.** *Development and Application of Hysteresis Steel Damper* (1992).

[19] **Ma X.** *Seismic design and behavior of self-centering braced frame with controlled rocking and energy-dissipating fuses* (2010).

[20] **Deierlien G., Hajjar J., Eatherton M., Billington S., Krawinkler H., Ma X.** *Seismically resilient steel braced frame systems with controlled rocking and energy dissipating fuses.* Proceedings of 2009 NSF Engineering Research and Innovation Conference, Honolulu, Hawaii (2009).

[21] **Eatherton M., Hajjar J., Deierlien G., Krawinkler H., Billington S., Ma X.** *Controlled rocking of steel-frame buildings with replaceable energy-dissipating fuses*. The 14th World Conference on Earthquake Engineering (2008).

[22] **Ma X., Borchers E., Pena A., Krawinkler H., Billington S., Deierlien G.** *Design and behavior of steel shear plates with openings as energy-dissipating fuses.* John A. Blume Earhquake Engineering Center, Stanford University; Internal Report (2011).

[23] **Ozaki F., Kawai Y., Tanaka H., Okada T., Kanno R.** *Innovative damage control systems using replaceable energy dissipating steel fuses for cold-formed steel structures.* Twentieth International Specialty Conference on Cold-Formed Steel Structures (2010).

[24] **Ozaki F., Kawai Y., Kanno R., Hanya K.** *Damage-Control Systems Using Replaceable Energy-Dissipating Steel Fuses for Cold-Formed Steel Structures: Seismic Behavior by Shake Table Tests.* Journal of Structural Engineering-Asce; 139: 787-95 (2013).

[25] **Dargush G.F., Soong T.T.** *Behavior of Metallic Plate Dampers in Seismic Passive Energy Dissipation Systems.* Earthquake Spectra; Volume 11, No. 4 (1995).

[26] **Nakata N., Schafer B.W., Madsen R.L.** *Seismic design of multi-story cold-formed steel buildings - the CFS-NEES archetype building.*

[27] **Cold-Formed Steel NEES**. http://www.ce.jhu.edu/cfsnees/index.php (Accessed 2013).

[28] **Federal Emergency Management Agency.** *Interim Testing Protocols for Determining the Seismic Performance Characteristics of Structural and Nonstructural Components.* FEMA 461 (2007).

[29] **Eatherton M.** *Large-scale cyclic and hybrid simulation testing and development of a controlled-rocking steel building system with replaceble fuses.* PhD Dissertation, University of Illinois at Urbana-Champaign (2010).

[30] **American Iron and Steel Institute.** *North American Standard for Cold-Formed Steel Framing - Product Data.* AISI S201-7 (2007).

[31] **Krawinkler H.** *Loading histories for cyclic tests in support of performance assessment of structural components.*

[32] **Abaqus (Simulia).** *Abaqus Analysis User's Manual* (version 6.11).

[33] **Zeinoddini V.M., Schafer B.W.** *Simulation of geometric imperfections in cold-formed steel members using spectral representation approach.* Thin-Walled Structures (2012).

[34] **American Iron and Steel Institute.** *Cold-formed Steel Design Manual* (2008).

Appendix

This Appendix presents the main numerical results of the parametric study of fuses. 60 different combinations of length, height, thickness and yielding stress have been analyzed, as indicated in Chapter 4.3. For each fuse specimen, five charts are reported in the following:

1. Time history of the shear force V in the fuse (chart at the top of the page);
2. Hysteretic curve $V-\Delta_{fuse}$ for the model of the single fuse link (mid left of the page);
3. Hysteretic curve $V-\Delta_{fuse}$ for the model of the fuse with side plates (mid right of the page);
4. Hysteretic curve $V-\Delta$ for the model of the single fuse link (bottom left of the page);
5. Hysteretic curve $V-\Delta$ for the model of the fuse with side plates (bottom right of the page).

It is recalled that Δ_{fuse} is the drift of the fuse, whereas Δ is the global drift of the wall: the relation between these two parameters is given by Eqn. (3.19), reported here:

$\Delta_{fuse}=\frac{w}{L}\cdot\Delta$ where w and L are, respectively, the width of the shear wall and length of the fuse.

Thus, the hysteretic curves 2-4 and 3-5 are basically identical, the only difference being the scale of the drift. To define the hysteretic behavior of the fuses, the charts with Δ_{fuse} are more significant, but the charts with the wall drift Δ are reported as well because the FEMA loading protocol has been applied according to the drift of the entire wall (Chapter 4.4).

The differences observed between the numerical models without and with side plates have been described and justified in Chapter 4.

Fuse 1 - L=200mm; b=60mm; t=5mm; σ_y=180MPa

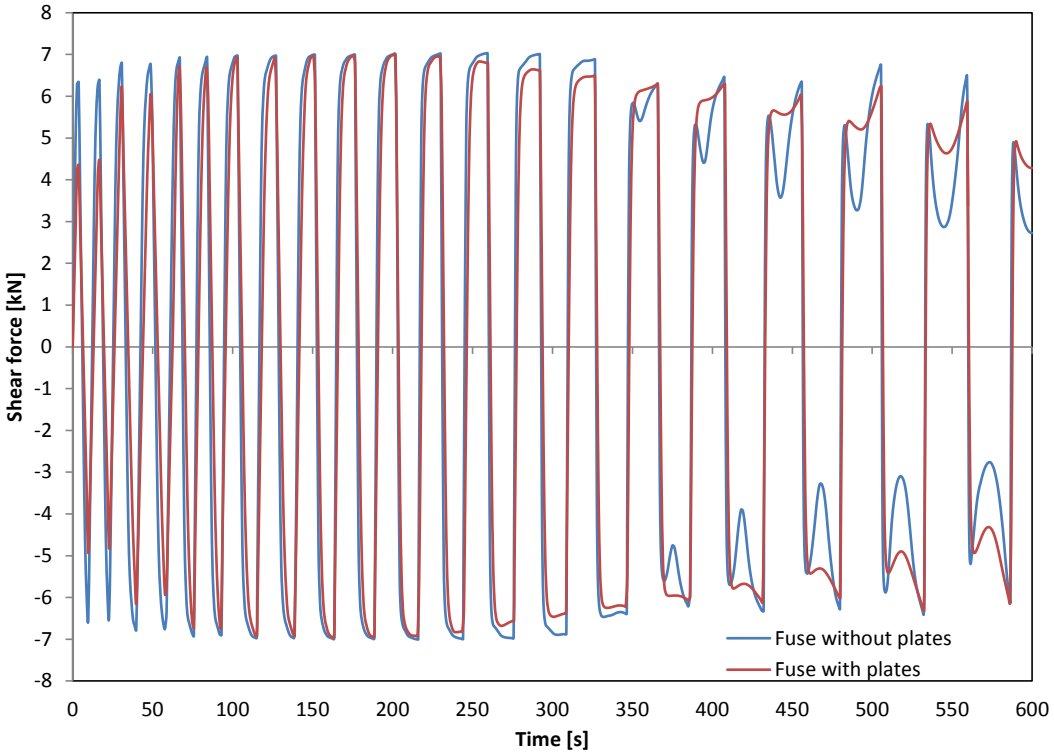

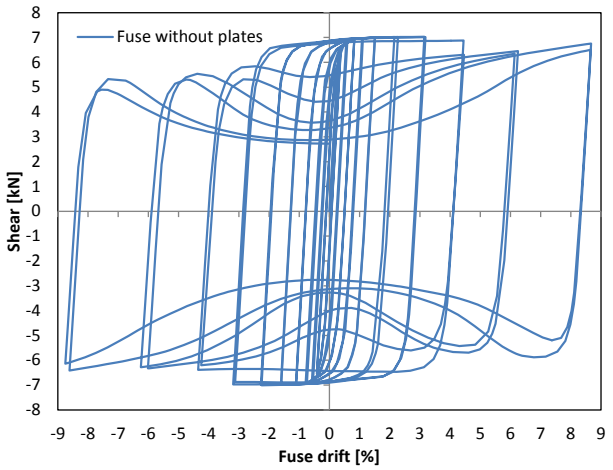

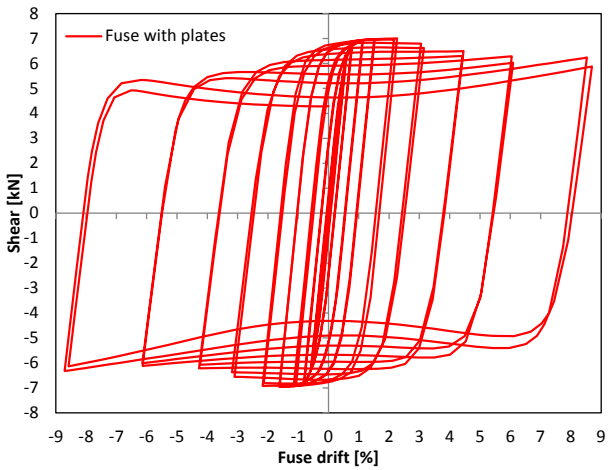

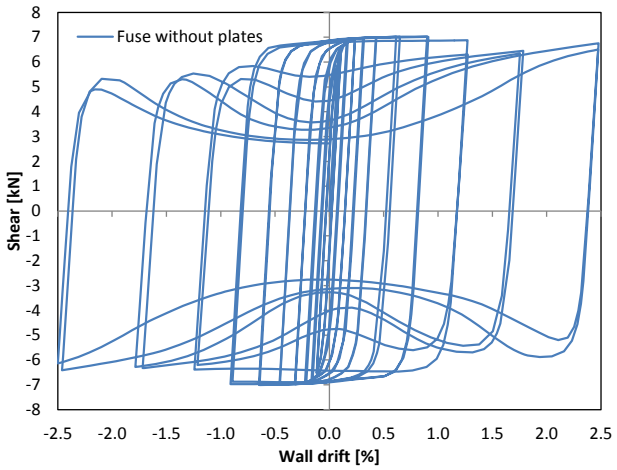

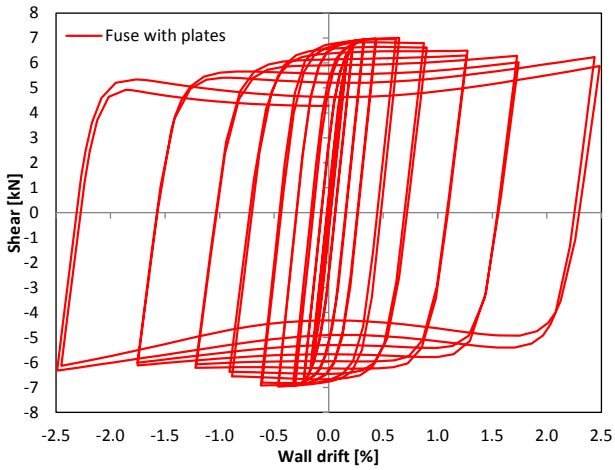

Fuse 2 - L=200mm; b=60mm; t=5mm; σ_y=250MPa

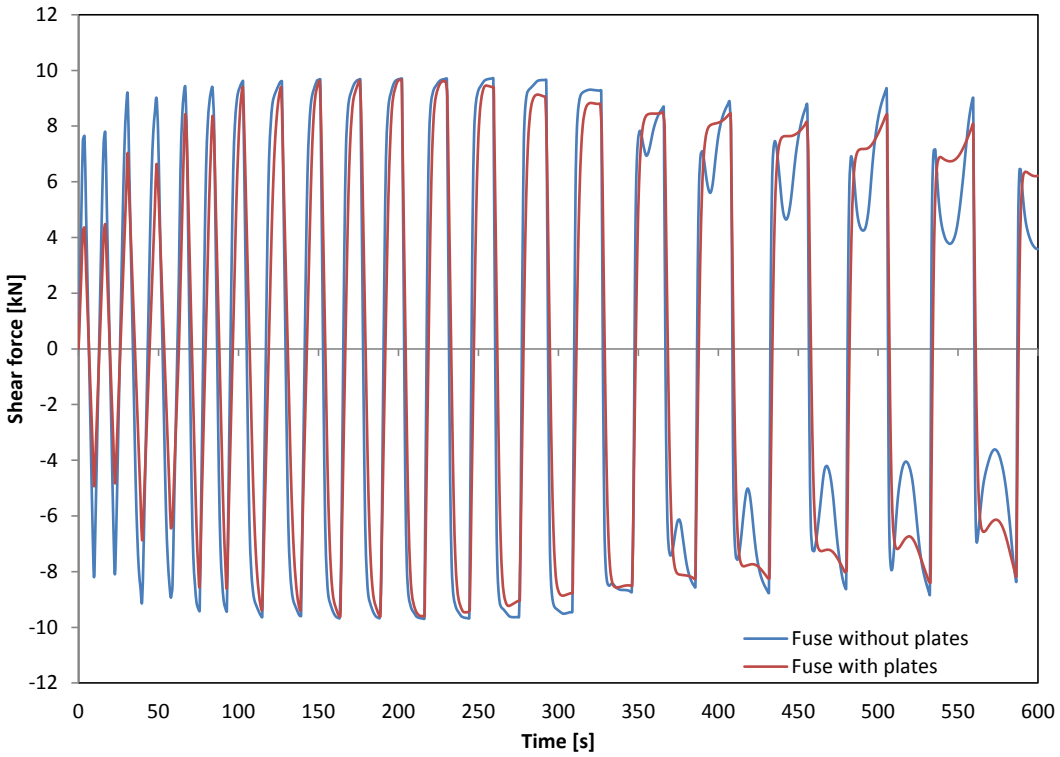

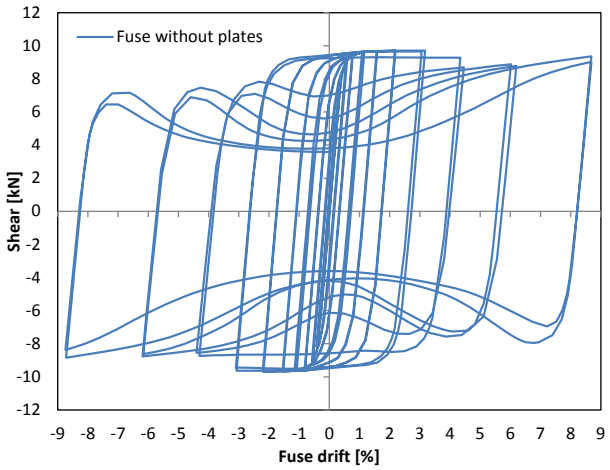

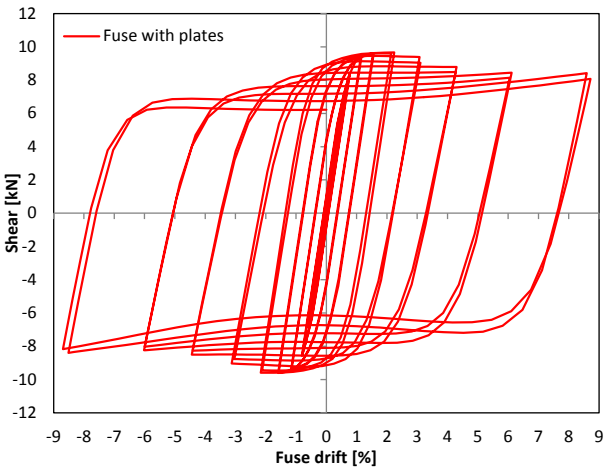

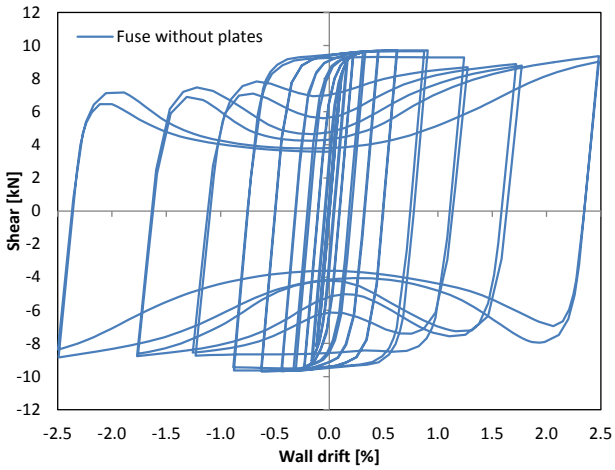

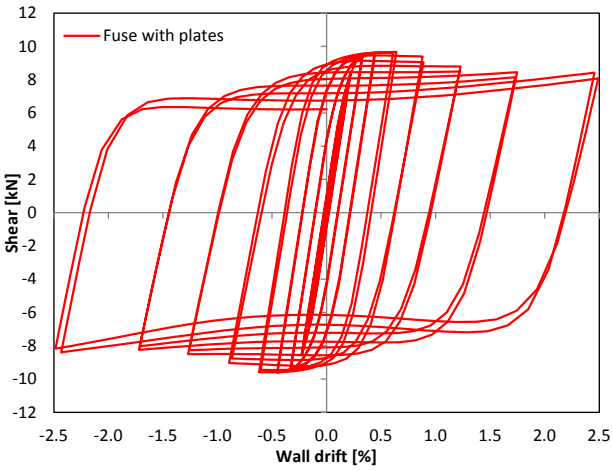

Fuse 3 - L=200mm; b=60mm; t=6mm; σ_y=180MPa

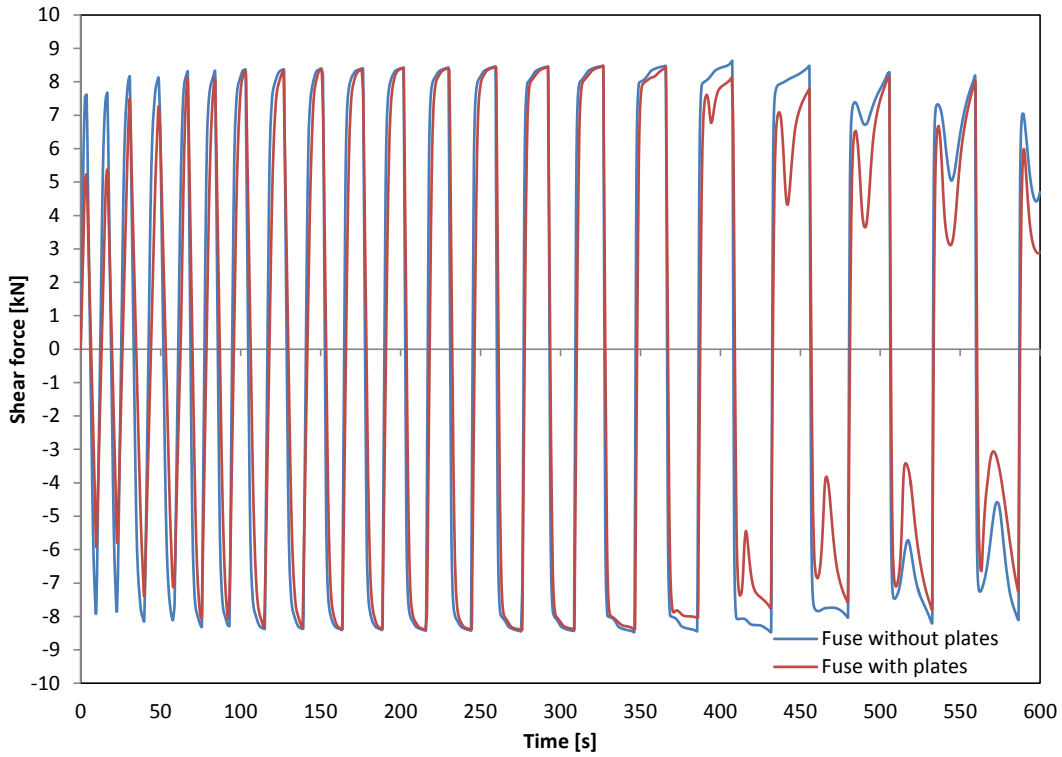

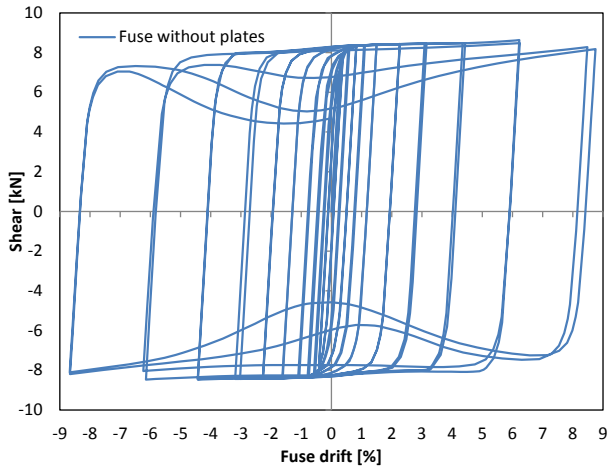

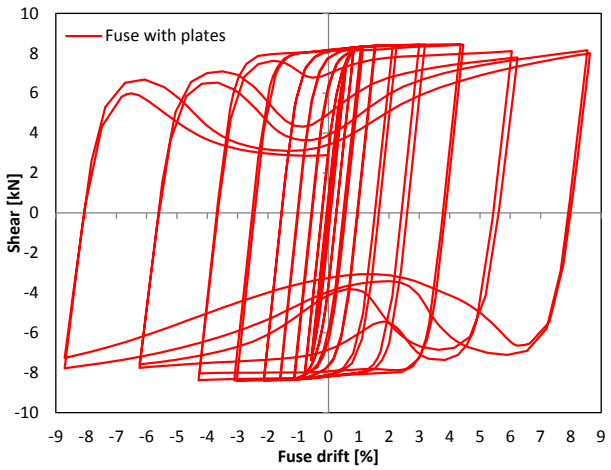

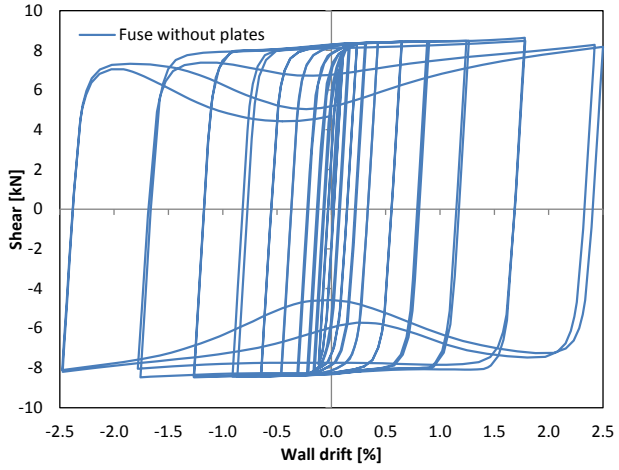

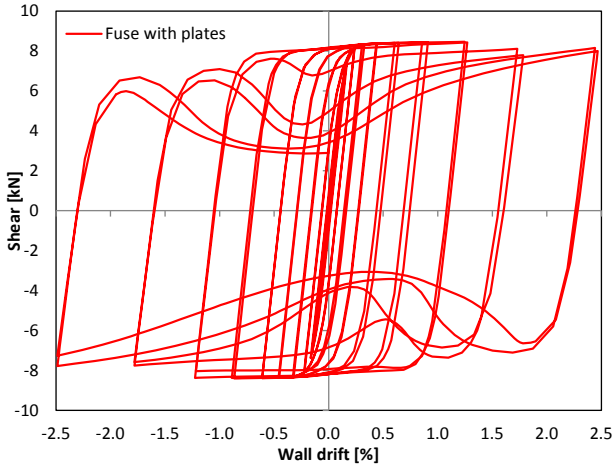

Fuse 4 - L=200mm; b=60mm; t=6mm; σ_y=250MPa

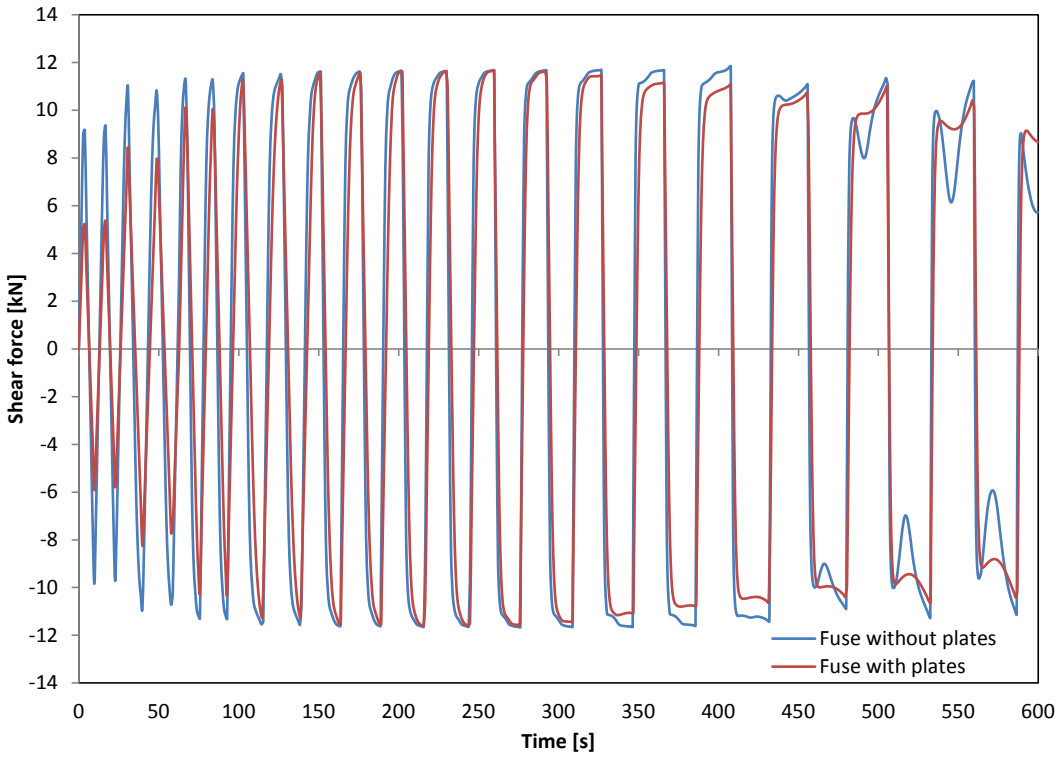

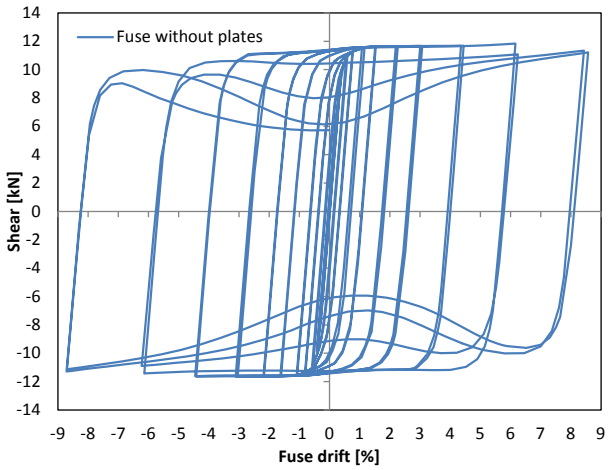

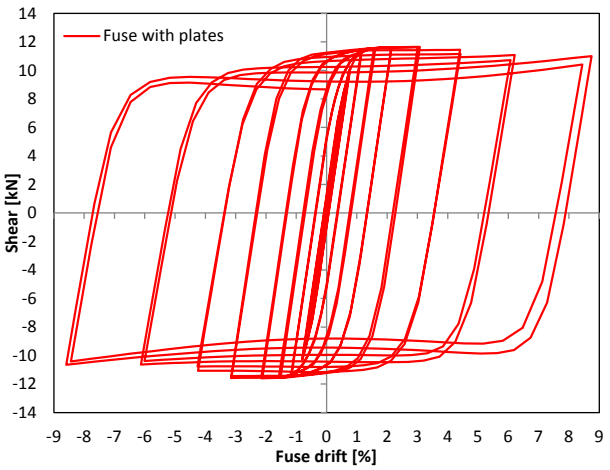

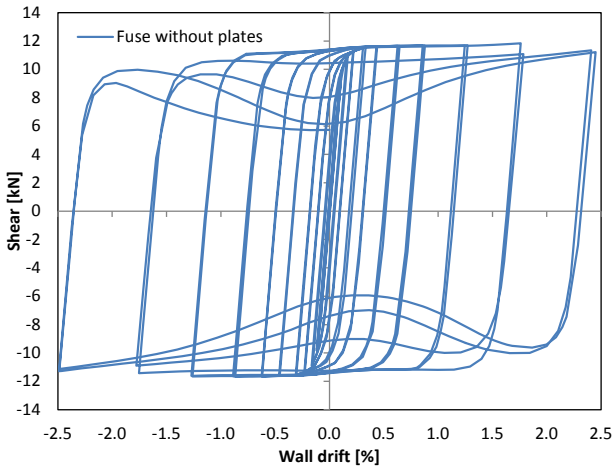

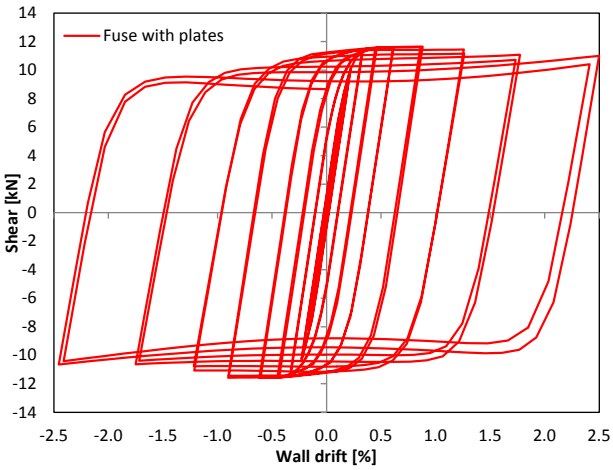

Fuse 5 - L=200mm; b=60mm; t=7mm; σ_y=180MPa

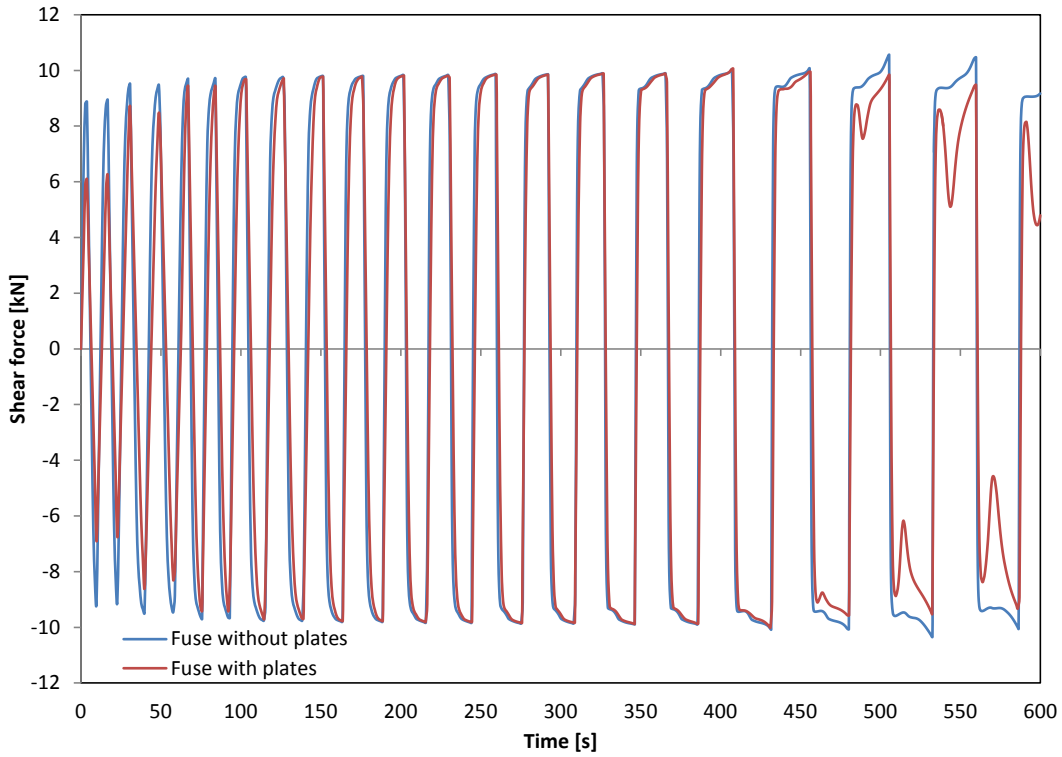

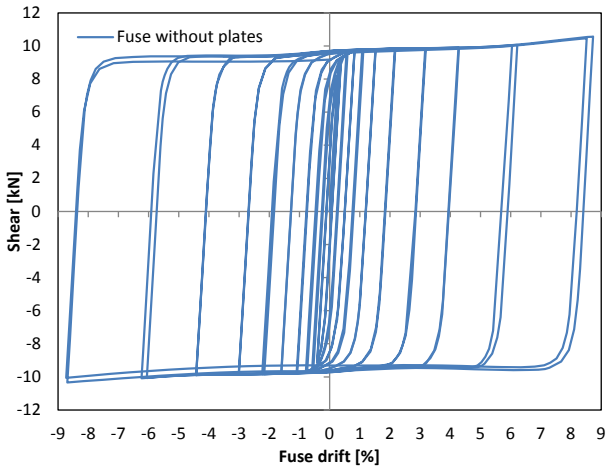

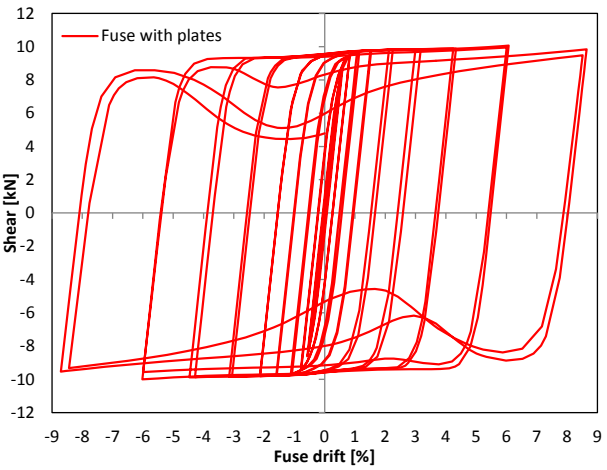

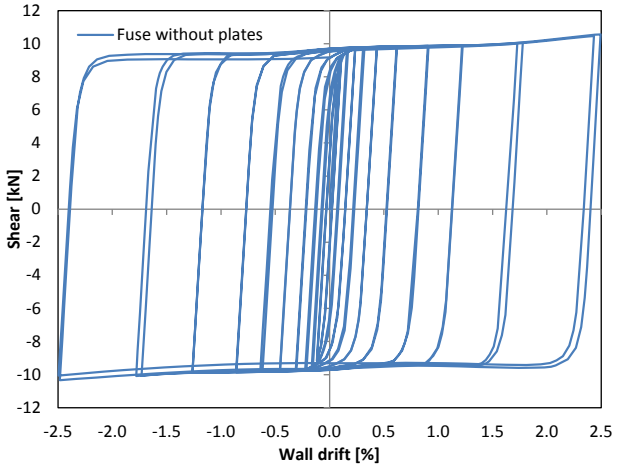

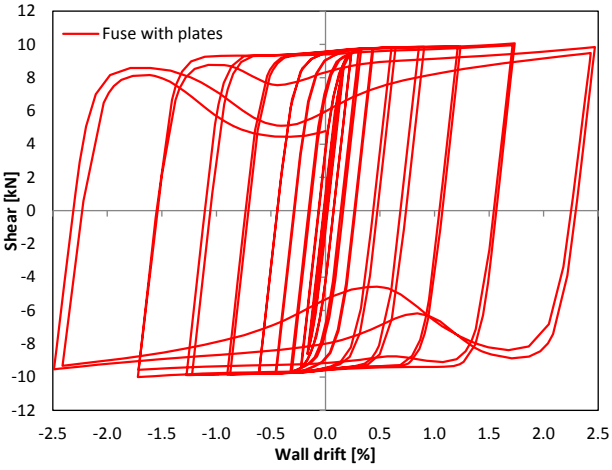

Fuse 6 - L=200mm; b=60mm; t=7mm; σ_y=250MPa

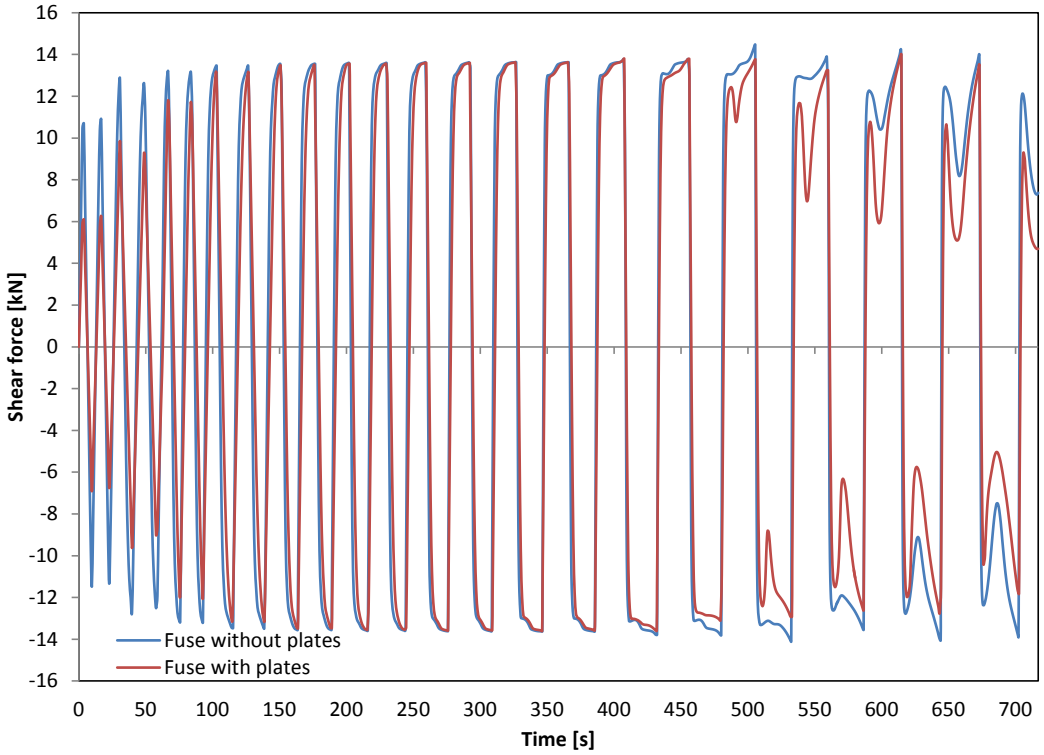

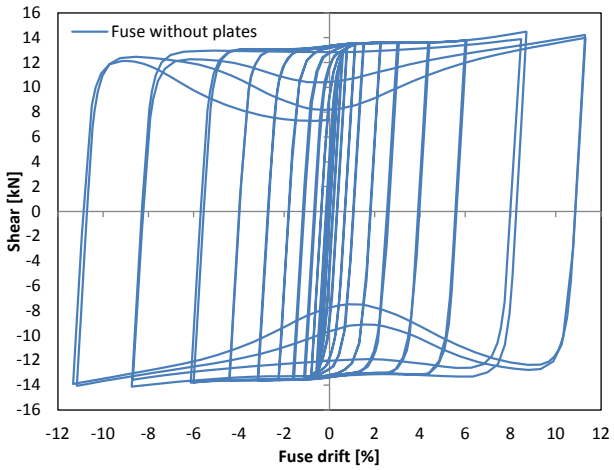

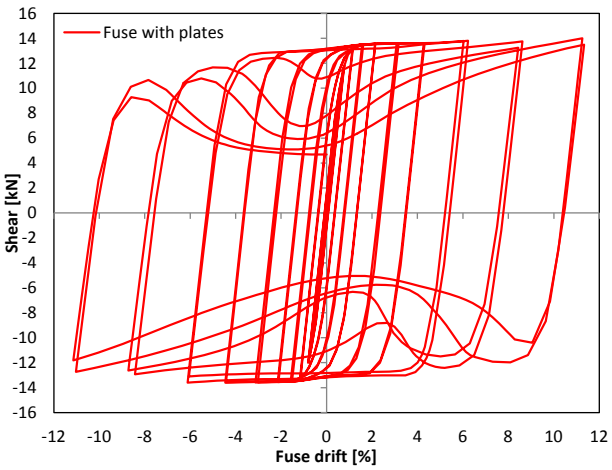

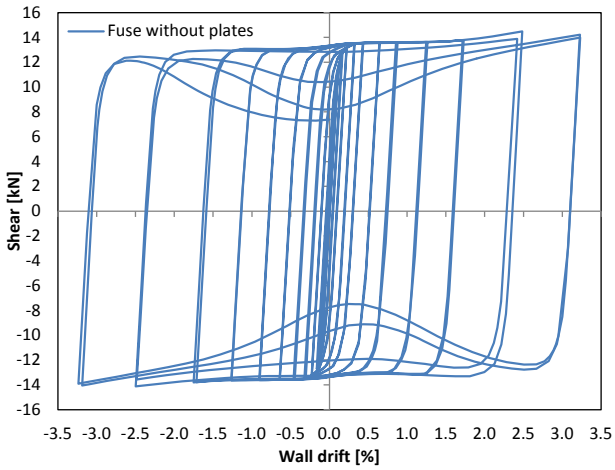

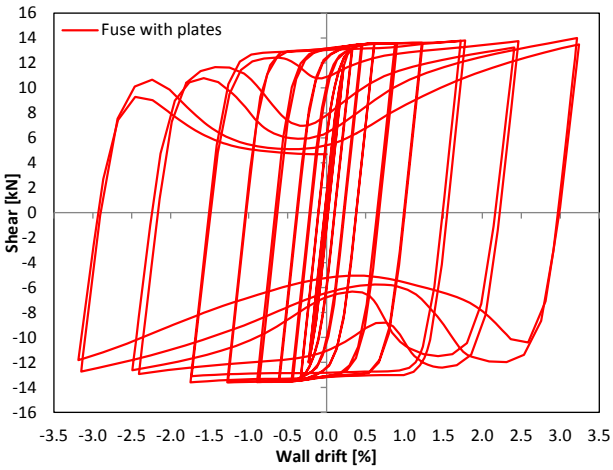

Fuse 7 - L=200mm; b=75mm; t=5mm; σ_y=180MPa

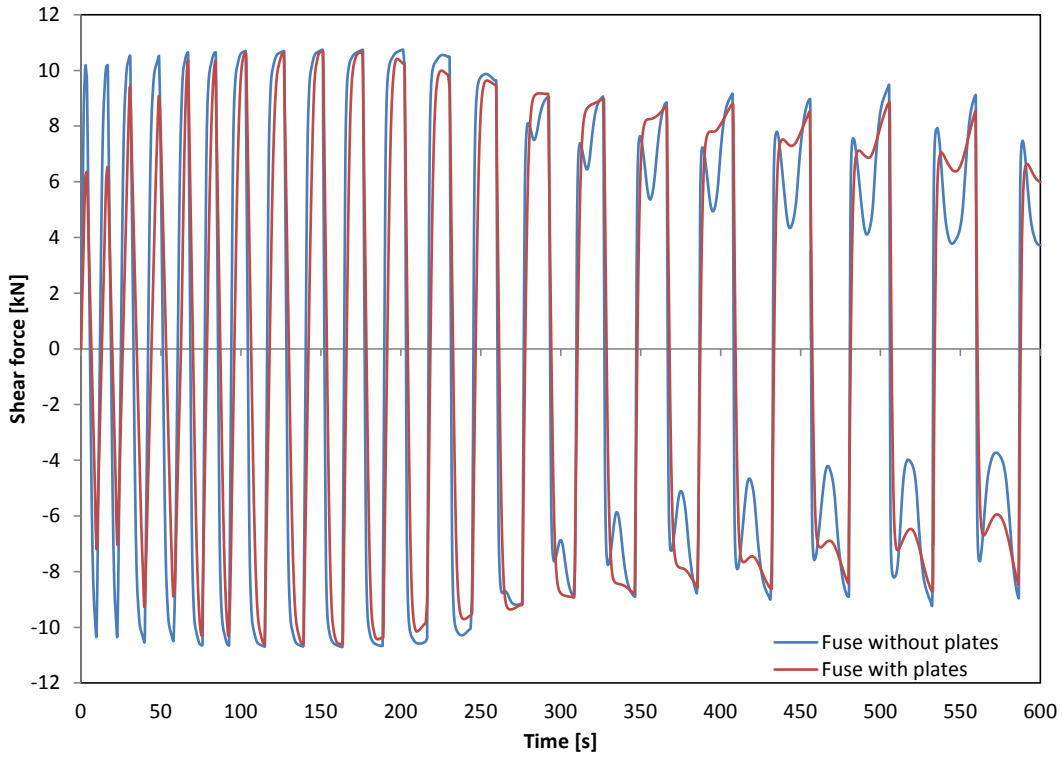

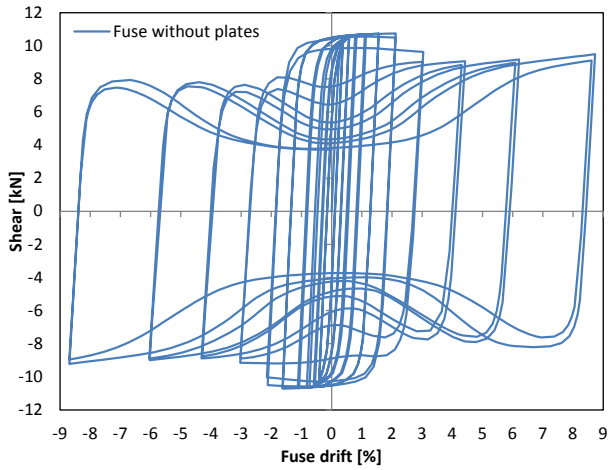

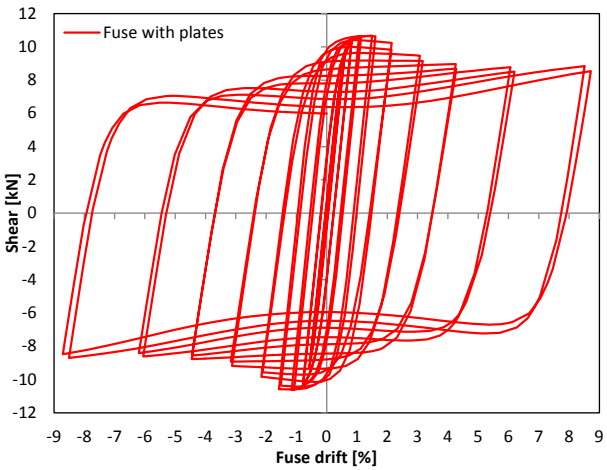

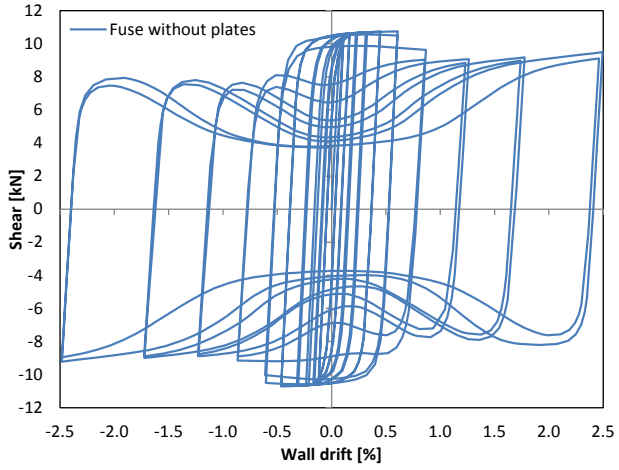

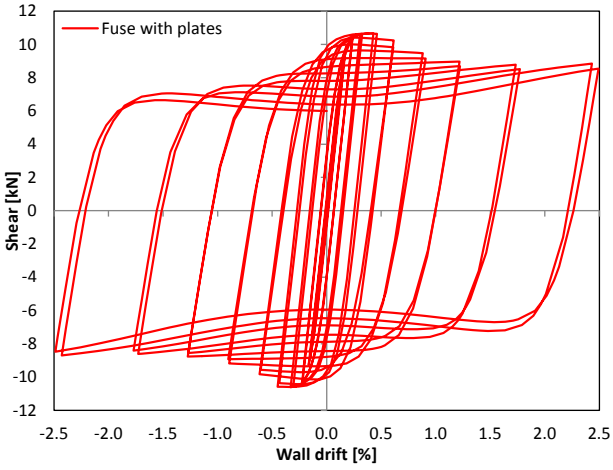

Fuse 8 - L=200mm; b=75mm; t=5mm; σ_y=250MPa

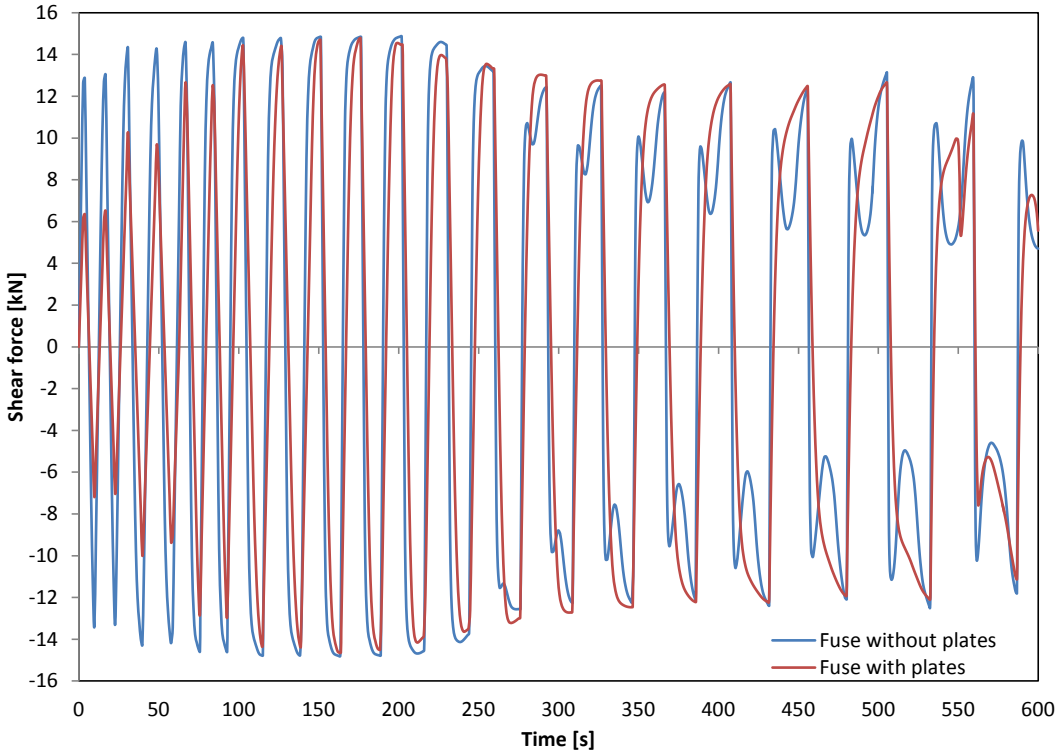

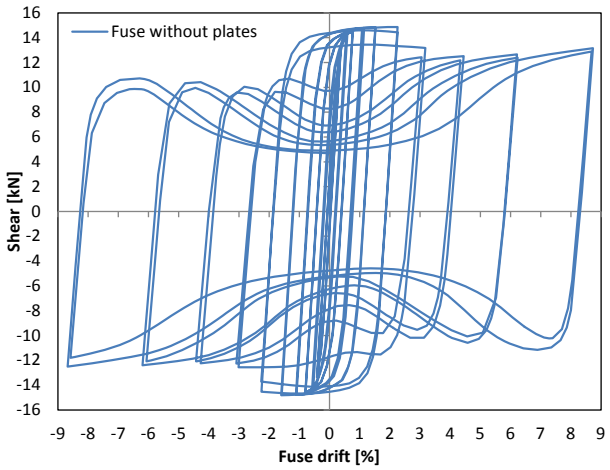

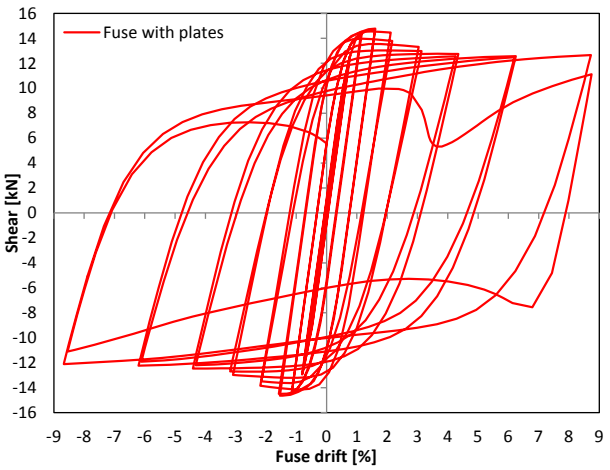

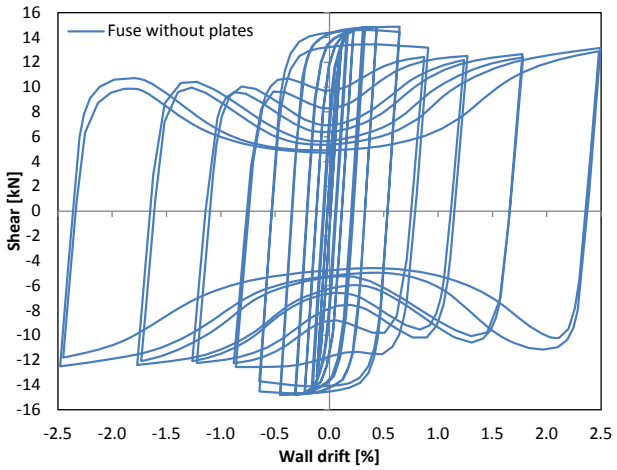

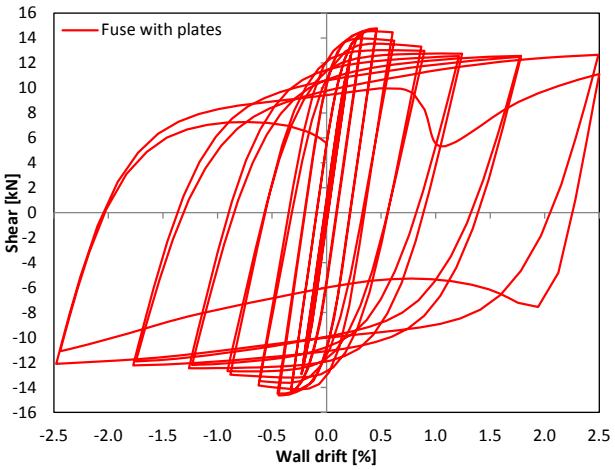

Fuse 9 - L=200mm; b=75mm; t=6mm; σ_y=180MPa

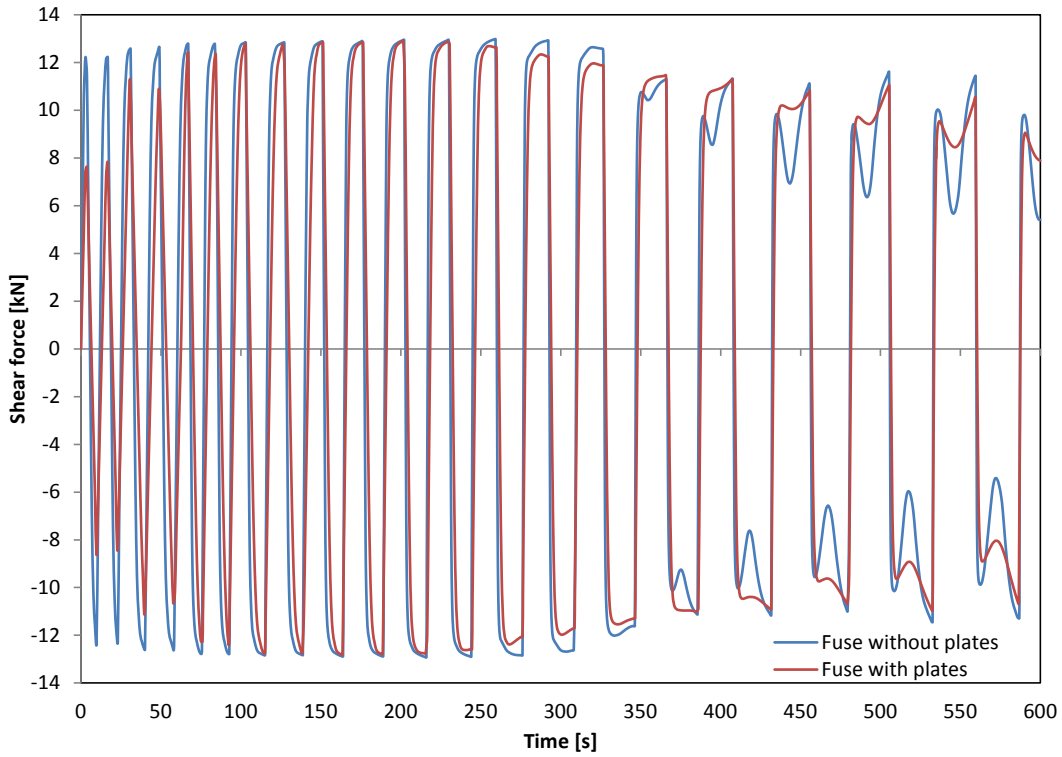

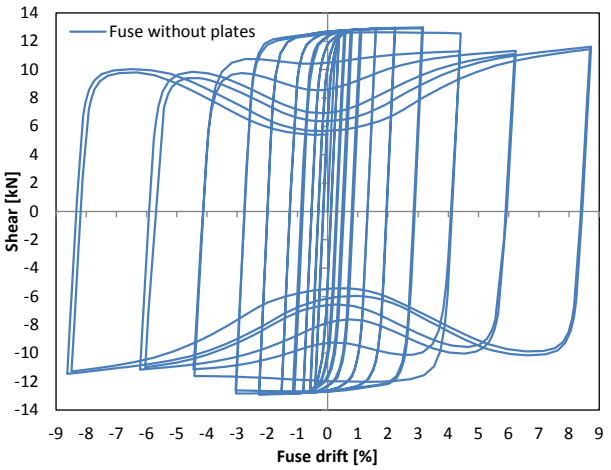

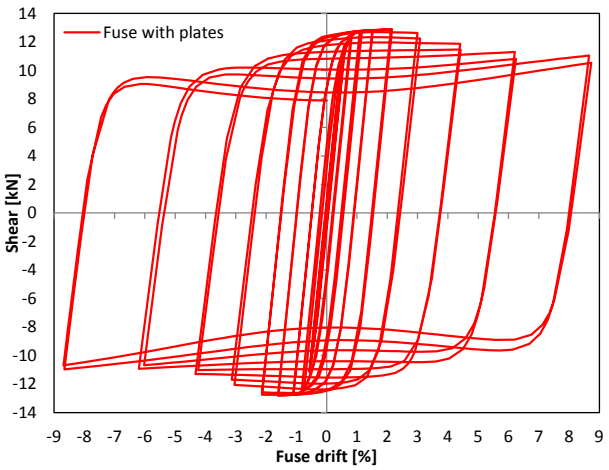

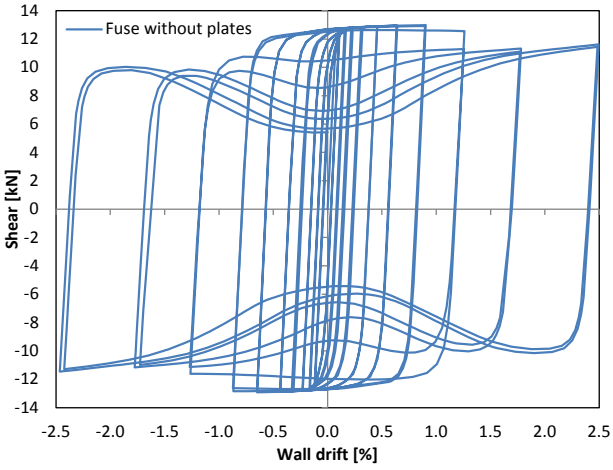

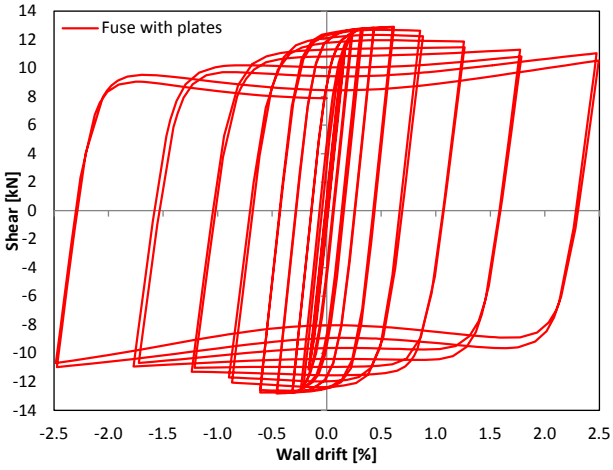

Fuse 10 - L=200mm; b=75mm; t=6mm; σ_y=250MPa

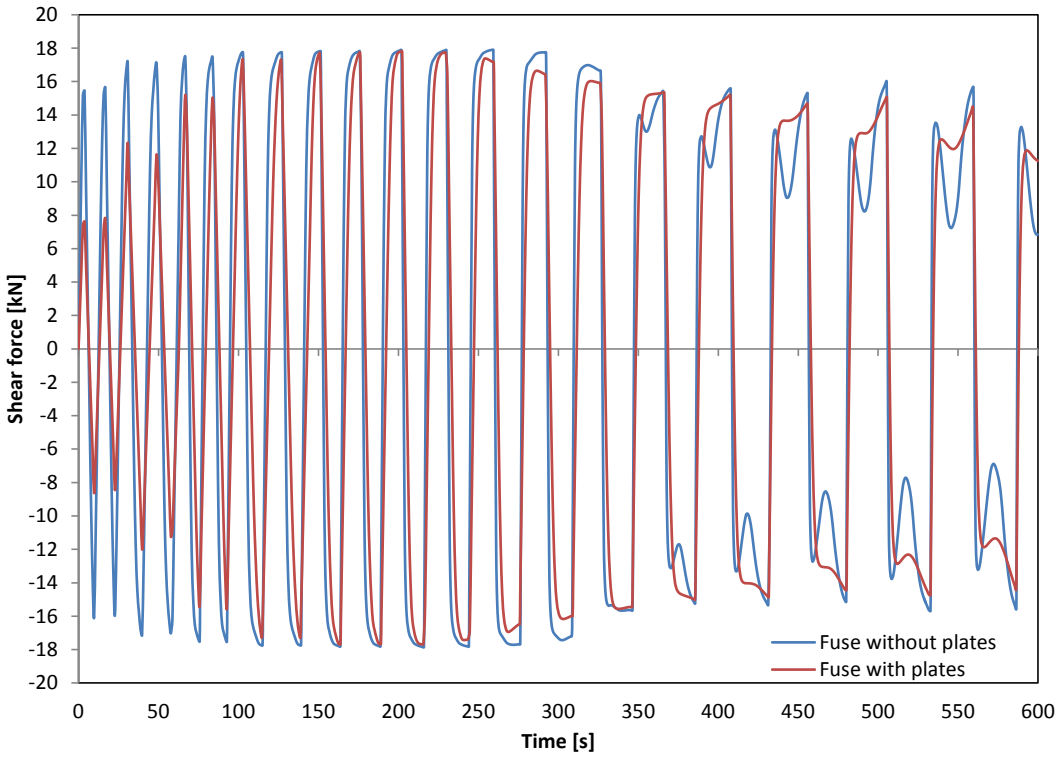

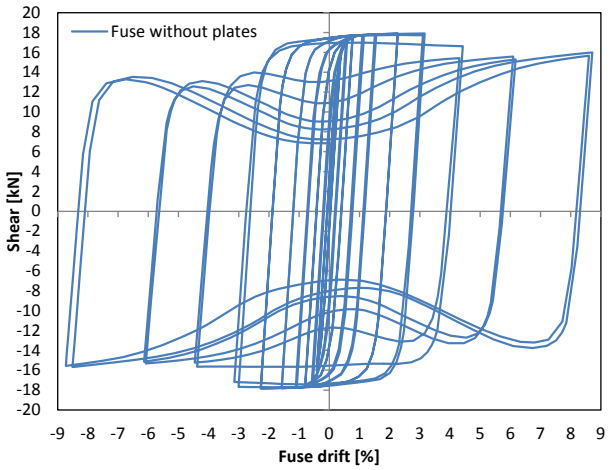

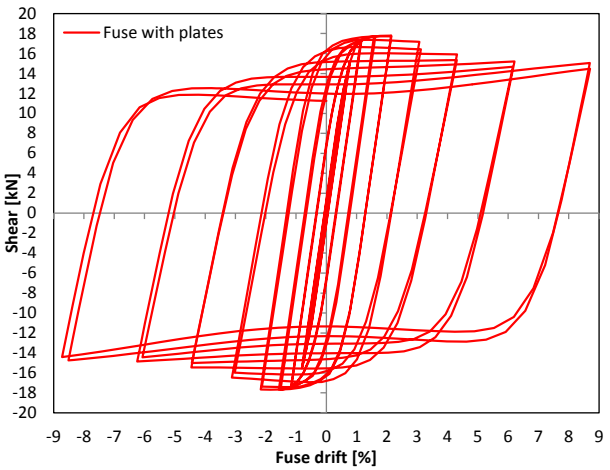

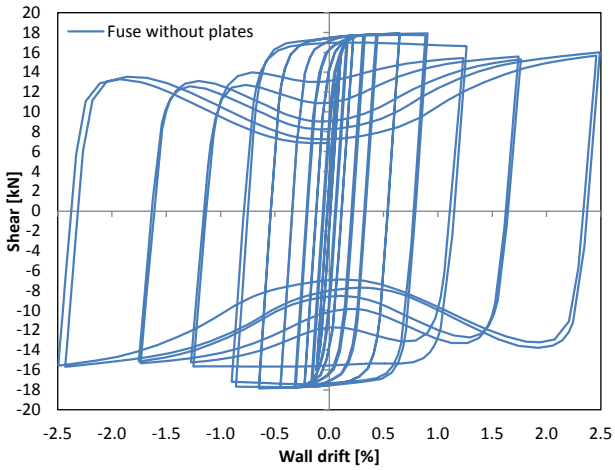

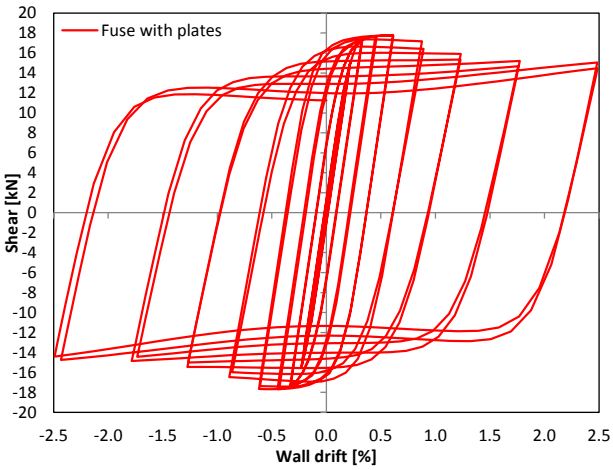

Fuse 11 - L=200mm; b=75mm; t=7mm; σ_y=180MPa

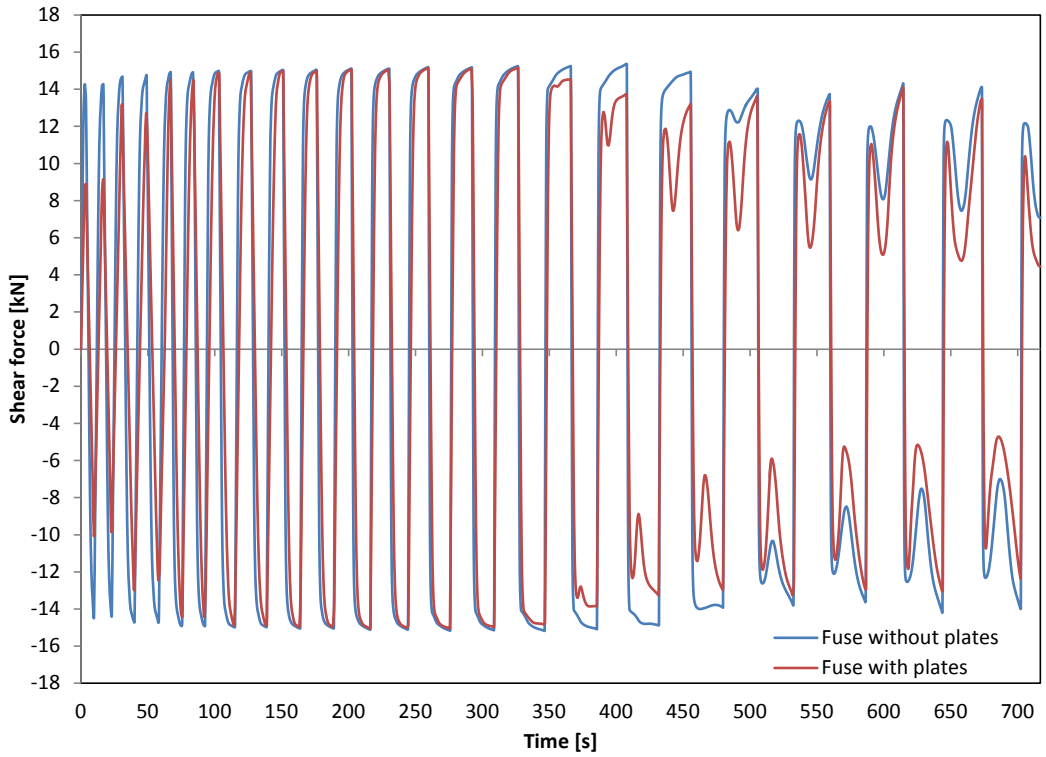

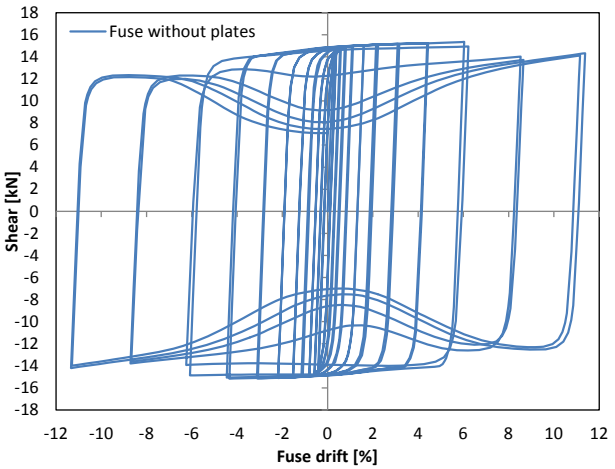

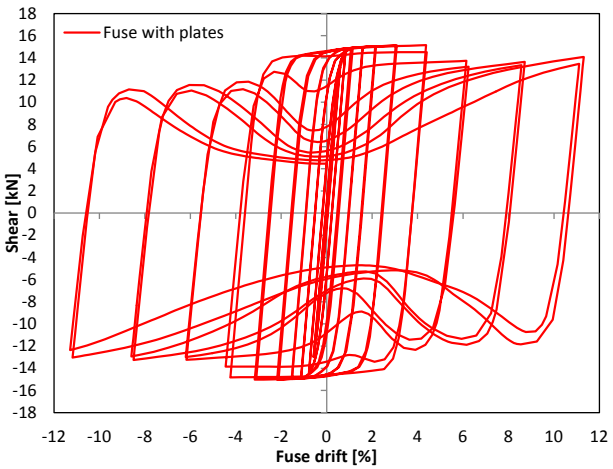

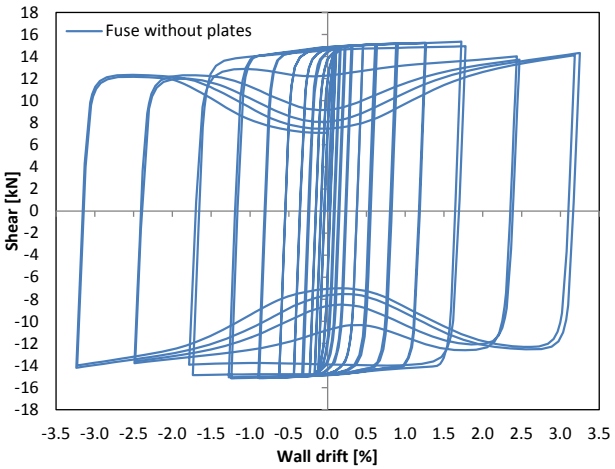

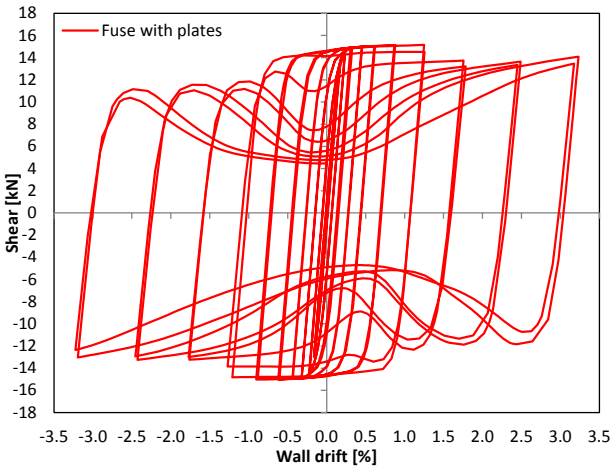

Fuse 12 - L=200mm; b=75mm; t=7mm; σ_y=250MPa

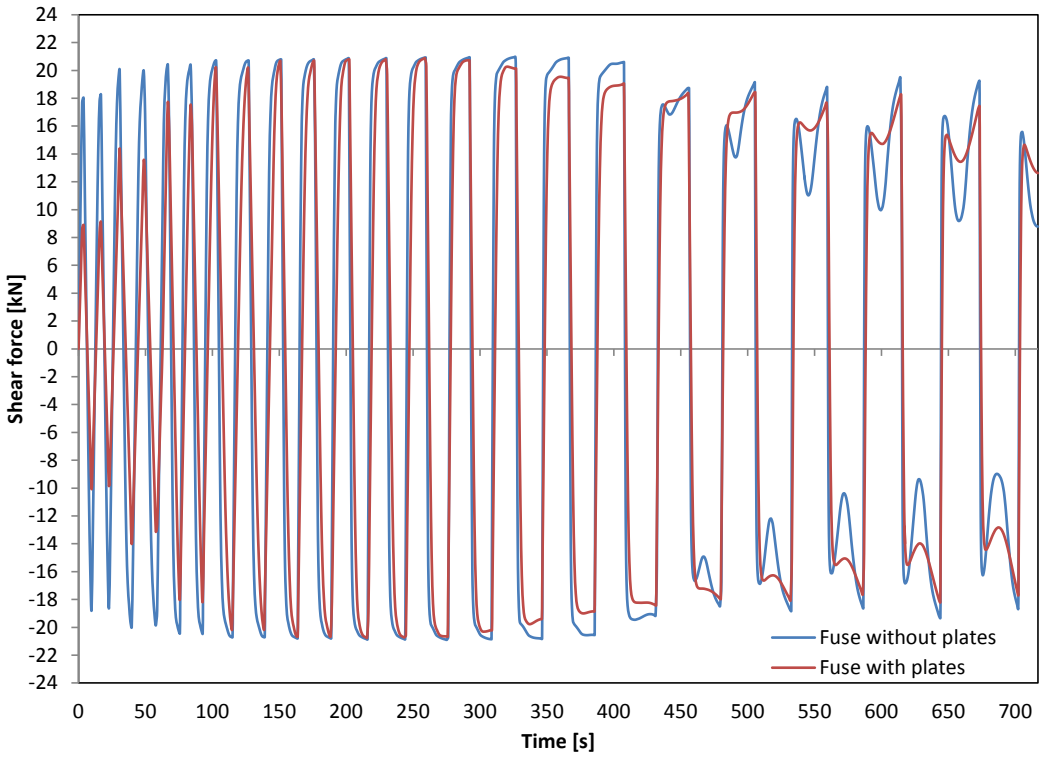

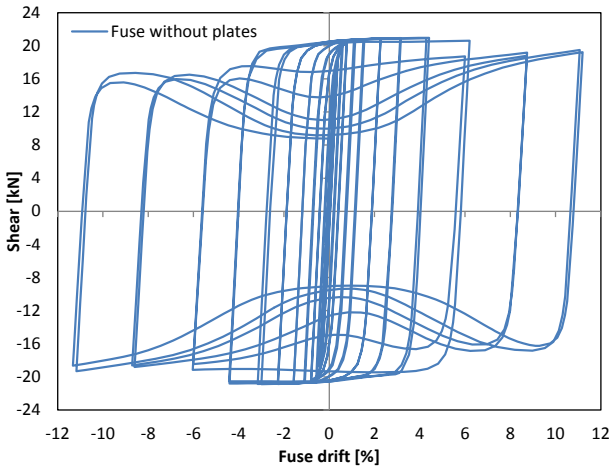

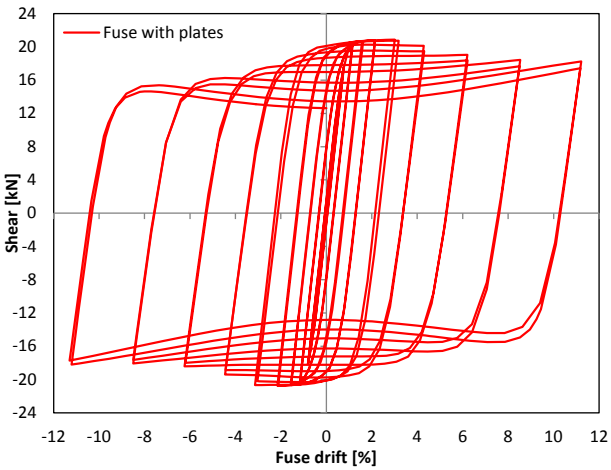

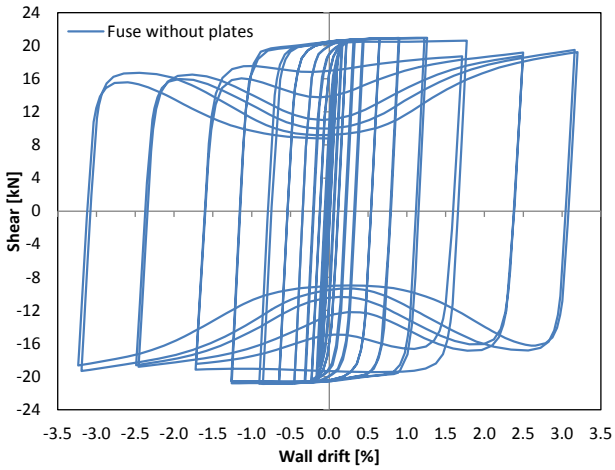

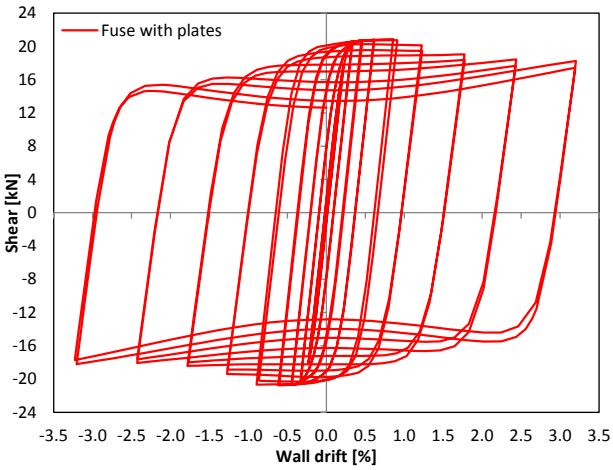

Fuse 13 - L=250mm; b=60mm; t=5mm; σ_y=180MPa

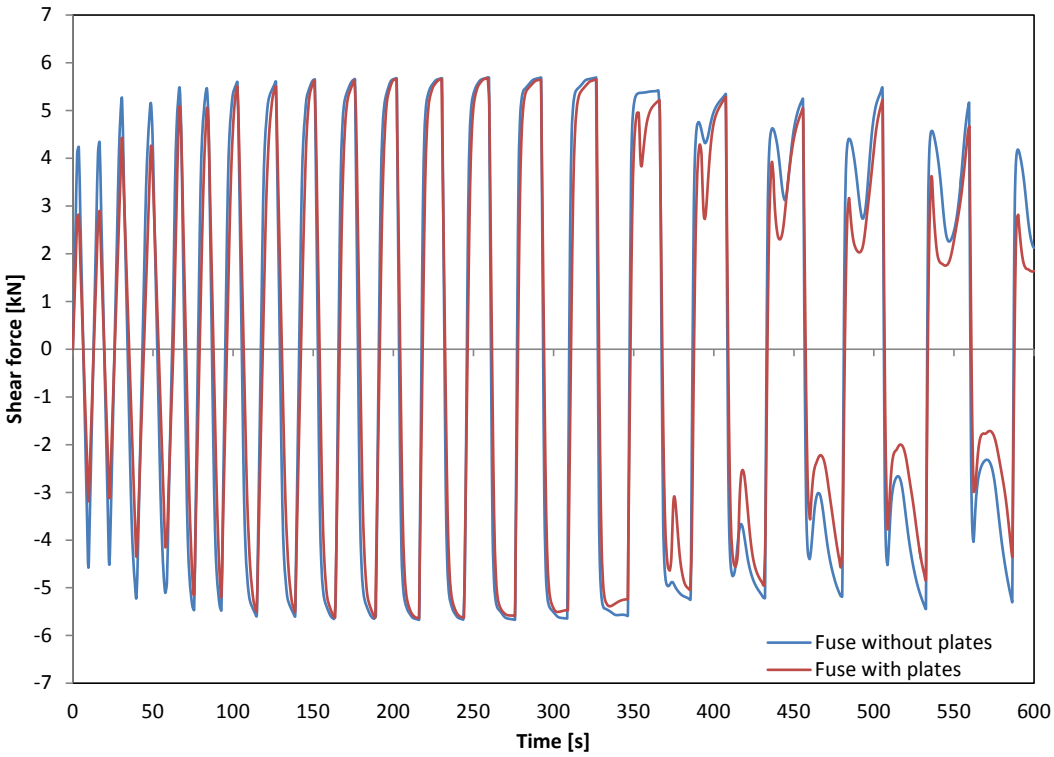

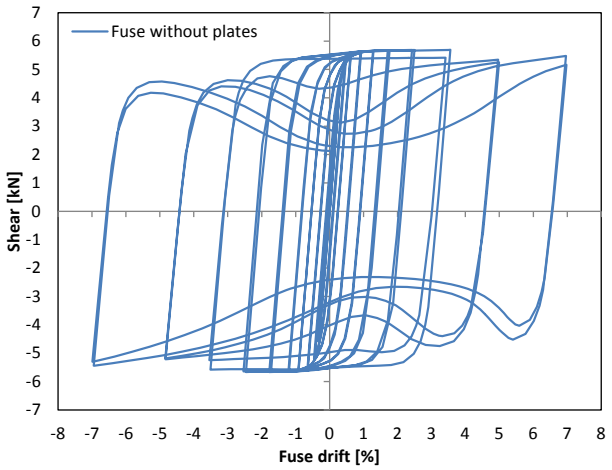

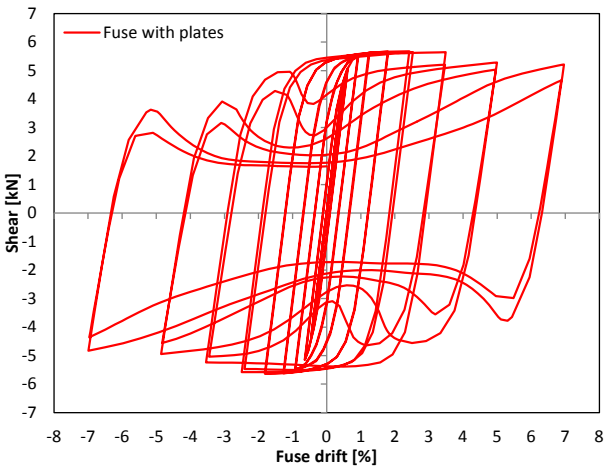

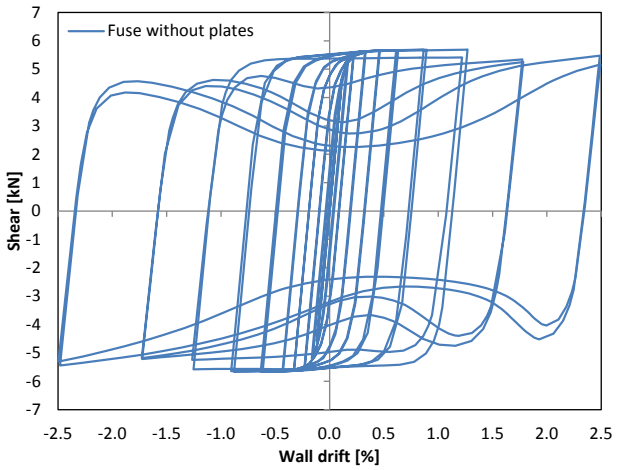

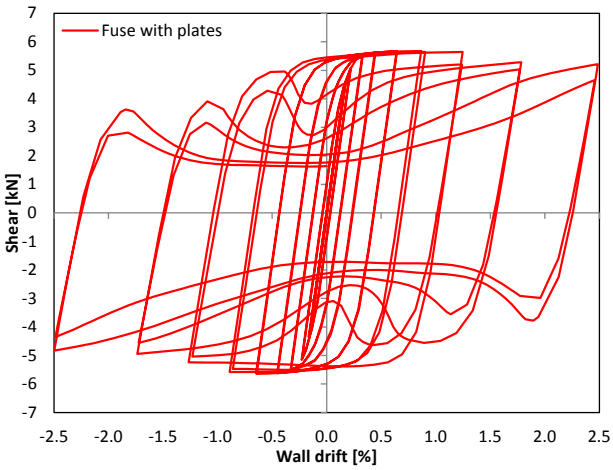

Fuse 14 - L=250mm; b=60mm; t=5mm; σ_y=250MPa

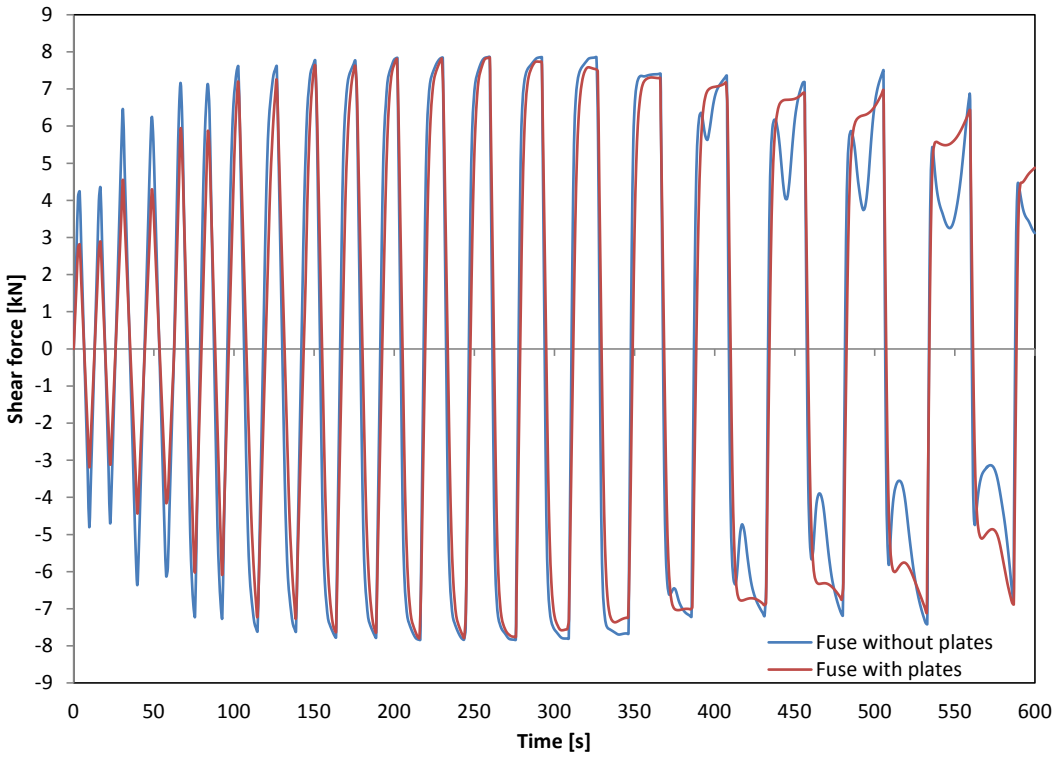

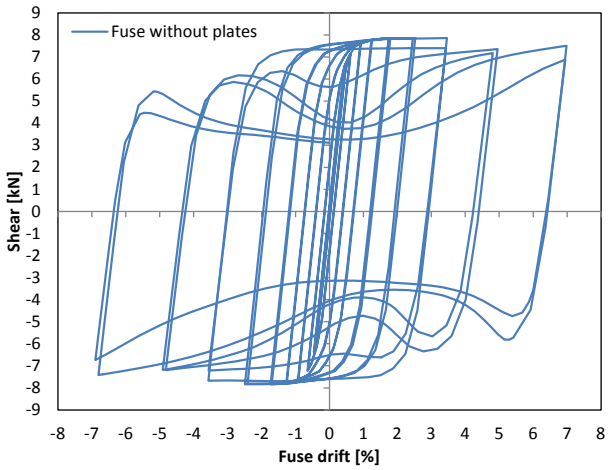

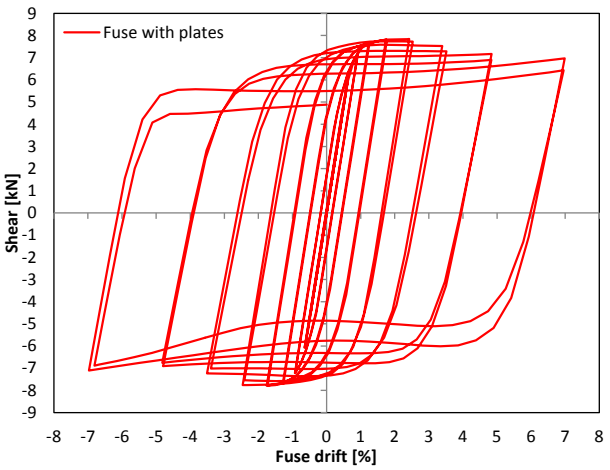

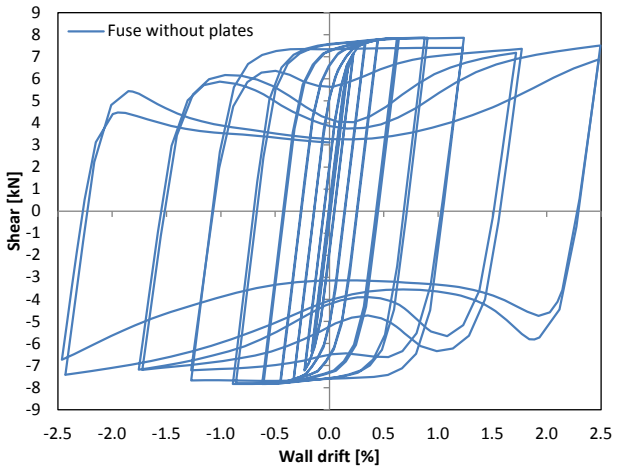

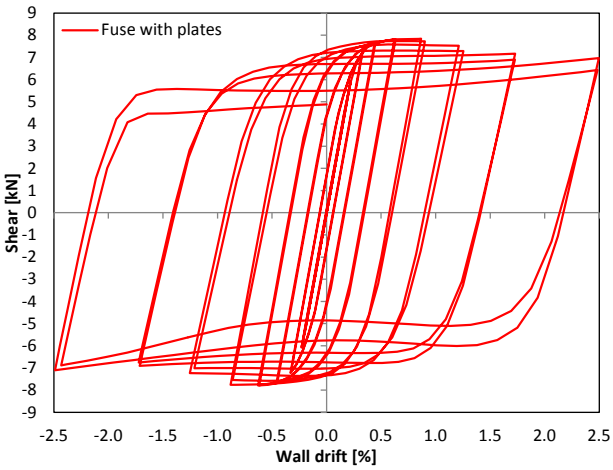

Fuse 15 - L=250mm; b=60mm; t=6mm; σ_y=180MPa

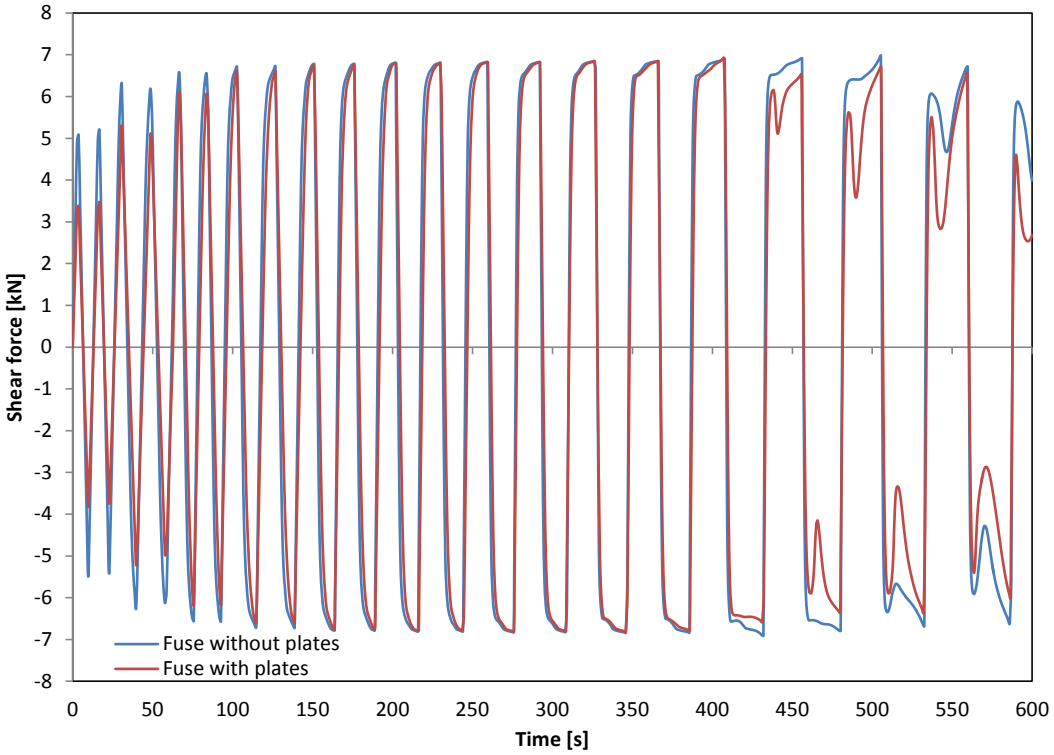

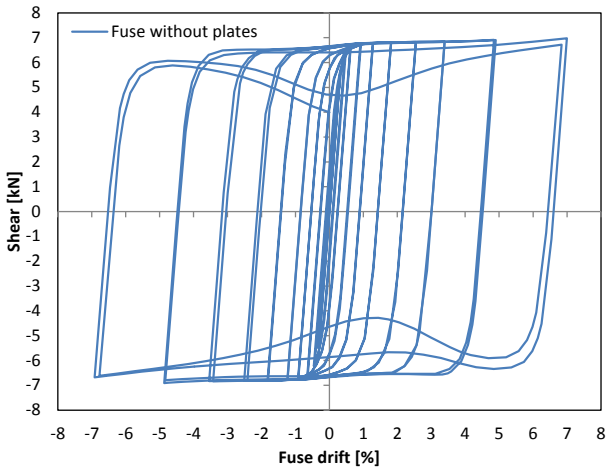

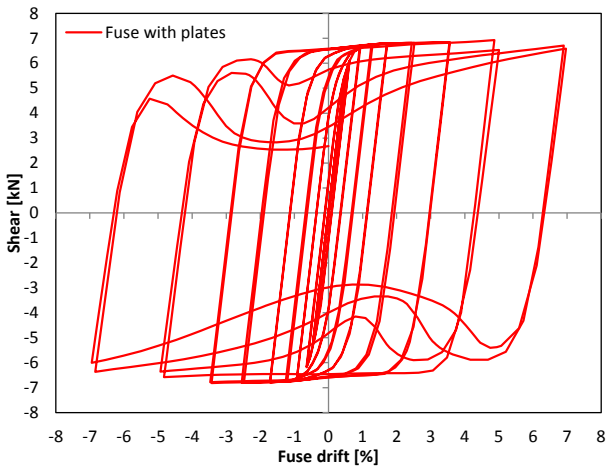

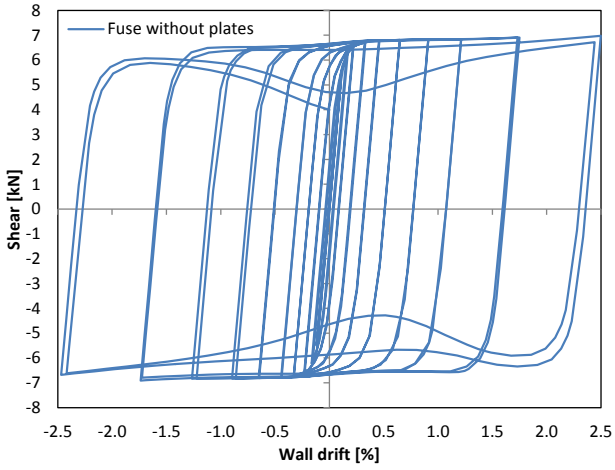

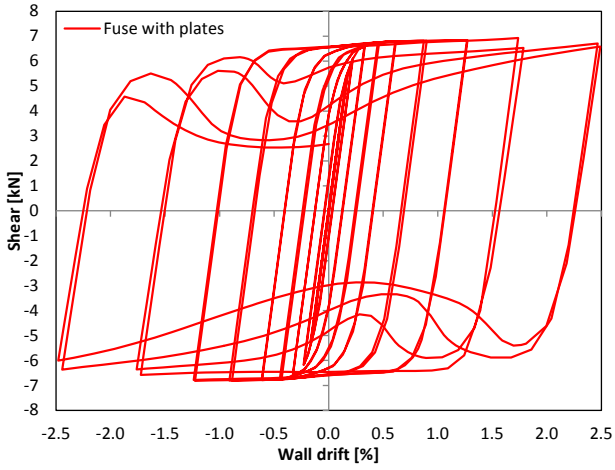

Fuse 16 - L=250mm; b=60mm; t=6mm; σ_y=250MPa

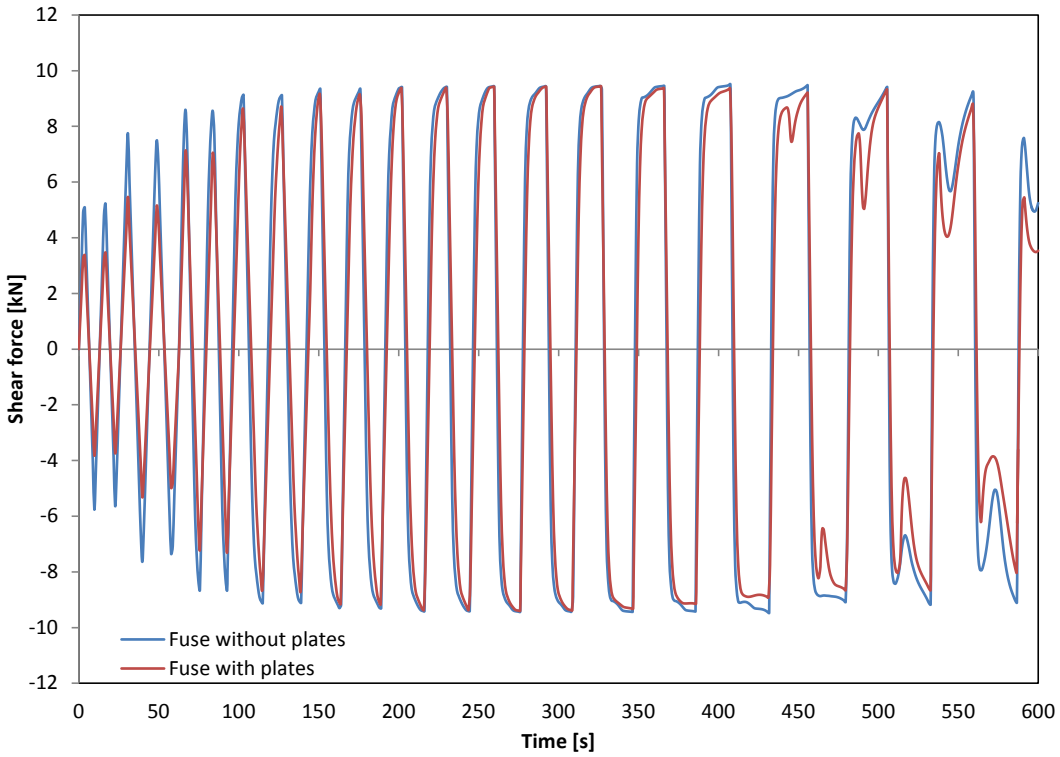

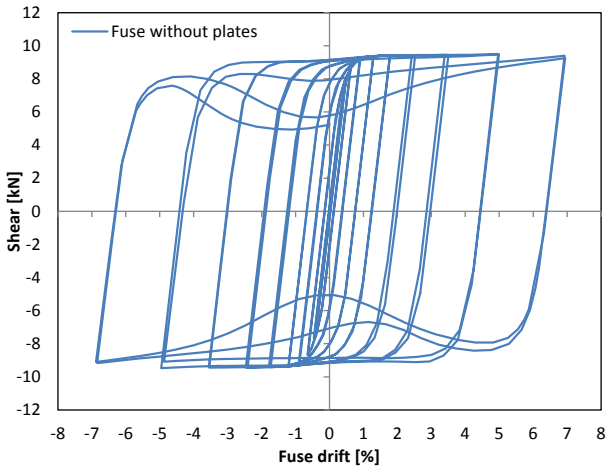

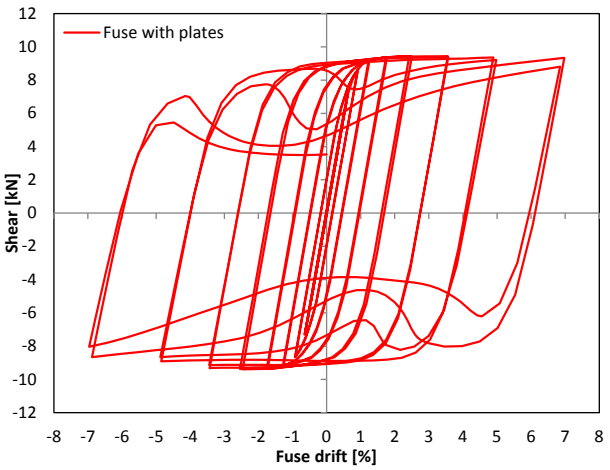

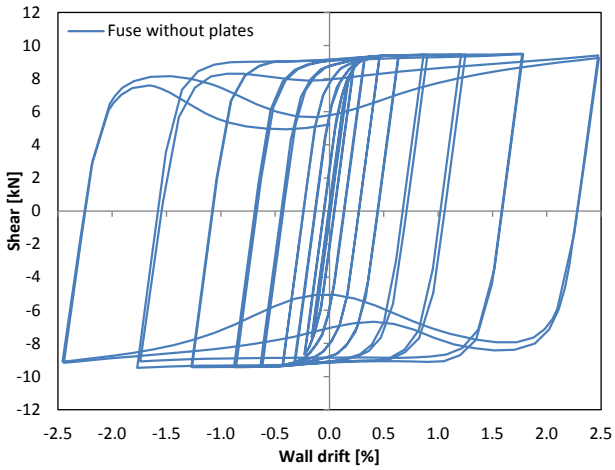

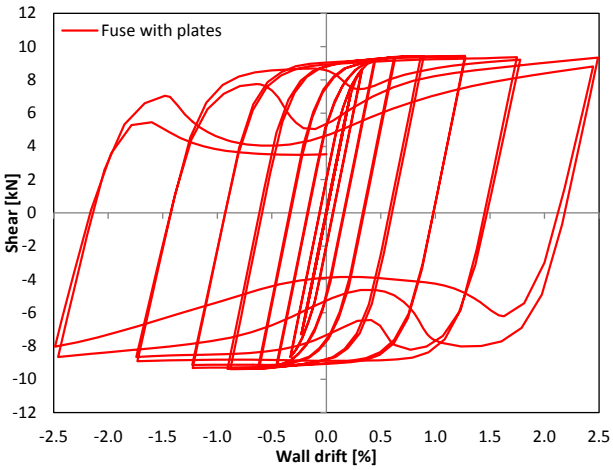

Fuse 17 - L=250mm; b=60mm; t=7mm; σ_y=180MPa

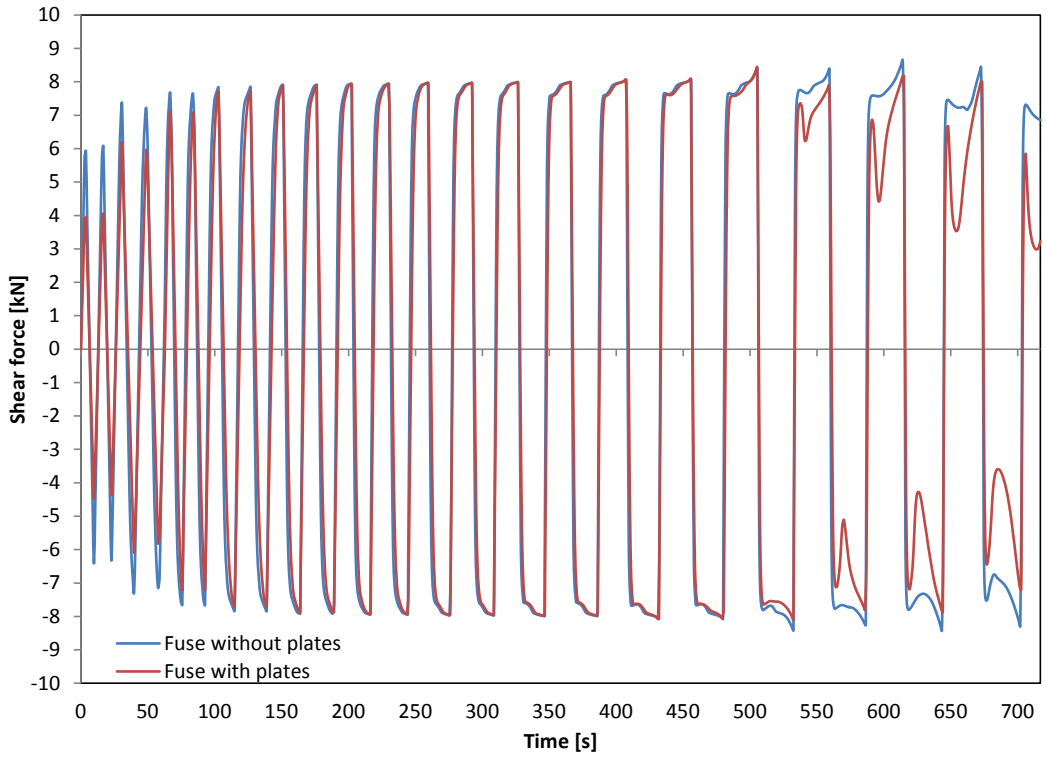

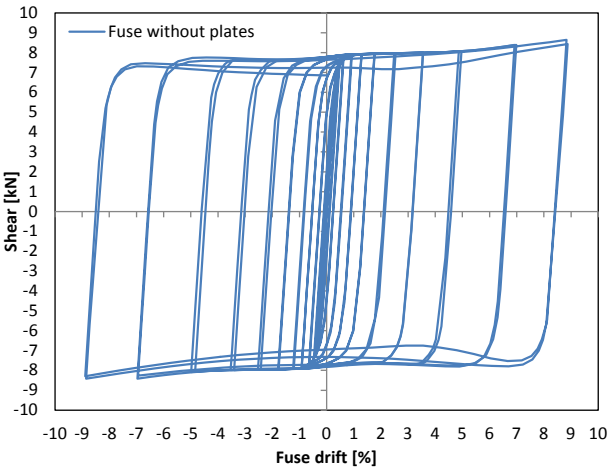

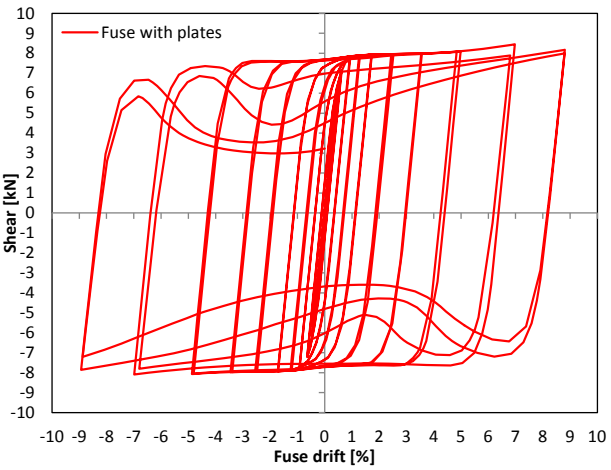

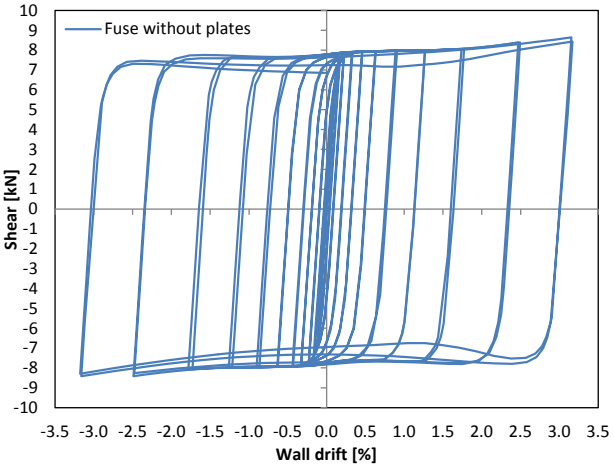

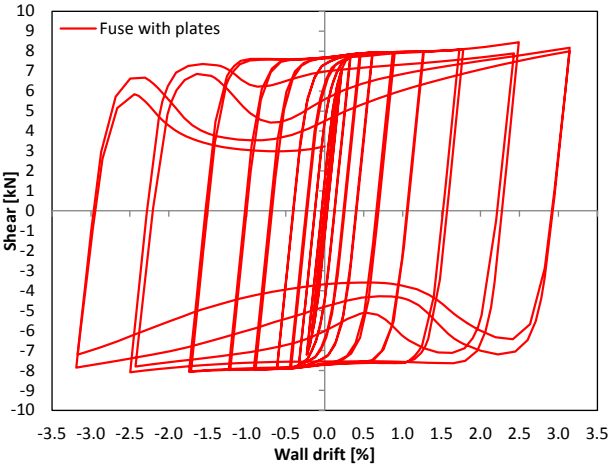

Fuse 18 - L=250mm; b=60mm; t=7mm; σ_y=250MPa

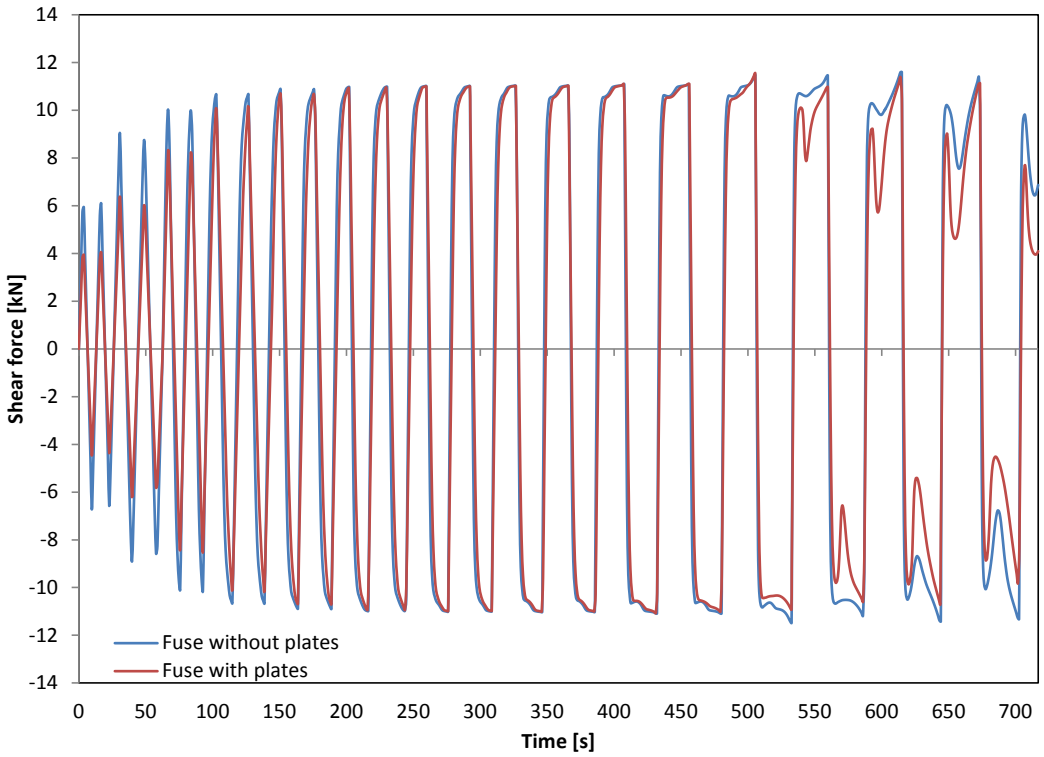

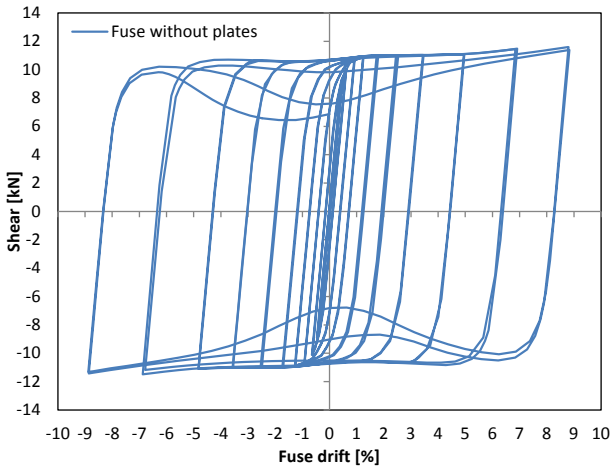

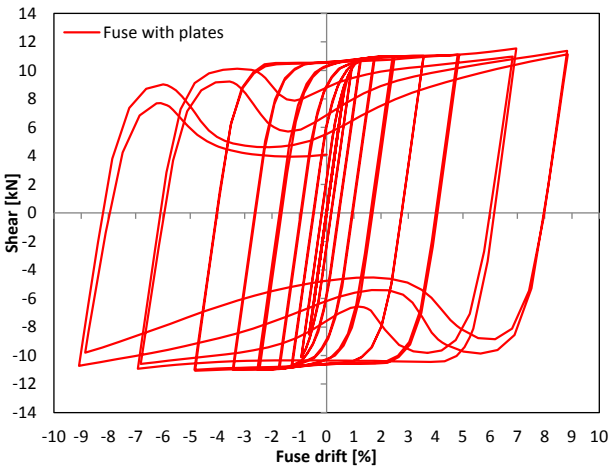

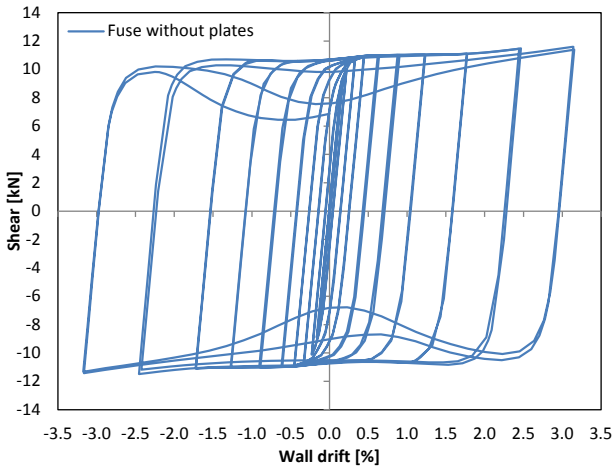

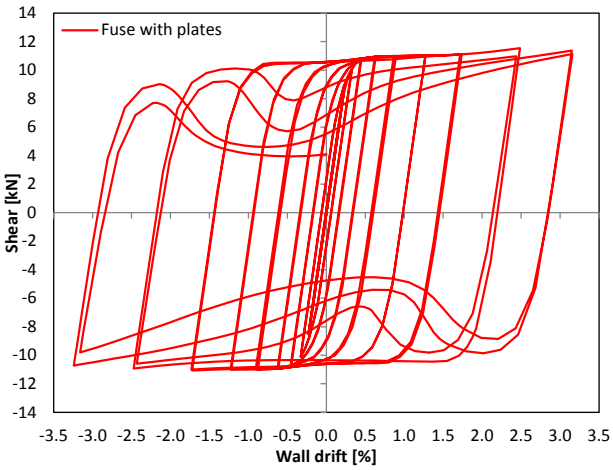

Fuse 19 - L=250mm; b=75mm; t=5mm; σ_y=180MPa

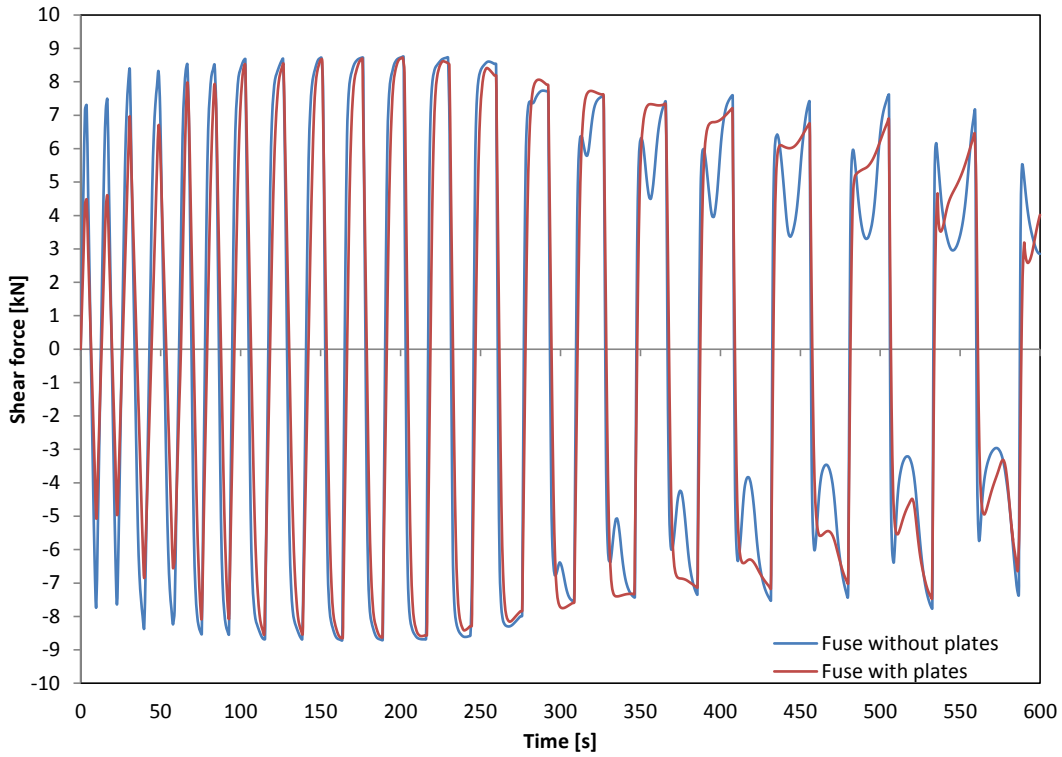

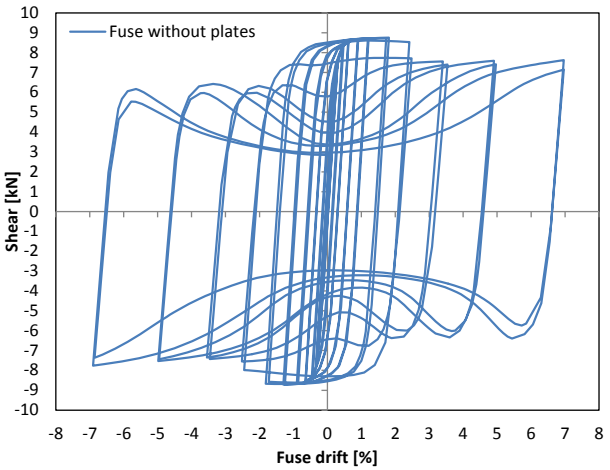

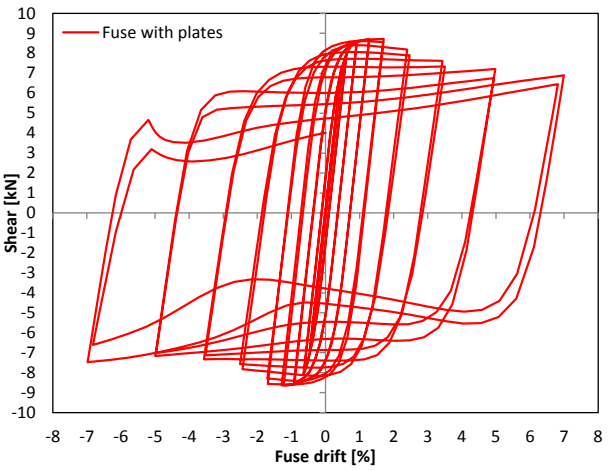

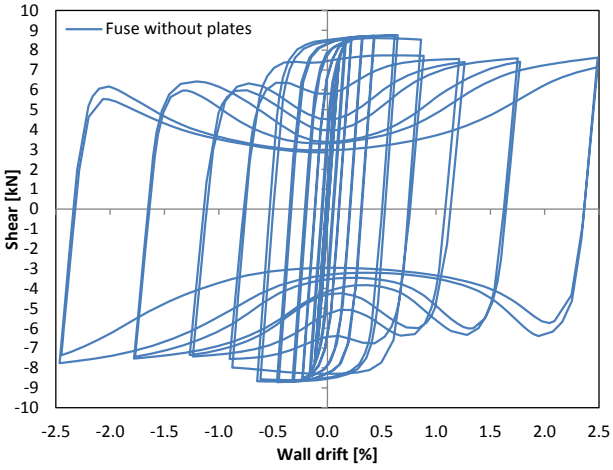

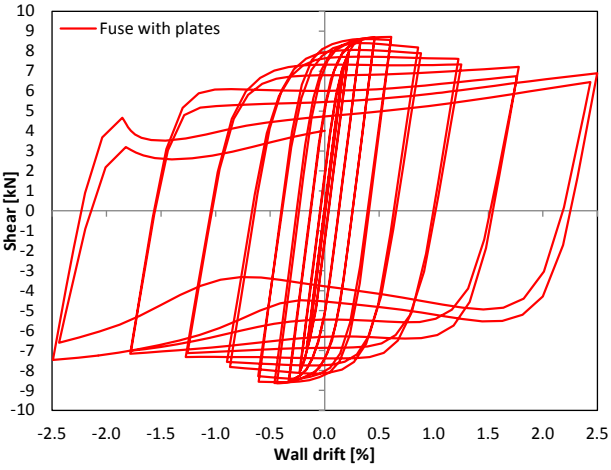

Fuse 20 - L=250mm; b=75mm; t=5mm; σ_y=250MPa

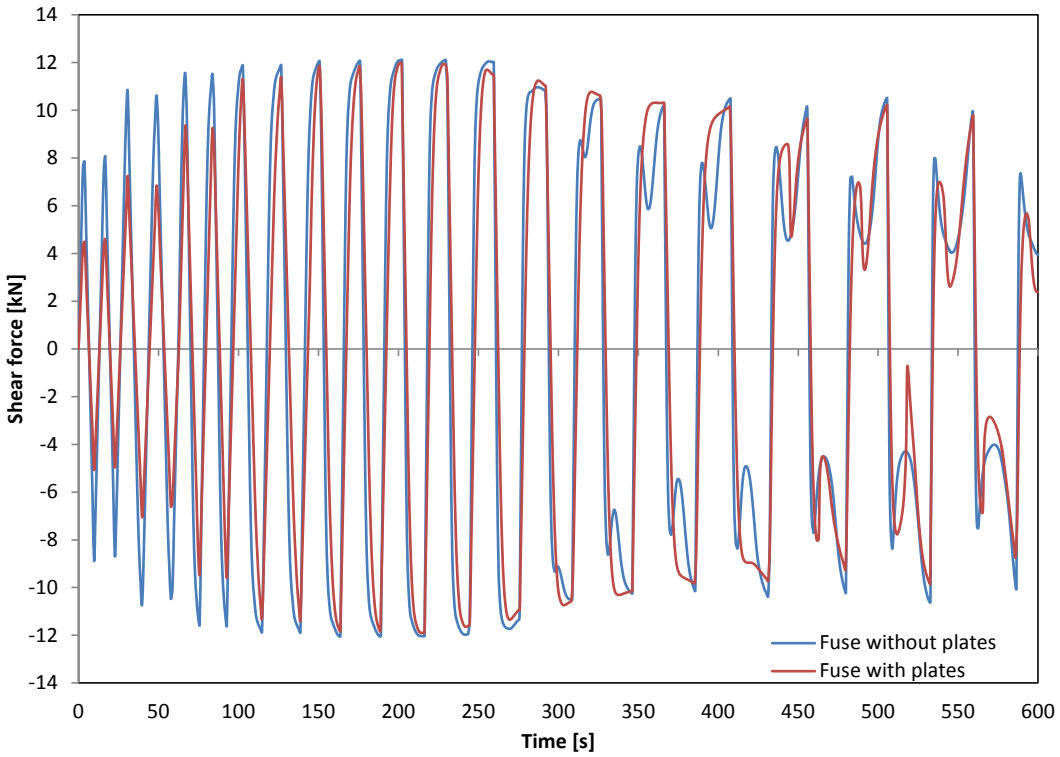

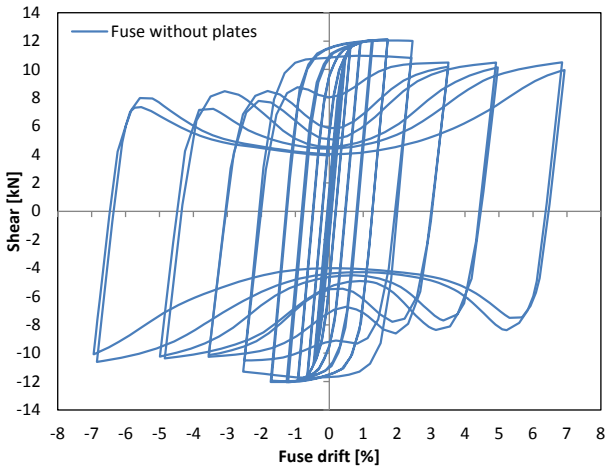

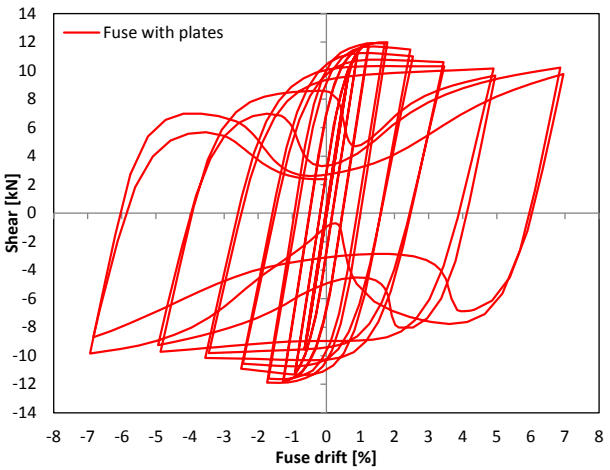

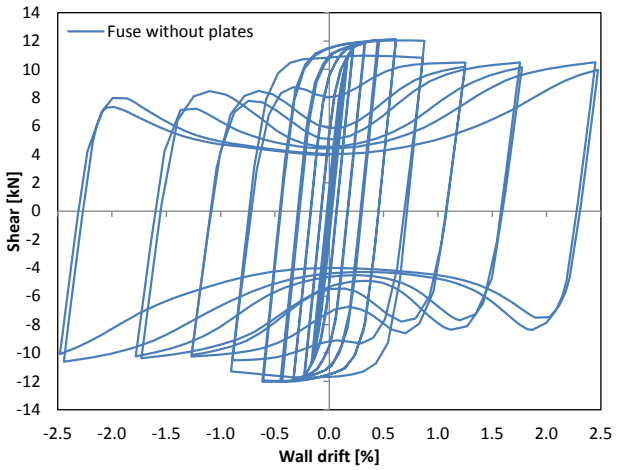

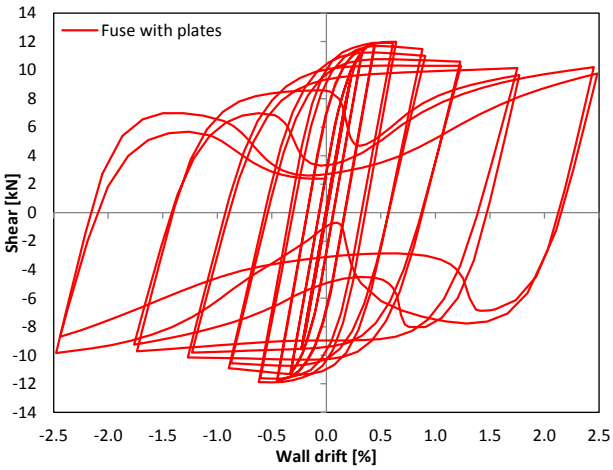

Fuse 21 - L=250mm; b=75mm; t=6mm; σ_y=180MPa

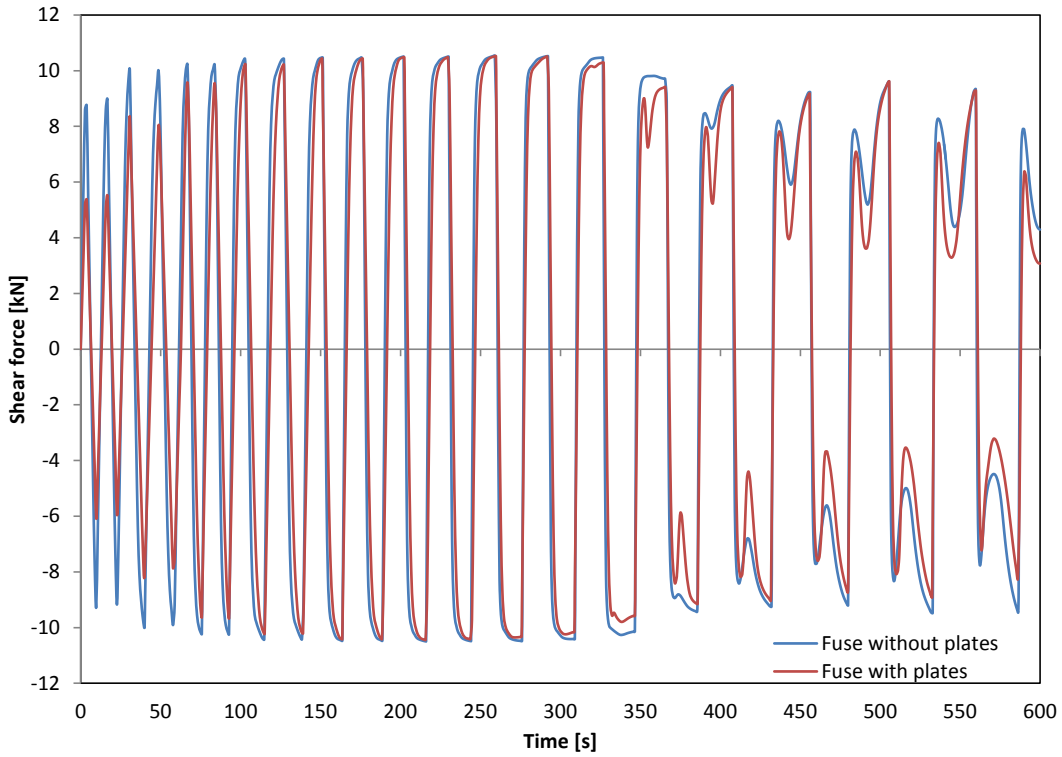

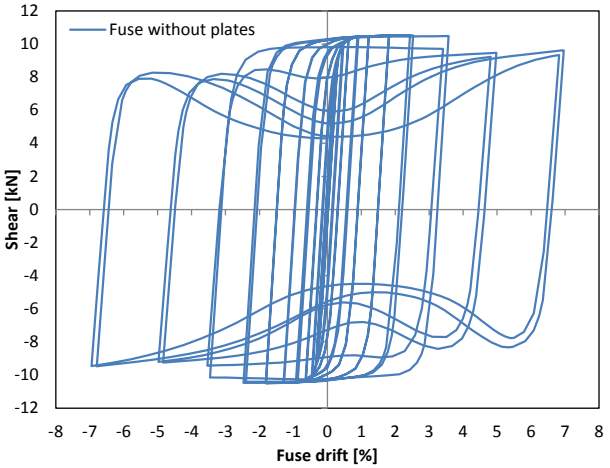

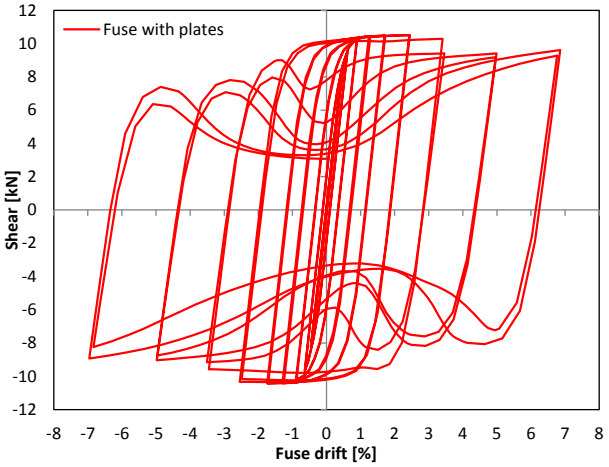

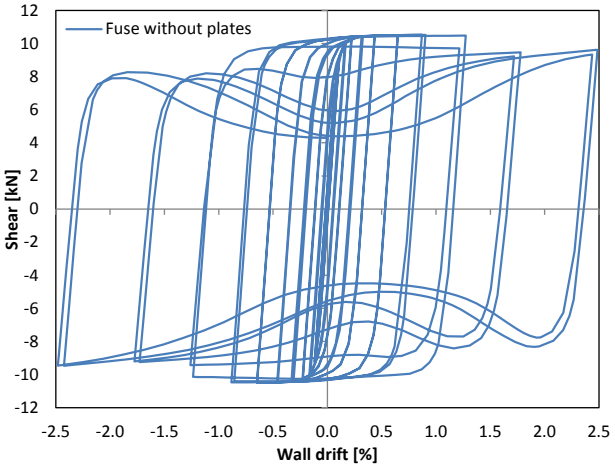

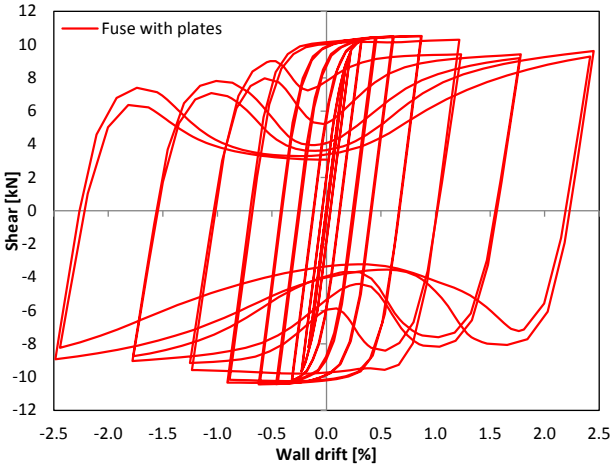

Fuse 22 - L=250mm; b=75mm; t=6mm; σ_y=250MPa

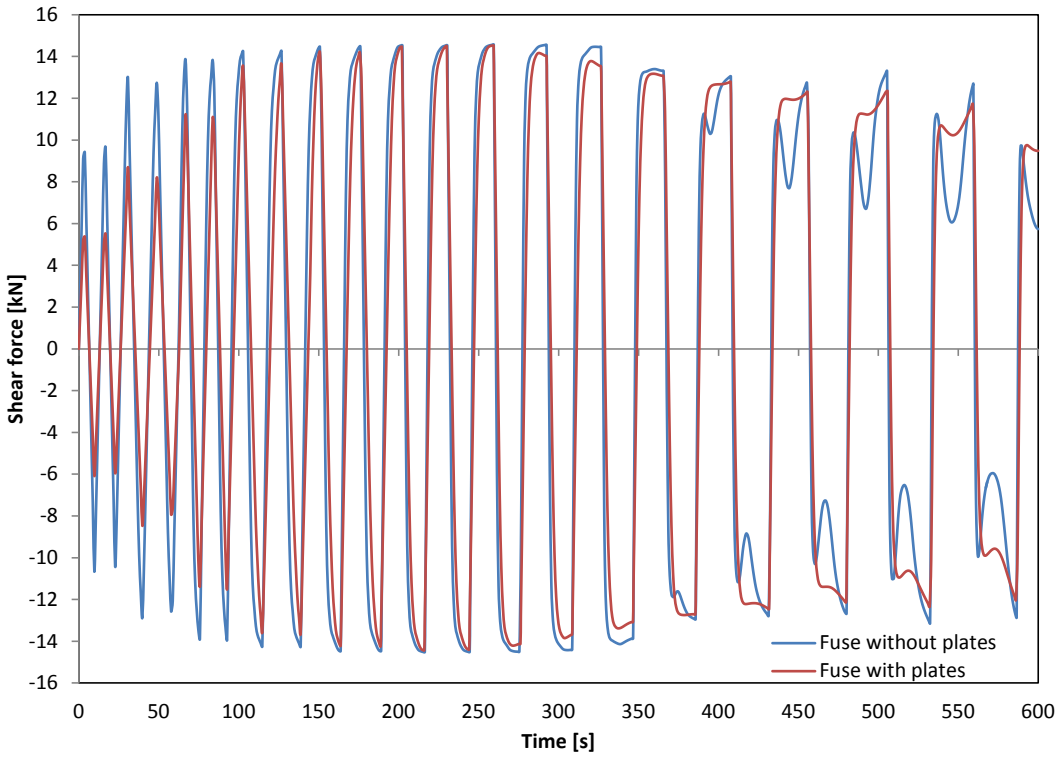

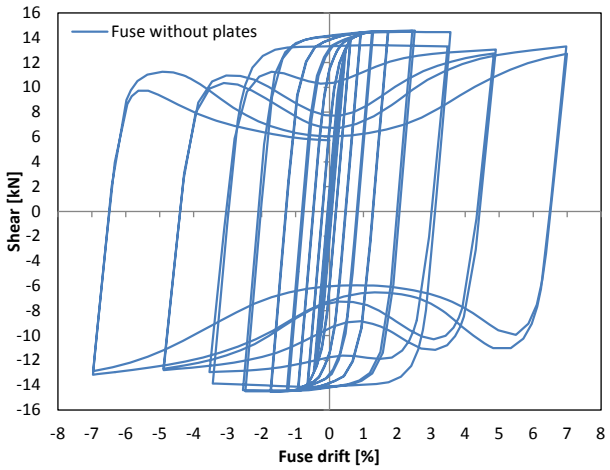

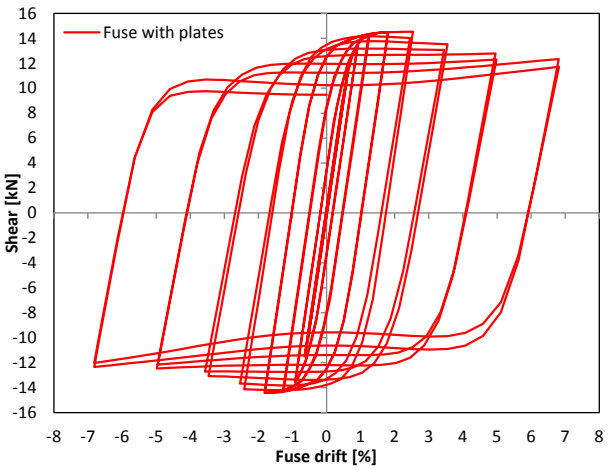

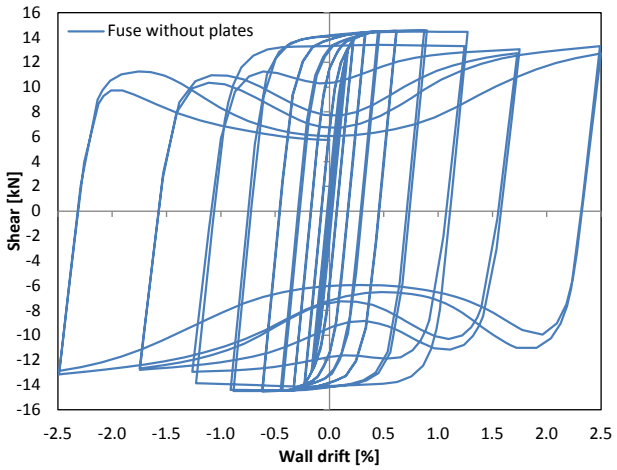

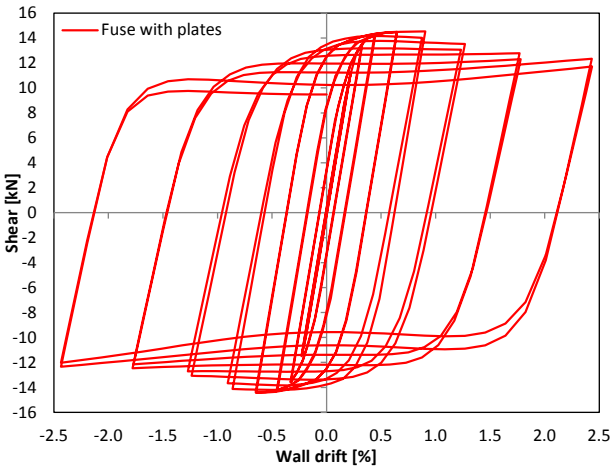

Fuse 23 - L=250mm; b=75mm; t=7mm; σ_y=180MPa

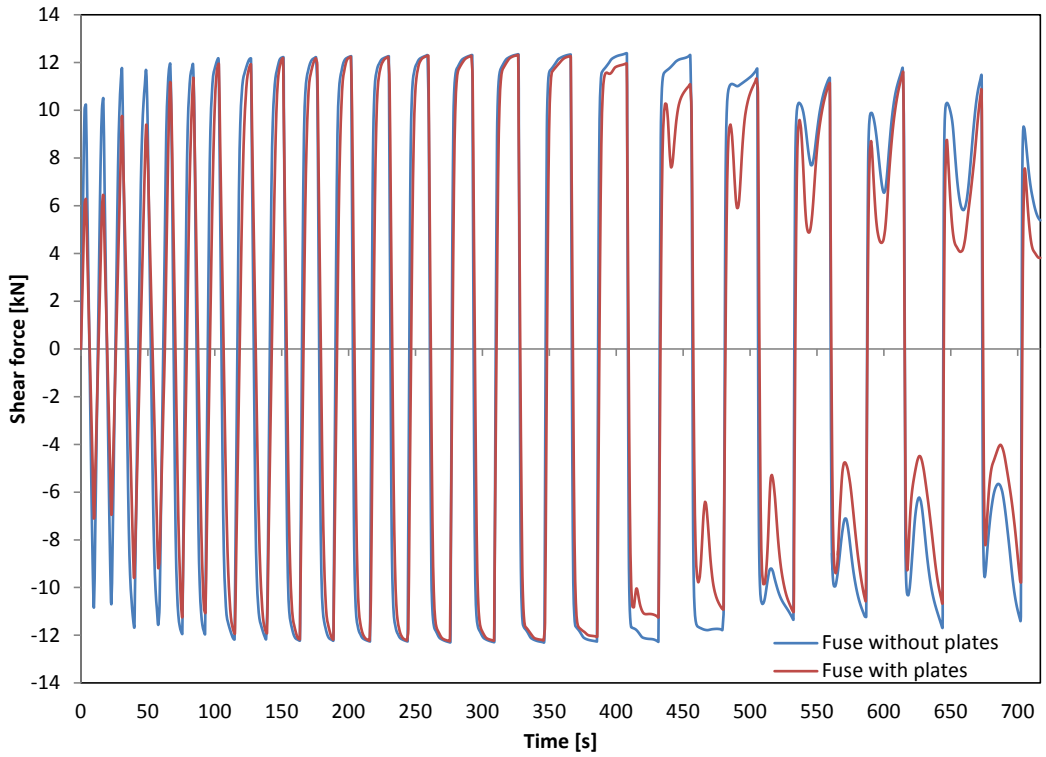

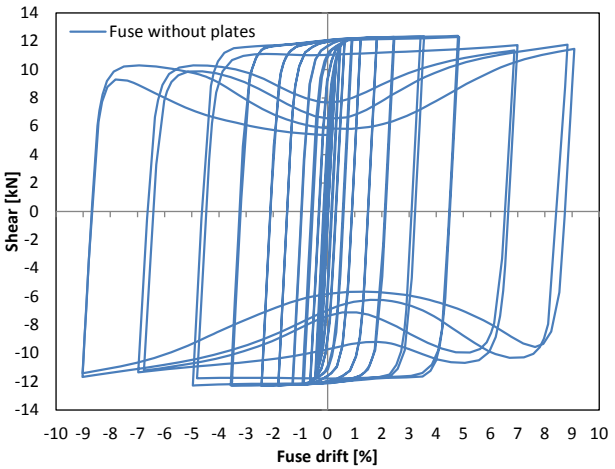

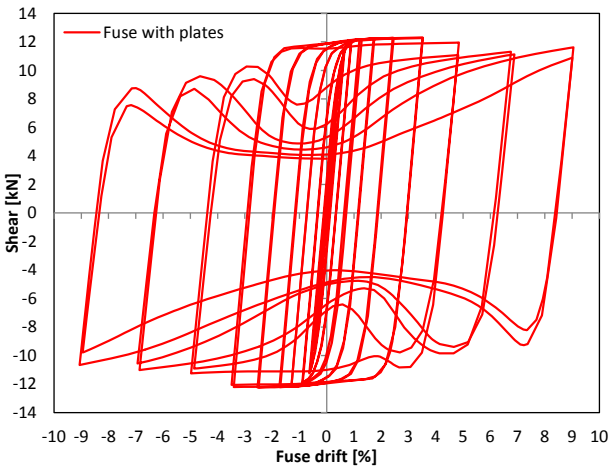

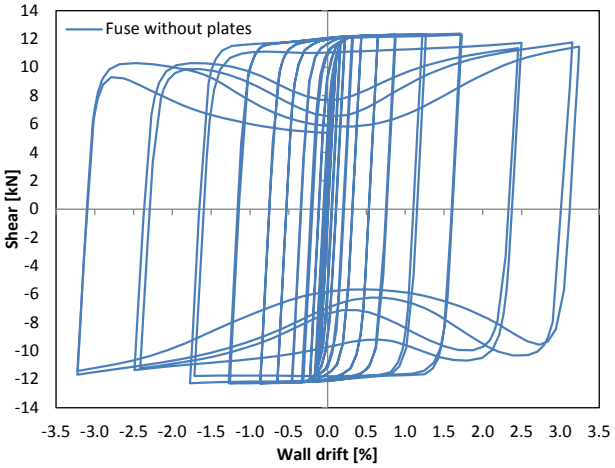

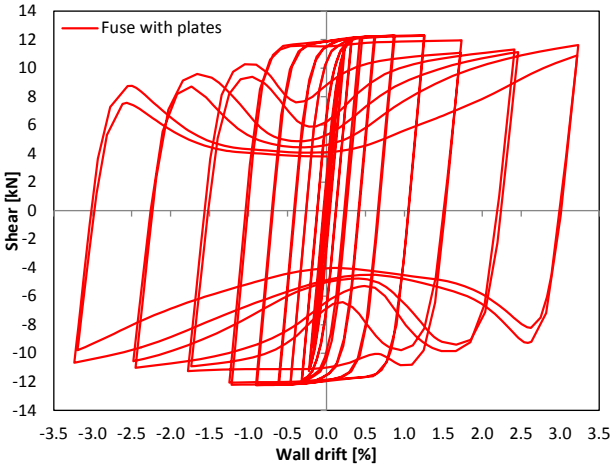

Fuse 24 - L=250mm; b=75mm; t=7mm; σ_y=250MPa

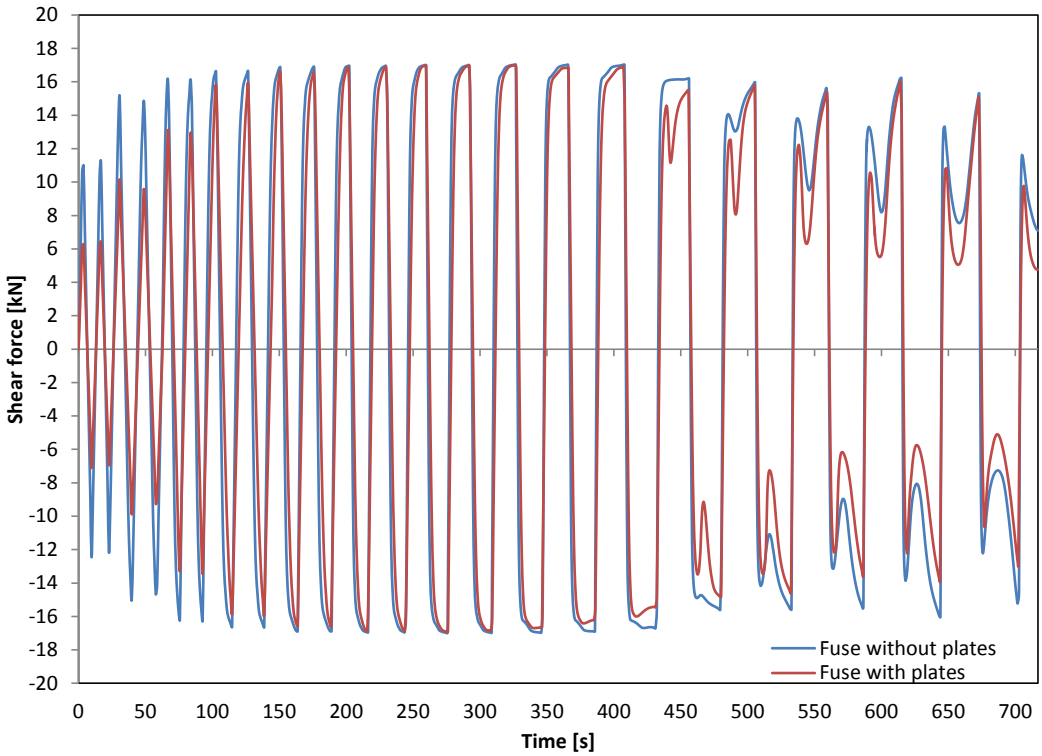

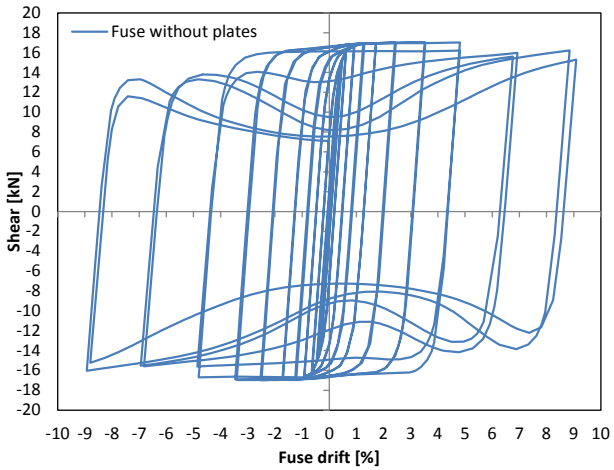

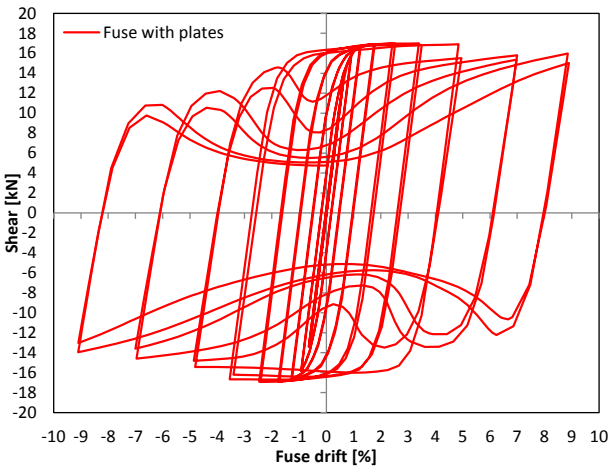

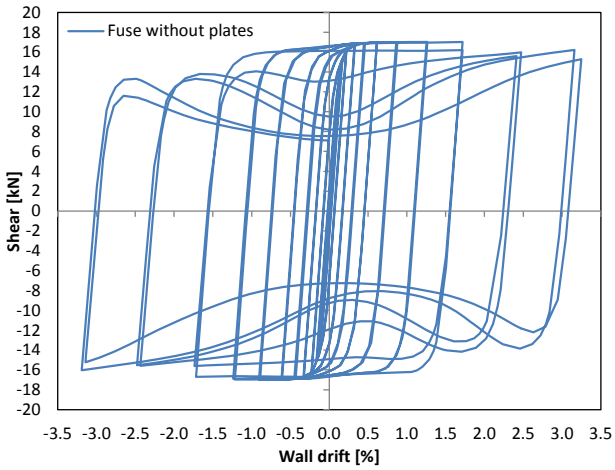

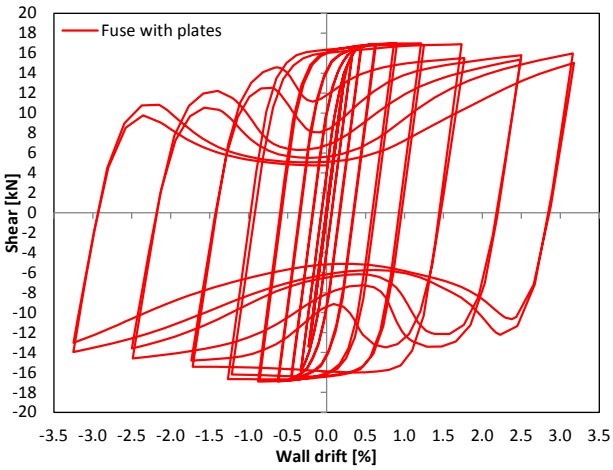

Fuse 25 - L=300mm; b=60mm; t=5mm; σ_y=180MPa

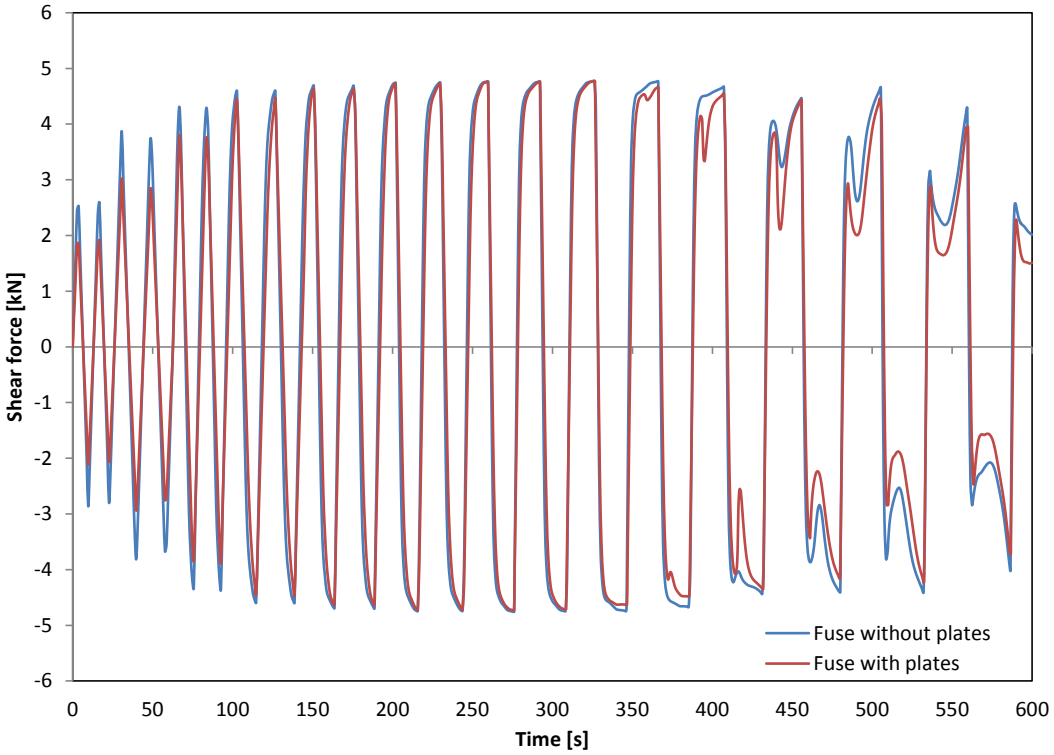

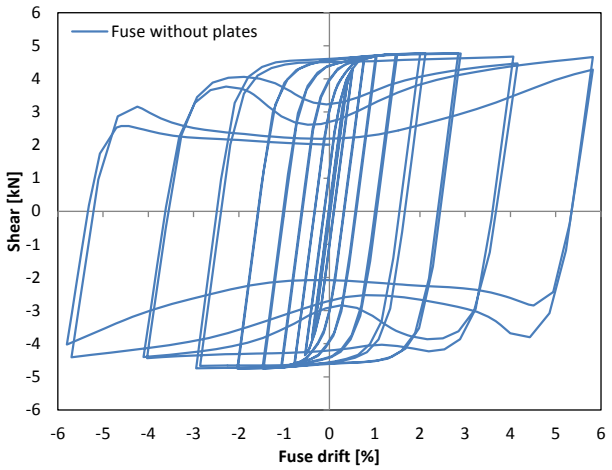

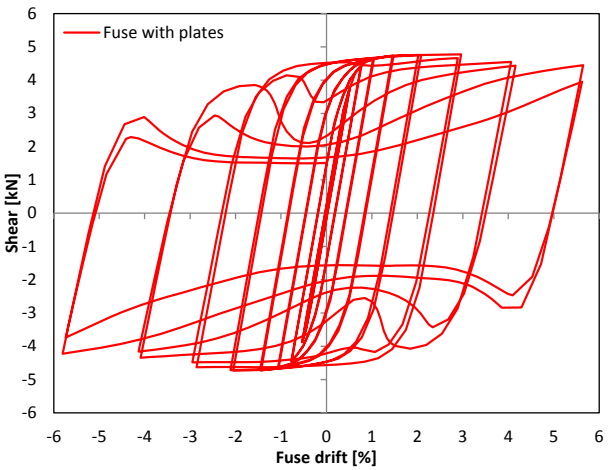

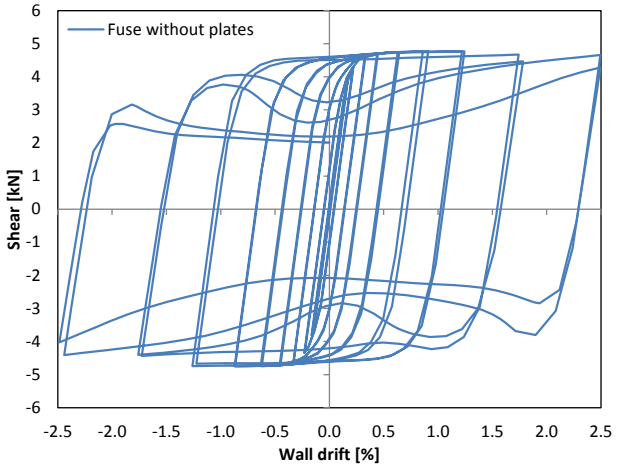

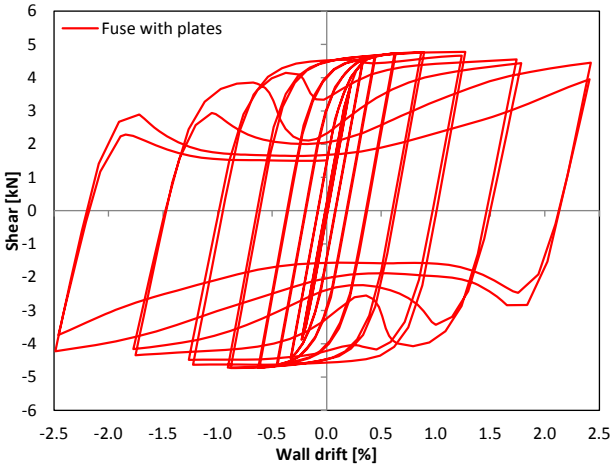

Fuse 26 - L=300mm; b=60mm; t=5mm; σ_y=250MPa

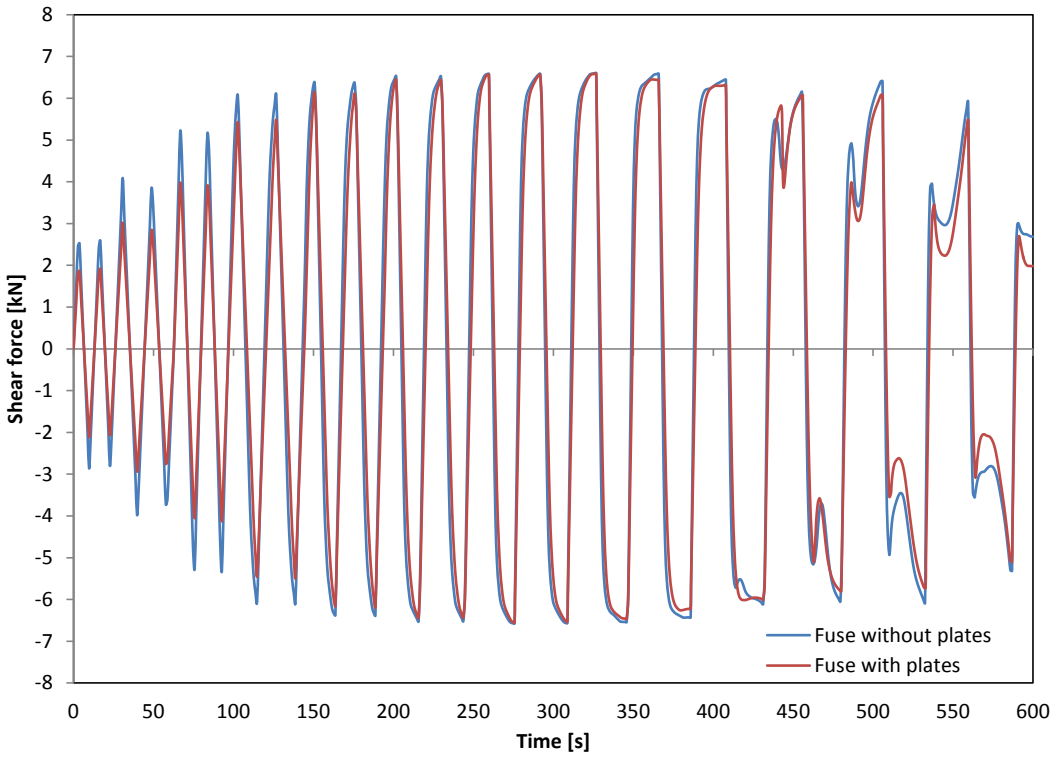

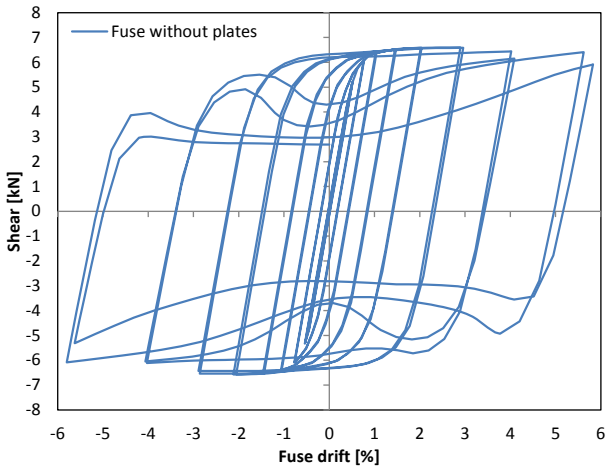

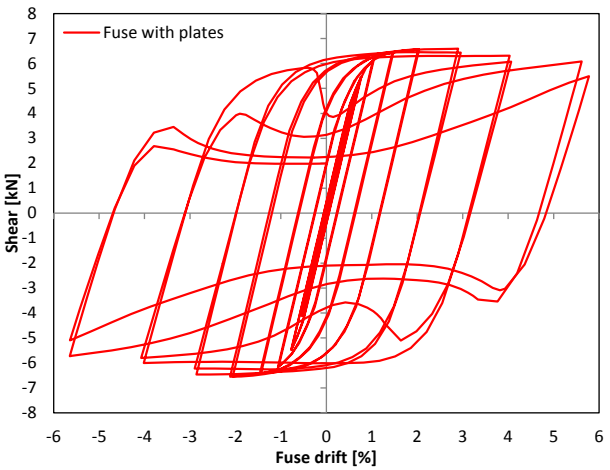

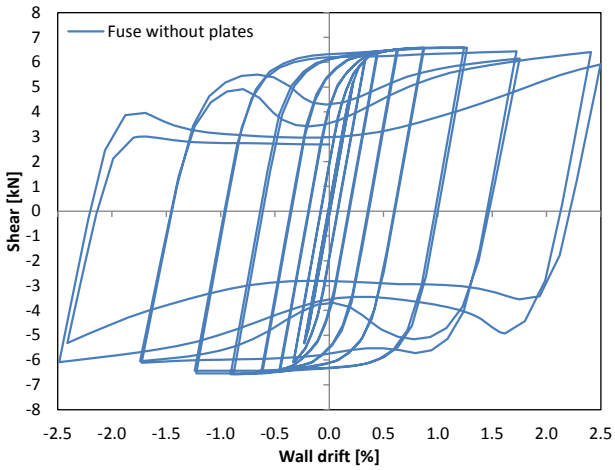

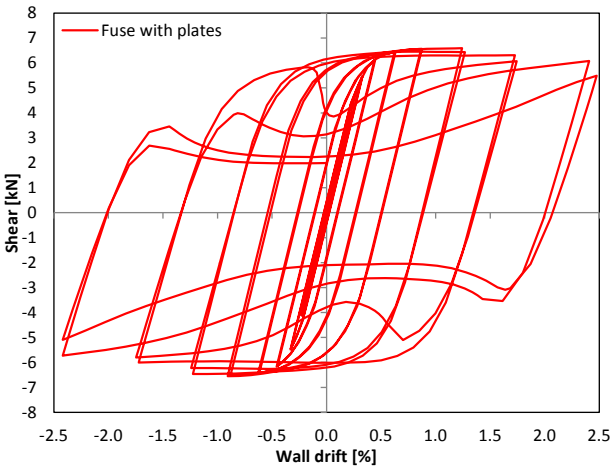

Fuse 27 - L=300mm; b=60mm; t=6mm; σ_y=180MPa

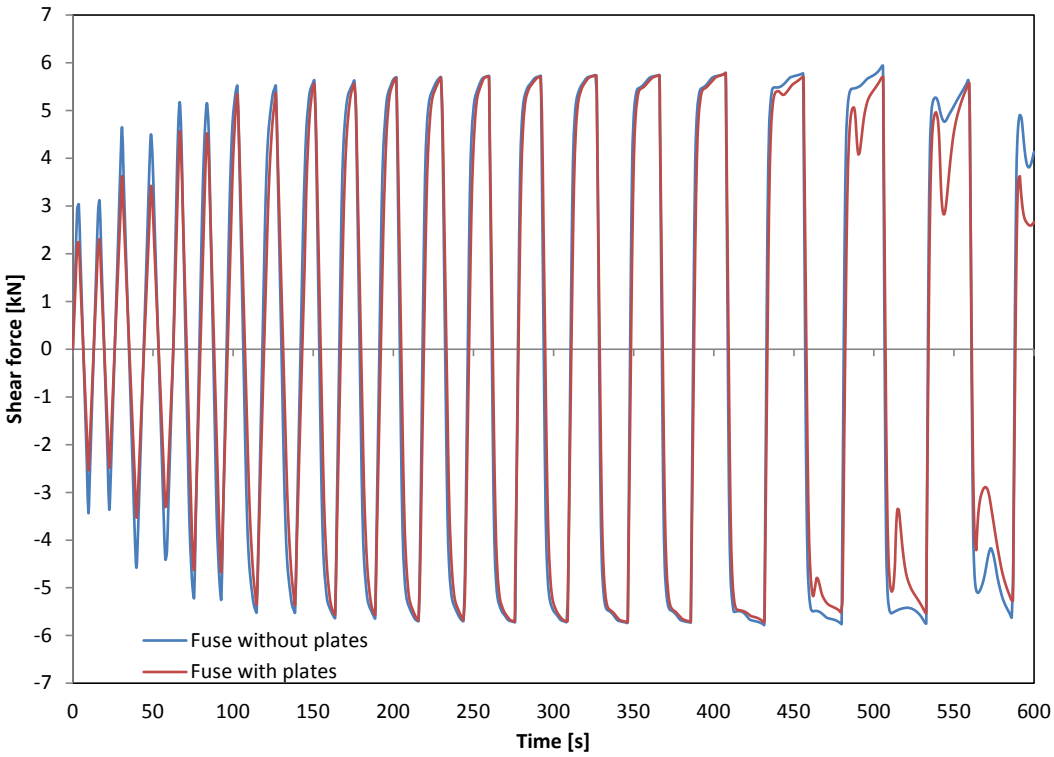

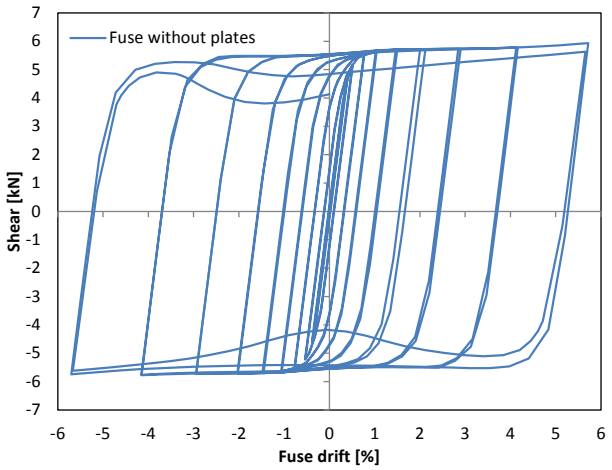

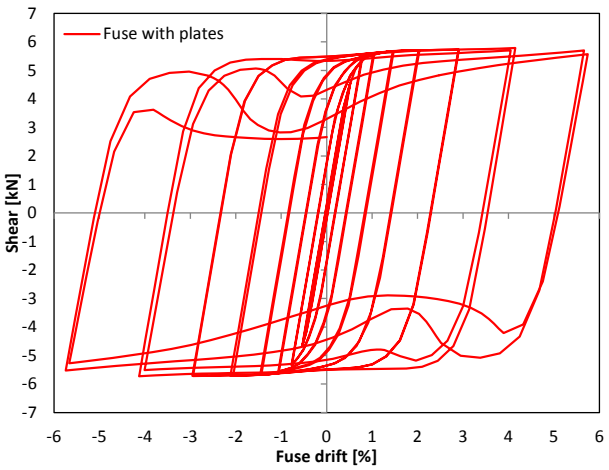

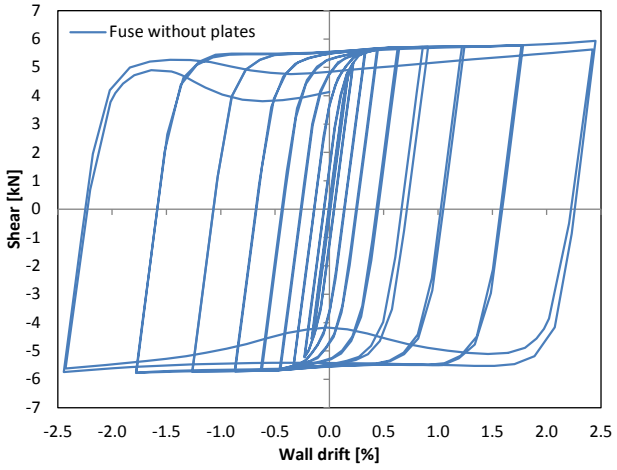

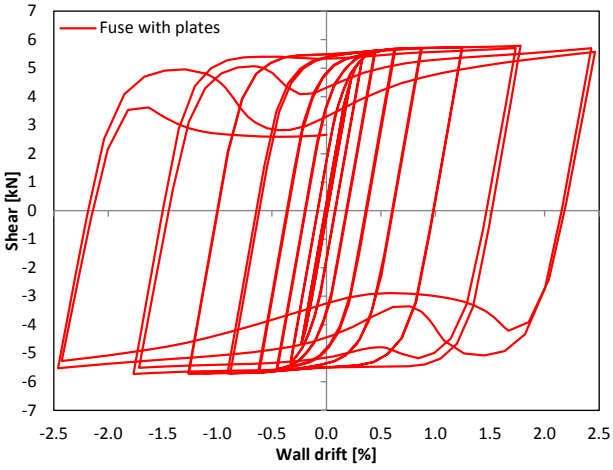

Fuse 28 - L=300mm; b=60mm; t=6mm; σ_y=250MPa

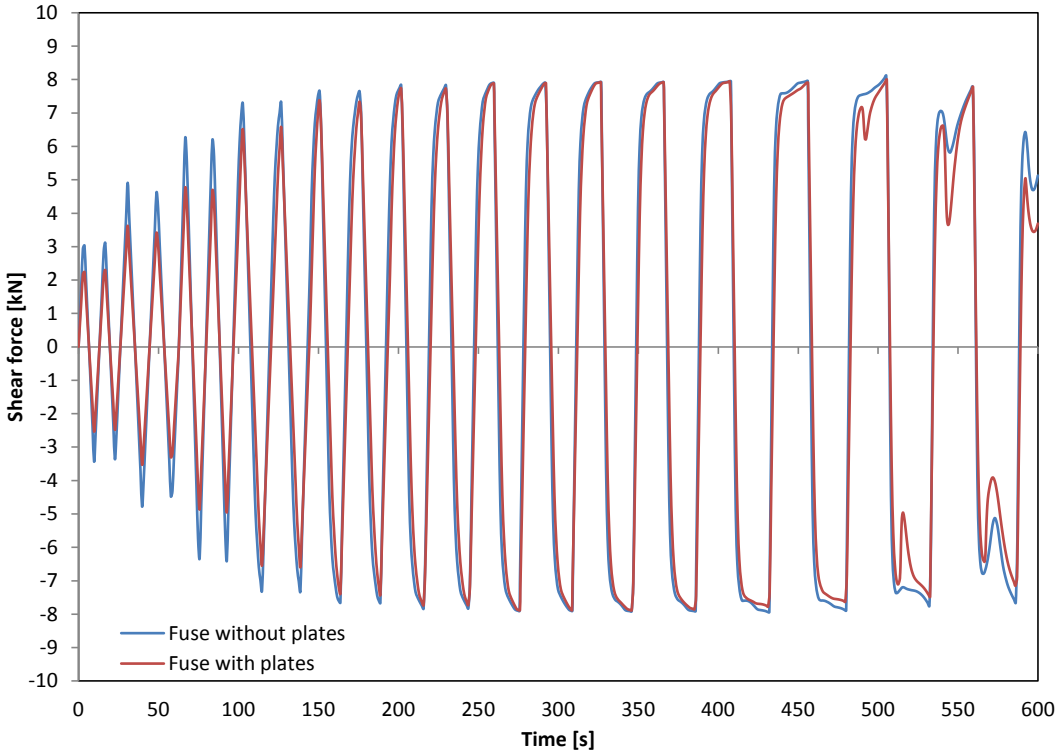

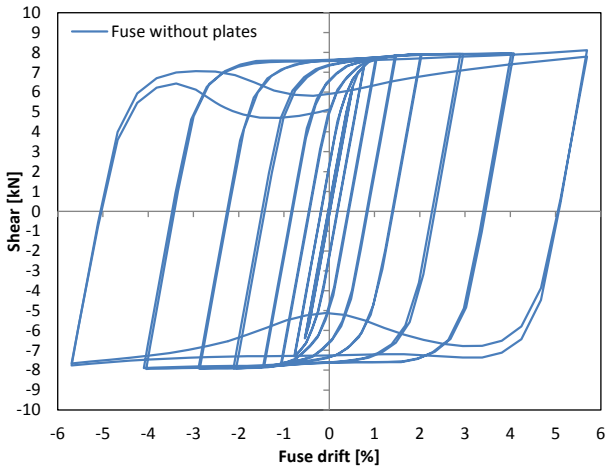

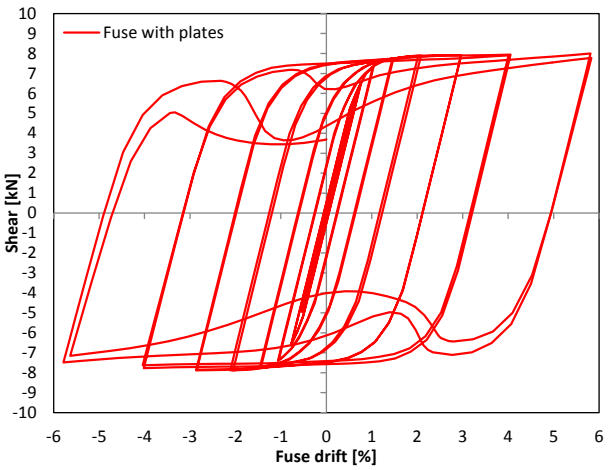

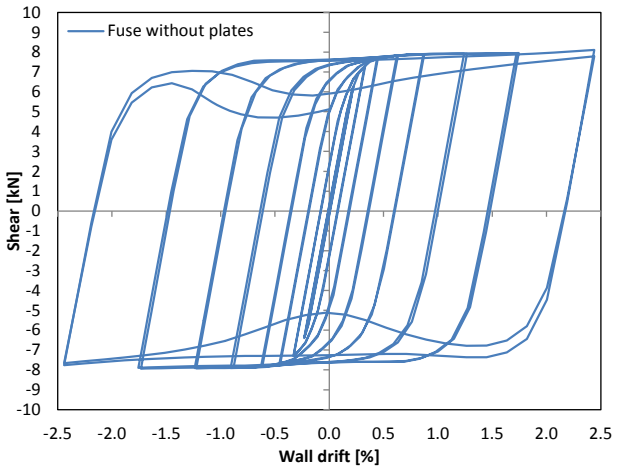

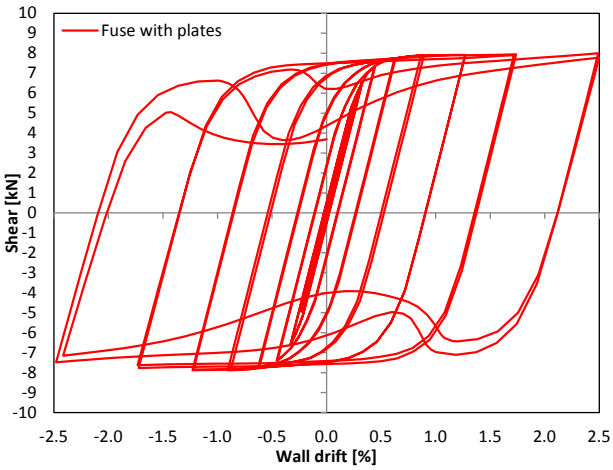

Fuse 29 - L=300mm; b=60mm; t=7mm; σ_y=180MPa

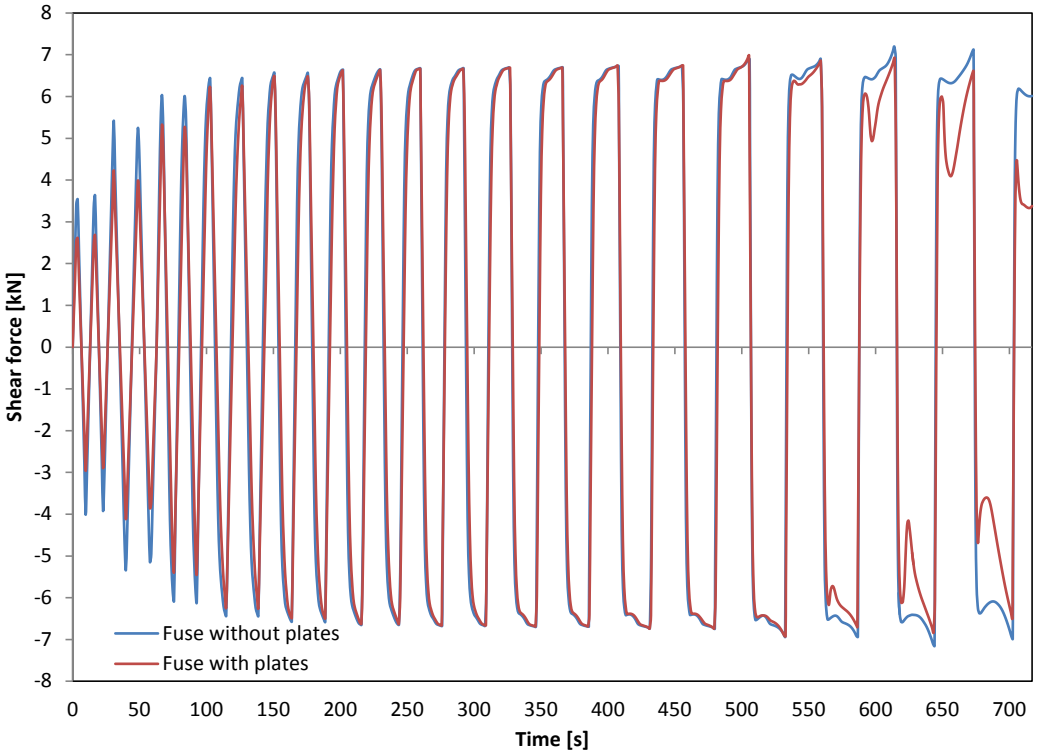

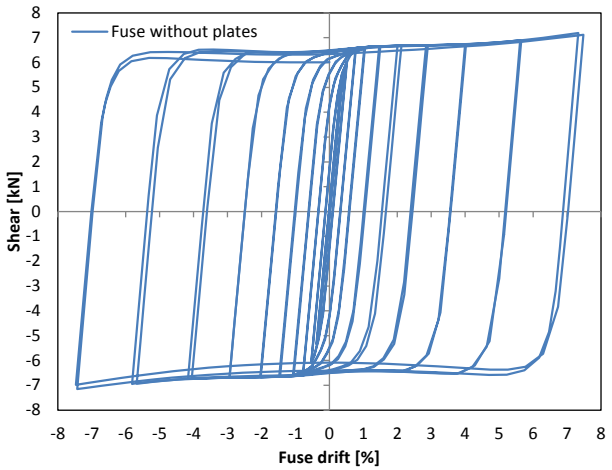

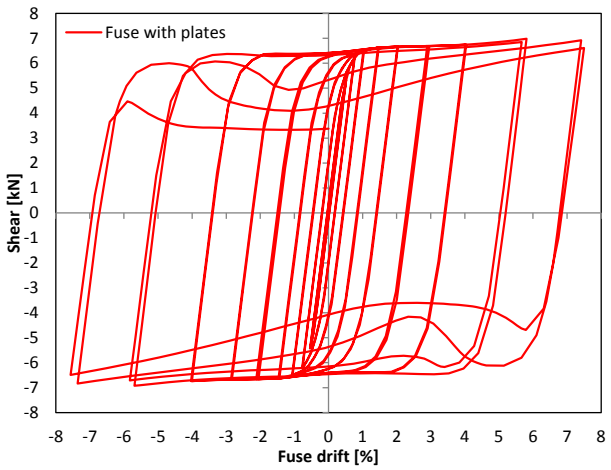

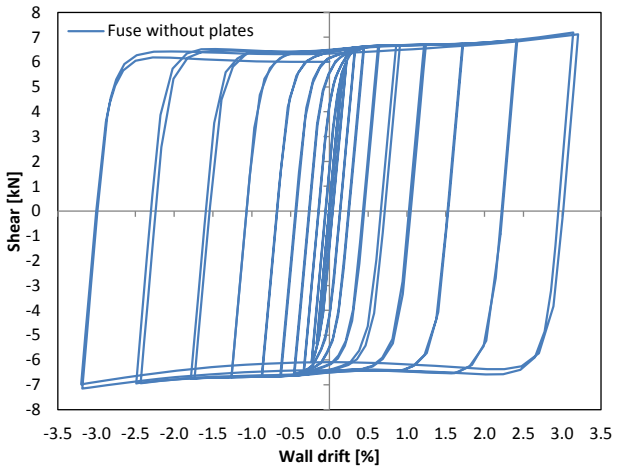

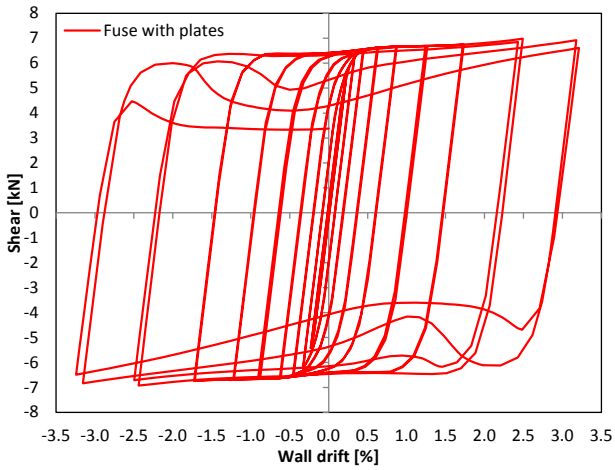

Fuse 30 - L=300mm; b=60mm; t=7mm; σ_y=250MPa

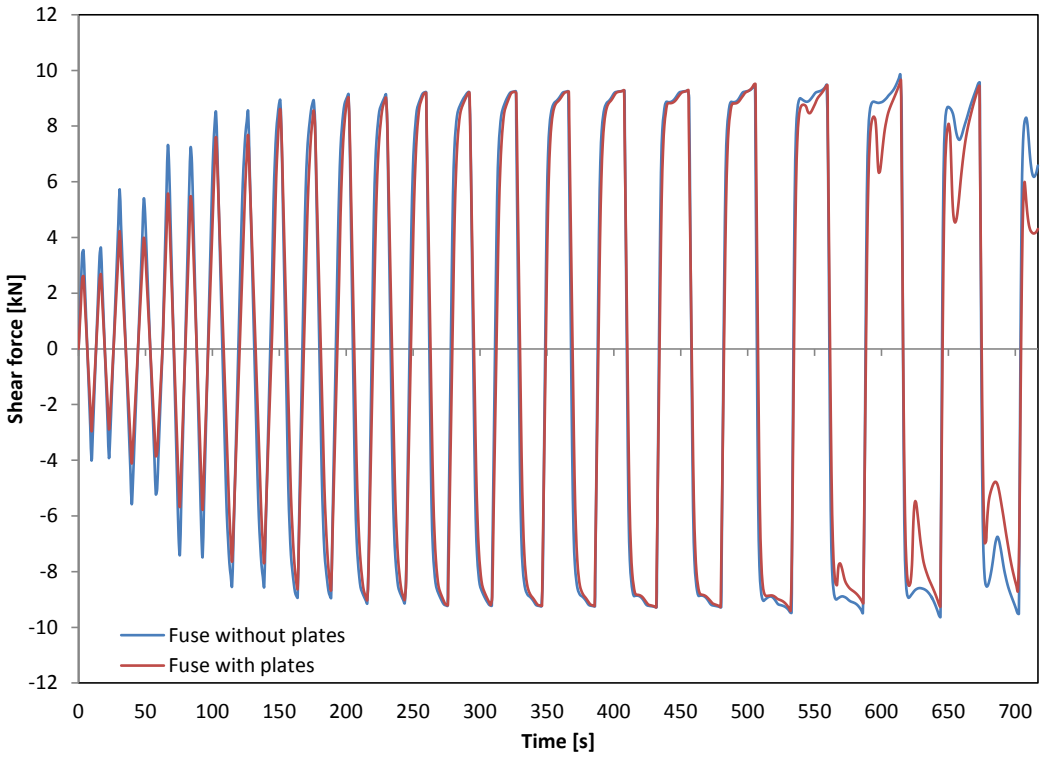

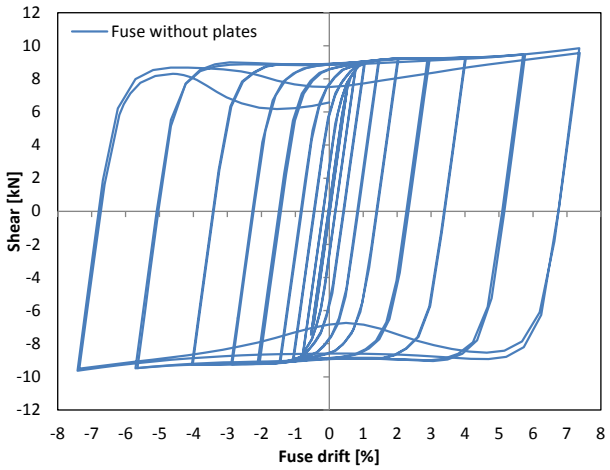

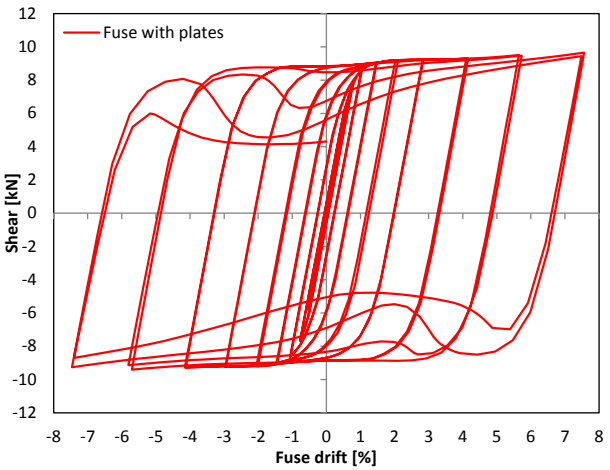

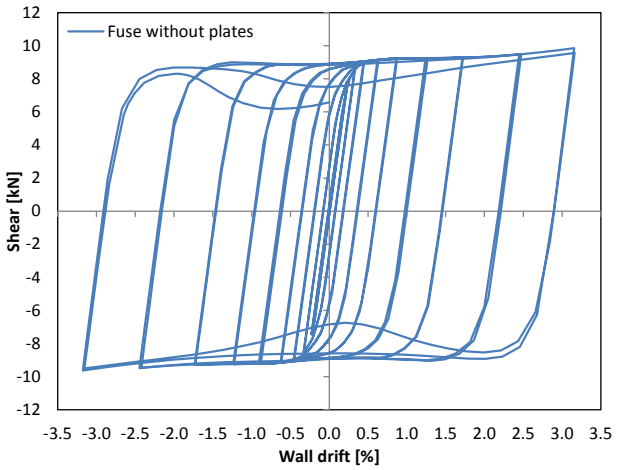

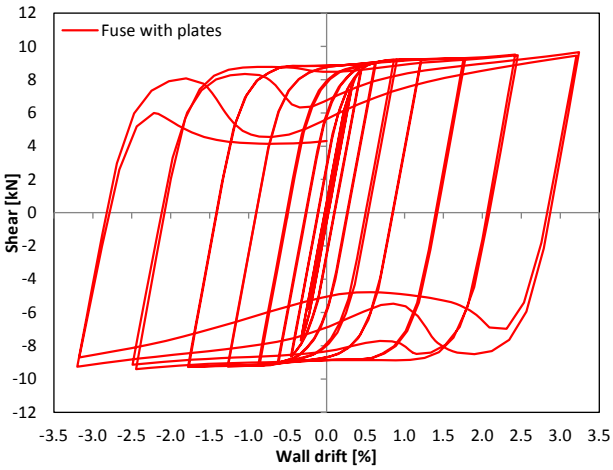

Fuse 31 - L=300mm; b=75mm; t=5mm; σ_y=180MPa

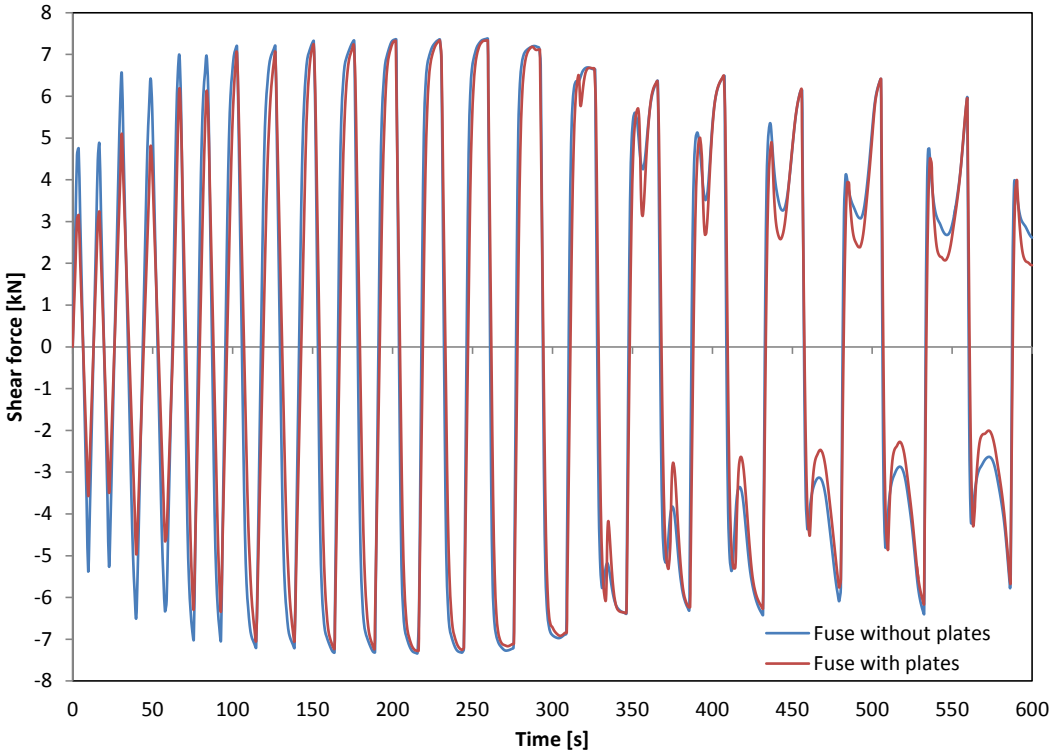

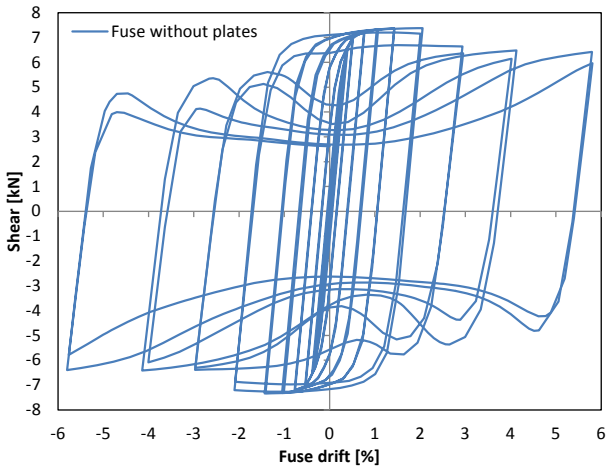

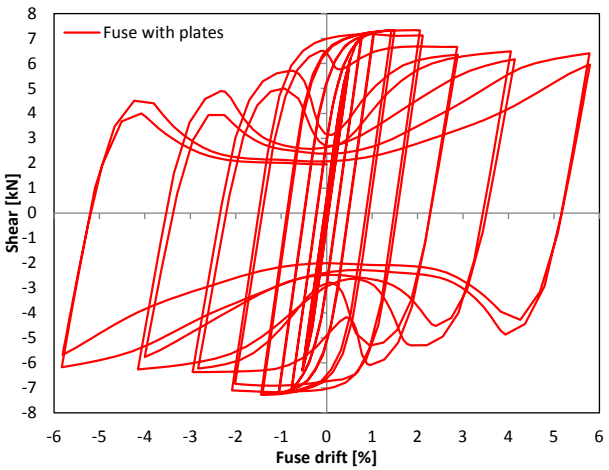

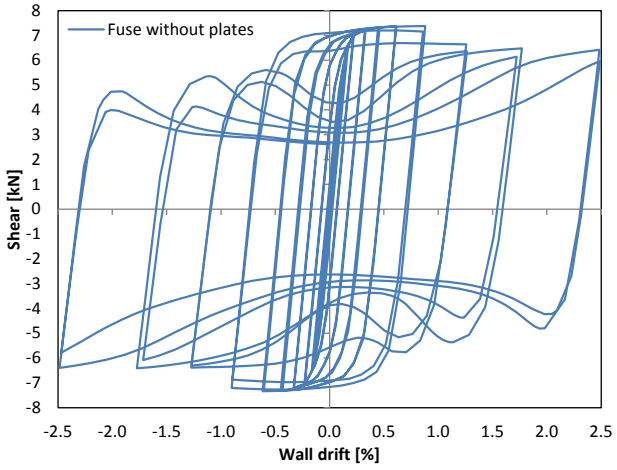

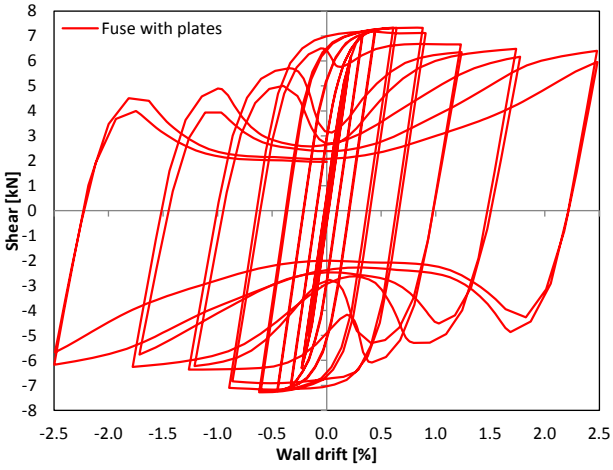

Fuse 32 - L=300mm; b=75mm; t=5mm; σ_y=250MPa

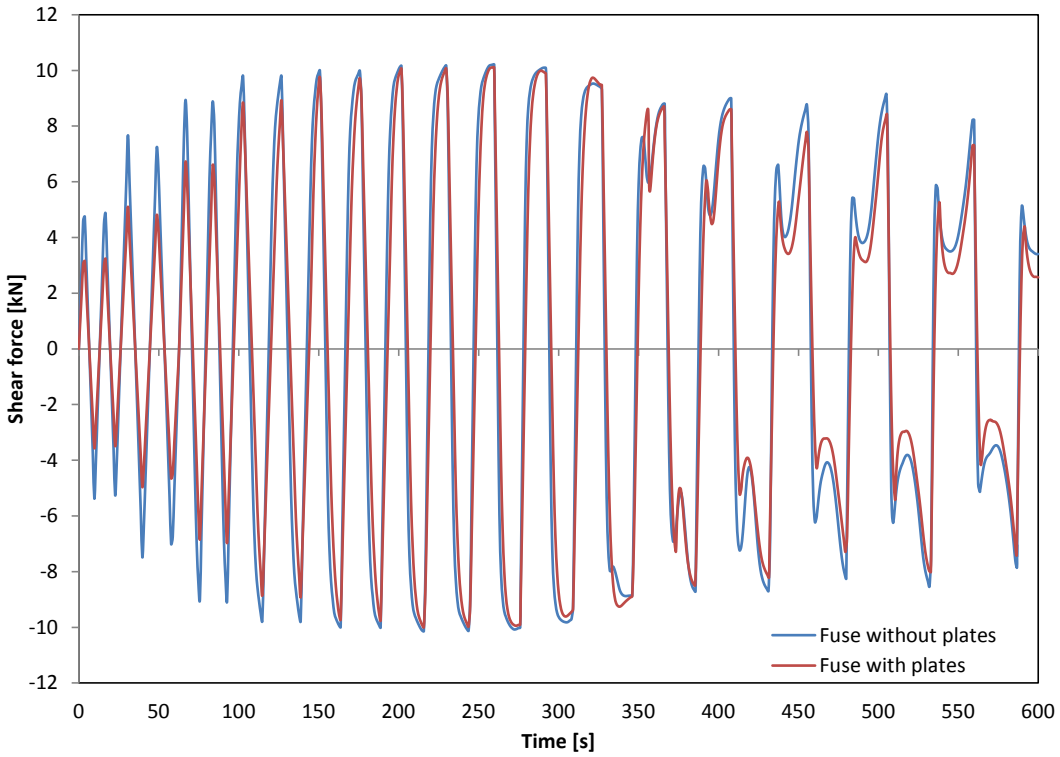

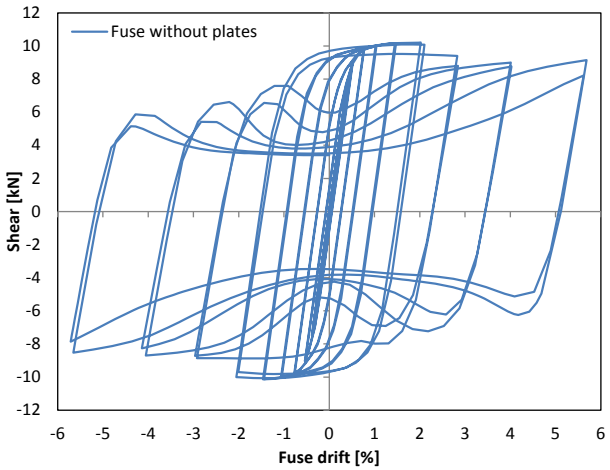

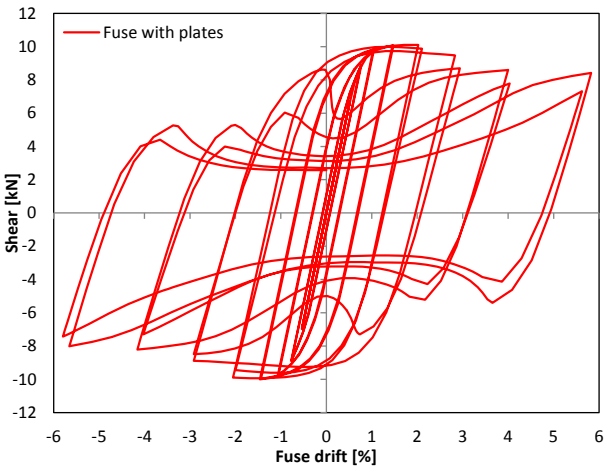

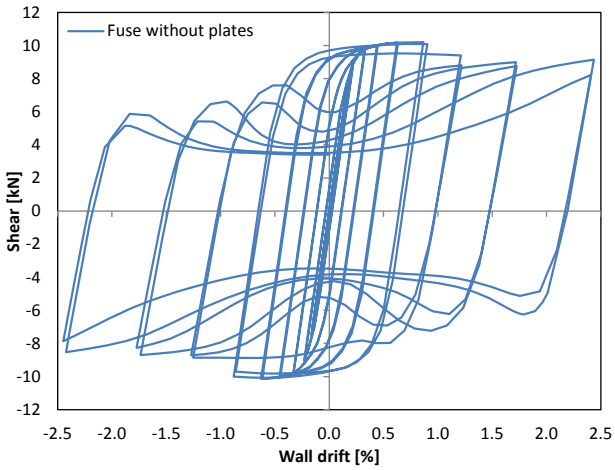

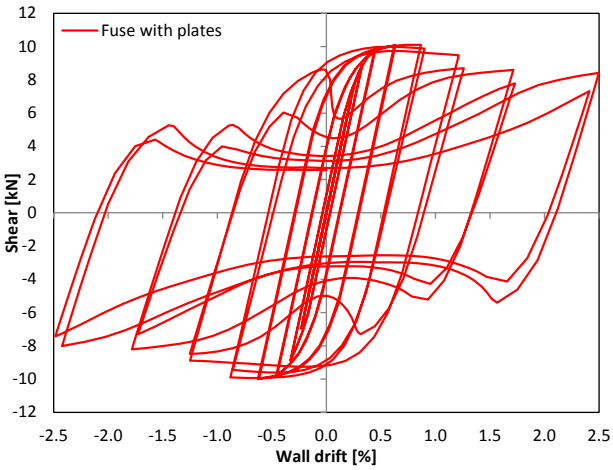

Fuse 33 - L=300mm; b=75mm; t=6mm; σ_y=180MPa

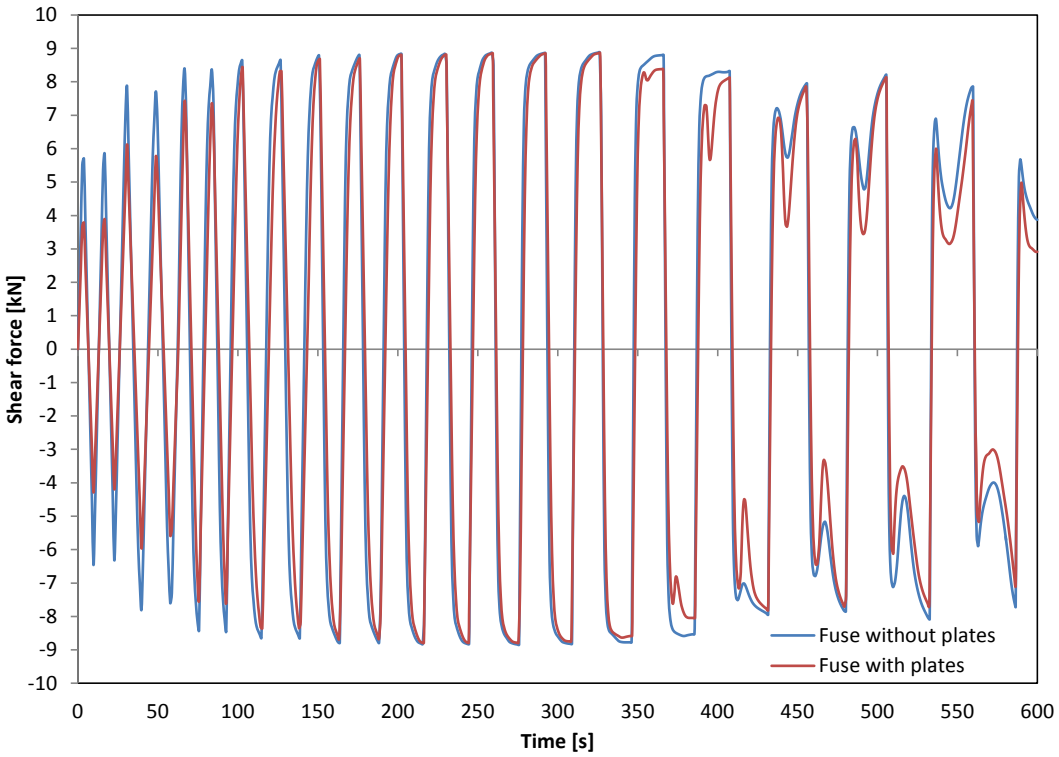

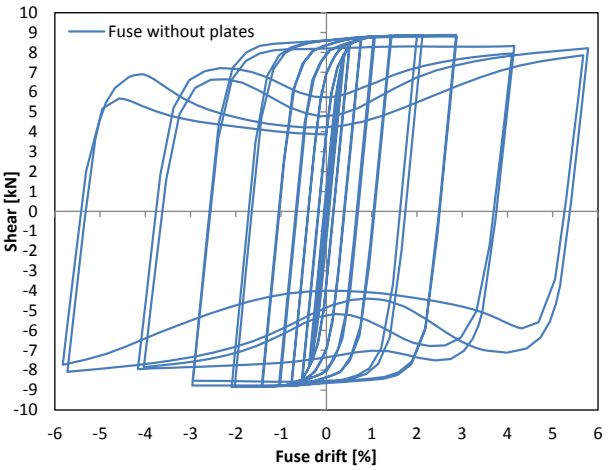

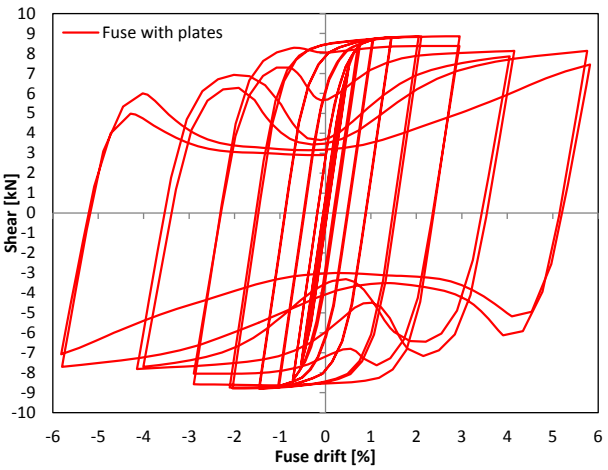

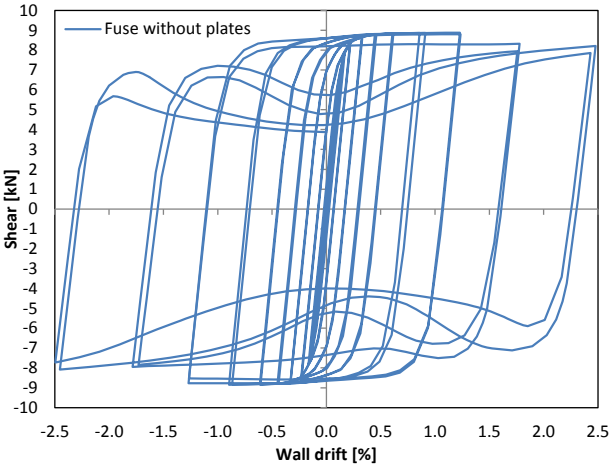

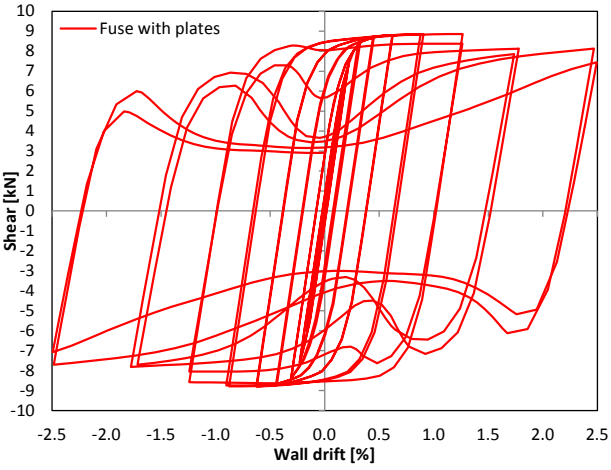

Fuse 34 - L=300mm; b=75mm; t=6mm; σ_y=250MPa

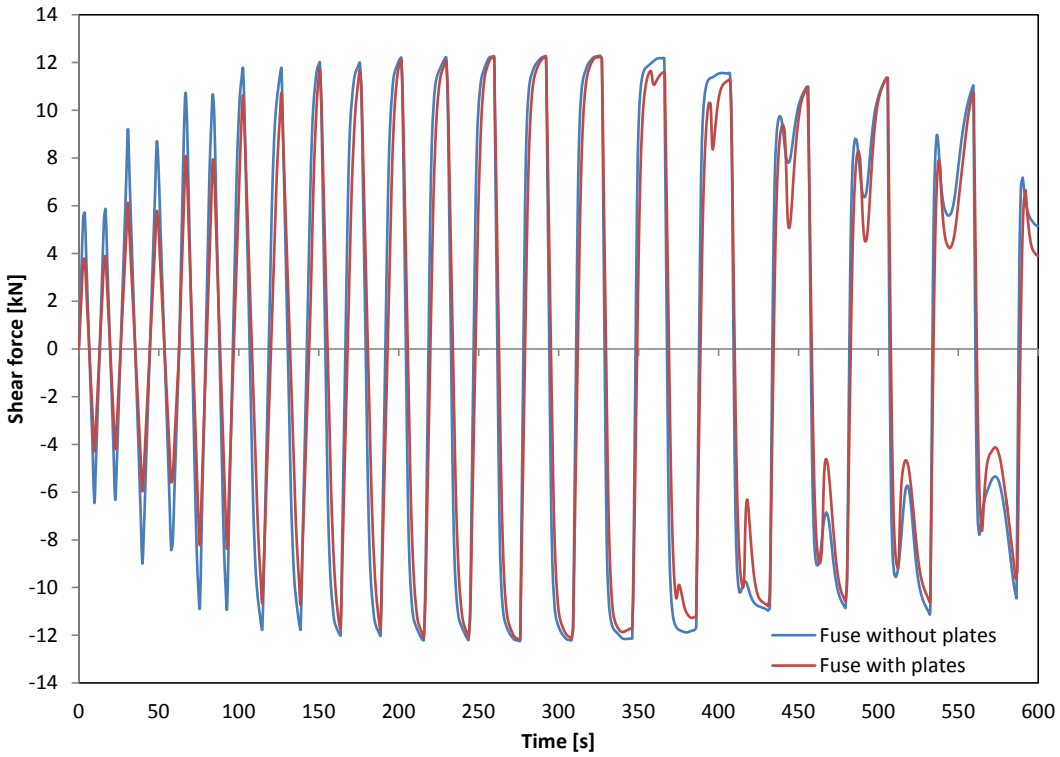

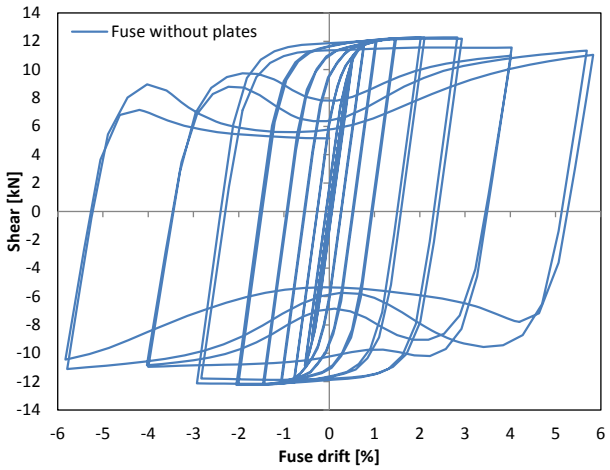

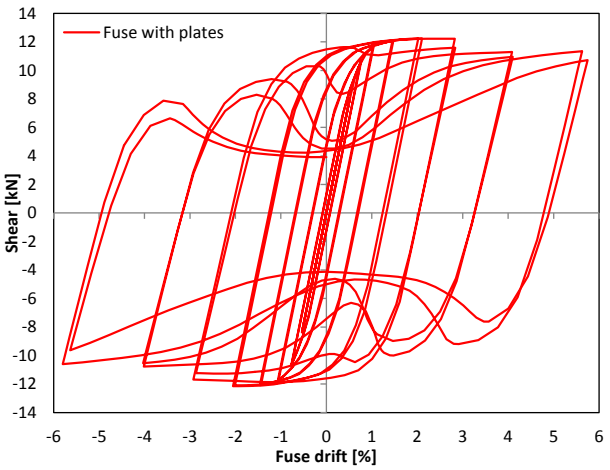

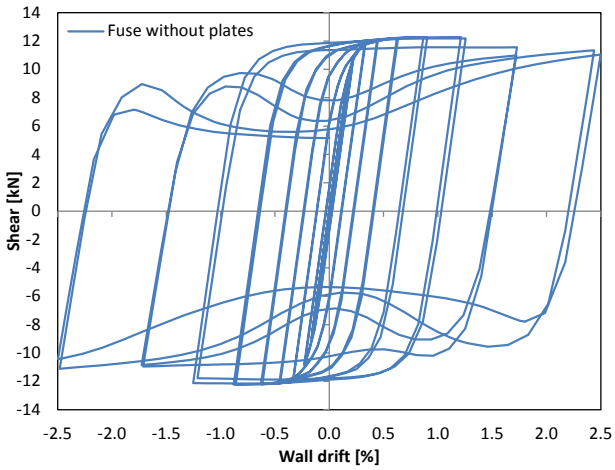

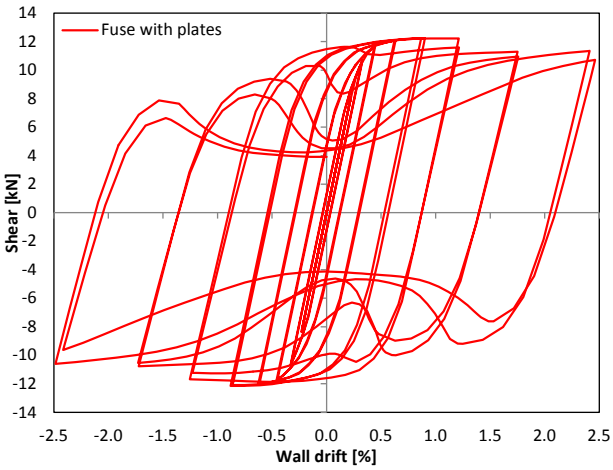

Fuse 35 - L=300mm; b=75mm; t=7mm; σ_y=180MPa

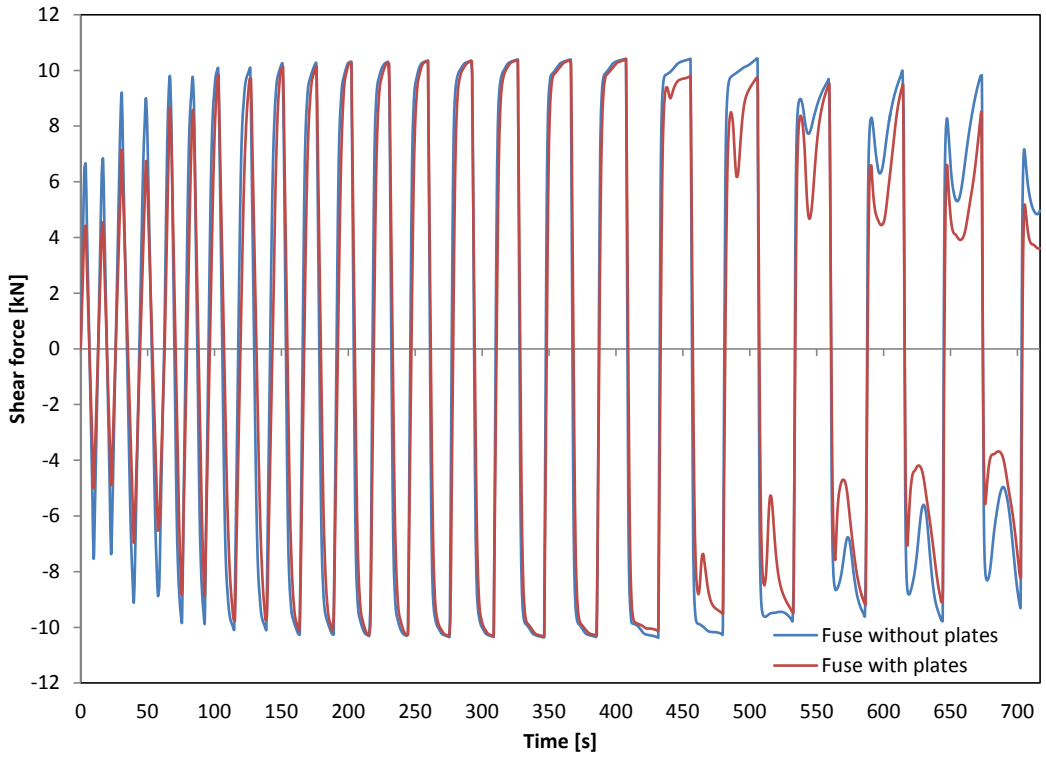

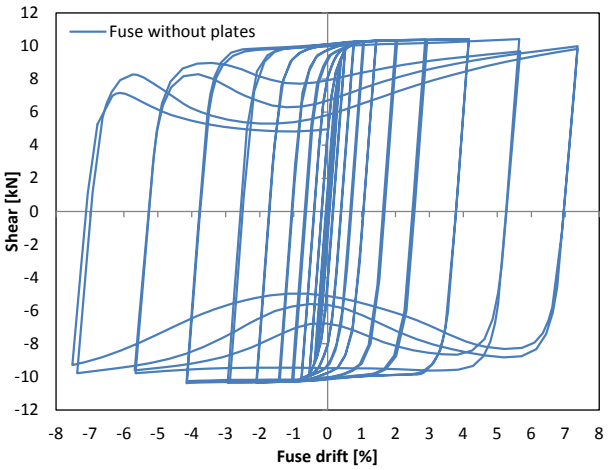

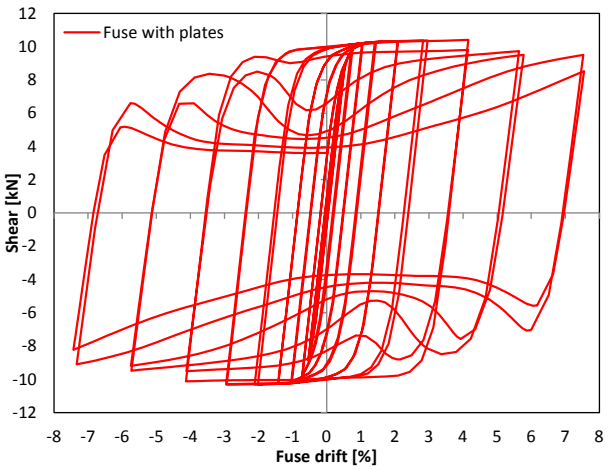

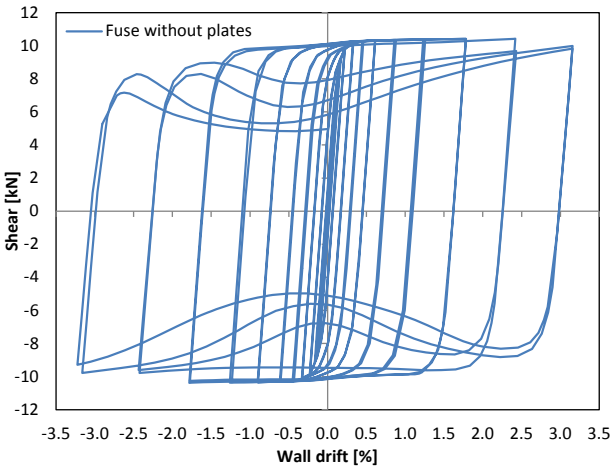

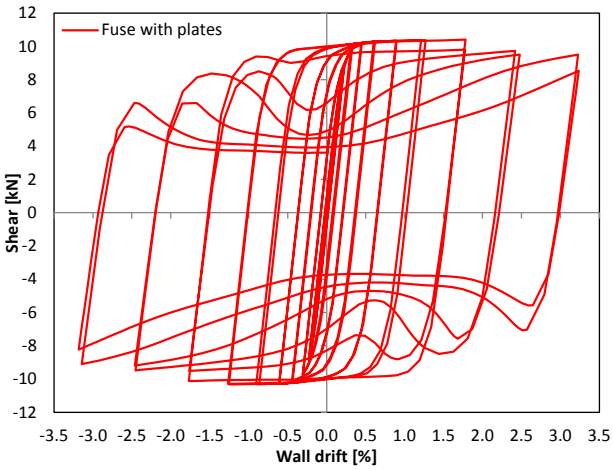

Fuse 36 - L=300mm; b=75mm; t=7mm; σ_y=250MPa

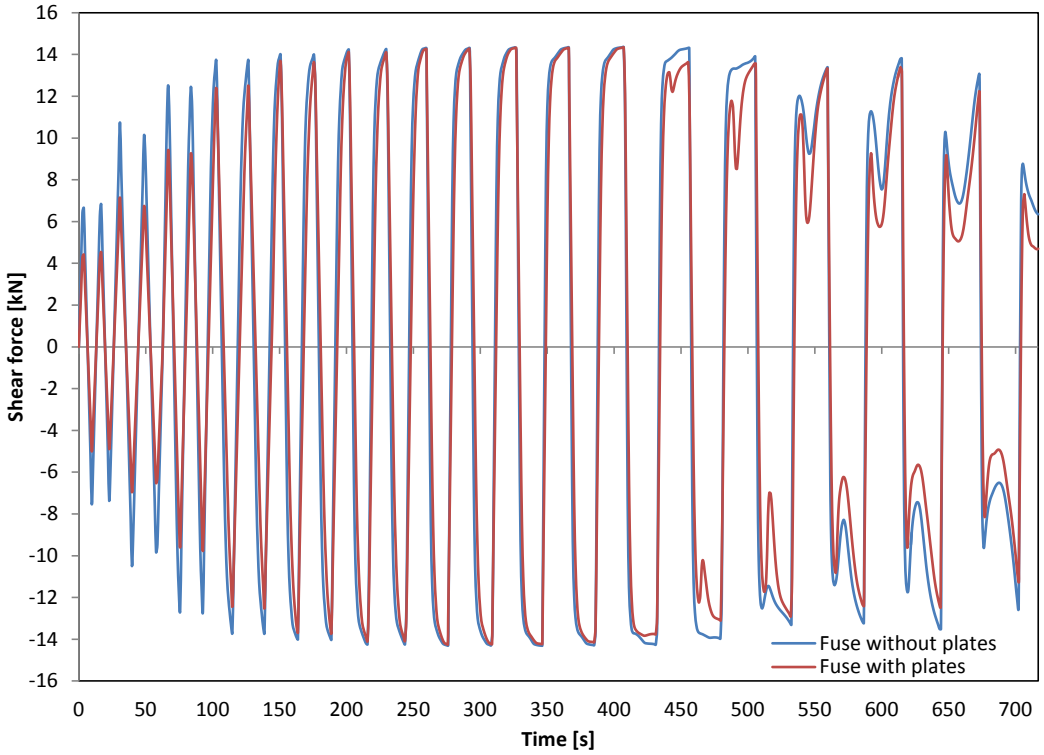

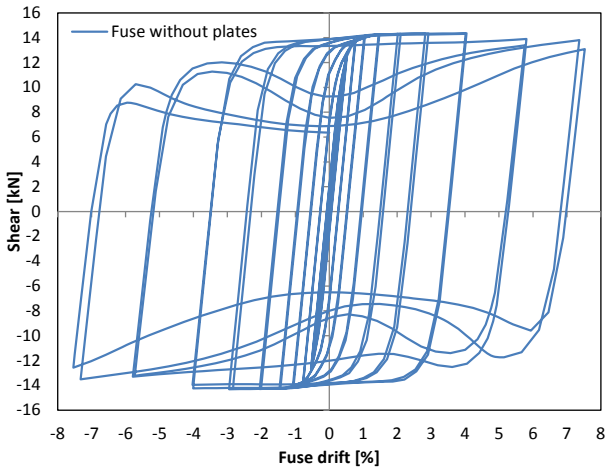

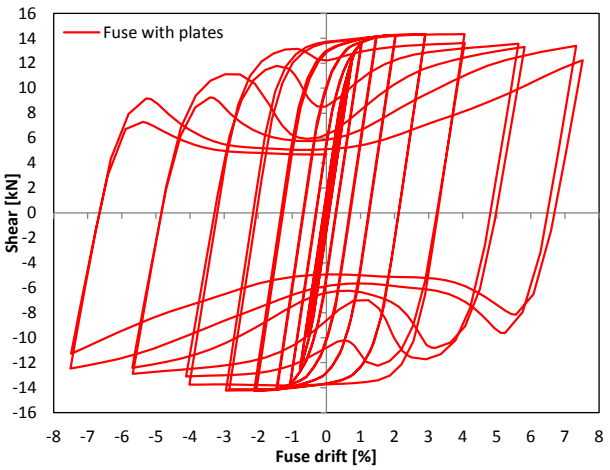

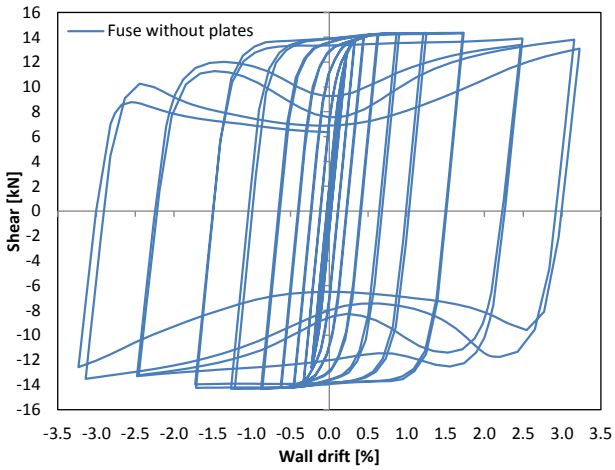

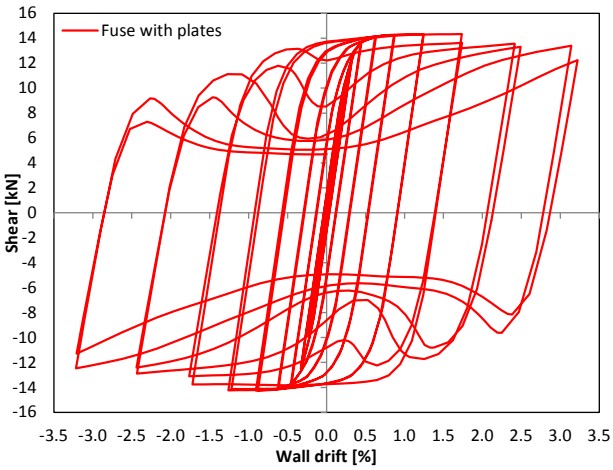

Fuse 37 - L=350mm; b=60mm; t=5mm; σ_y=180MPa

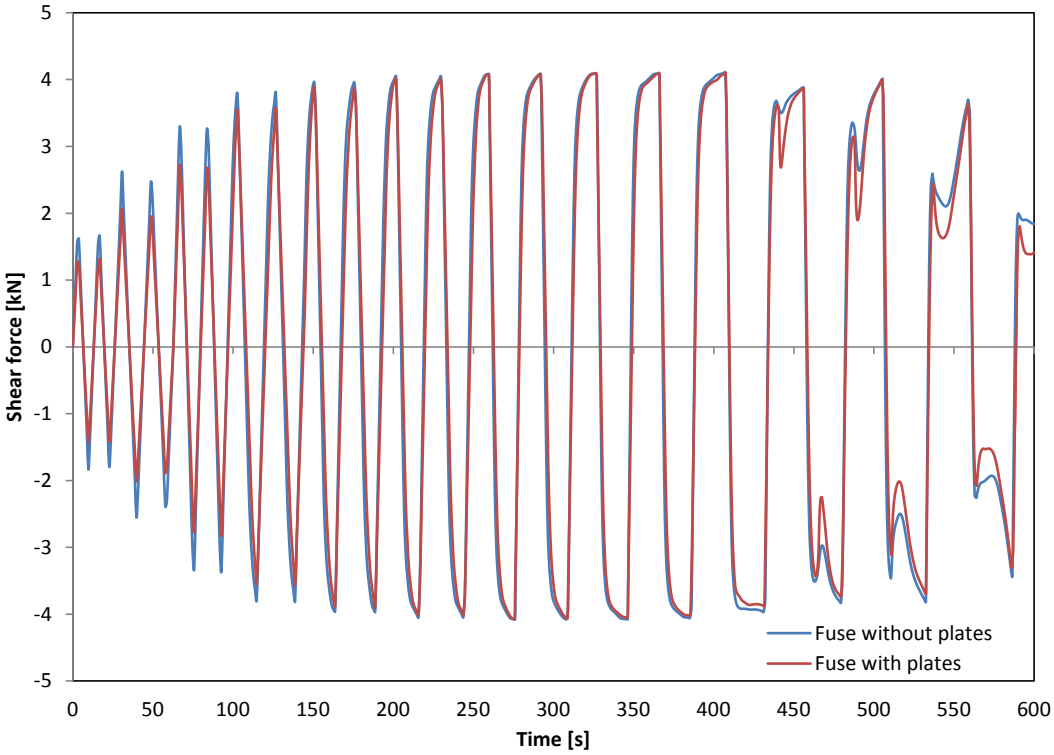

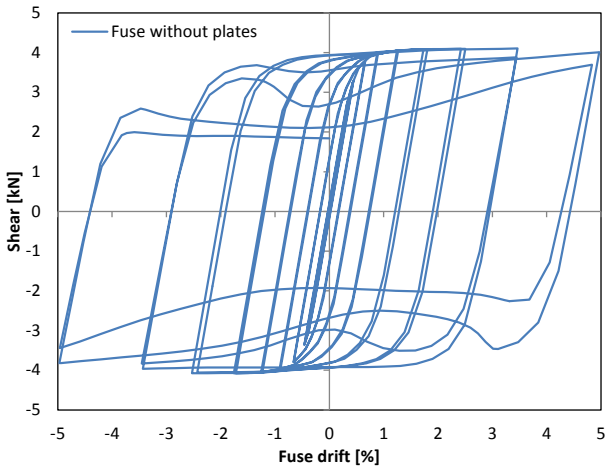

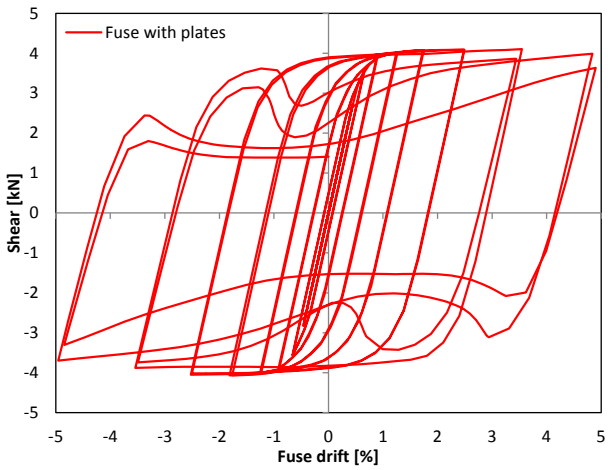

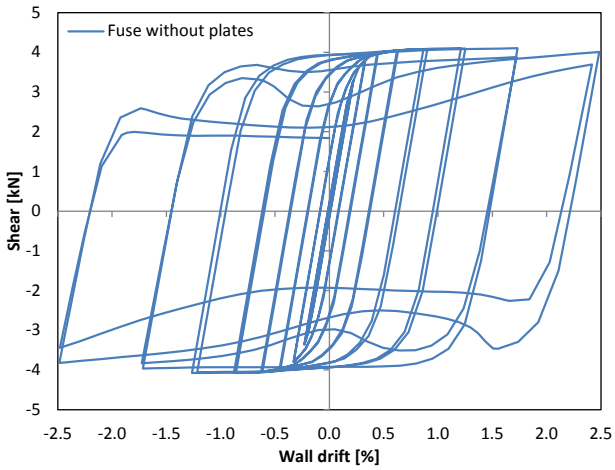

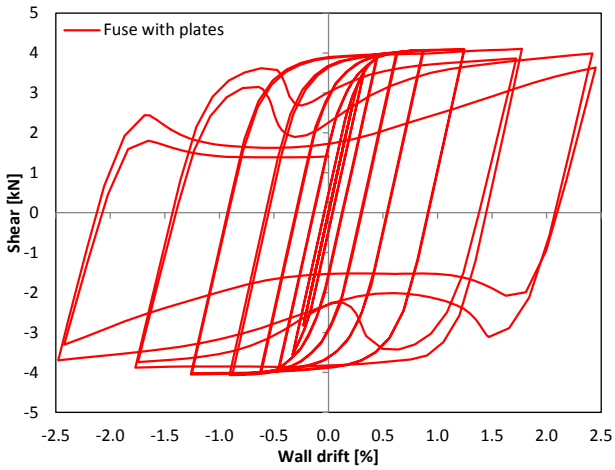

Fuse 38 - L=350mm; b=60mm; t=5mm; σ_y=250MPa (*)

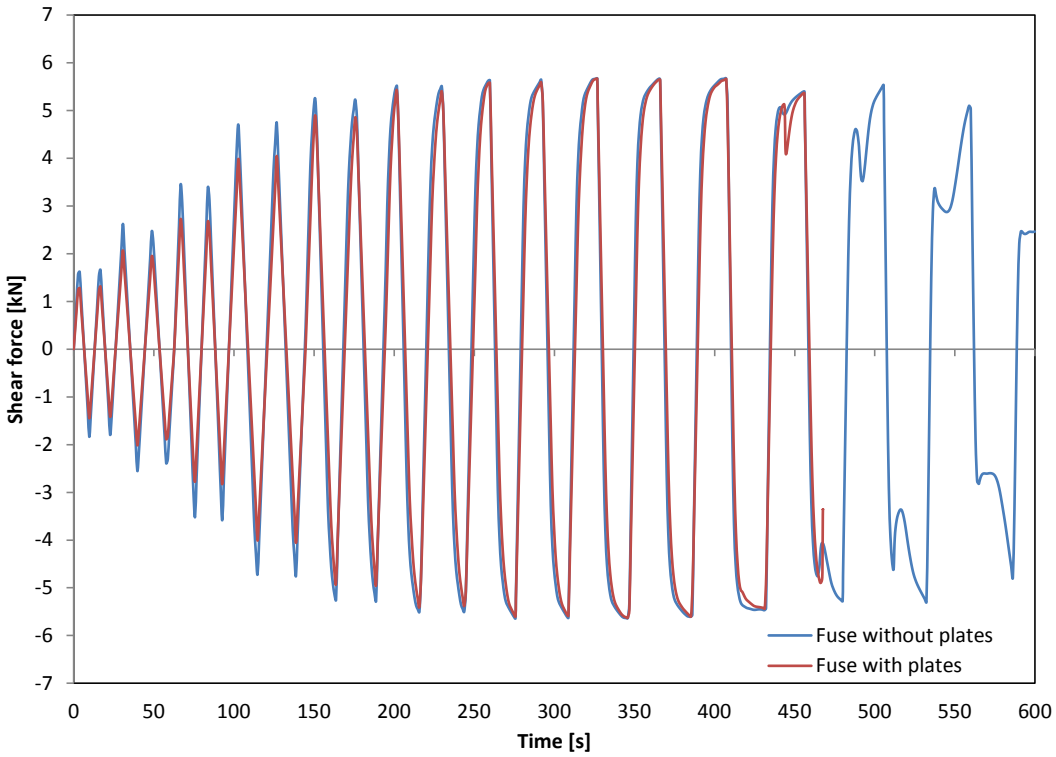

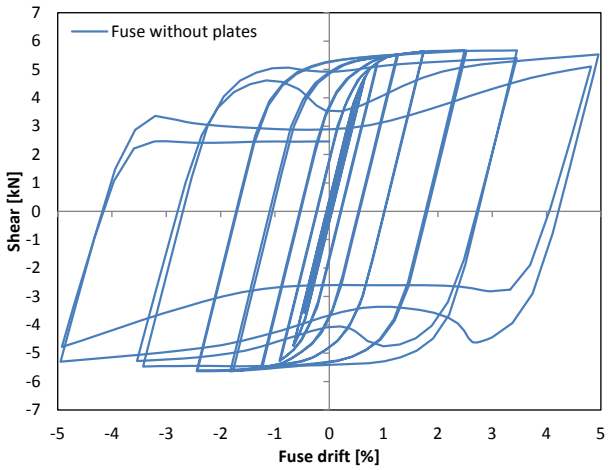

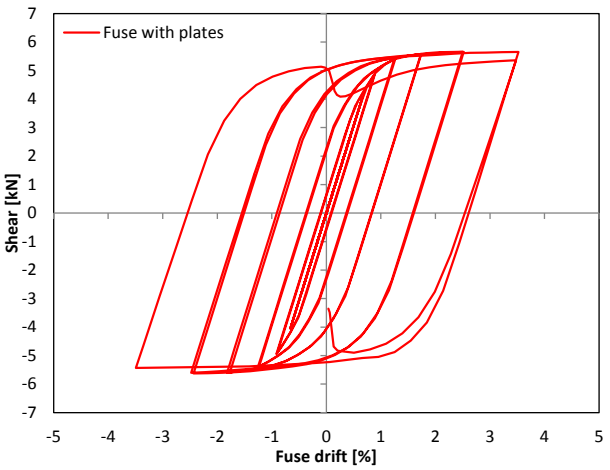

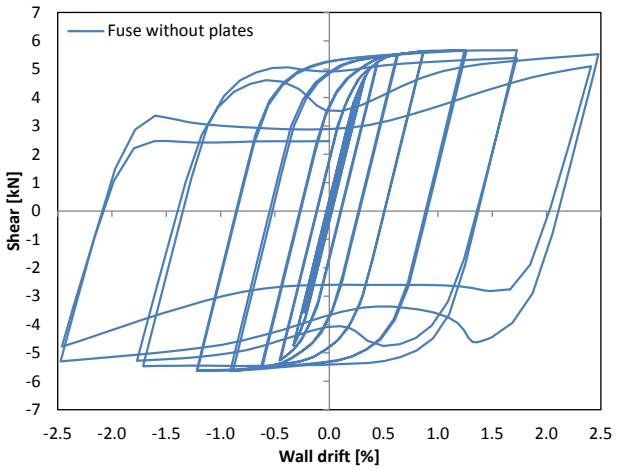

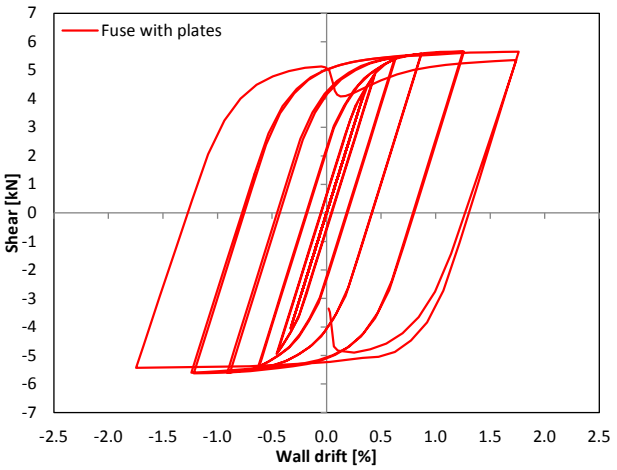

(*): the numerical analysis of the fuse with plates terminated prematurely due to lack of convergence.

Fuse 39 - L=350mm; b=60mm; t=6mm; σ_y=180MPa

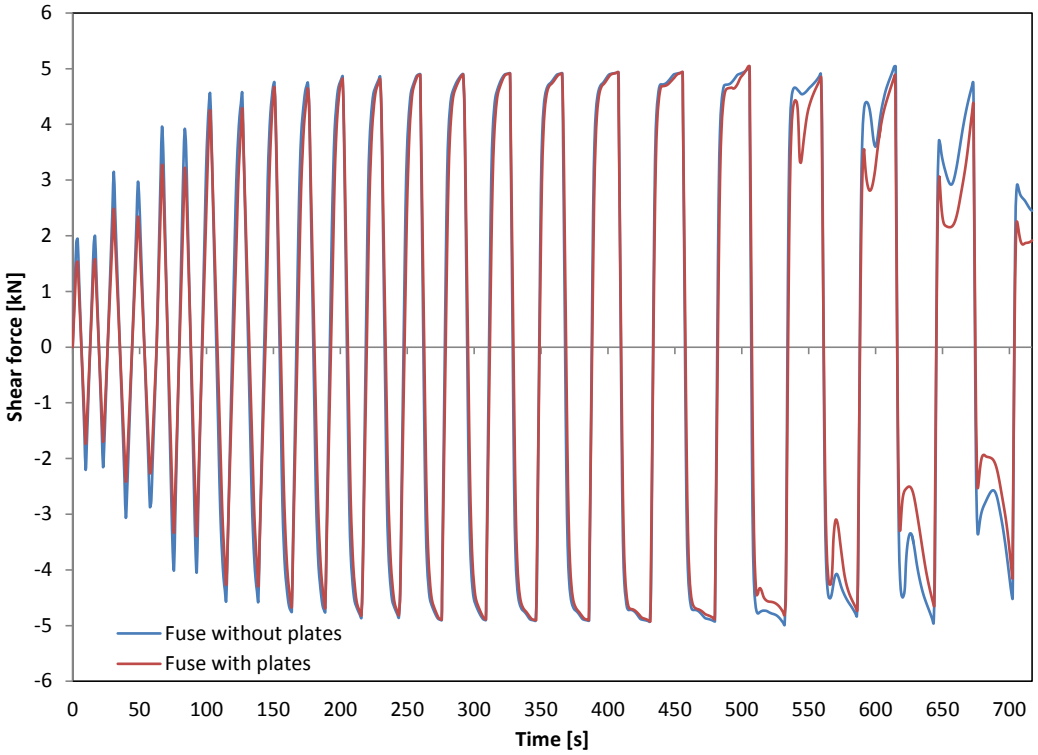

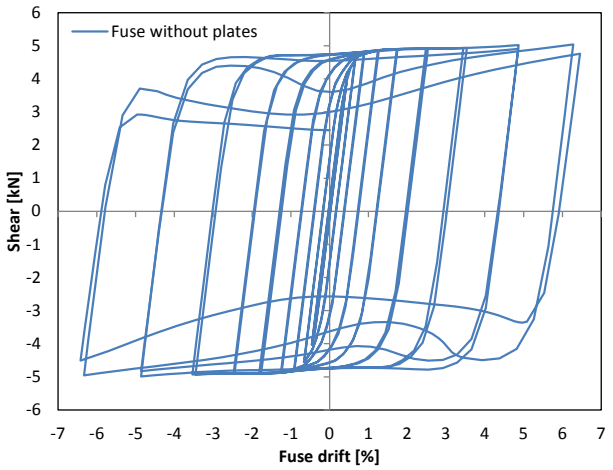

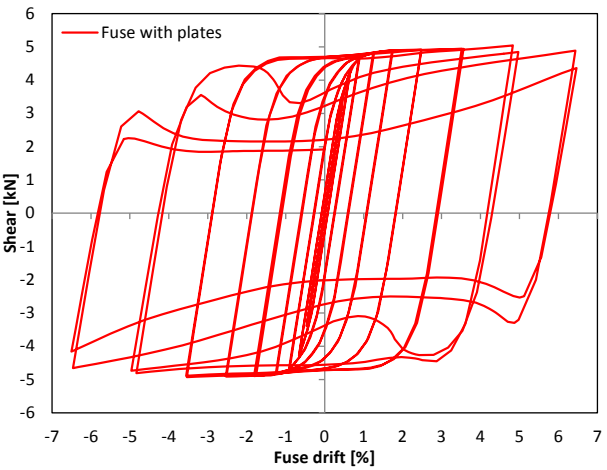

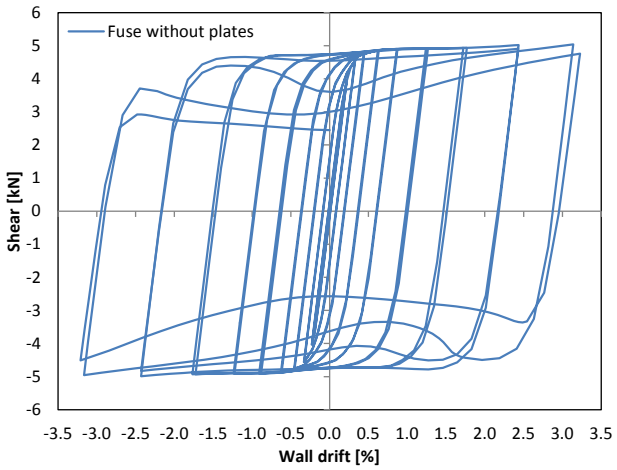

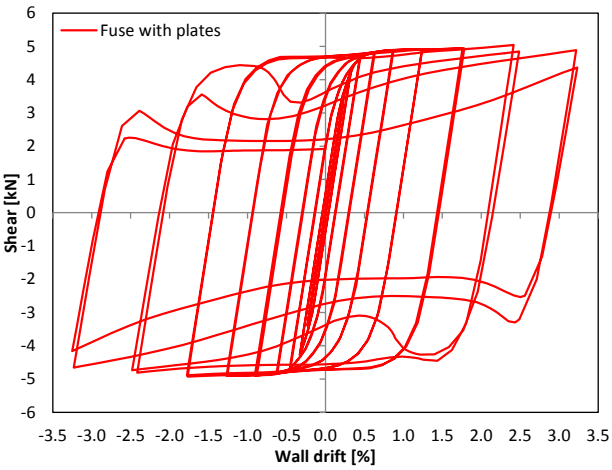

Fuse 40 - L=350mm; b=60mm; t=6mm; σ_y=250MPa

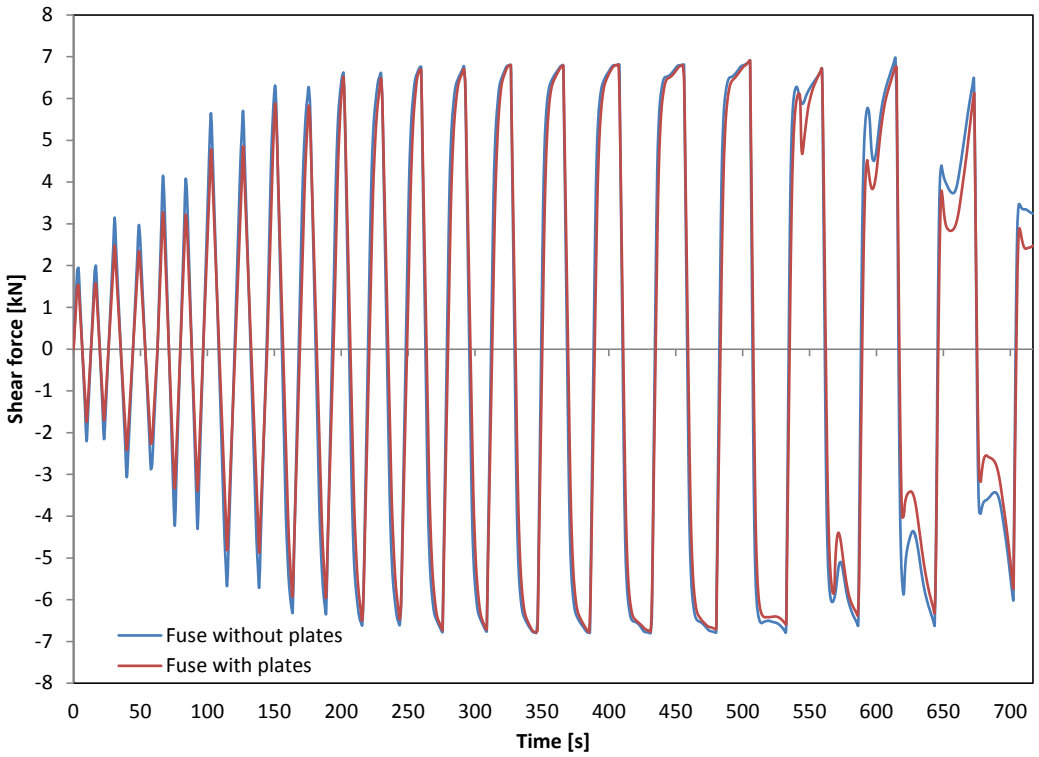

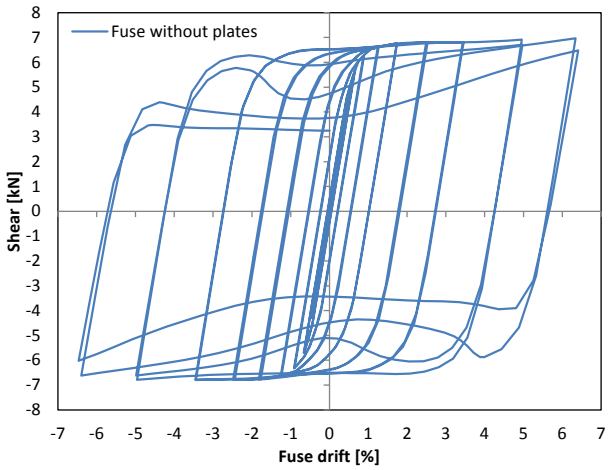

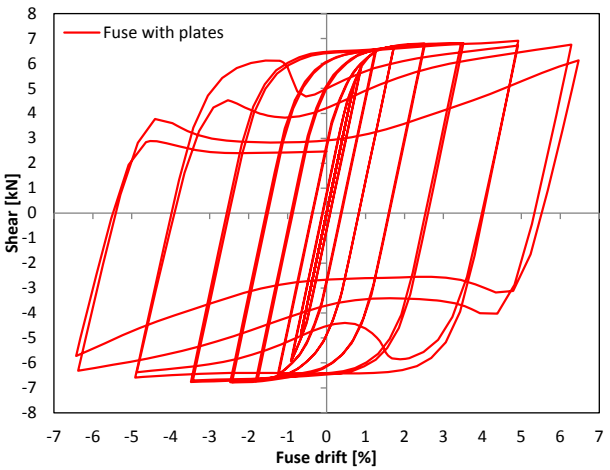

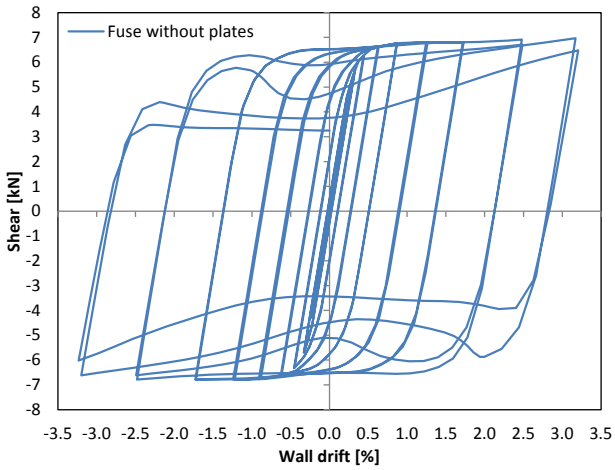

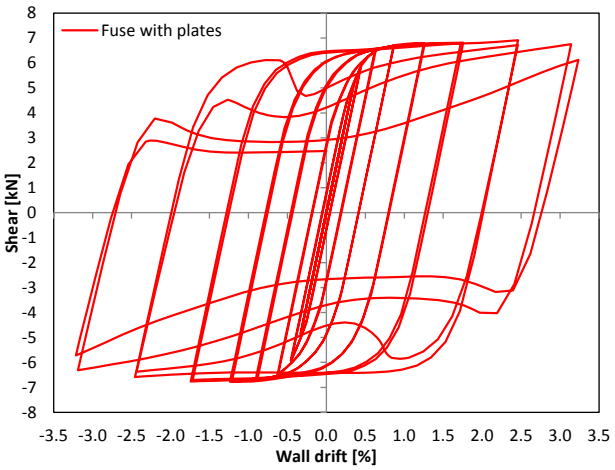

Fuse 41 - L=350mm; b=60mm; t=7mm; σ_y=180MPa

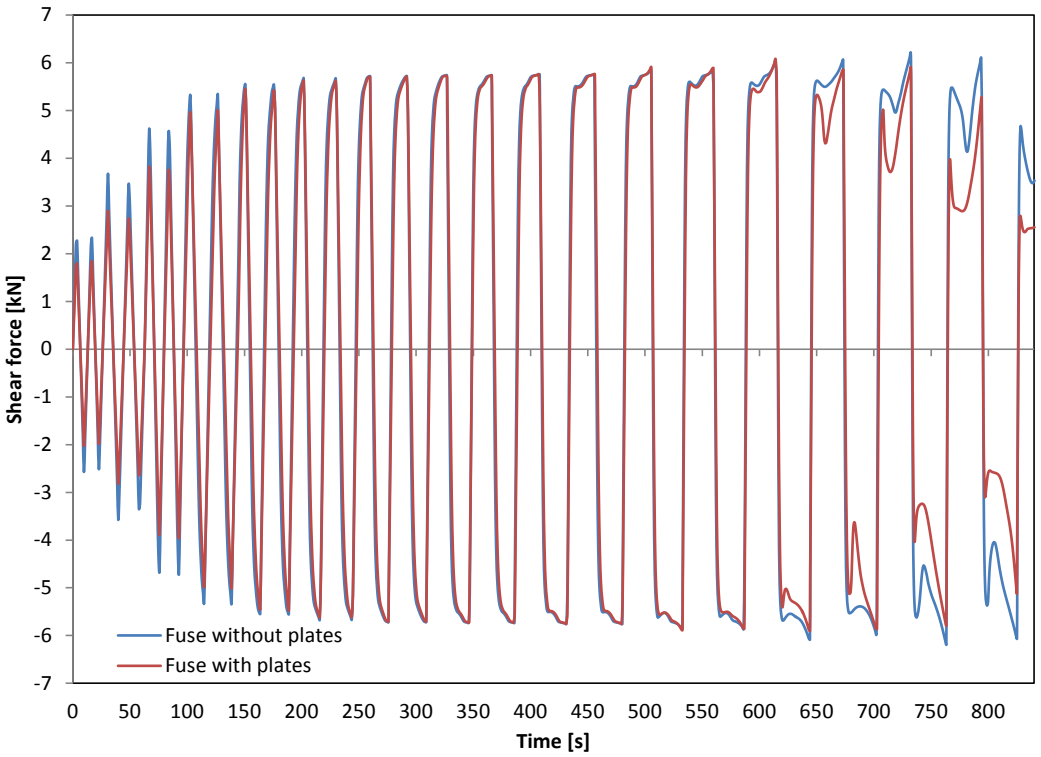

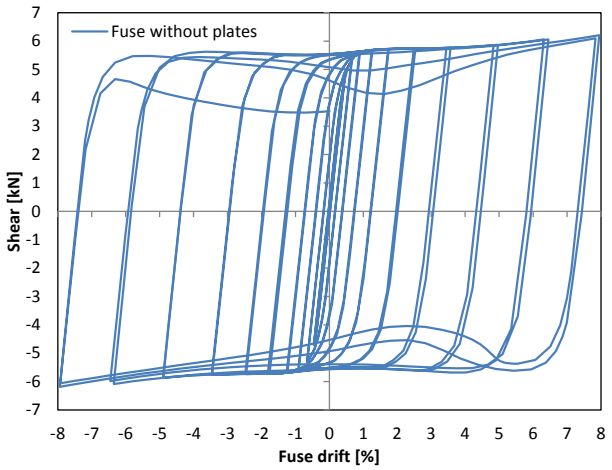

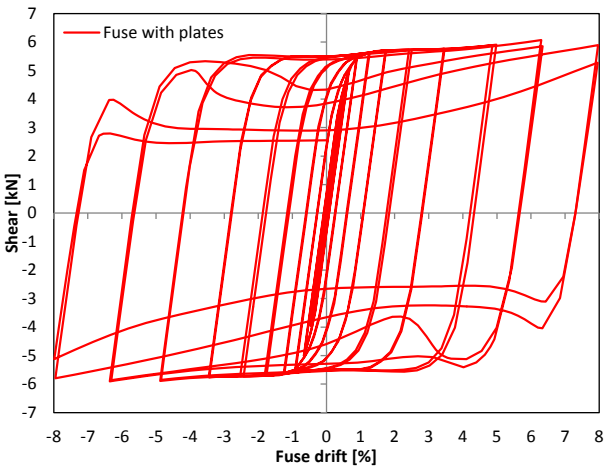

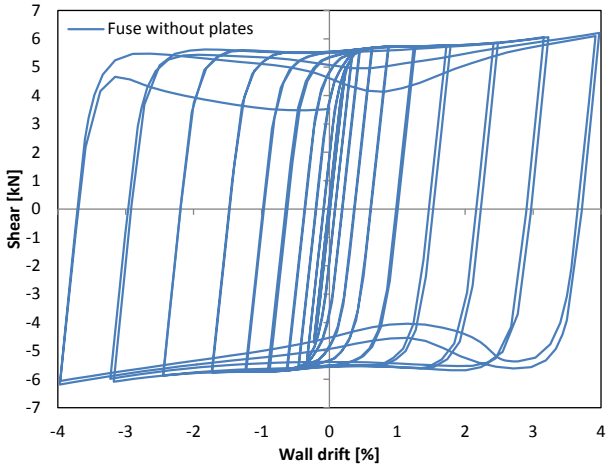

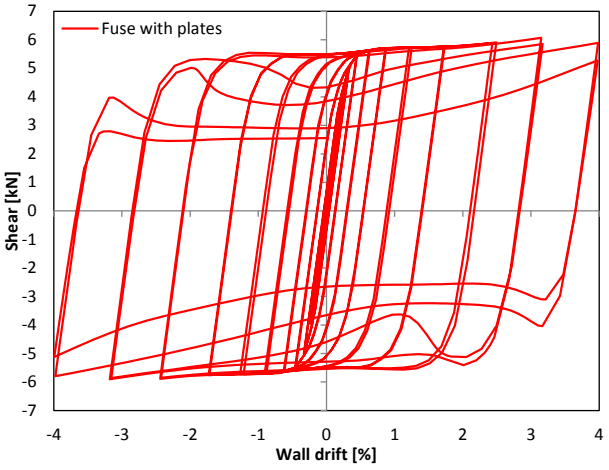

Fuse 42 - L=350mm; b=60mm; t=7mm; σ_y=250MPa

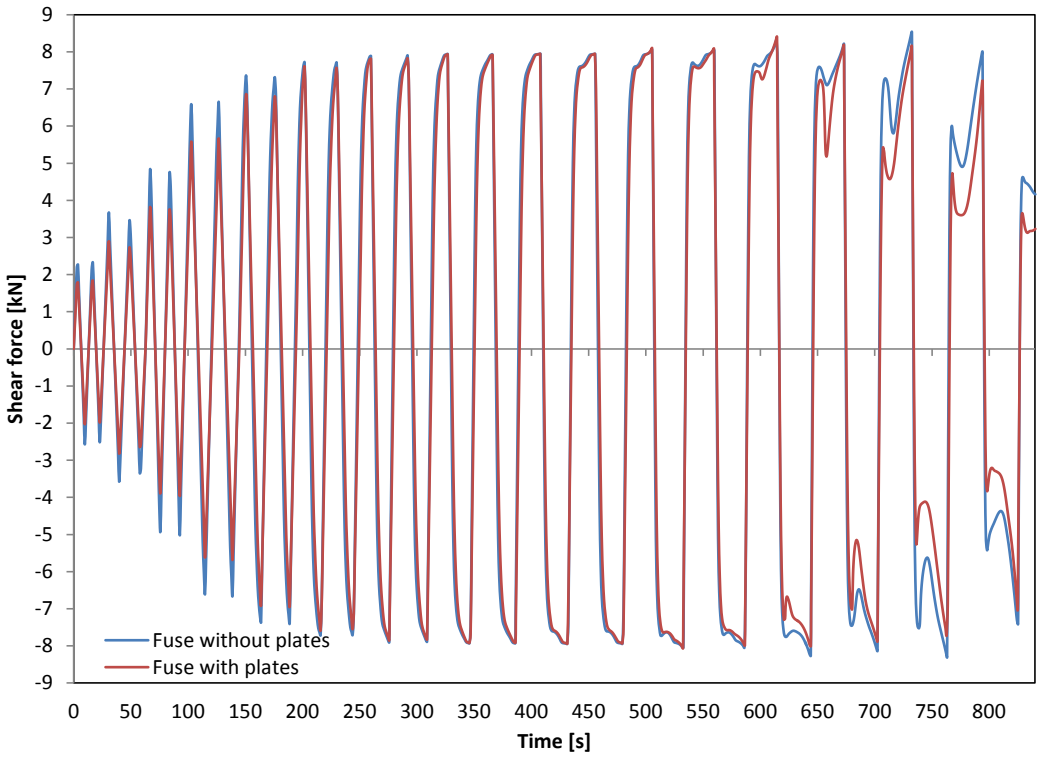

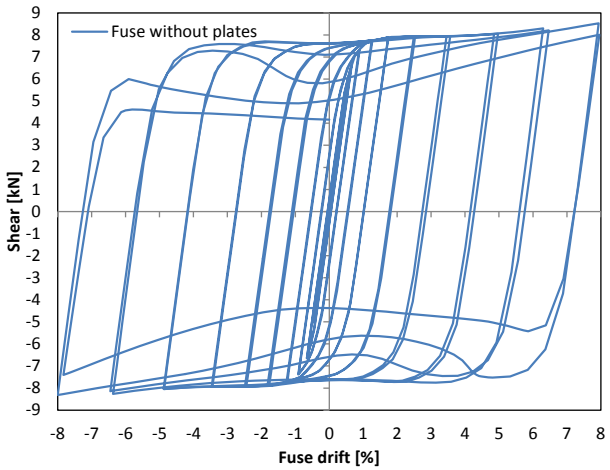

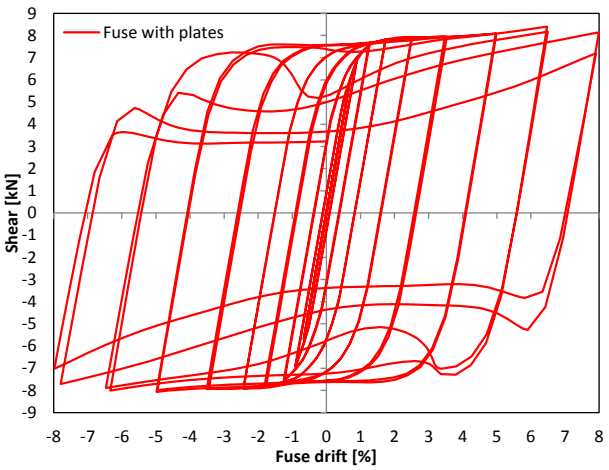

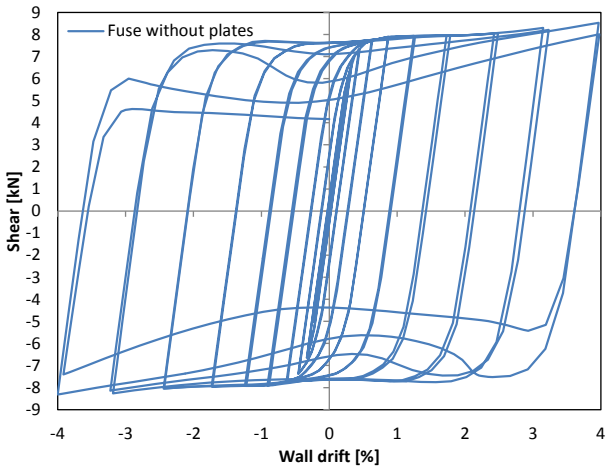

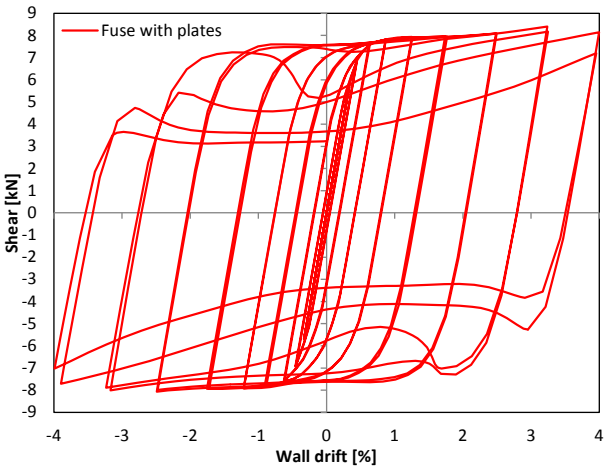

Fuse 43 - L=350mm; b=75mm; t=5mm; σ_y=180MPa

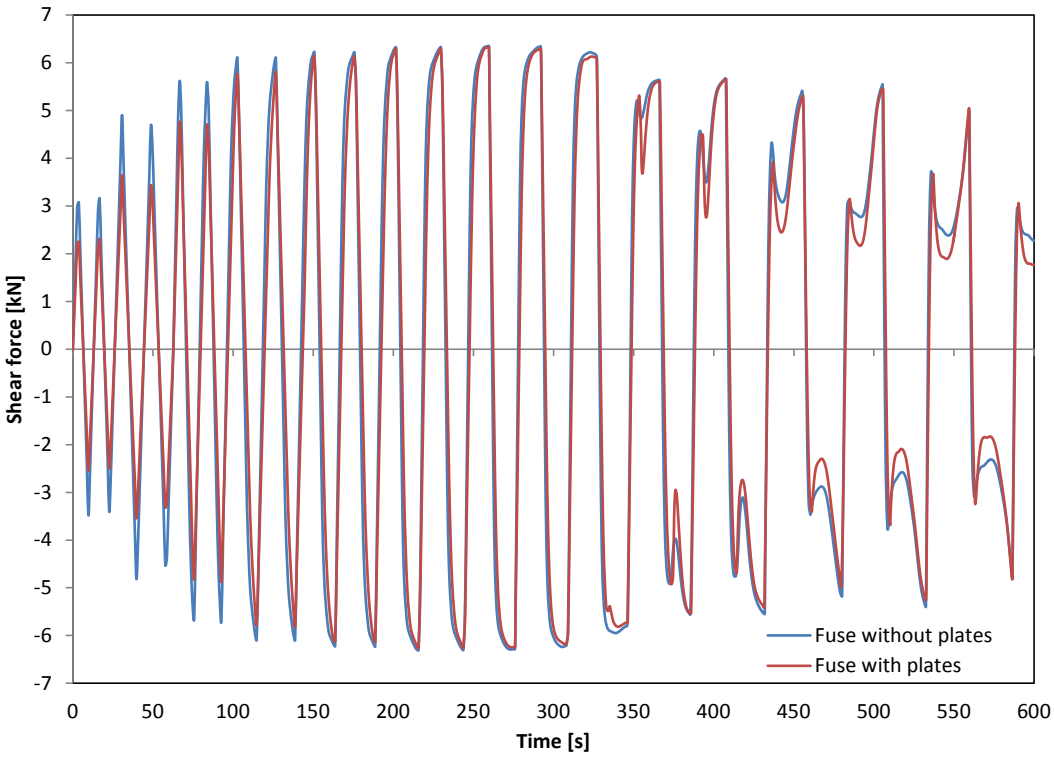

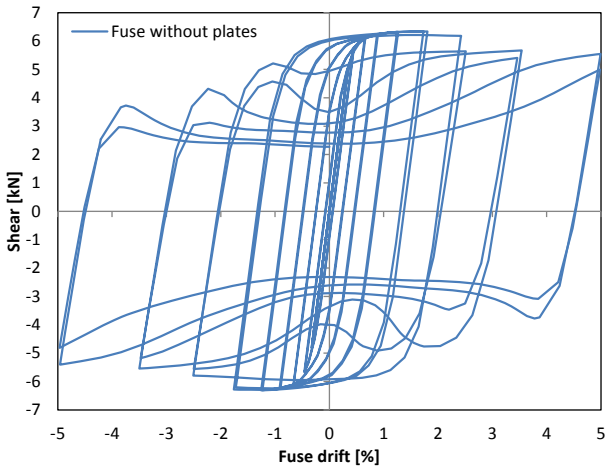

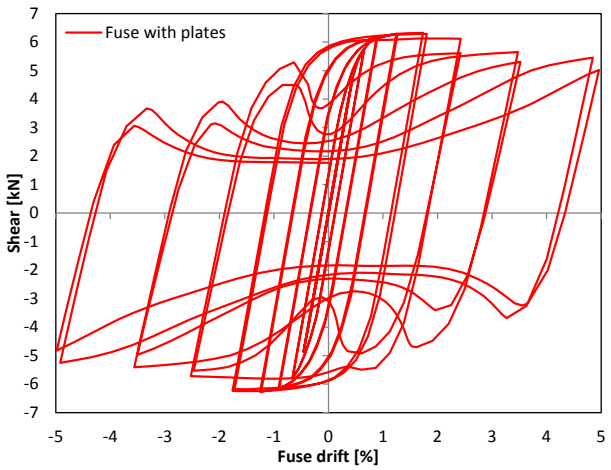

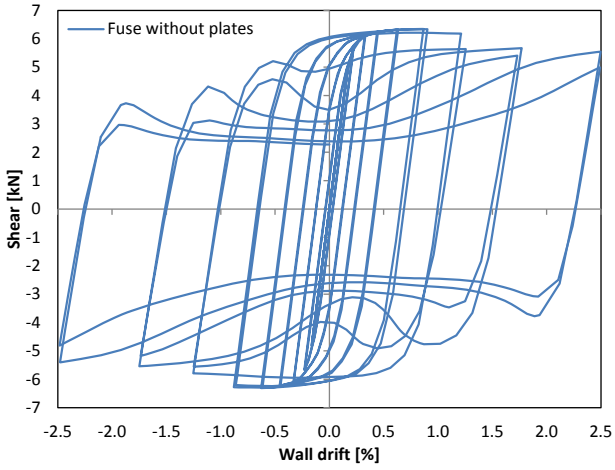

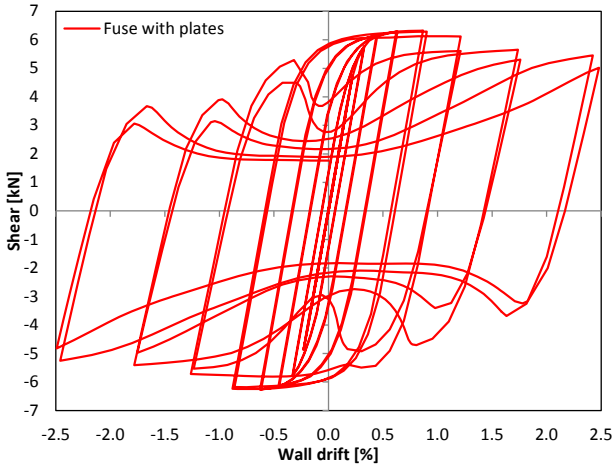

Fuse 44 - L=350mm; b=75mm; t=5mm; σ_y=250MPa

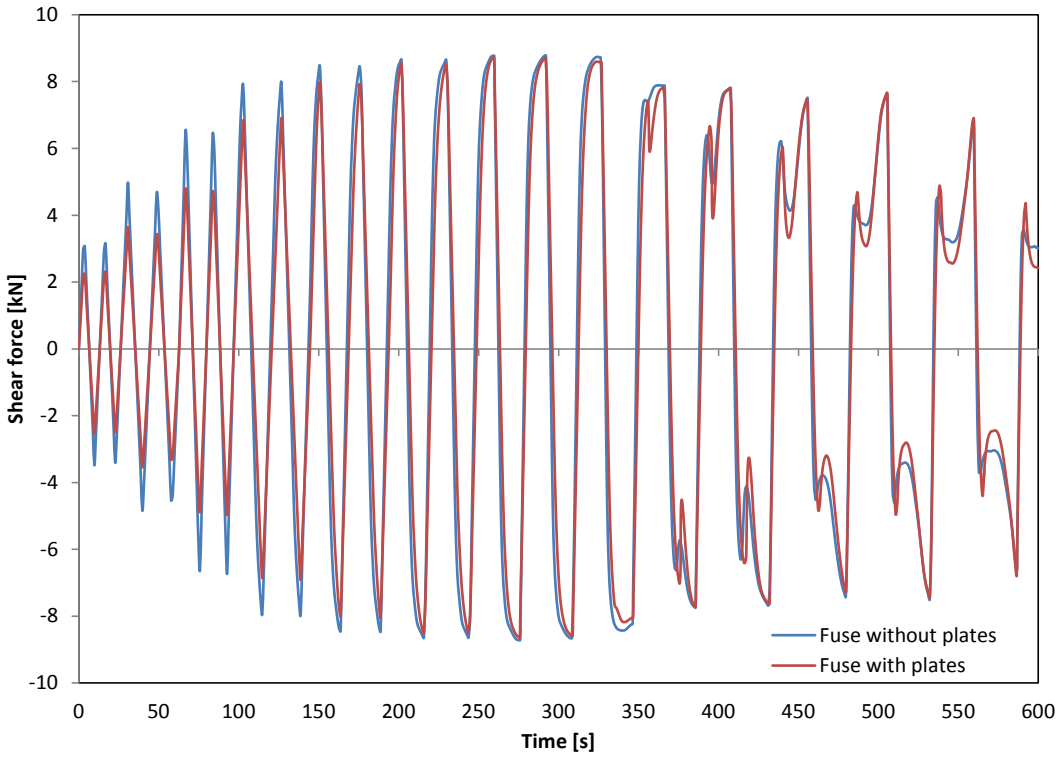

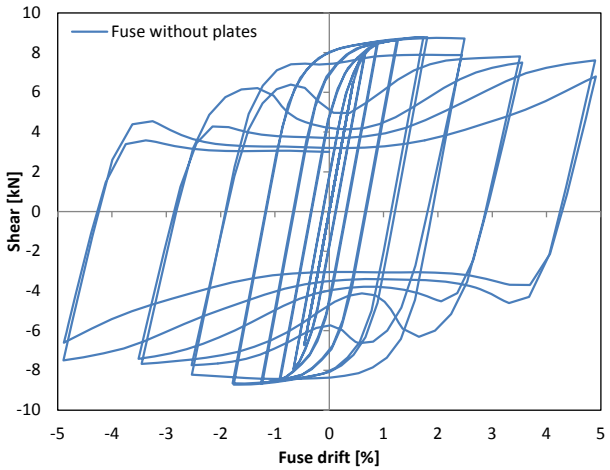

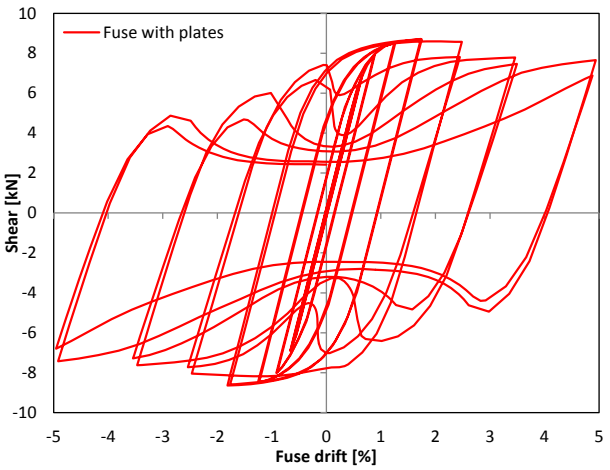

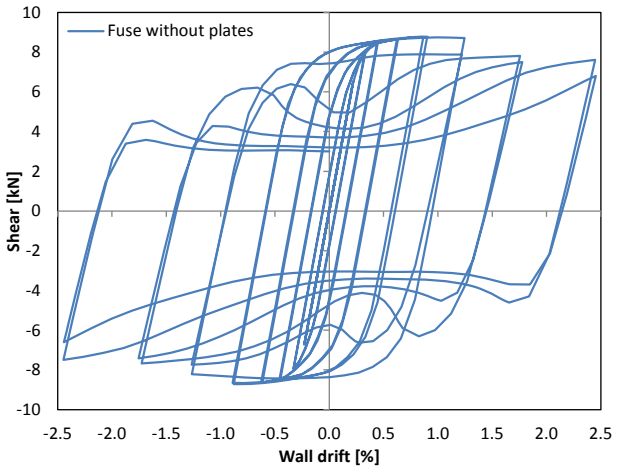

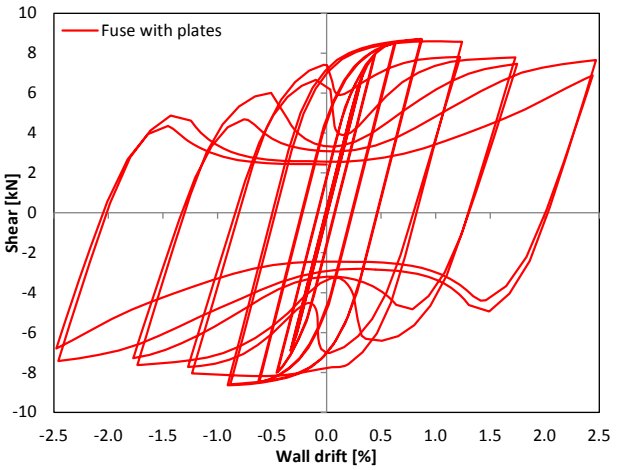

Fuse 45 - L=350mm; b=75mm; t=6mm; σ_y=180MPa

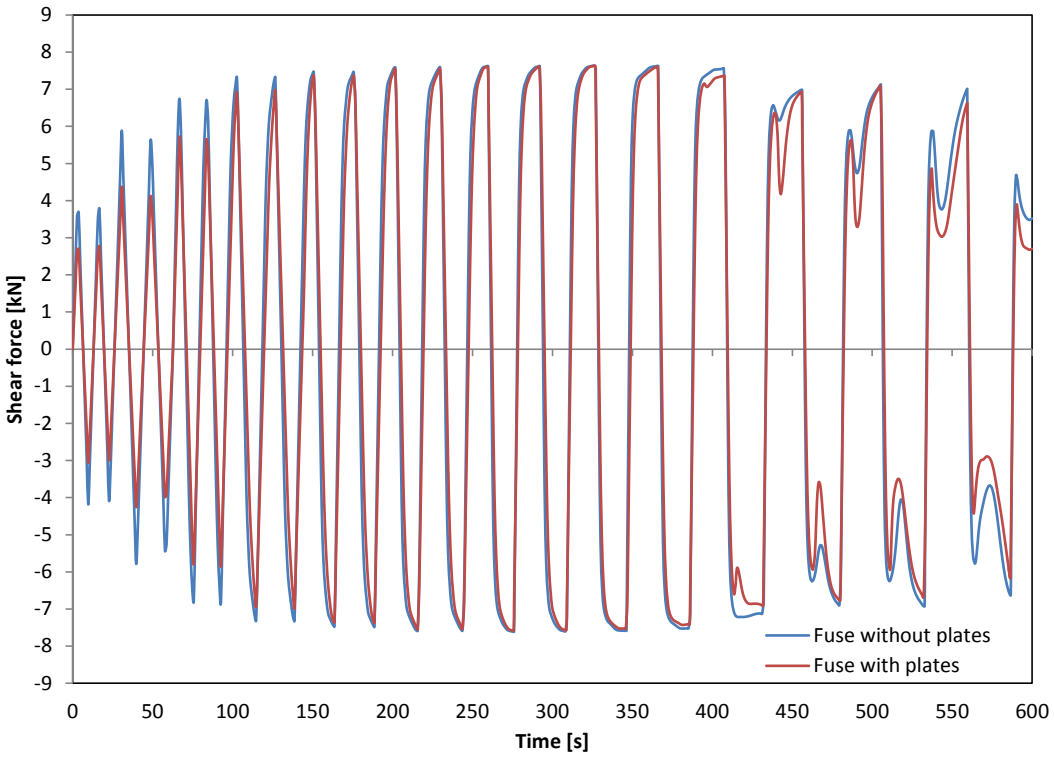

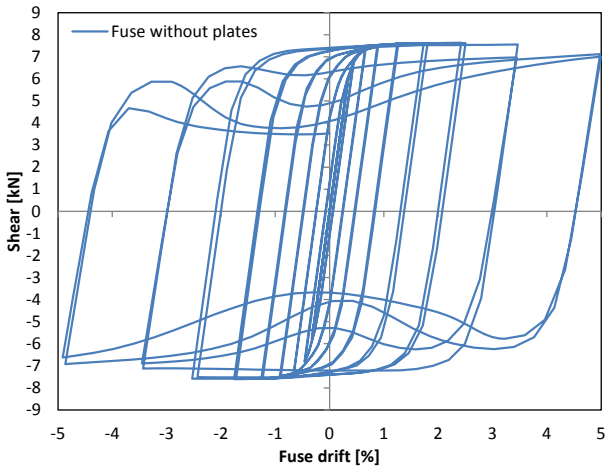

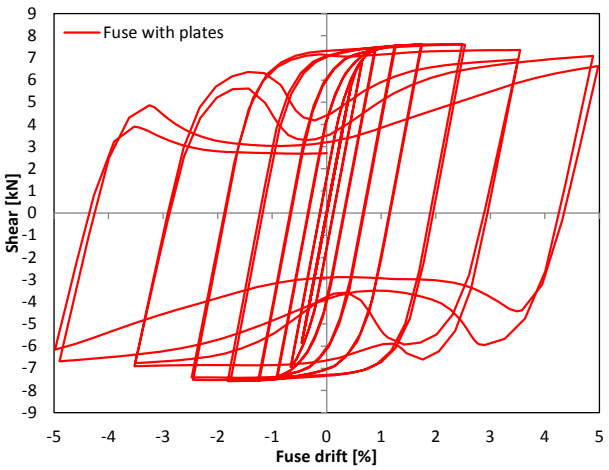

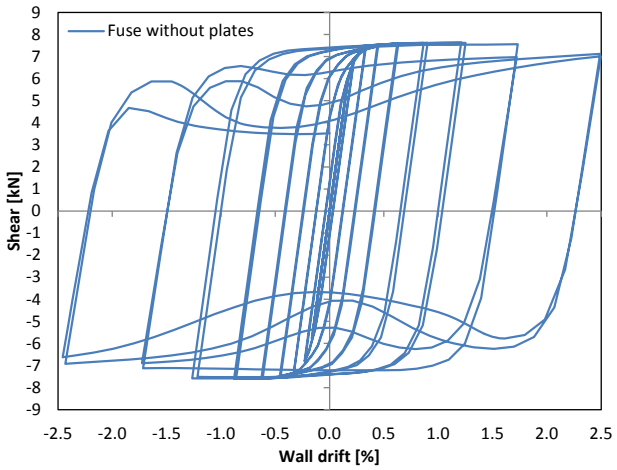

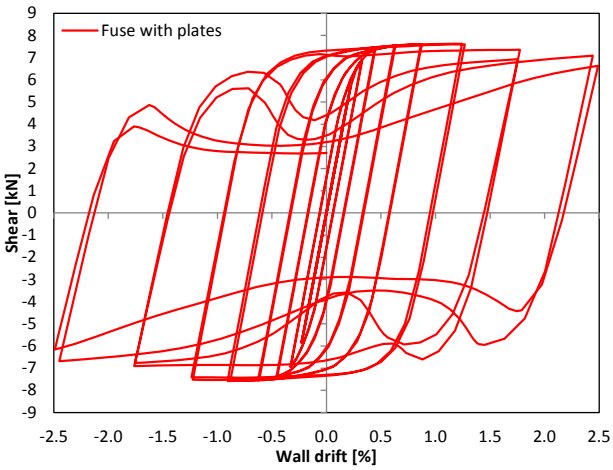

Fuse 46 - L=350mm; b=75mm; t=6mm; σ_y=250MPa

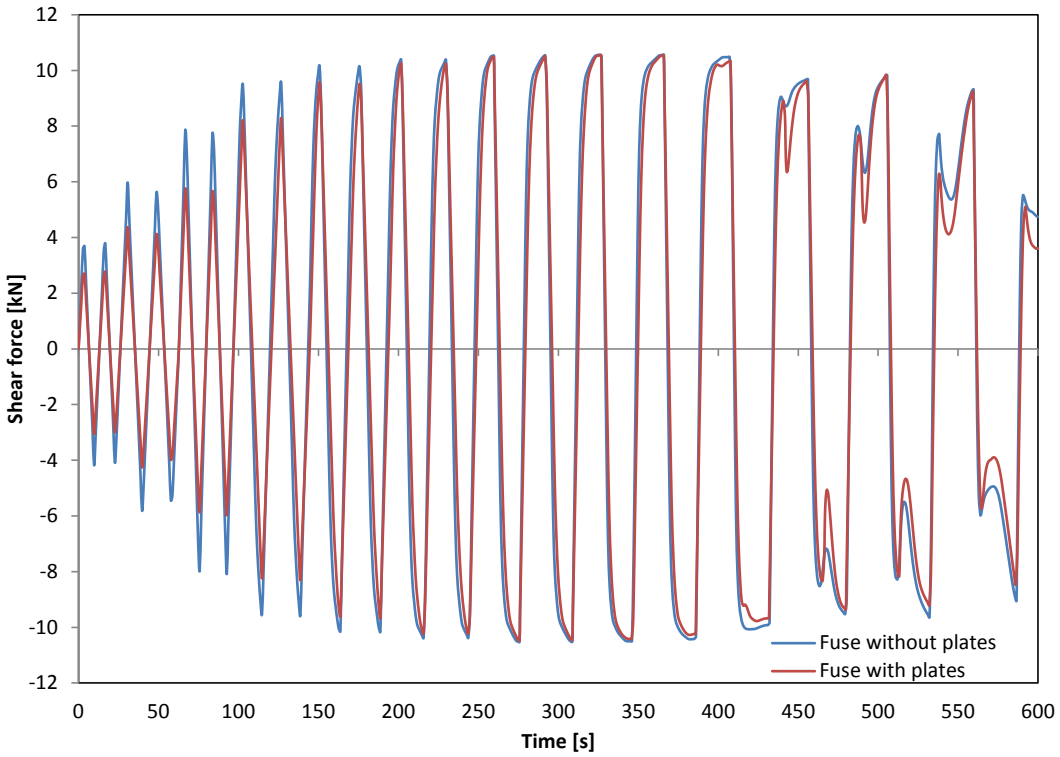

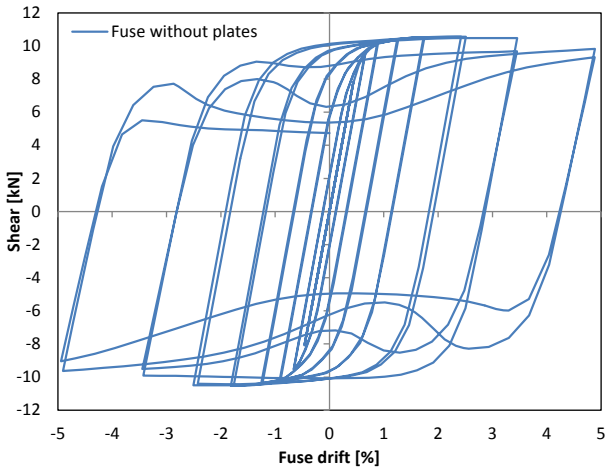

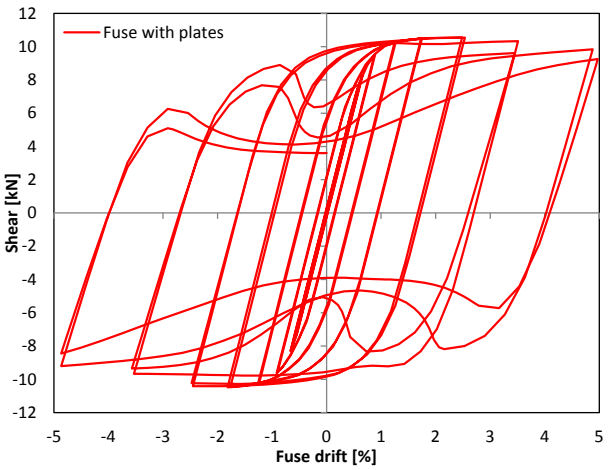

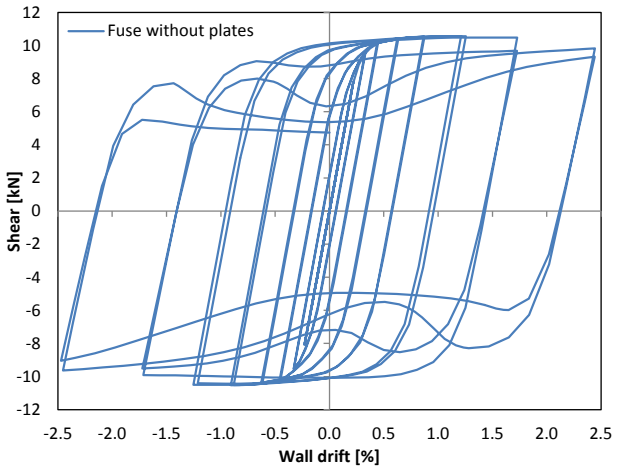

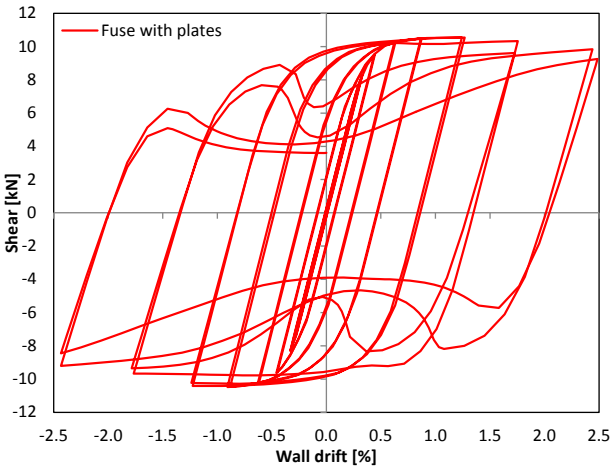

Fuse 47 - L=350mm; b=75mm; t=7mm; σ_y=180MPa

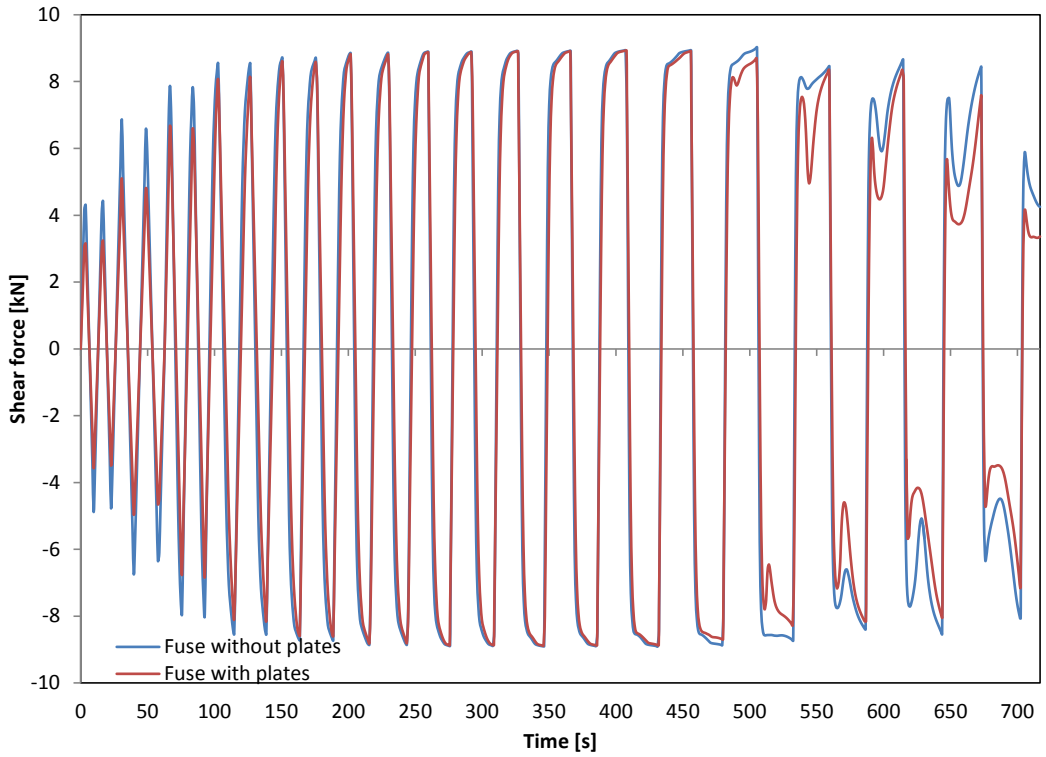

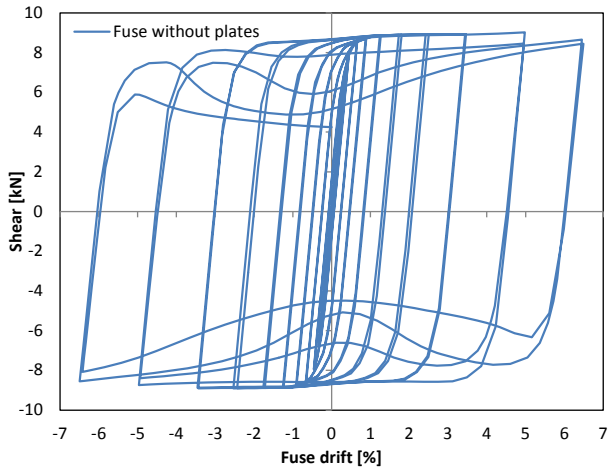

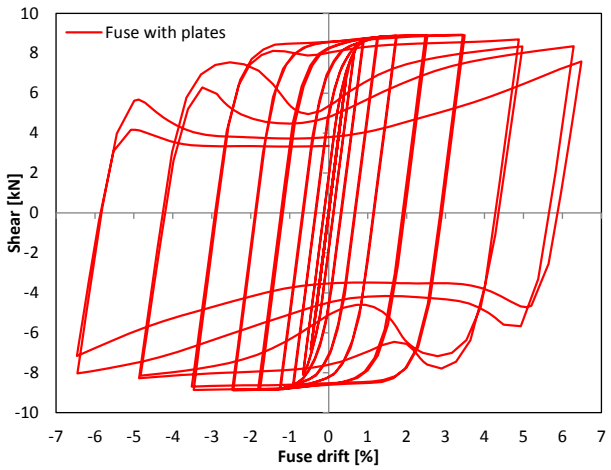

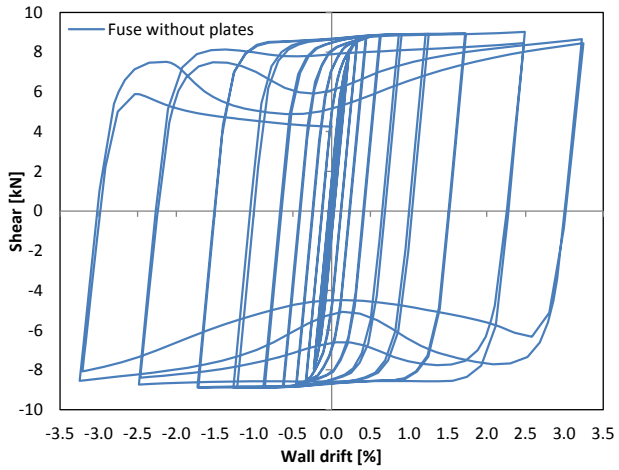

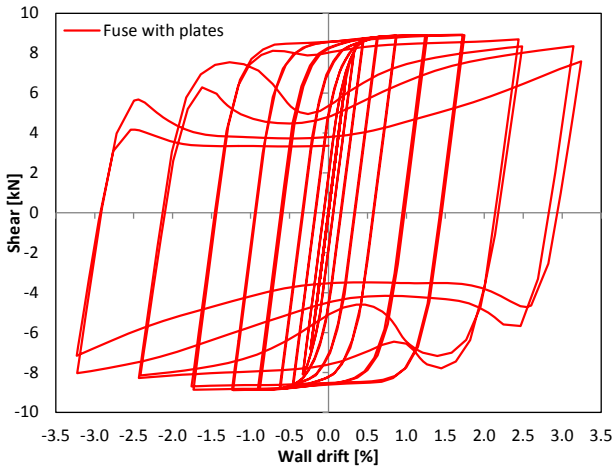

Fuse 48 - L=350mm; b=75mm; t=7mm; σ_y=250MPa

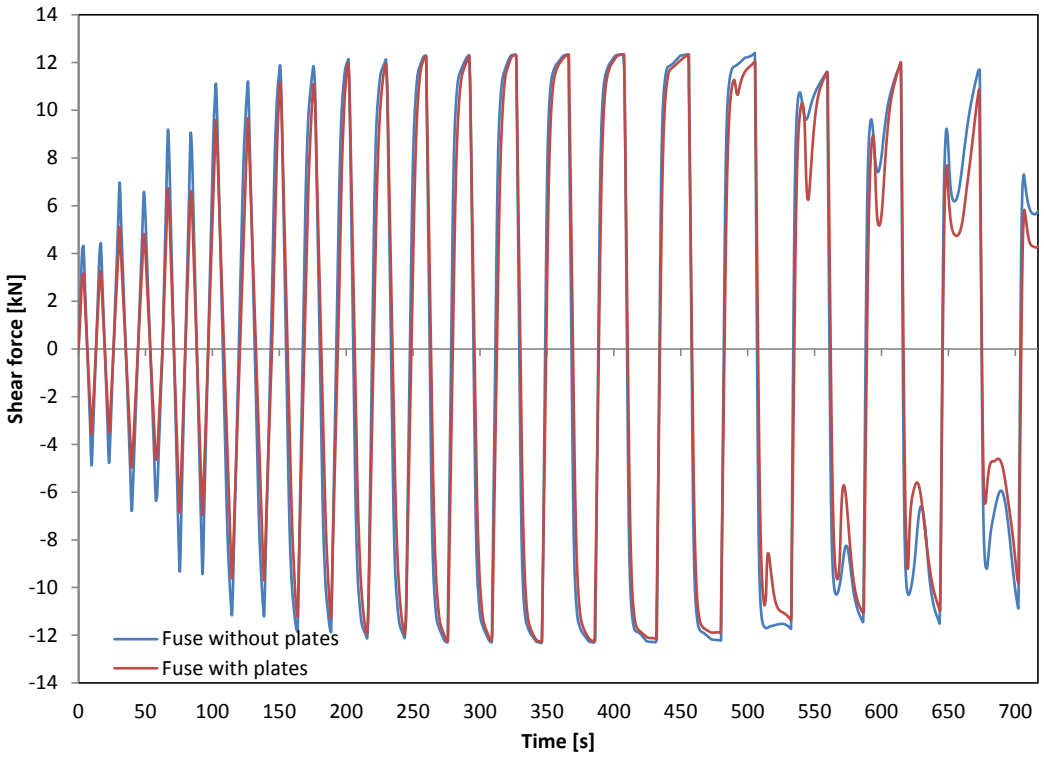

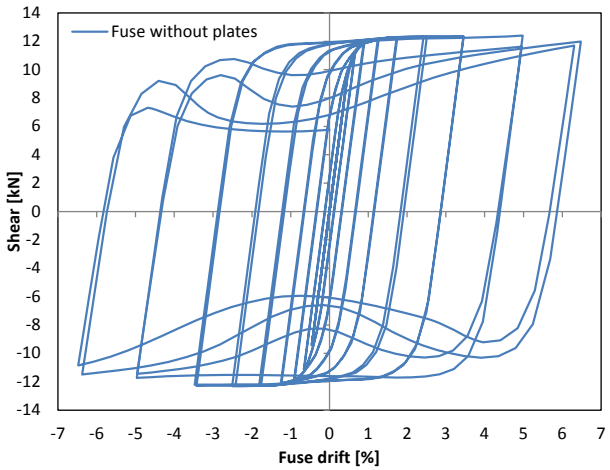

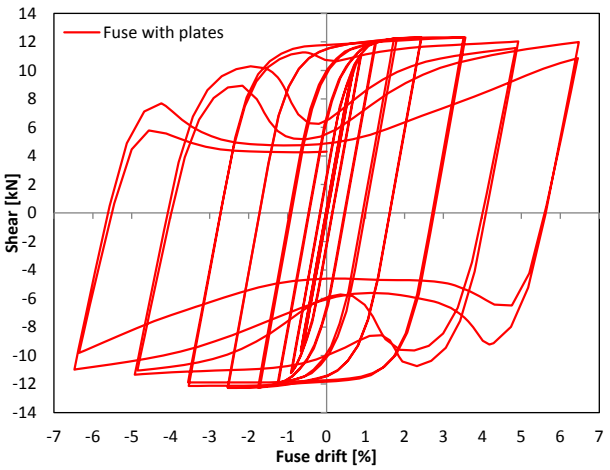

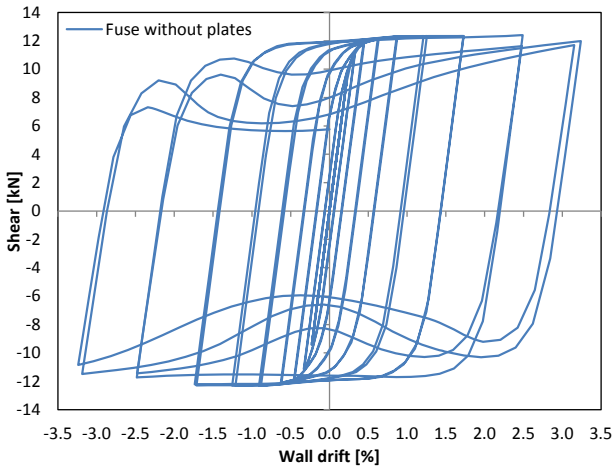

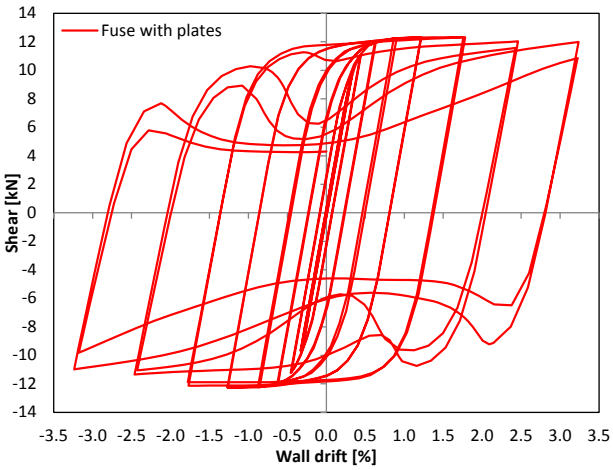

Fuse 49 - L=400mm; b=60mm; t=5mm; σ_y=180MPa

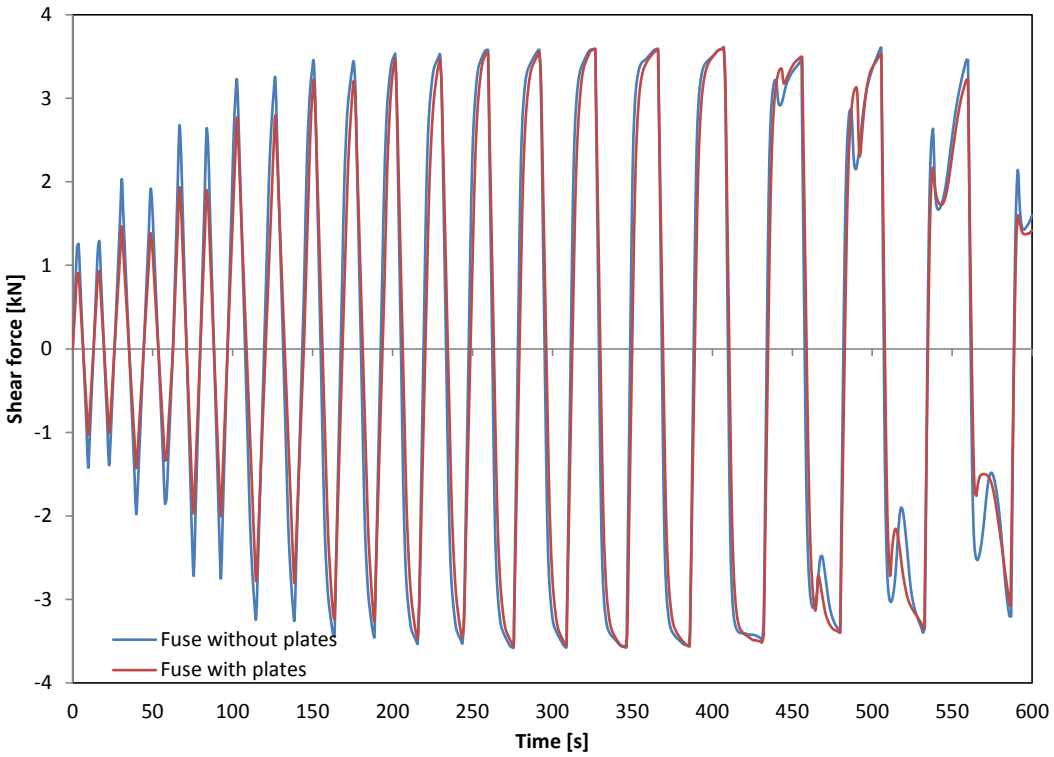

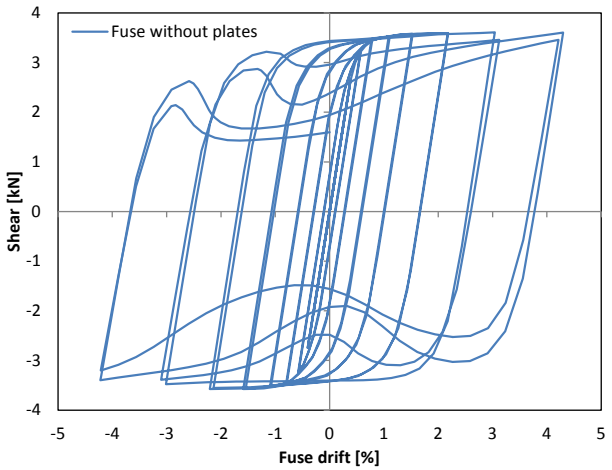

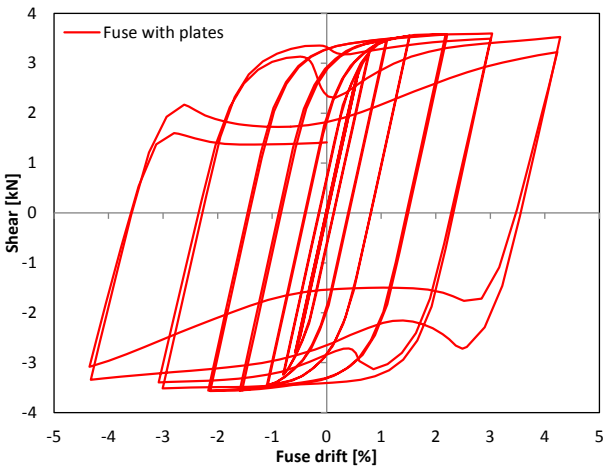

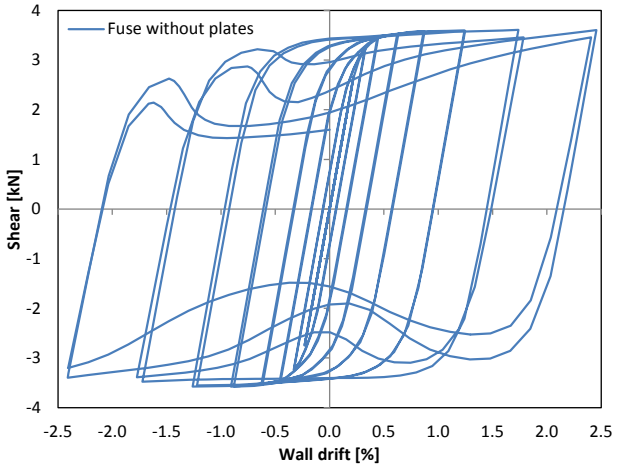

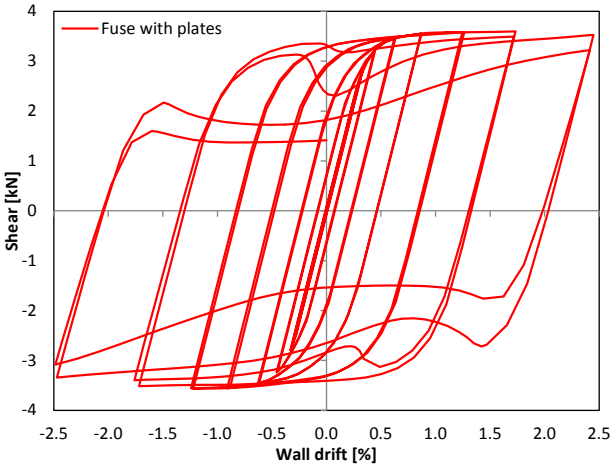

Fuse 50 - L=400mm; b=60mm; t=5mm; σ_y=250MPa (*)

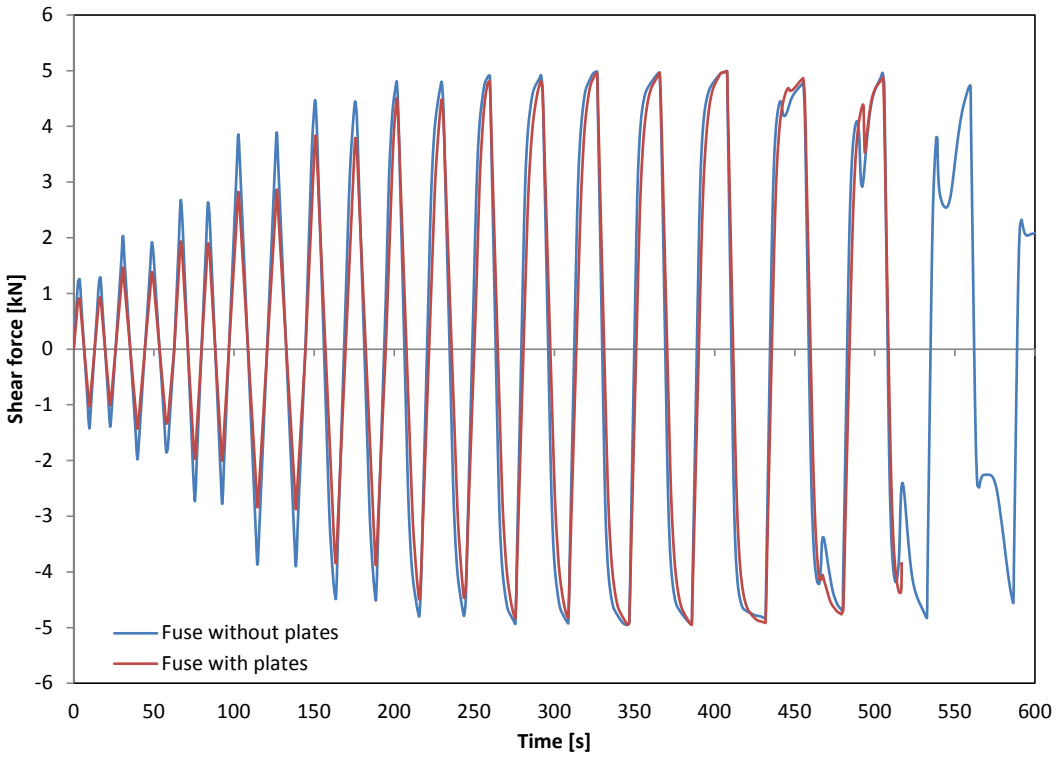

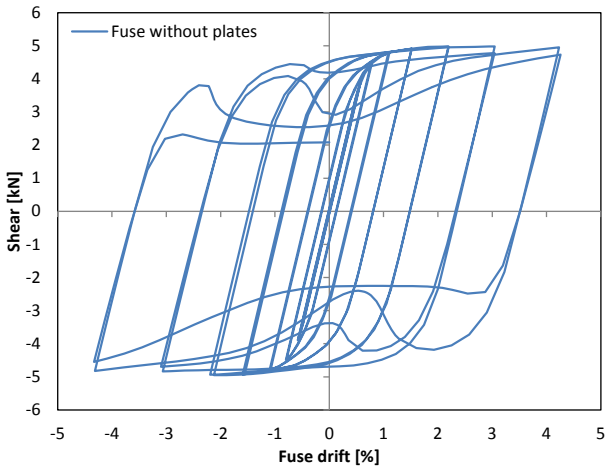

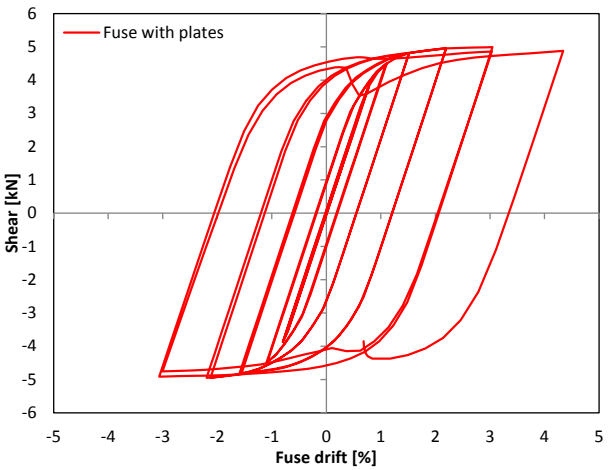

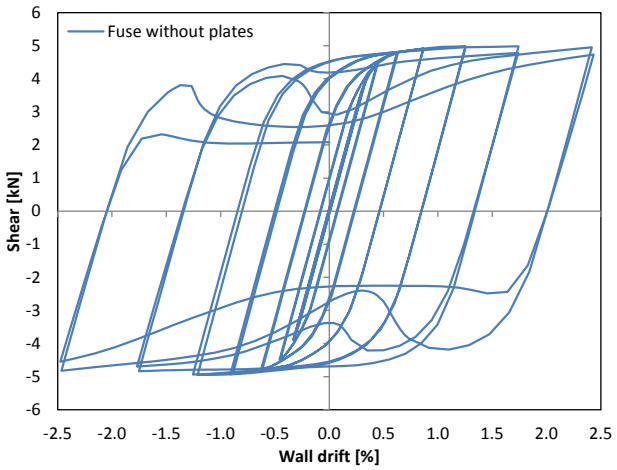

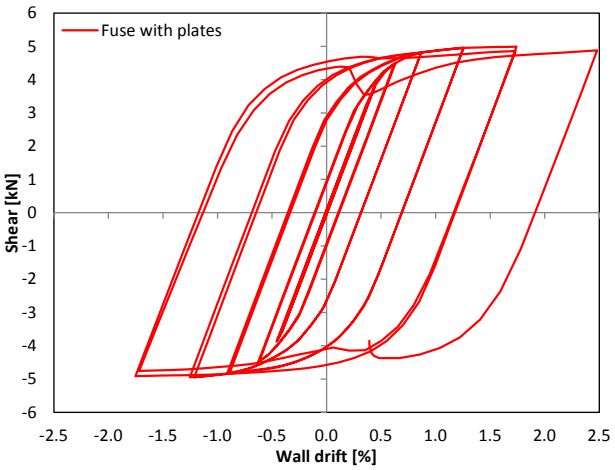

(*): the numerical analysis of the fuse with plates terminated prematurely due to lack of convergence.

Fuse 51 - L=400mm; b=60mm; t=6mm; σ_y=180MPa

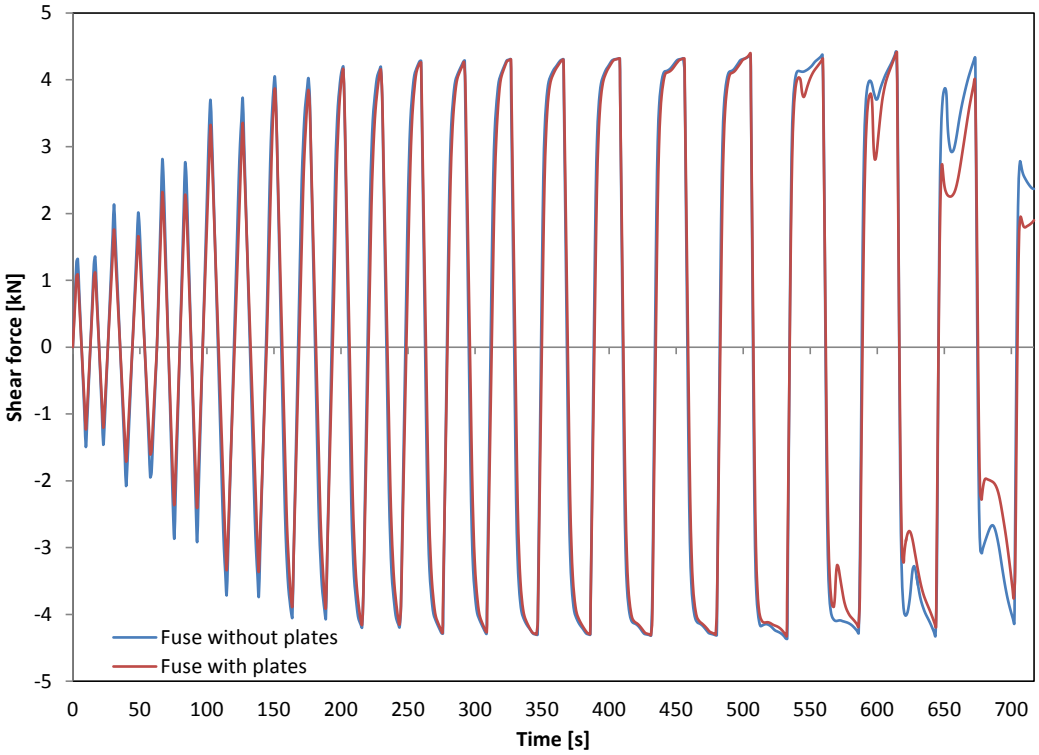

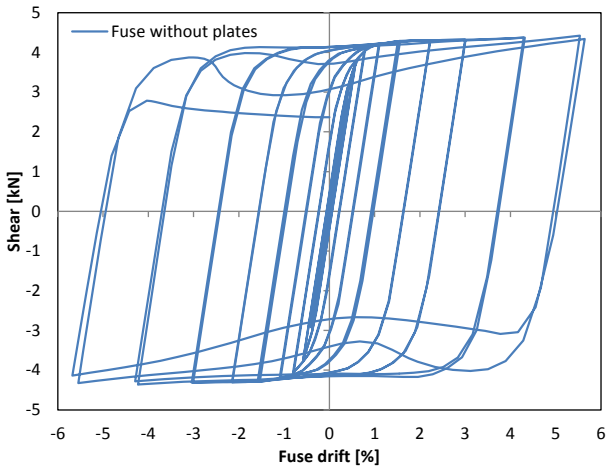

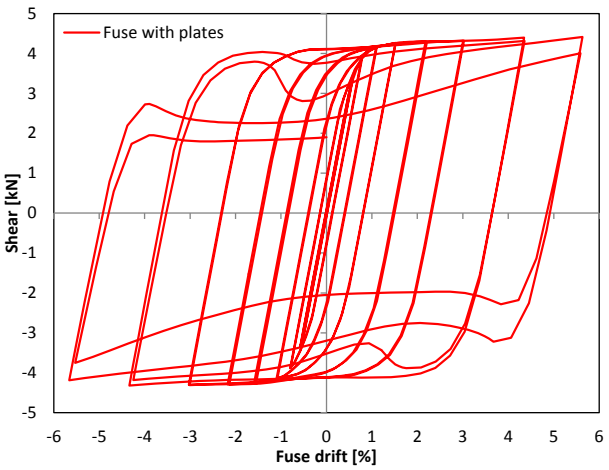

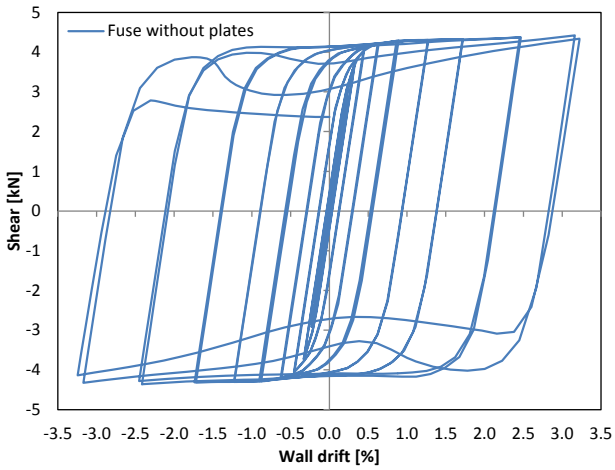

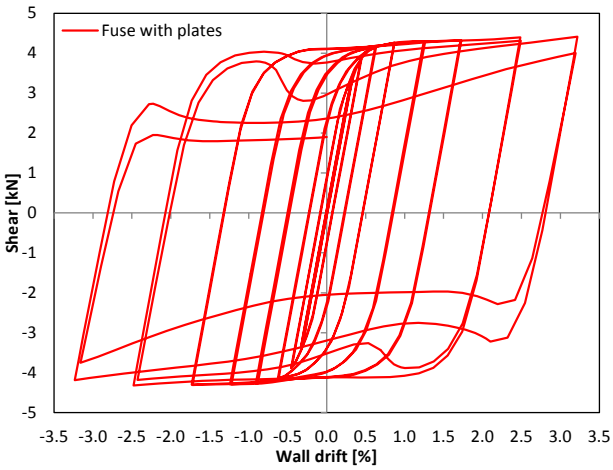

Fuse 52 - L=400mm; b=60mm; t=6mm; σ_y=250MPa

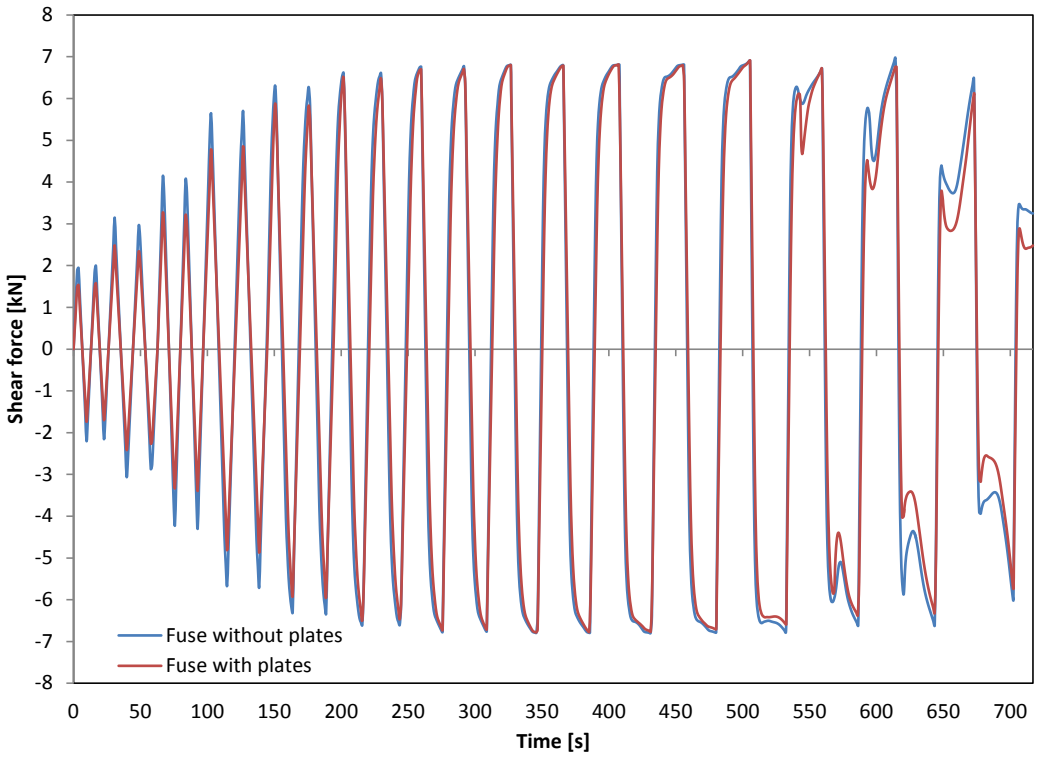

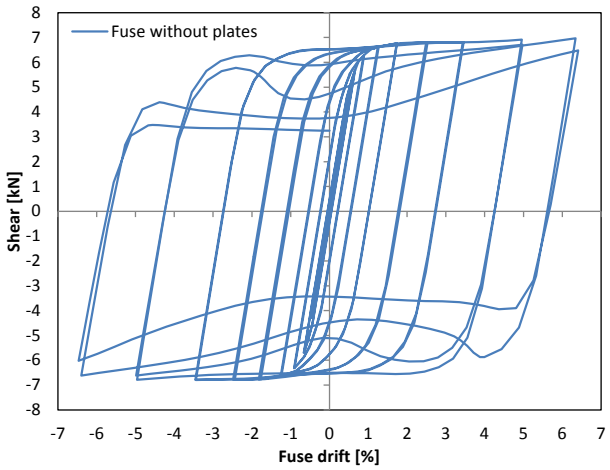

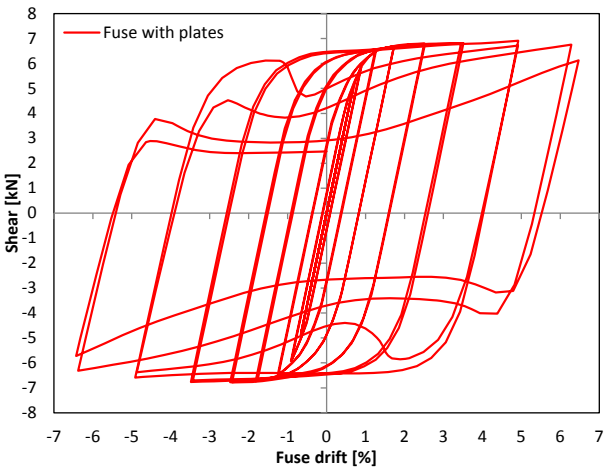

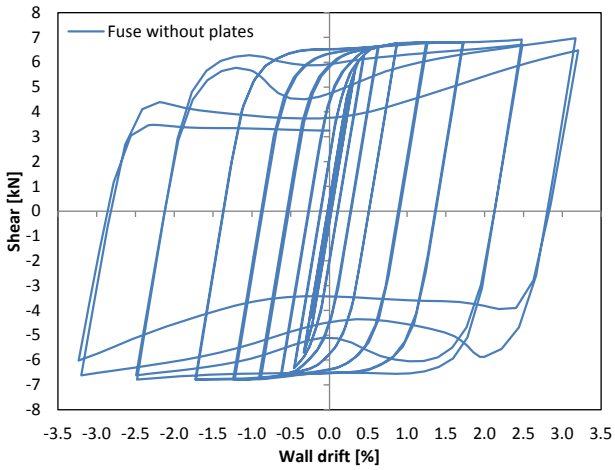

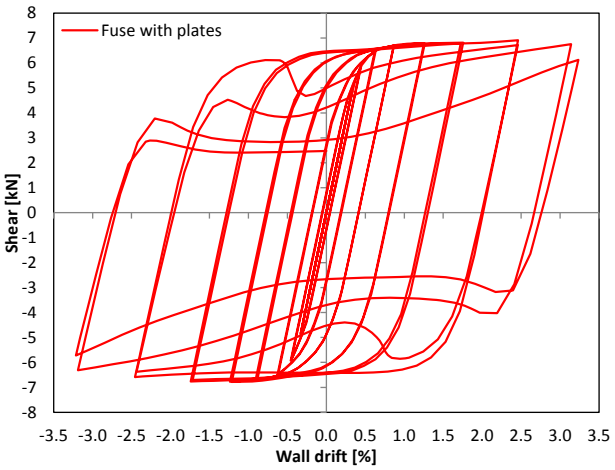

Fuse 53 - L=400mm; b=60mm; t=7mm; σ_y=180MPa

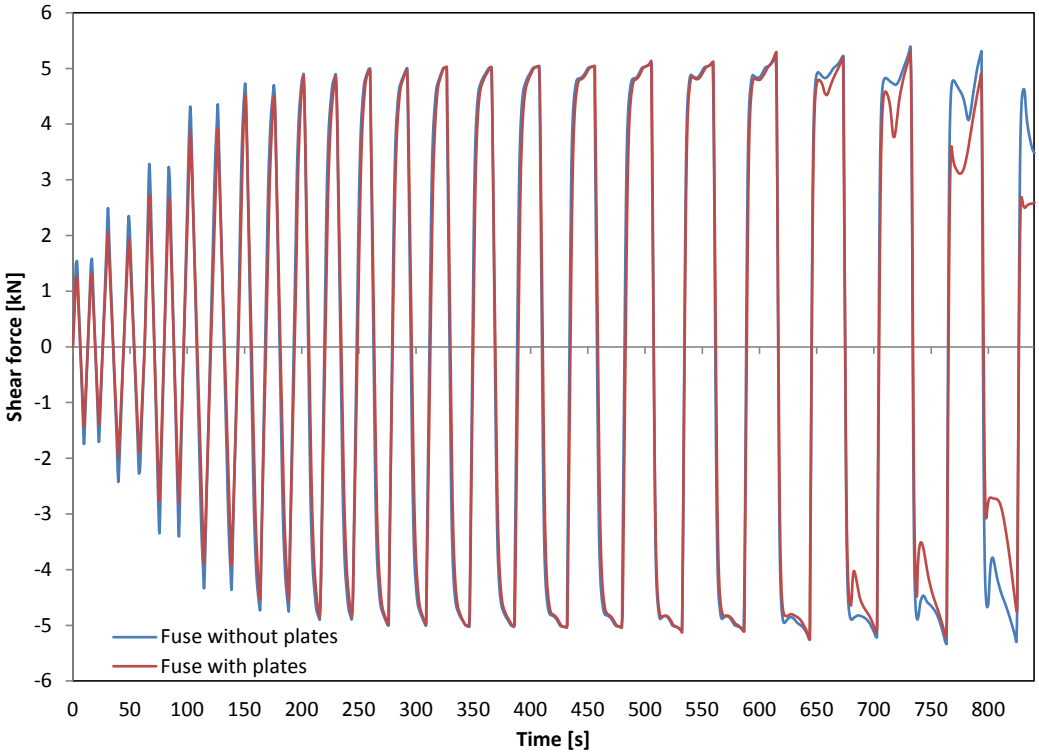

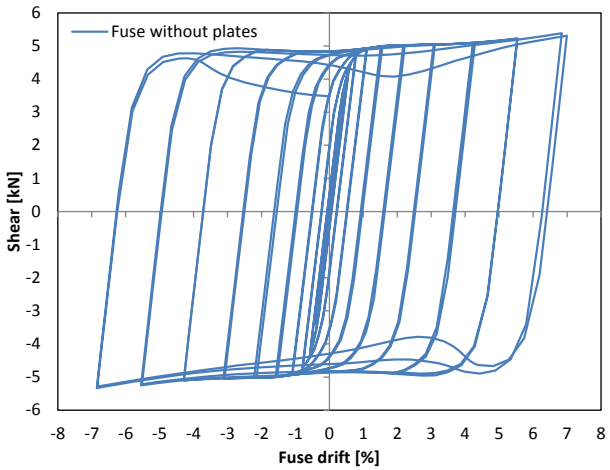

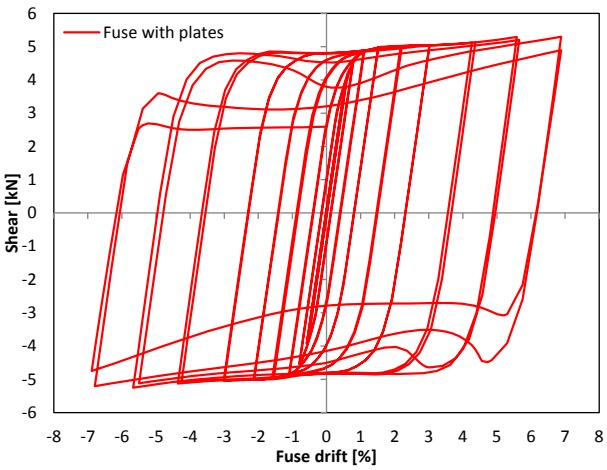

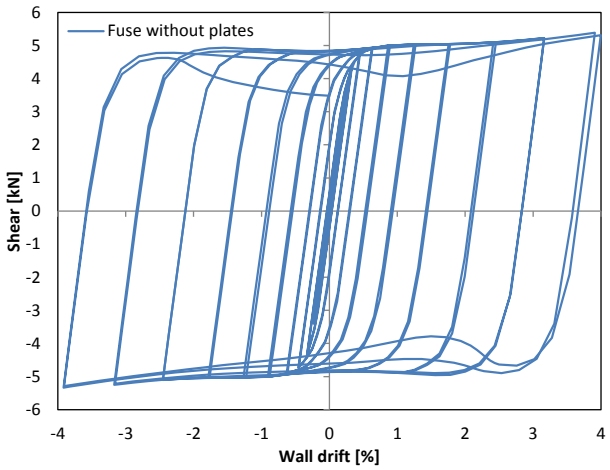

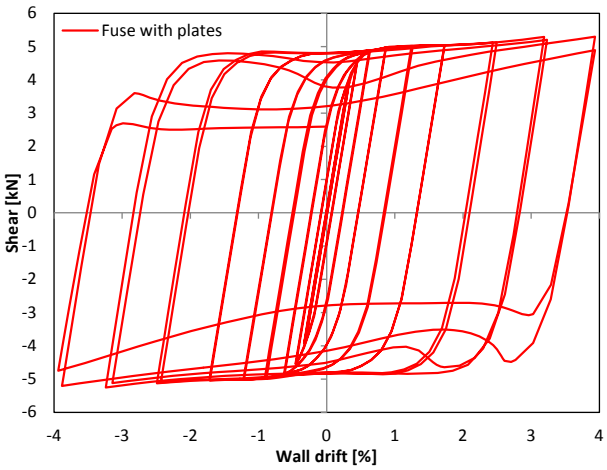

Fuse 54 - L=400mm; b=60mm; t=7mm; σ_y=250MPa

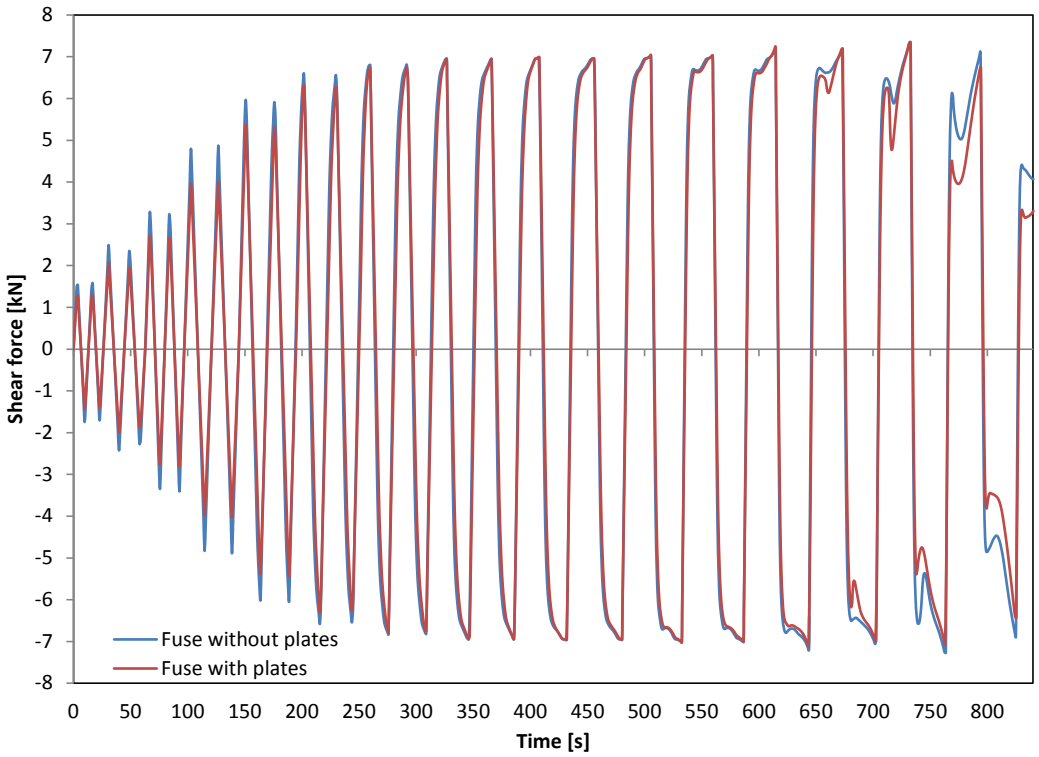

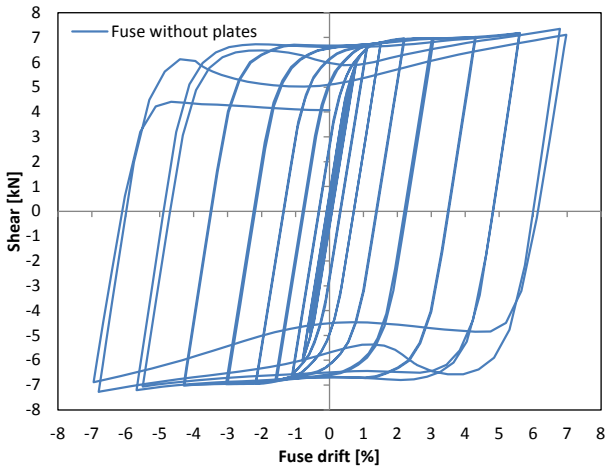

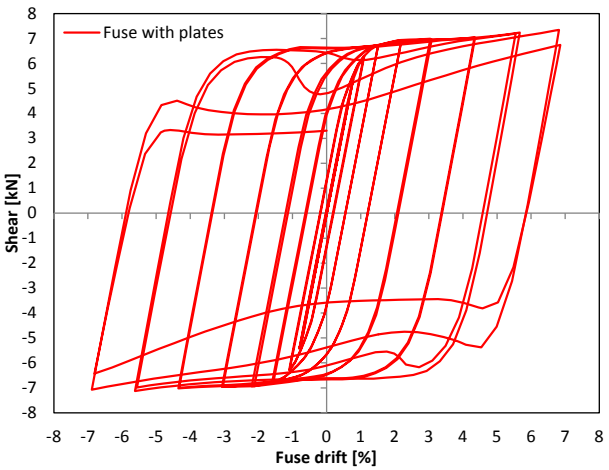

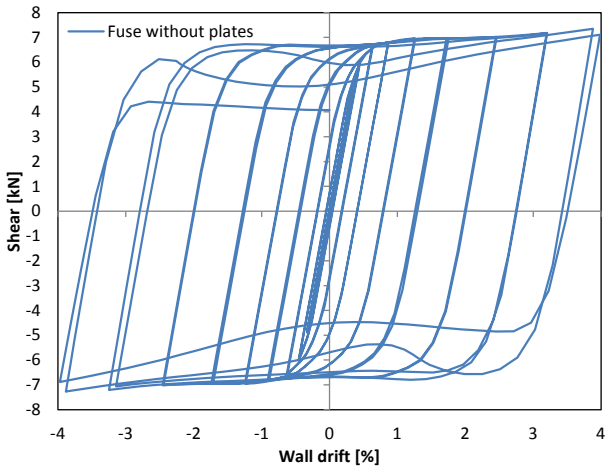

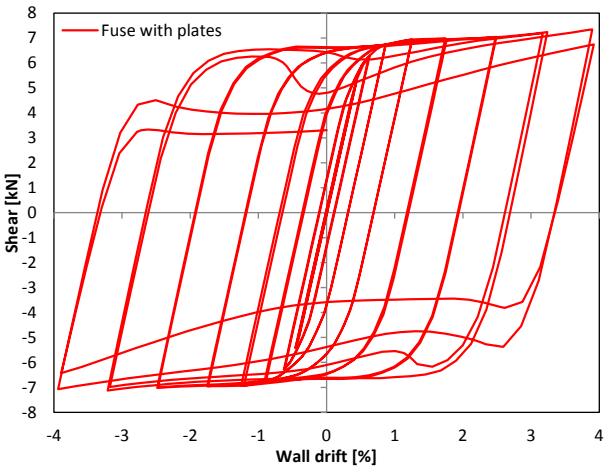

Fuse 55 - L=400mm; b=75mm; t=5mm; σ_y=180MPa

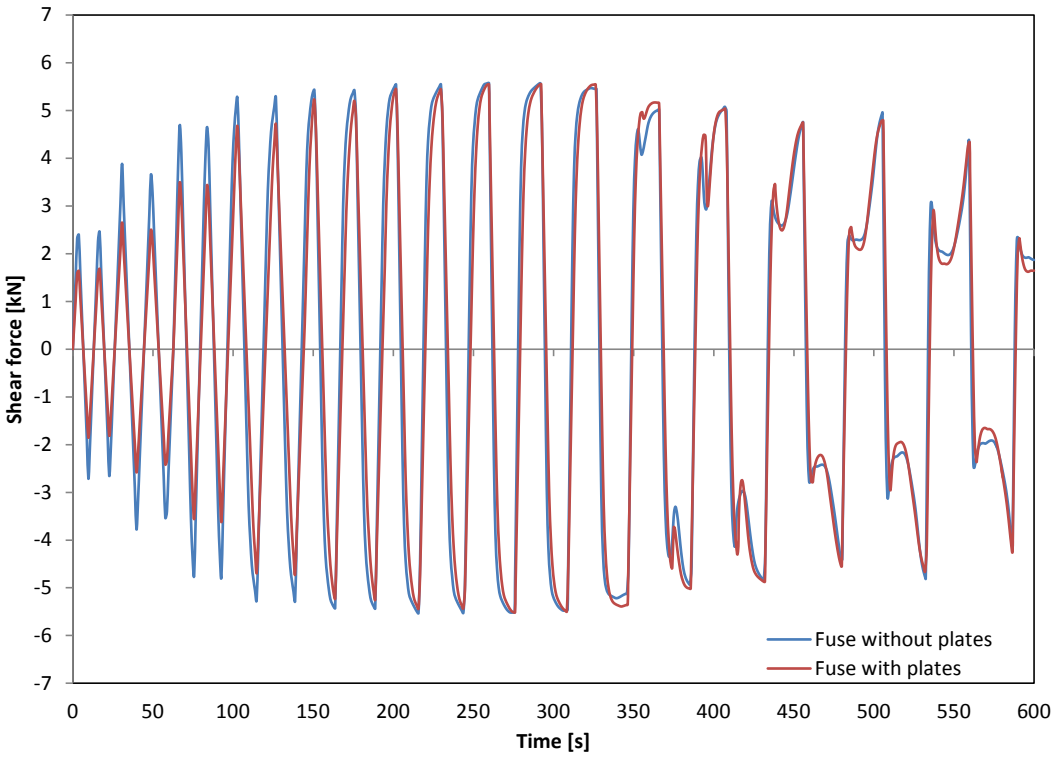

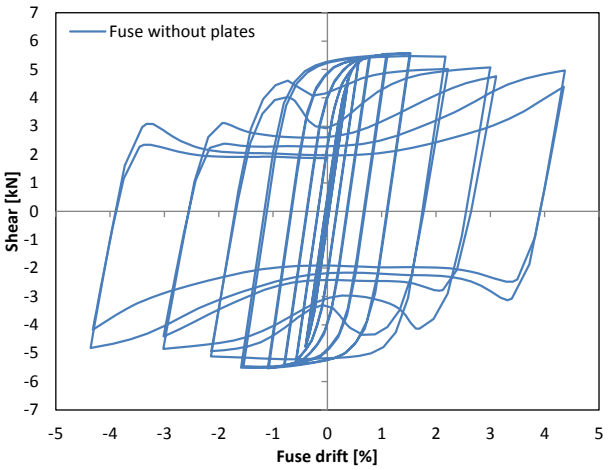

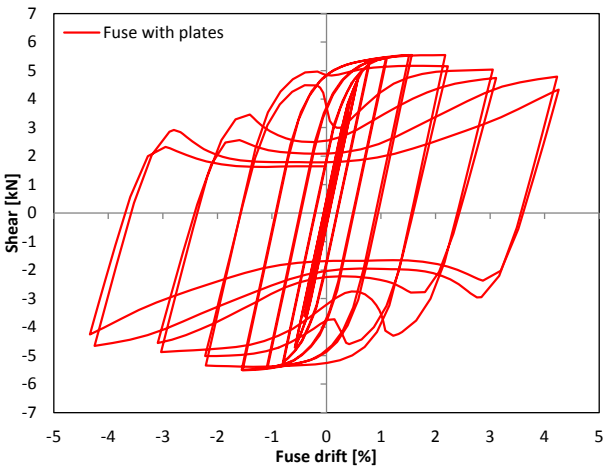

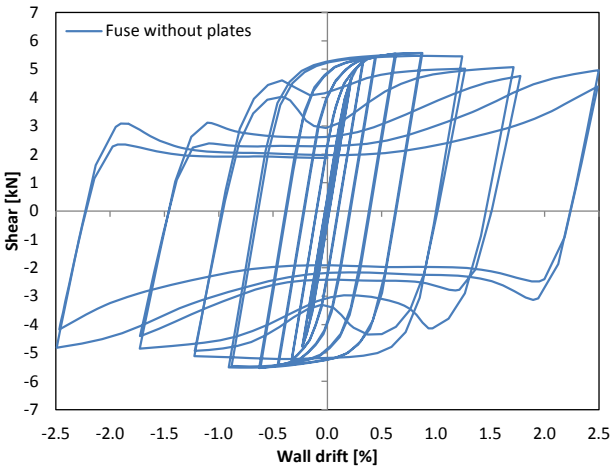

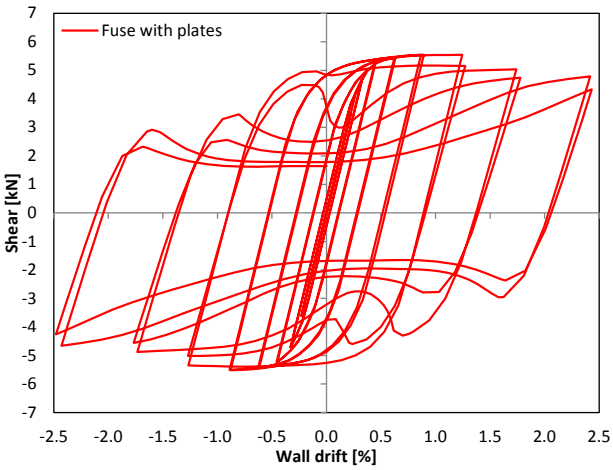

Fuse 56 - L=400mm; b=75mm; t=5mm; σ_y=250MPa (*)

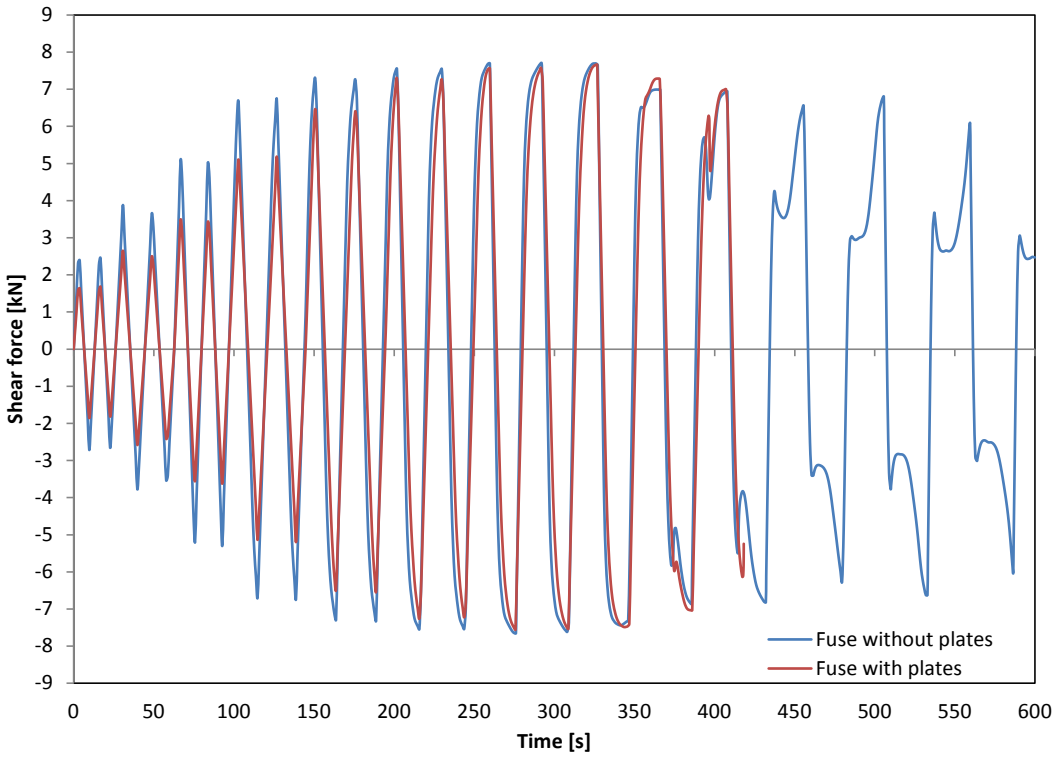

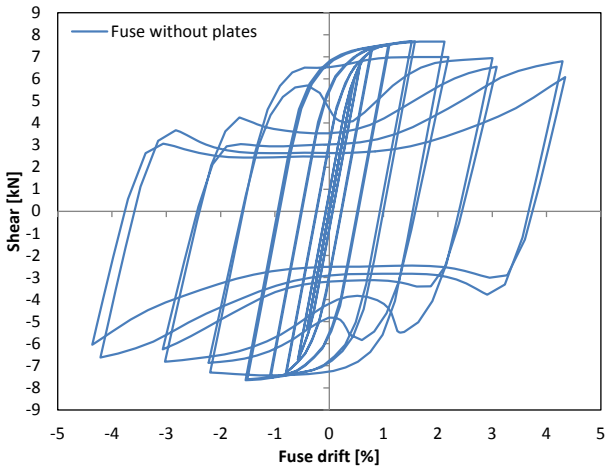

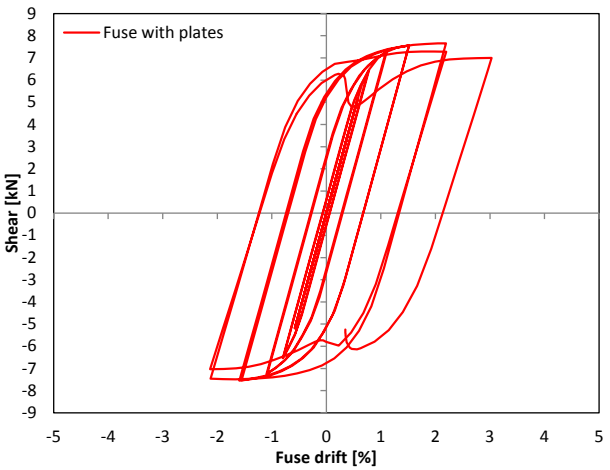

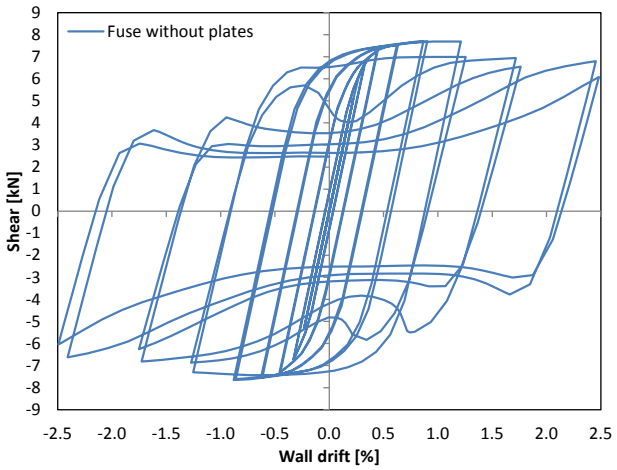

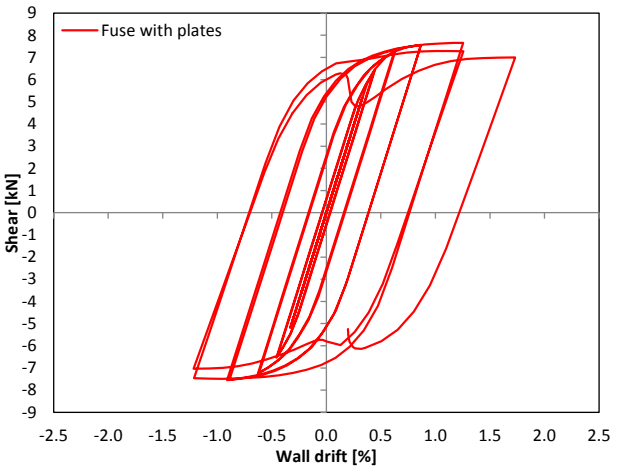

(*): the numerical analysis of the fuse with plates terminated prematurely due to lack of convergence.

Fuse 57 - L=400mm; b=75mm; t=6mm; σ_y=180MPa

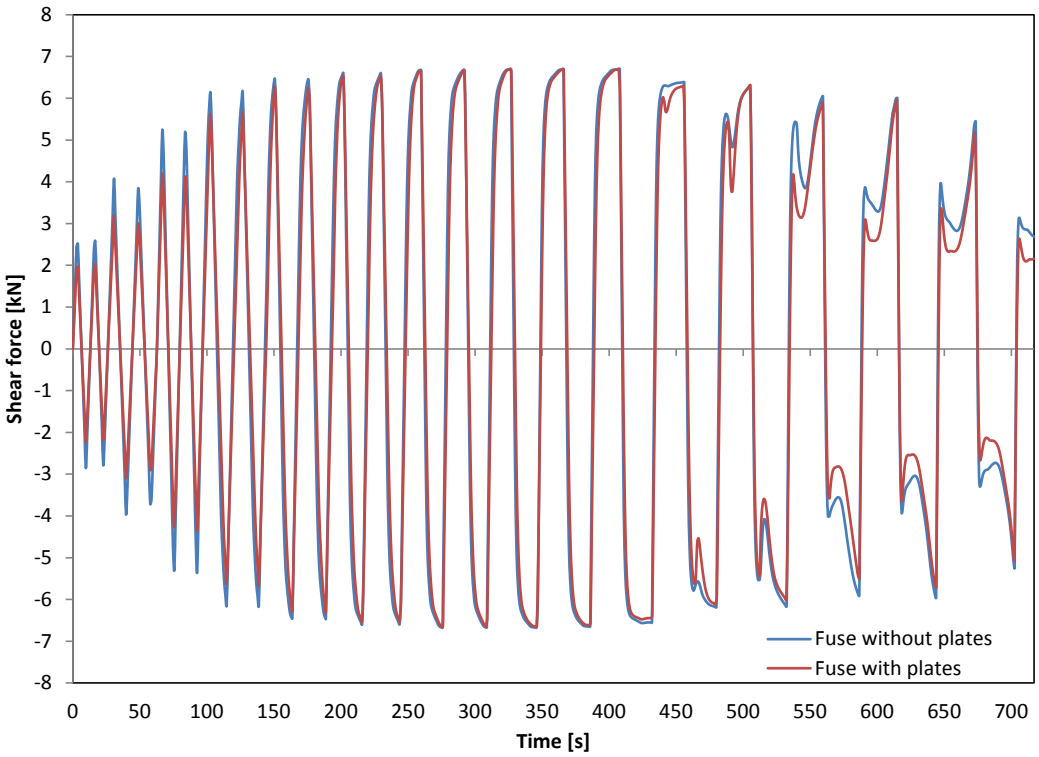

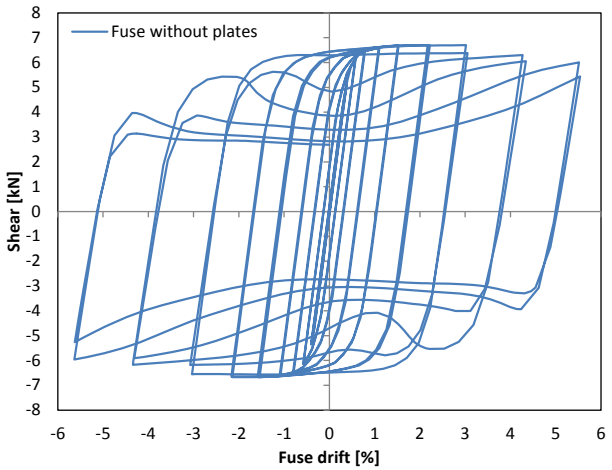

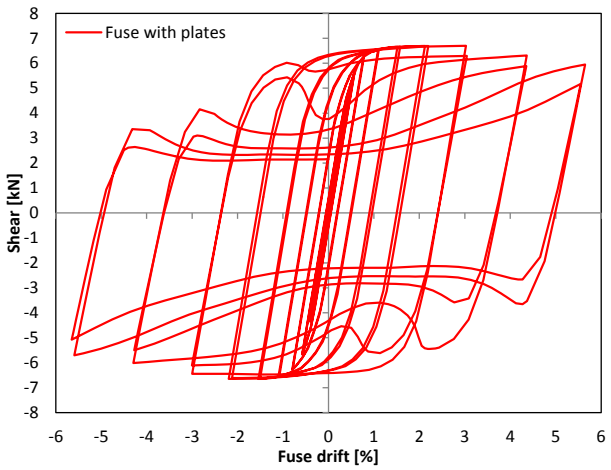

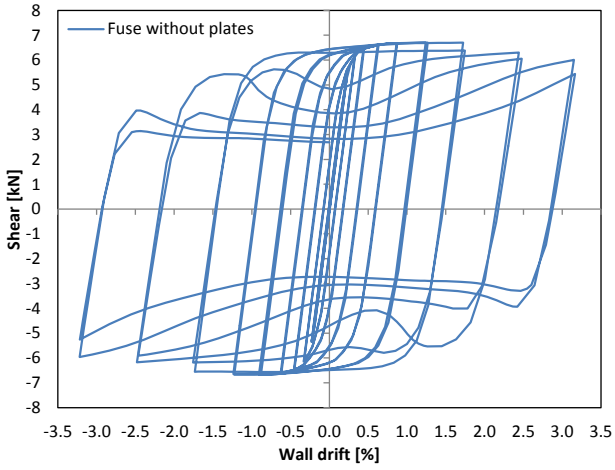

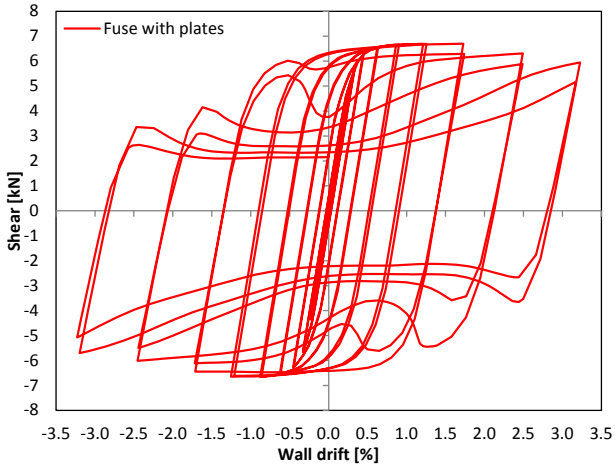

Fuse 58 - L=400mm; b=75mm; t=6mm; σ_y=250MPa

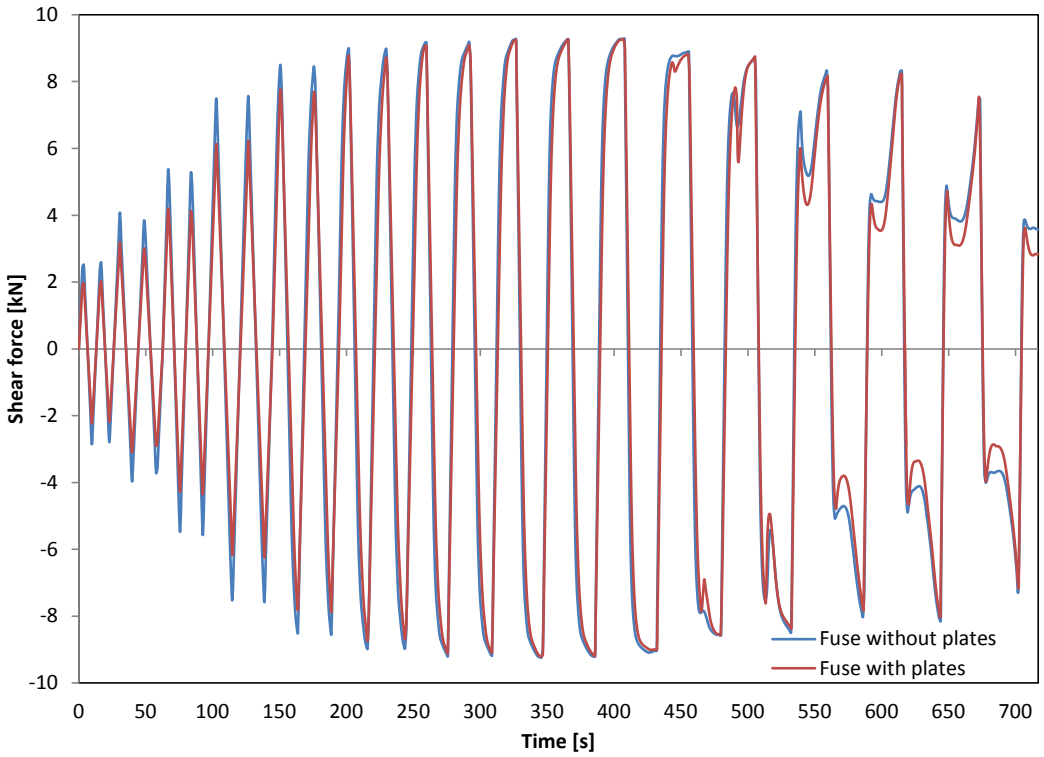

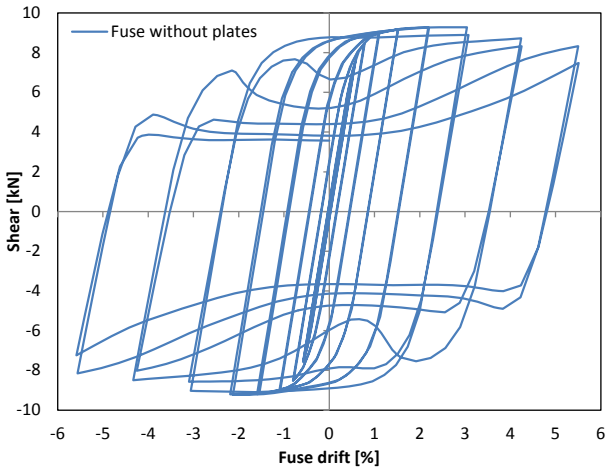

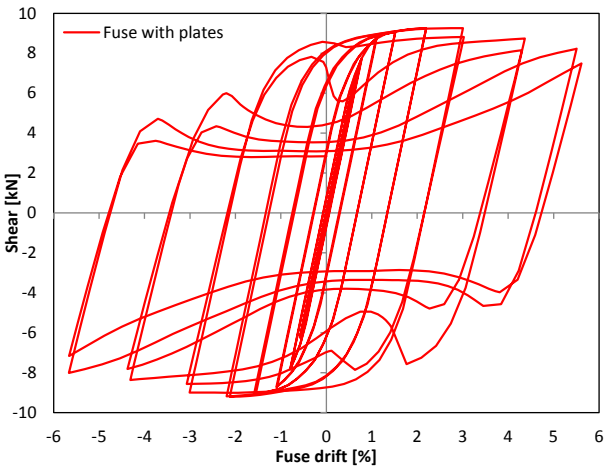

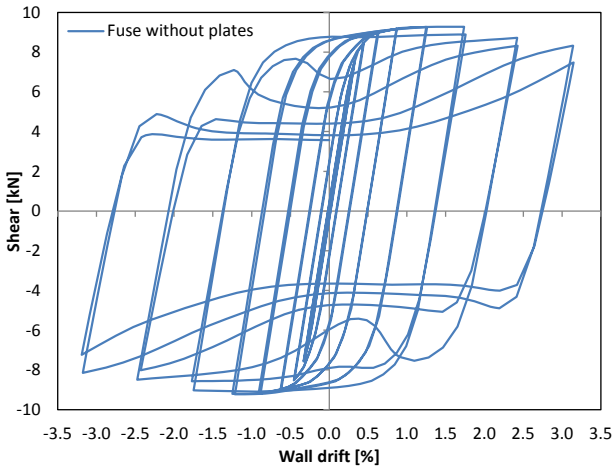

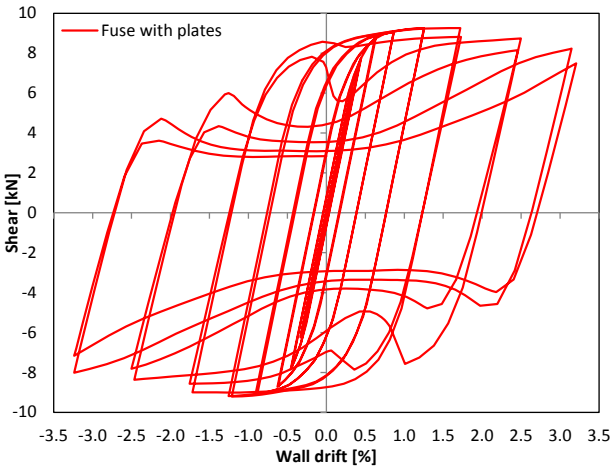

Fuse 59 - L=400mm; b=75mm; t=7mm; σ_y=180MPa

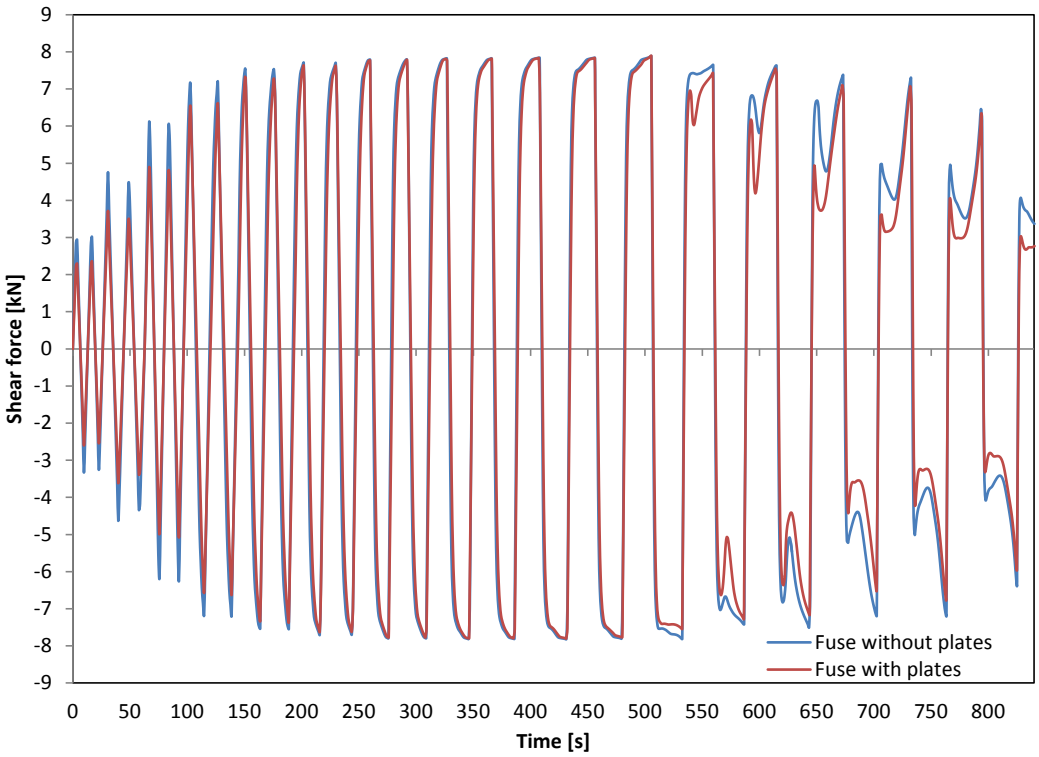

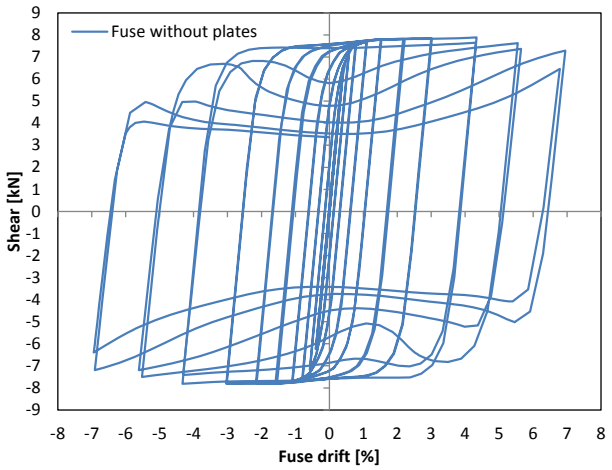

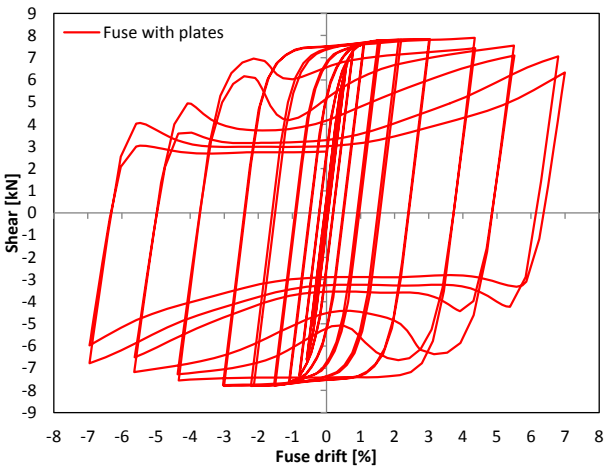

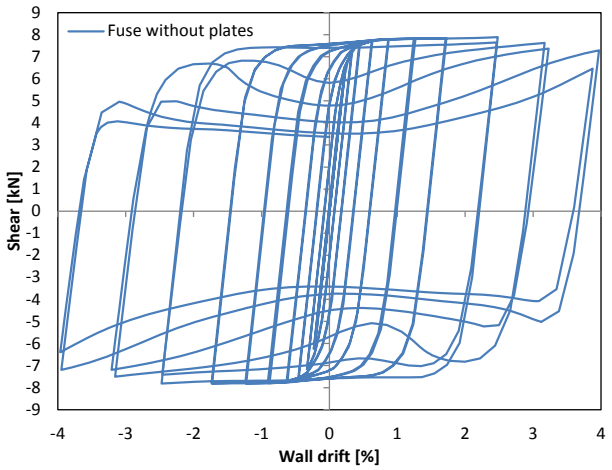

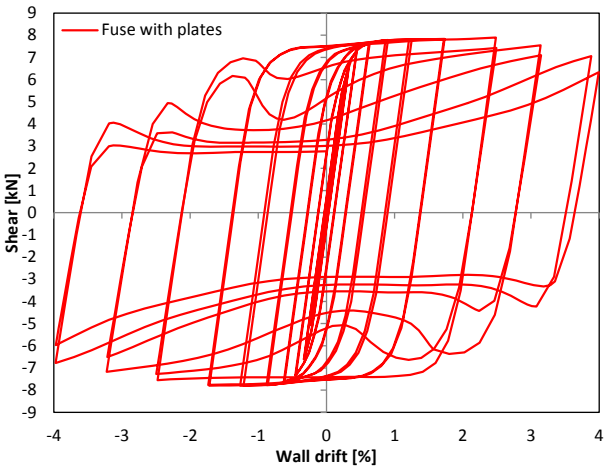

Fuse 60 - L=400mm; b=75mm; t=7mm; σ_y=250MPa